Control of Interface Reactions in SiC/Ti Composites And An X-Ray Diffraction Study Of Interdiffusion Between Al Thin Films and Ti Substrates

by

Venkatraman B. Rao

dissertation submitted to the Graduate Faculty of the Virginia Polytechnic Institute and State University in partial fulfillment of the requirements for the degree of

DOCTOR OF PHILOSOPHY

in

Materials Engineering Science

APPROVED:

C. R. Houska

D. P. H. Hasselman

J. L. Lytton

K. L. Reifsnider

C. W. Smith

October, 1980
Blacksburg, Virginia

ACKNOWLEDGEMENTS

The author would like to express his sincere thanks to Dr.C.R.Houska who has been a source of inspiration and provided the challenge and assistance required to complete this work. Thanks are also due to Drs.D.P.H.Hasselman, J.L.Lytton, K.L.Reifsnider and C.W.Smith who, unselfishly devoted their time and knowledge while participating as members of my committee. Dr.J.Greene from the University of Illinois is thanked for his assistance and knowledge imparted to me in the area of thin film technology.

Thanks are also due to Drs.J.Unnam, D.R.Tenney, B.A.Stein and R.T.Swan from Nasa-Langley Research Center for their interesting and timely discussions. The financial assistance of the Nasa-Langley Research Center is gratefully acknowledged.

Grateful appreciation and admiration is due to Mr.Harry C.Dudley,III, technician for the X-ray laboratory, who worked harder and longer hours than was ever asked of him. Thanks also go to the following colleagues and friends, who for obvious reasons, are being ranked in chronological sequence of my assosiation with them: Victor Gehman, Dick Yesensky, Nagender Naidu, Terry Smith, Augusto Peneloza and Karl Wiederman. A special thanks goes to Satish I. Rao for

helping with the sometimes arduous tasks often encountered during the completion stages. Appreciation is also extended to my loving wife Manjula B. Rao for her patience and assistance in typing (scripting) this thesis. She spent long hours during the completion of this thesis, assisting and providing loving care and encouragement, and words cannot express my sincere thanks to her.

The author wishes to express his thanks to the members of his family for their loving care and encouragement.

TABLE OF CONTENTS

ACKNOWLEDGEMENTS ii

Chapter page

I. INTRODUCTION 1

II. REVIEW OF LITERATURE 5

Control of Interface Reactions in SiC/Ti composites: 5
Interdiffusion in the Titanium Aluminum System . 13
Interdiffusion in the Composition Range Between 0 and 25 at.% Ti 14
Interdiffusion in the Composition Range Between 25 and 100 at.%Ti 18

III. THEORY 38

Basic diffraction equations for determining composition profiles. 38
Computer Simulation of Intensity Bands: . . . 45
Diffusion Equations: 50
Two-Phase Plating Problem with Constant D: . 52
Two-Phase Plating Problem with Variable D: . 57

IV. EXPERIMENTAL PROCEDURES 59

Sample Preparation 59
Planar Composites for Studying Control of Interfacial Reactions: 59
Planar Composites for Diffusion Studies: . . 69
Annealing Procedure: 71
Planar Composite Samples for Control of Interface Reactions 71
Planar Composites for Diffusion and Reaction Studies: 75
X-ray Measurements 77
X-ray Measurements on Planar Composites . . . 79
X-ray Measurements on Planar Composites for Diffusion Studies 81
Microscopy 83
Preparation of the $TiAl_3$ Powder Standards . . . 84
Annealing Procedure 84

X-ray Diffraction Measurements 86

V. COMPUTER SIMULATION TECHNIQUES 87

Simulation of Diffracted Intensity Bands 87
Two-Phase Iterative Solution to obtain Diffusion Coefficients 96
Computer Simulation of Integrated Intensities of the Ti-Al Compounds 100
Simulation of $TiAl_3$ Integrated Intensities 100
Simulation of the Ti_3Al and Ti_2Al Phases . 101

VI. RESULTS AND DISCUSSION 103

Control of Interface reactions in Planar Composites 103
Lattice Parameters 112
Optical Microscopy 116
Relative Reaction Rates 118
Interface Reactions in Al thin films on Titanium Substrates 141
Control of Interface Reactions in $SiC/Ti_3Al/Ti$ Planar Composites. 151
Relative Reaction Rates 153
Diffusion Studies on the Al/Ti Thin Films . . 158
Low Temperature Diffusion Studies 158
High Temperature Diffusion Studies 167
Determination of Diffusion Coefficients . . . 187
Low Temperature Case 187
High Temperature Case 189
Computer Simulations of the Integrated Intensities of Ti-Al Compounds 200

VII. CONCLUSIONS 206

REFERENCES 209

APPENDIX 1 217

APPENDIX 2 232

APPENDIX 3 242

APPENDIX 4 254

APPENDIX 5 284

APPENDIX 6 292

APPENDIX 7 297

LIST OF TABLES

Table		page
1.	Diffusion Coefficients for Al Diffusion in Alpha-Titanium	19
2.	Phase Changes in the Titanium-Aluminum System	28
3.	Results of the Layer growth in various diffusion couples[32]	34
4.	Summary of the structures of the phases occuring in the Ti-Al System	37
5.	Specimen Data Sheet for SiC/Ti Planar Composites	61
6.	Specimen Data Sheet for SiC/Al/Ti Planar Composites	62
7.	Specimen Data Sheet for The SiC/Mo_5Si_3 /Ti Planar Composites	63
8.	Specimen Data Sheet for Mo_5Si_3 /Ti Planar Composites	65
9.	Spectrographic Analysis of The Aluminum Target	66
10.	Spectrographic Analysis for the Mo_5Si_3 Target	67
11.	Spectrographic Analysis of the SiC Target	68
12.	Specimen Data Sheet for SiC/Ti_3Al/Ti Planar Composites	70
13.	Specimen Data Sheet for Al(1 micron)/Ti Planar Composites	72
14.	Specimen Data Sheet for Al(0.5 microns)/Ti Planar Composites	73
15.	Lattice Parameter, Absorption and Reflectivity Data for the Ti-Al system with CuK_{α_1} radiation	89
16.	Table showing the Half-Width values used in the Computer Simulations	91
17.	Integrated intensities and two theta positions for the SiC/Ti system annealed at 875°C for various times.	106

18. Integrated intensities and two theta positions for the SiC/Al/Ti system annealed at 875°C for various times. 110

19. Integrated intensities and two-theta positions for the SiC/Mo_5Si_3/Ti planar composites 113

20. Lattice Parameter Data for the SiC/Ti System . . . 117

21. Table showing the ratios for Ti_5Si_3/Ti reflection pairs for the SiC/Ti system 134

22. Table showing the ratios for Ti_5Si_3/Ti reflection pairs for the SiC/Al/Ti system 135

23. Table showing the ratios for Ti_5Si_3/Ti reflection pairs for the SiC/Mo_5Si_3/Ti system 136

24. Comparison of the layer or random assumption for $TiAl_3$ at 635°C , 1/2 hour. 144

25. Integrated intensities and two theta positions for the SiC/Ti_3Al/Ti samples annealed at 875°C for various times. 154

26. Table showing the ratios for Ti_5Si_3/Ti reflection pairs for the SiC/Ti_3Al/Ti system 156

27. Diffraction data for Al/Ti standards for 635°C, 1/2 hr 160

28. Diffraction data for Al/Ti standards for 635°C, 1 hr 162

29. Pearson Parameters and Error Function Coefficients for 635°C 163

30. Diffraction data for Al/Ti standards for 900°C, 1/2 hr 173

31. Diffraction data for Al/Ti standards for 900°C,1 hour. 175

32. Diffraction data for Al/Ti standards for 900°C,4hrs 177

33. Pearson parameters and the Error function coefficients for (900°C) 186

34. Integrated intensities and two-theta positions for $TiAl_3$ 202

35. Table showing the Integrated Intensities of Ti_3Al and Ti_2Al from several investigations. 205

36. Table showing the Integrated Intensities for Titanium obtai- from theoretical (computer) calculations. 296

37. Table showing the Integrated Intensities for Ti_5Si_3 obtained from theoretical (computer) calculations. 297

LIST OF FIGURES

Figure		page
1.	The Titanium-Aluminum Phase Diagram after H. Margolin[59].	20
2.	The Titanium-Aluminum Phase Diagram[74,26].	21
3.	Important Ti-Al Phase Diagrams from Several Investigations.	25
4.	Lattice Parameter versus Composition Data for the Ti-Al System(ref. 49).	29
5.	Results from the van Loo and Rieck study.	36
6.	Cross-section of specimen illustrating an irradiated region.	40
7.	Schematic of the intensity band for a single phase system.	44
8.	Schematic representation of composition profiles for finite two phase systems.	56
9.	Schematic of the X-ray diffraction geometry.	78
10.	Illustration of the four rotational axis.	80
11.	Initial conditions and conservation of Al atoms, for diffusion studies.	93
12.	Schematic representation of the composition profiles for the low temperature diffusion studies.	95
13.	Schematic representation of the composition profiles for the high temperature diffusion studies.	97
14.	Photomicrograph of the SiC/Ti sample annealed at 875°C for 2 hours.	119
15.	Photomicrograph of the SiC/Ti sample annealed at 875°C for 1/2hr, showing flaking.	120
16.	Photomicrograph of the SiC/Ti sample annealed at 875°C for 1/2hr showing reaction zone.	121

17. Photomicrograph of the SiC/Ti sample annealed at 875°C for 1 hour. 122

18. Photomicrograph of the SiC/Ti sample annealed at 875°C for 4hours showing a depletion zone. . . 123

19. Photomicrograph of a SiC/Ti sample annealed at 875°C for 6 hours. 124

20. Photomicrograph of a SiC/Al/Ti sample annealed at 875°C for 1/2 hr, showing discontinuous zones. 125

21. Photomicrograph of a SiC/Al/Ti sample annealed at 875°C for 2 hours. 126

22. Photomicrograph of a SiC/Mo_5Si_3/Ti sample annealed at 875°C for 1/2 hr. 127

23. Photomicrograph of a SiC/Mo_5Si_3/Ti sample annealed at 875°C for 2 hours. 128

24. Schematic of a SiC/Ti planar composite used to illustrate equivalent absorption path lengths. 131

25. Schematic of a SiC/Al/Ti planar composite used to illustrate equivalent absorption path lengths. 132

26. Schematic of a SiC/Mo_5Si_3/Ti planar composite used to illustrate equivalent absorption path lengths. 133

27. Reaction rate curves for the various planar composite systems. 139

28. Reaction kinetics for the 1 micron Al film samples. 148

29. Reaction kinetics for the 0.4 and 0.5 micron Al film samples. 150

30. Computer simulations of the (101) intensity band, 635°C (1/2hr). 165

31. Composition profiles for the simulations of the (101) intensity band, 635°C (1/2 hr). 166

32. Computer simulations of the (101) intensity band, 635°C (1hr). 168

33. Composition profiles for the simulations of the (101) intensity bands, 635°C (1 hr). 169

34. Computer simulations of the (101) intensity band, 635°C (2hrs). 170

35. Composition profiles for the simulations of the (101) intensity band, 635°C (2 hrs). 171

36. Computer simulations of the (101) intensity band, 900°C (1/2 hr). 179

37. Computer simulations of the (101) intensity band, 900°C (1hr). 180

38. Computer simulation of the (101) intensity band, 900°C (4 hrs). 181

39. Composition profiles for the simulations of the (101) intensity band, 900°C (1/2 hr). 183

40. Composition profiles for the simulations of the (101) intensity band, 900°C (1hr). 184

41. Composition profiles for the simulations of the (101) intensity band, 900°C (4hrs). 185

42. Simulation of the composition profiles, 635°C (1/2hr), to obtain diffusion coefficients. . . 190

43. Simulations of the composition profiles, 635°C (1hr) to obtain diffusion coefficients. 191

44. Simulations of the composition profiles , 900°C (1/2hr), to obtain diffusion coefficients. . . 192

45. Simulations of the composition profiles, 900°C (1hr), to obtain diffusion coefficients. . . . 193

46. Simulations of the composition profiles, 900°C (4hrs), to obtain diffusion coefficients. . . . 194

47. Diffusion coefficient data from the present study. 196

48. Comparisons of the diffusion coefficients from the present study with those in the literature. . . 198

49. Activation energies plotted against composition for aluminum diffusion in alpha-titanium. 200A

50. Side-view of the Perkin-Almer sputtering system. 258
51. Control Panel. 222
52. Perkin Elmer Auto Pump-down Control Panel. 229
53. Photograph showing vacuum units. 231
54. Photograph showing RF generator and compressor. . 232
55. The TiAl unit cell. 293

Chapter I

INTRODUCTION

Composites containing SiC fibers and a Ti matrix have generated considerable interest in recent years. This results from an anticipated improvement in the high temperature mechanical properties over composites containing Al matrices. The major problem still to be overcome is the physical chemical behaviour of the SiC/Ti interface at fabrication temperatures (approx. 850°C). Ideally, only a thin bonding film is desired after fabrication with essentially zero growth during the actual service conditions.

In this study, two mechanisms (barrier and rejection mechanism) which lower the growth rate of silicides and carbides about the SiC/Ti interface, were investigated. Because Si atoms must be transported through the interfacial silicide film to provide further growth of the film, the formation of films having the lowest rate of transport must be encouraged. Silicide films with the composition M Si (M= Ti or Mo) are known to have a low rate of Si transport. Therefore, the stability of SiC/Ti composites containing a Mo Si barrier film was investigated relative to the SiC/Ti interface without a barrier. The second mechanism involves the rejection of a metal atom into the matrix from the interface and tending to saturate it. The matrix satu-

rated with this atom has a lower tendancy to react with the SiC film. Samples containing Al films were studied to investigate the effectiveness of Al as an exchange atom in controlling silicide growth.

X-ray diffraction was employed as the major tool for this investigation because it is capable of providing detailed kinetic data on the earliest stages of the interface reactions, nondestructively. To perform a true test of adhesion, only planar samples were used. Cylindrical or spherical geometries may contain additional elastic stresses which obscure the interpretation of interface adhesion. Compressive stresses acting on an interior barrier film could reduce the tendancy for crack propagation or flaking. Consequently, only planar samples were used in order to reduce geometrical complications.

One of the major goals of this study was to determine the potential coating that could be used to reduce silicide formation and then to design an optimum hot-pressing cycle for fabrication of these composites. Reaction rate studies could be performed by thermal treatments (similar to the hot-pressing stage) given to several planar composite systems. The major silicide product associated with SiC/Ti matrix reactions has been Ti_5Si_3. Consistent results can be obtained if it is assumed that the rate limiting step is

the diffusion of Si from the SiC filament to the substrate producing mainly Ti_5Si_3. Based on this assumption, a quantitative X-ray method was used to inter-relate the rate of silicide formation. These preliminary results strongly supported the use of Al films on Ti foils in the preparation of SiC/Ti matrix composites.

The next stage in the investigation demanded the optimum thickness of the protective coating (Al) to be used to fabricate composites. For this, a detailed knowledge of the reaction kinetics of Al thin films on titanium substrates was necessary. Although a vast amount of data in the literature was available, most of this data dealt with bulk materials of both elements. This necessitated the use of Al/Ti planar composites and the study of the reaction kinetics, under conditions similar to those encountered during hot-pressing. Also, these samples could serve as internal standards for comparison.

The reaction kinetics on Al thin films served a second purpose. It allowed us to obtain important information on the exact processes occuring at the interface during the fabrication. This is basic to the understanding of silicide reduction during fabrication and also it is essential in designing the proper hot-pressing cycle. While serving this purpose, the data from the reaction kinetics was used to

advantage to obtain composition profiles by a previously developed X-ray diffraction, simulation technique. From these profiles, useful information such as composition dependent diffusion coefficients were obtained.

Studies on the interdiffusion in the Ti-Al system until now, have resulted in a lot of confusion due to contradictory findings. Most of this confusion resulted from differences in reaction kinetics due to sample size, reaction times used, etc. While it is not the purpose of the present investigation to clarify all the contradictions, it is intended that this study help provide some insight into the reaction kinetics in thin Al films on titanium substrates. Some attempt has been made to explain the occurence of the Ti_3Al and Ti_2Al phases in some instances, using a computer modelling technique based on the structures of these phases. The experimental relative integrated intensities of the $TiAl_3$ phase (using a diffractometer), as well as computer simulated values are also included.

Chapter II

REVIEW OF LITERATURE

2.1 CONTROL OF INTERFACE REACTIONS IN SIC/TI COMPOSITES:

In recent years, considerable interest has developed in titanium matrix composites, especially in the area of blades for advanced gas turbine engines. Titanium composites are attractive for applications requiring a stronger matrix and higher temperature capabilities than resin or aluminum-matrix composites. Applications requiring high stiffness and low weight in the 205-627°C (477-900°K) temperature range will benefit from the development of titanium matrix composites.

Borsic* reinforced titanium matrix composites have been fabricated with axial tensile strength, axial elastic modulus, and transverse elastic modulus greater than those of the titanium matrix[1]. This effect is more pronounced when one considers the specific strength or specific stiffness, since the volume fraction of the low density fiber can be extended to as high as 0.5. Also, it was demonstrated that the transverse tensile strength and modulus of Borsic/Titanium at elevated temperatures, are considerably better than those for Boron/Aluminum composites[1].

---

* A commonly used name for Boron-Silicon Carbide.

Above 550°C (823°K), problems of the surface and structural stability had to be solved to make Titanium composites suitable for industrial applications. Most of the previous work done on Titanium composites made use of a Ti-6Al-4V or a Ti-3Al-2.5V alloy as the matrix[1,3]. Some work was also done on commercially pure Ti-A55 and Beta-III alloy (11.5%Mo, 6.0%Zr, and 4.5%Sn)[3]. Some of this work was related to problems encountered with thermal stability, filament splitting, filament -matrix compatibility and mechanical strength. The primary emphasis was placed on optimizing the consolidation parameters in an effort to maximize the as-fabricated composite strengths. The fibers used for reinforcement of these various Ti-base matrix materials were either Boron, Borsic or SiC.

Titanium matrix composites have not reached their full potential because of problems associated with instabilities at the fiber/matrix interface or loss of fiber strength at elevated temperatures. A more detailed understanding of the interfacial reaction kinetics and the behavior of the fiber are required if new processes and materials are to be developed for improving the high temperature stability of these materials.

Elevated temperature studies[4] on borsic reinforced Ti-3Al-2.5V alloy composites revealed certain interesting

features. Extensive interfacial reactions resulted in the formation of the brittle silicides (Ti_5Si_3, $TiSi_2$, and TiSi) during the early stages of the reaction. For higher exposure temperatures and longer times, borides (TiB_2, Ti_3B_4 and TiB) of titanium were also formed. The mechanical strength of the composite was observed to decrease in proportion to the increase in the amount of silicides and the size of the reaction zone at the fiber/matrix interface.

Schob , et al.[5] have reported that in the presence of aluminum, a C49 type orthorhombic Ti(Al)Si phase forms in preference to the C54 type $TiSi_2$ phase. The elevated temperatures studies on Borsic/Ti-3Al-2.5V [4] confirmed the formation of large amounts of $TiSi_2$ (C54 type). The absence of the C49 type disilicide suggests that Al was being rejected from the reaction zone. The Al rejection mechanism has also been verified by electron microprobe data[6]. The importance of this behavior in composites containing Al will be discussed at a later stage in relation to the 'Aluminum Rejection Mechanism'.

Earlier work had indicated that the high temperature stability of SiC filaments could be effectively utilized in a Ti matrix composite[7]. Also the availability and lower cost of SiC filaments over either Boron or Borsic filaments showed promise for SiC reinforced composites. Consolidation

subjects the composite to more severe conditions than what are normally anticipated during actual service. Therefore, a major limitation in the use of these composites was the physical chemical behavior of the SiC/Ti interface at fabrication temperatures.

An examination of the limited kinetic data in the literature dealing with the interfacial stability of SiC/Ti composites may lead one to conclude that they are incompatible. However, the same conclusion might have been made about the B/Al system before the concept of protective coatings as first suggested by Metcalfe[8]. He showed that for the B/Al system if solid rather than liquid fabrication techniques are used, a relatively stable interface is formed between a boron oxide film and the oxide on aluminum. As a consequence many investigations are being centered on finding a similar protective mechanism for SiC/Ti composites.

According to Metcalfe, two types of bonds are of importance for the SiC/Ti system[8]. These are reaction bonds associated with the compounds TiC, Ti_5Si_3 and $TiSi_2$, and the "exchange reaction bond" in which a two stage reaction is believed to occur. Previous investigations[9,13] of the reactions between SiC and Ti or Ti alloys are based primarily on optical or scanning electron microscopy and electron microprobe data. Consequently, the early stages of the reaction, which are of considerable importance, have not

received enough attention. Because of resolution limitations with the electron microprobe, quantitative data has only been obtained in the over reacted state, i.e. with reaction zones in excess of 1 micron, where the mechanical properties have already deteriorated.

The SiC reaction with Ti proceeds by the simultaneous recession of the filament and the growth of the reaction zone into Ti[10] without porosity. A small amount of Ti is found in the SiC filament after diffusion treatments and TiC exists as a dispersed phase within the reacted zone. Interface motion was reported to be parabolic. Saturation of Ti with dissolved C increases the rate of transformation[13]. Before saturation the Ti matrix acts as a sink for C atoms thereby removing this atom from the reaction zone.

Although some reaction at the interface is desirable, continued reaction to form a new compound beyond a maximum size is undesirable. At this point, the new compound at the interface is generally more degrading to mechanical properties than simple solution. The compound is usually brittle and its strain to fracture is lower than the filament. Cracks may form if the reaction results in a reduction in the specific volume.

The fact that control mechanisms are not described in the literature for SiC/Ti composites may simply reflect a

lower overall research effort. In the case of titanium diboride, the degree of stoichiometry is important because of additional lattice vacancies generated with boron deficiency. The diboride can be made stoichiometric by the proper additions of V[12]. This, as expected, has a large effect on atomic transport and therefore the interface reaction. A similar variation in stoichiometry of the commonly observed $TiSi_2$ phase has not been reported. Consequently, the existence of this control mechanism is not known in the SiC/Ti system.

A second interface control mechanism which appears to be understood in the B/Ti(Al) system could also play an important role for the SiC/Ti(Al) system. This is the exchange reaction bond which can be described by the following two step reaction beginning with a solid solution of Al in Ti:[8].

1. $Ti\ (Al)_{ss} + B = (Ti, Al)\ B_2$

2. $Ti + (Ti, Al)\ B_2 = Ti\ B_2 + Ti\ (Al)_{ss}$

The first reaction is governed by kinetic considerations and not by equilibrium thermodynamics. In the second reaction, the trend is toward thermodynamic equilibrium which results

in the rejection of Al into the Ti(Al) matrix. When Al is rejected, the matrix adjacent to the diboride becomes enriched in Al and retards further transformation. The rate of growth therefore depends upon the rate of diffusion of Al away from the interface. Rejection of Al by the exchange reaction occurs in the system B/Ti-8Al-1Mo-1V. Exchange reactions should also be important in the SiC/Ti(Al) system since Al alone does not form silicides. It should be noted that in the $TiSi_2$ phase Al replaces Si according to the formula $TiAl_{0.3-0.6}\ Si_{1.7-1.4}$ [14] and for $MoSi_2$ the corresponding formula is $MoAl_{1.3}\ Si_{0.7}$ [14]. Clearly the disilicide of Mo is able to accomodate more Al. In the case of B/Al composites, AlB is formed[15] and decomposes at 975°C (1248°K). For TiB_2, melting occurs at 2850°C (3123°K)[15] which is considerably more stable than AlB_2. The exchange reaction requires a second element such as either Al or Mo that form diborides of lower stability.

In the SiC/Ti system, two or more silicides are formed depending upon specimen size. The most recent binary phase diagram[16] for Si/Ti indicates that all silicides are stoichiometric. However, recent data in the literature indicates that this diagram is in error below 1000°C[17]. Consequently whether any one of the silicides can be adjusted to the stoichiometric composition to reduce the Si flux is

not really known at this time. It is known that the M_5Si_3 phase can greatly lower the Si flux. The following data at 1100°C (1373 °K) for the Mo-Si system[18] illustrates this point:

$$D_{MoSi_2} = 2.2 \times 10^{-5} \text{ cm}^2 \text{ sec}^{-1}$$
$$D_{Mo_5Si_3} = 7.5 \times 10^{-7} \text{ cm}^2 \text{ sec}^{-1}$$
$$D_{Mo} = 1.2 \times 10^{-4} \text{ cm}^2 \text{ sec}^{-1}$$

All of the above diffusion coefficients (DC) refer to Si diffusion. If these data are normalized to the DC for Si diffusion in Mo, one finds

$$\frac{D_{MoSi_2}}{D_{Mo}} = 0.18 \qquad \frac{D_{Mo_5Si_3}}{D_{Mo}} = 6.1 \times 10^{-3}$$

indicating that the $MoSi_2$ phase is not much better as a barrier than pure Mo. However, the Mo_5Si_3 phase represents a barrier far superior to the other two. It has been found that W_5Si_3, Nb_5Si_3 and Ta_5Si_3 are even more effective barriers with Ta_5Si_3 being the most effective[19]. The M_5Si_3 silicides generally have the highest melting points. However, they are not always formed in thin film reactions between Si and M, indicating that although they are highly stable, the kinetics of formation are less favorable than for other silicides. Dietrich[17] and Gehman[20] have shown

that for a thin film of Si crystal, only $TiSi_2$ and TiSi are formed. Thicker Ti coatings are required in this system if the Ti_5Si_3 phase is to be observed. It is well known that in some cases the diffusion flux of metal atoms is much smaller than for Si in these compounds, and that growth requires the transport of Si through the silicide to the silicide/metal interface.

A second mechanism that was described earlier is the exchange mechanism. In this case, a film of Al can be located between the Ti matrix and the SiC. As previously mentioned, Al has only limited solubility in the bonding silicide film and is largely rejected by the advancing silicide interface.

2.2 INTERDIFFUSION IN THE TITANIUM ALUMINUM SYSTEM

The Ti-Al phase diagram has been the subject of many investigations. The importance of the binary system has been principally two-fold. First, these studies have been instigated because of the importance of aluminide coatings on Ti. The other reason (and a more academic one) was mainly because the results of several investigations are very confusing and a clearer understanding of the Ti-Al system (especially the Ti rich side) was desirable. Therefore the purpose of this section is to discuss the literature on the

Ti-Al system in two seperate parts (Ti rich and Al rich sides) with the intent to provide some clarification of those results.

2.2.1 Interdiffusion in the Composition Range Between 0 and 25 at.% Ti

The interaction between Ti and molten Al, i.e. at temperatures above 660°C (933 °K), has been investigated by several authors[21-24]. In these circumstances a two-phase coating layer of $TiAl_3$ and Al was formed, rapidly growing according to a linear time-dependence.

On the other hand, studies on interdiffusion between solid Al and Ti-Al alloys have been initiated only recently. Van Loo and Rieck[25] coated pure Ti as well as Ti-Al alloys (upto 75 at.%Ti) in several ways, with a pure solid Al layer and studied interdiffusion in the temperature range between 516-642°C (789 -915°K). They observed that in each case a well adhered layer of $TiAl_3$ is formed. Also, no other intermetallic compounds formed and they did not observe any solid solution of Al in Ti. Using a microprobe analysis they obtained penetration curves on various diffusion-couples by scanning 50 squares, each of 100x100 microns cross sectional area. Their results showed that the $TiAl_3$ layer has an initial linear growth stage which is characterized (microscopically) by a regular shape of the $TiAl_3$ layer and small

inclusions of pure Al. After prolonged heating, the growth was no longer linear and the resulting layer was very irregular before becoming parabolic. They pointed out that for greater amounts of Al present in the starting alloy, the longer is the duration of the linear growth stage and that the growth rate is faster. The initial linear period was described to be due to an oxide layer on the Ti alloys.

Another interesting result of the van Loo and Rieck's[25] study was the discovery of the Ti_8Al_{24} phase. Using X-ray diffraction they found, that at temperatures of about 585°C, the diffusion layer consists of a mixture of two modifications of $TiAl_3$, viz. the one already mentioned and which will henceforth be denoted as "$TiAl_3$" and a hitherto unknown modification which was described as a superlattice of $TiAl_3$. This modification has nearly the same "a" parameter but has a "c" parameter which is 4 times as large as that of $TiAl_3$, thus containing 8 molecules/cell. The lattice parameters of this phase which they denoted as "Ti_8Al_{24}" resemble rather closely** those of the compound Ti_9Al_{23} as given by Raman and Schubert[26]. They[25], used a microprobe analysis and showed unambiguously that the

---

**

van Loo and Rieck[25]	Raman and Schubert[26]
a = 3.875±0.004 A	a = 3.85 A
c = 33.84±0.04 = 4x8.46 A	c = 33.46 = 4x8.365 A
c/a = 4x2.183	c/a = 4x2.173

chemical composition of both modifications is indeed TiAl within the experimental error of ±0.5 at %.

Samples annealed at 638°C showed only the $TiAl_3$ modification. The structure of $TiAl_3$, formed at 638°C does not change on subsequent annealing at 585°C for 120 hours. Also, Ti_8Al_{24}, formed at 585°C and then annealed at 638°C for 137 hours, does not change its crystal structure either. The two temperatures suggest a rough dividing line for stability of either modification at around 600°C.

Other investigations[27-29] have shown that other phases of the Ti-Al system should also be present along with TiAl in the low temperature region. However, van Loo and Rieck[25] with a series of well planned experiments have shown that the cause for one to observe only the TiAl phase is one that arises due to kinetics. They concluded that at low temperatures, diffusion in the $TiAl_3$ compound was very much faster than in the other intermetallic compounds and therefore these were present in only immeasurably thin layers.

Schubert et. al.[26,30,31] report the existence of the compounds $TiAl_2$, Ti_5Al_{11}, Ti_9Al_{23} and $TiAl_3$. van Loo and Rieck[32] observed a phase Ti_2Al_5 which they believed was probably the same as the compound Ti_5Al_{11} reported by Schubert et. al.[26,30,31].

Analyzing that part of the $TiAl_3$ growth kinetics that showed a parabolic time dependence, in the temperature range 516-642°C (789-915°K), van Loo and Rieck calculated for the integrated diffusion coefficient, as defined by Wagner[33]:

$$D_o = (7\pm2)\times10^{-3}\ cm^2\ sec^{-1}$$

$$Q = 22.6\pm1.2\ kcal\ mole^{-1}$$

According to these investigations[25], the values for the activation energy as well as for the frequency factor are low. This is a strong indication for the influence of grain boundary or, more generally, short-circuit diffusion. This indication was corroborated by the very small grains that were formed. Another explanation of the low values for the activation energy and frequency factor might be the very fast diffusion along a lattice direction with an abnormally high vacancy concentration as first proposed by Kidson et.al.[34] and Heumann et. al.[35-37]. However, since they observed very small grains in the layer, they concluded that this was less likely to be the cause although they did not rule it out completely. The parabolic growth of the $TiAl_3$ layer is not in contradiction to a short circuit mechanism, provided that the layer thickness is much larger than the distances between dislocations or grain boundaries[32].

Pouliquen, Offret and de Fouquet[38] employed electron microprobe analysis to study the interdiffusion of Al and Ti. Their results agree with those of van Loo and Reick[25] in that the main phase was $TiAl_3$ and that the growth of $TiAl_3$ characterizes the diffusion kinetics. The diffusion data they obtained is given in Table 1a[38].

Pokoev et.al.[39] studied Al diffusion in alpha-titanium by X-ray diffraction at 700-850°C in a vapor deposited Al layer 0.1 to 0.4 microns thick on Ti foil 0.8mm thick. Their results are summarized in Table 1 b.

2.2.2 Interdiffusion in the Composition Range Between 25 and 100 at.%Ti*

The study by many investigators[40-60] of the Ti-rich part of the Ti-Al system, has resulted in many inconsistencies thus making the system appear very complicated. Figures 1[59] and 2[74,26] are the commonly accepted phase diagrams of the Ti-Al system.

Some of the earliest studies[61-63] have indicated extensive solubility of Al in both alpha and beta titanium. Ence and Margolin, as a result of work on the Ti-Al-O system[64,65] have shown that the alpha solubility of aluminium is considerably restricted, and found that a compound

---

* Note: Unless otherwise stated all percentages used will be in atomic % of a second phase.

TABLE 1

Diffusion Coefficients for Al Diffusion in Alpha-Titanium

Table 1a
Pouliquen et al.[38]

Temp. C	D in $TiAl_3$ $cm^2\ s^{-1}$	D (Al in Ti) $cm^2\ s^{-1}$	D (Ti in Al) $cm^2\ s^{-1}$ (estimated)
560	-	0.17×10^{-10}	0.14×10^{-10}
590	0.066×10^{-10}	0.20×10^{-10}	0.09×10^{-10}
611	0.235×10^{-10}	0.35×10^{-10}	0.24×10^{-10}
648	0.900×10^{-10}	0.57×10^{-10}	0.44×10^{-10}
590-648	Q=62.18 kcal $g\text{-atom}^{-1}$	-	-
560-648	-	Q 30 kcal $g\text{-atom}^{-1}$	-

Table 1b
Pokoev et al.[39]

Temp. C	D x 10^{10} cm^2/sec.	D cm^2/sec.	Q kcal/mol
850	4.3		
800	2.5		
750	1.4		
700	0.66		
700-850	-	9.7×10^{-5}	27.5

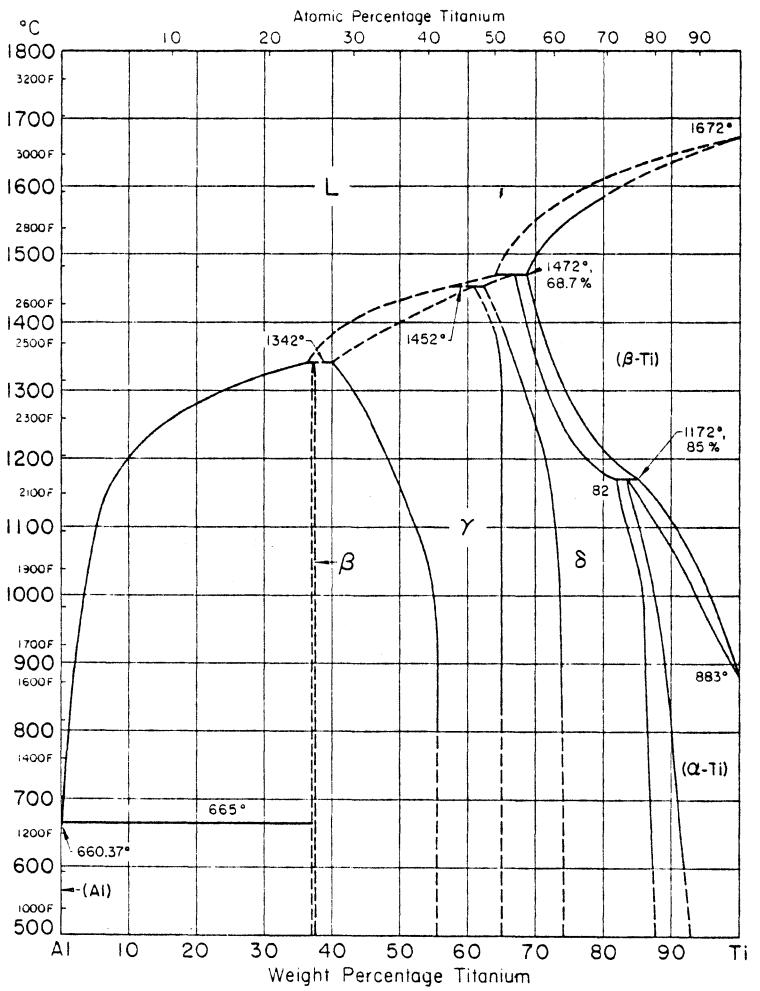


Figure 1. The Titanium-Aluminum Phase Diagram after Harold Margolin (59).

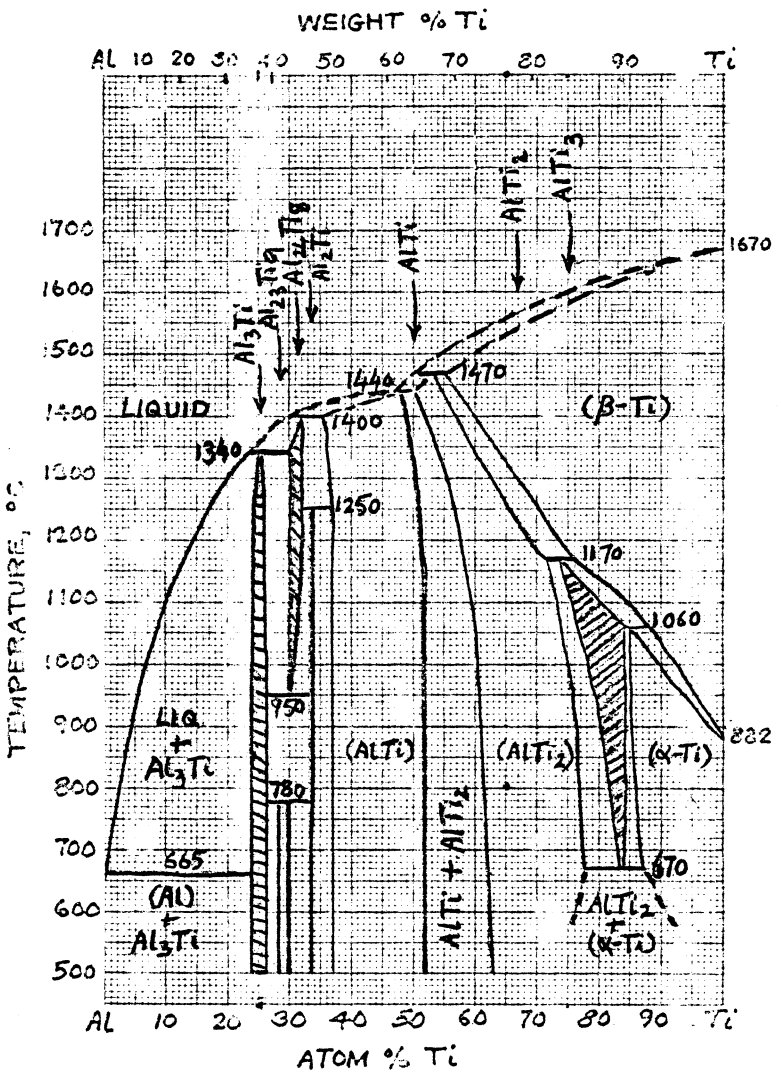


Figure 2. The Titanium-Aluminum Phase Diagram [74,26].

Ti_2Al[66] existed in the region formerly designated as alpha[61-63]. This structure was identified as hexagonal with c/a=0.803. Pietrokowsky confirmed the existence of this phase and pointed out that the structure was isomorphous with Ti_3Sn[67]. Although the existence of Ti_2Al has been confirmed by others[68-71], there has been considerable disagreement regarding the composition and mode of formation.

A detailed reinvestigation of the Ti-Al syatem has been published by Sagel et.al.[72]. The tentative diagram indicated two phases, alpha and epsilon occuring in the former all alpha region. The alpha' phase has the same structure as Ti_2Al and was indicated as having a broad region of solubility. Epsilon, a tetragonal phase, was shown to form within the alpha' solubility region.

As a result of unpublished work[73], Ence and Margolin disagreed with the interpretation of Sagel et.al.[73], although some common features existed. To clarify prevailing uncertainties, Ence and Margolin[74] investigated the titanium-rich portion of the Ti-Al phase diagram upto 34% Al. They observed the delta (Ti_2Al) phase which is hexagonal with lattice parameters a= 5.775 A, c=4.638A and c/a=0.803. The delta (Ti_3Al) is formed by the peritectic reaction:

beta +liquid $\longrightarrow$ delta (Ti_2Al).

Similarly the epsilon (TiAl) phase is formed by the reaction:

delta (Ti_2Al) + liquid $\longrightarrow$ epsilon (TiAl).

Furthermore, they[74] showed that the gamma (Ti_3Al) phase is formed by the peritectoid reaction:

beta + delta $\longrightarrow$ gamma (Ti_3Al)

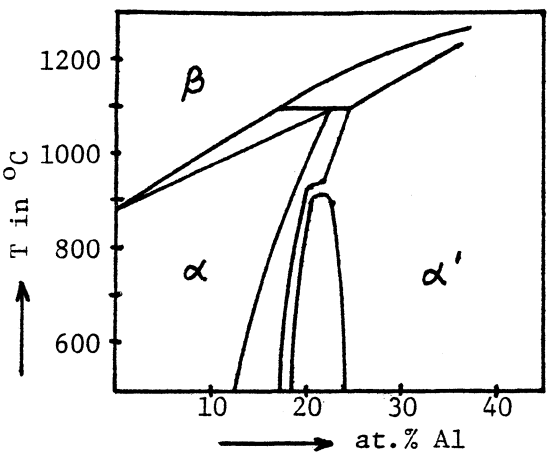
at about 16.5 pct Al at 1170°C (1443°K). The crystal struture of the gamma (Ti_3Al) phase was interpreted as hexagonal with the lattice parameters a=11.52A, C=4.65A and c/a=0.404. The gamma phase is not stable but transforms on cooling. The transformation product of the gamma phase, the gamma' phase, appears to be hexagonal and similar to alpha titanium. They showed that increase of aluminium additions stabilize gamma and this phase can be retained on quenching. The outcome of their work also shows that the solubility of Al in Ti is rather restricted and is about 8% Al at 800°C. The possibility or an eutectoid reaction:

gamma $\longrightarrow$ alpha + delta

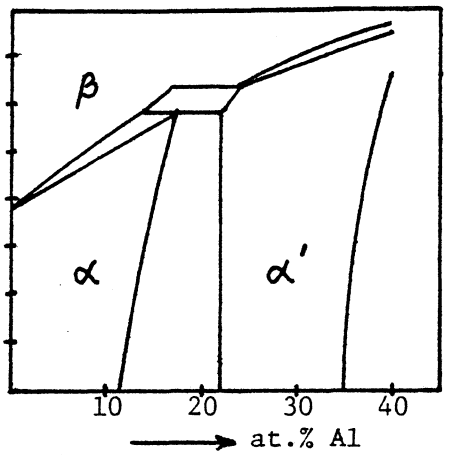
occuring below 700°C was also indicated.

Some investigators have reported the formation of compounds such as Ti_9Al, Ti_6Al and Ti_2Al[41-45] but later investigations by others[50-60] have not confirmed these phases. As a consequence these phases are normally left out of the phase diagrams. Figures 3a-3e, show the most important results on the Ti rich part of the system.

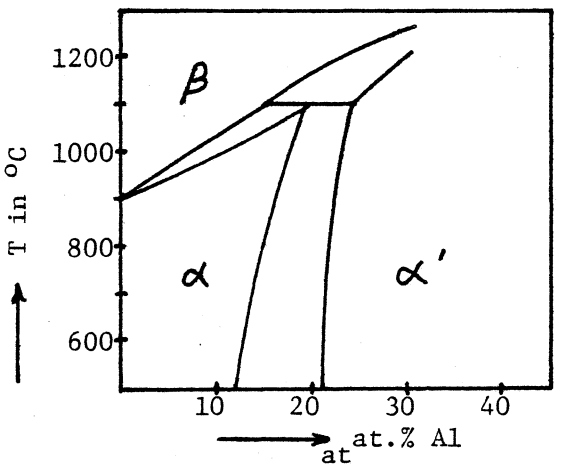
Several investigators reported compound formation in the composition range 0 to 40 at.% Al, and limited solid solubility (less than 10 at.% Al). However, no one explained why the earliest investigators[61,62] observed solid solubility extending to 36 at.% Al at room temperature. It was shown later[71,75], that in alloys containing 16.5 at.% Al, striated microstructures were produced by quenching from just below the $\alpha/(\alpha+\beta)$ boundary. Although ductile in this condition, these alloys were embrittled on ageing in the range 400-650°C without any significant change in microstructure. The existence of a superlattice based on the Ti_3Al composition was first briefly reported by Clark and Terry[68] and subsequently confirmed by Anderko, Sagel and Zwicker[69]. Clark et.al[49] used optical metallography, electrical-resistance measurements and X-ray diffraction in an attempt to discover the modifications needed to the phase diagram to accommodate the Ti_3Al superlattice.



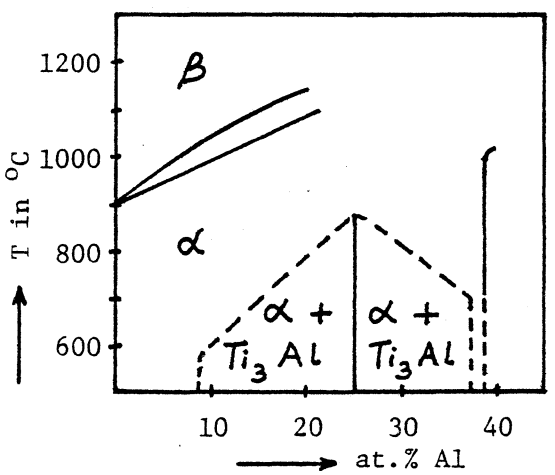
a) Clark et al. (49)



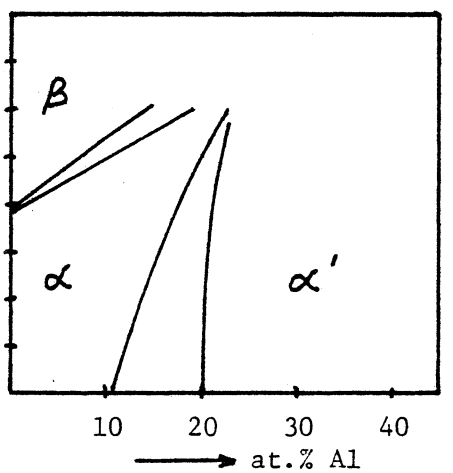
b) Kornilov et al. (50)



c) Tsujimoto (52)



d) Crossley (53)



e) Blackburn (56)

Figure 3. The Ti-rich side of the Ti-Al System.

They observed that the ($\alpha + \beta$) field extended up to 34.5 at.% Al. In the range 13.2-19.5 at.% Al, alloys quenched from a temperature close to the $\alpha/(\alpha+\beta)$ phase boundary had striated microstructures. They found that the occurance of striations depends on both quenching temperatures and the severity of the quench. Direct observation of a hot surface failed to reveal striations at 1000°C, although they became apparent after the surface was cooled to room temperature. A two phase field ($\alpha+\alpha'$) was established over the range 17.8-22.3% Al at temperatures well below the ($\alpha+\beta$) field. The duplex ($\alpha+\alpha'$) structure was differentiated from the striated structures because the coarseness of the alpha' phase increases with annealing time, whereas striated structures are not so affected.

By measuring the variation of resistence with temperature, Clark et.al[49] determined the $\alpha/(\alpha+\alpha')$ boundaries for various compositions of Al. Resistance vs. temperature plots showed a maxima at a certain temperature for a specific composition, and was related to entry into the two phase field ($\alpha+\alpha'$). The exit from the field was masked by the sluggishness of the reaction at low temperatures and by non-equilibrium conditions. When the variation of the temperature coefficient of resistance as a function of composition was studied, the curves showed a maximum at 25% Al,

consistent with the existence of a superlattice based on the ideal composition Ti_3Al. Thus the electrical-resistance measurements confirmed the existence of a superlattice with the ideal composition Ti_3Al and established the phase changes shown in Table 2.

X-ray diffraction studies[49] were performed and were reported to be hampered by the extreme slowness of the system in reaching equilibrium, and by the sensitivity of the system to strains such as might be introduced by quenching stresses. X-ray diffraction photographs did not show any anomalies between the limits 0-12 and 23-38.5% Al and the a and c lattice parameters were found to be on smooth curves when plotted against composition (see Figure 4[49]).

In these ranges no significant changes of lattice parameters were observed between specimens quenched from just below the $\alpha/(\alpha+\beta)$ boundary and those allowed to cool slowly in the furnace. The two parts of the 'c' parameter curve can be regarded as being continuous but the two parts of the 'a' parameter curve are clearly discontinuous. Diffraction photographs of all alloys containing >25% Al showed weak superlattice reflections corresponding to a doubling of the a dimension[68,69]. It was impossible[49] to suppress the ordering reaction in this region by quenching from temperatures close to the $\alpha/(\alpha+\beta)$ boundary.

TABLE 2

Phase Changes in the Titanium-Aluminum System

by Clark et al.[49]

Comp. at. % Al	Temp. °C	Boundary	Method
12	850	Limit of striations	Res./Comp.
16	850	$\alpha / (\alpha + \alpha')$	Res./comp.
16.5	850	$\alpha / (\alpha + \alpha')$	Res.Temp.
18	920	$\alpha / (\alpha + \alpha')$	Res./Temp.
16.5	850	$\alpha / (\alpha + \alpha')$	Res.Quench. Temp.
19.5	980	$\alpha / (\alpha + \alpha')$	Res./Quench. Temp.

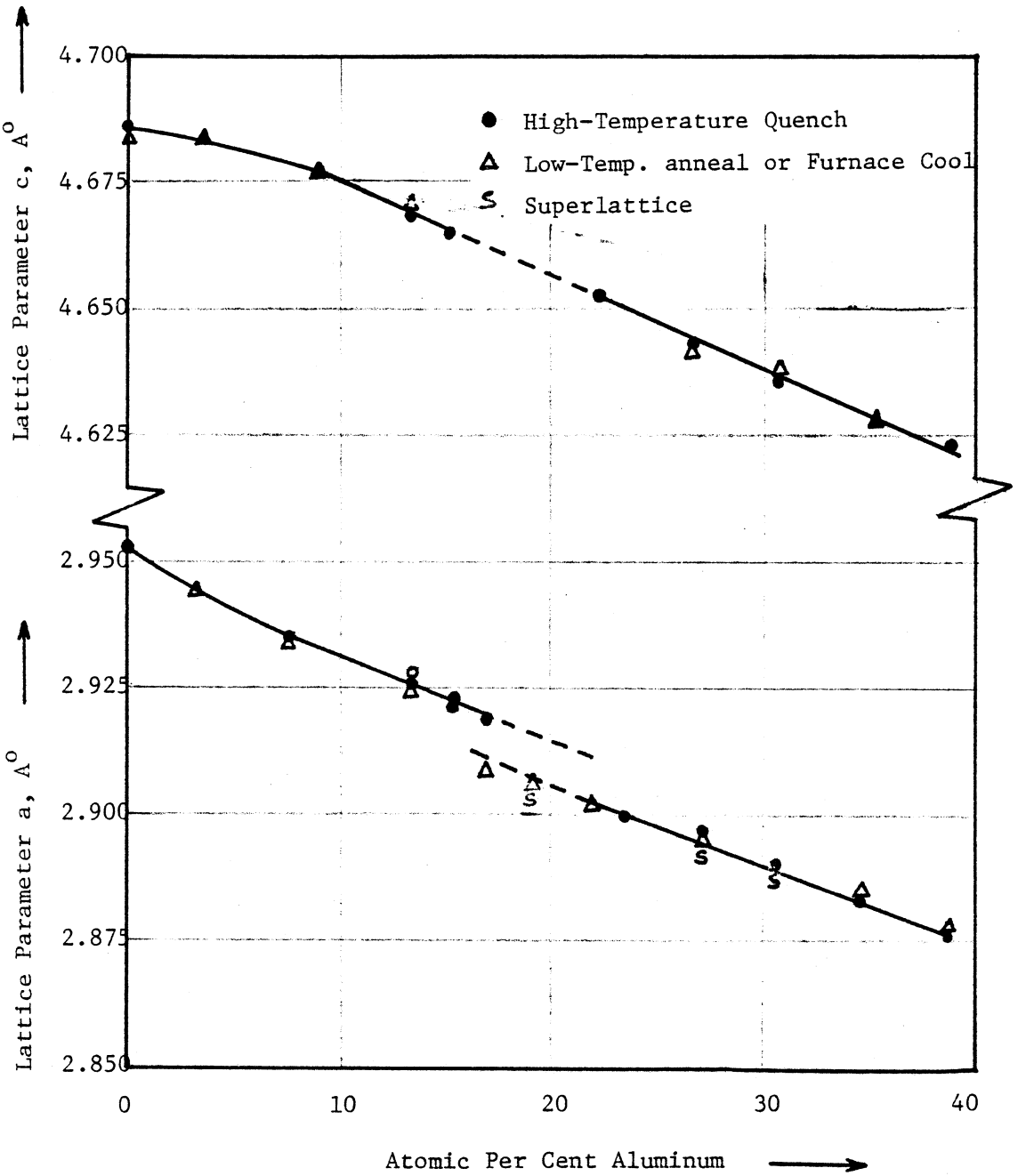


Figure 4. Lattice Parameter Plotted Against Composition For The Titanium-Aluminum System [49].

Between 12 and 25% Al, the lattice parameters were no longer independent of ageing and quenching temperatures. Also, certain "hkl" reflections show systematic broadening, followed at a lower temperature by a splitting into two components. The separation of the components was greatest for reflections having h or k large and absent when h and k are both zero. The diffraction pattern was accounted for by a duplex structure ($\alpha+\alpha'$) in which the components have two a parameters but a common c parameter, rather than by a single phase of symmetry lower than hexagonal.

A pronounced broadening of X-ray reflections having high h or k indices was observed for some alloys in the range 650-850°C (923-1123°K)[49]. For an alloy of given composition the degree of broadening was a function of annealing temperature and increased as the $\alpha/(\alpha+\alpha')$ boundary was approached. The broadening was also found to increase with time of annealing at a given temperature. Annealing at a lower temperature caused the broad reflections to split up into two relatively sharp components.

Clark et.al[49] concluded from their results that the two parts of the lattice parameter/composition curve (Figure.4) can therefore be regarded as the 'a' parameter curves of disordered and ordered alloys respectively. They also found that the diffraction patterns (for a 13.2% alloy)

showed clearly a duplex structure around 600°C, although some reflections were broad. They were not certain whether equilibrium had been reached. However, compared to the main phase the new phase had an increased lattice parameter and the photographs suggested the existence of two disordered phases.

van Loo and Rieck[32] studied the interdiffusion of Al in Ti using diffusion couples between Ti or Ti alloys and Al. They observed that for couples in which Ti was one of the starting materials, below the transition temperature of Ti, diffusion was characterized by two facts - viz, the absence of solid solution of Al in Ti and the non-parabolic growth of the phases arising. In their earlier work[25], they explained such a behavior as being due to an oxide film. However one of their experiments showed a behavior similar to the order-disorder phenomena as observed by Clark et.al[49]. During the preparation of one of their diffusion couples and as a result of an accidental temperature rise, they formed a 40 micron thick solid solution in a Ti(5% Al) alloy. Microprobe analysis showed a smooth penetration curve in a concentration region in which, strictly speaking, a two-phase region ought to have formed during cooling. After annealing at 837°C for 240 hours, they did not notice any detectable change in the thickness of the diffusion

layer. Also, the penetration curve did not show any alteration, although they observed a slight tendancy to developing a phase boundary at αTi-Ti_3Al. They reported thus: "This experiment proves that at temperatures below the transition point of titanium (below 880°C or 1153°K), diffusion proceeds very slowly in the Ti-rich solid solution and in the compound Ti_3Al, and there is no further extension of the layer of solid solution. We therefore believe that the absence of the solid solution is caused by an abnormally low volume diffusion coefficient in this phase, viz, $< 10^{-13}$ cm^2 /sec".

The conclusion of low diffusivity of Al in alpha-Ti by van Loo and Rieck[32] is in disagreement with the findings of Goold[76]. He reports for the diffusion couple Ti(6.9% Al)-Ti(13.4% Al) at 834°C (1107°K) a frequency factor of $1.6x10^{-5}$ cm^2 /sec and an activation energy of 23,700 cals/mole. At 834°C(1107°K) this gives a diffusion coefficient of $1.15x10^{-10}$ cm^2 /sec and according to van Loo and Rieck[32] this indicates a diffusion zone of about 200 microns. Therefore they[32] conclude that the diffusion zone found by Goold may have been formed as a result of the method of preparation of the couple.

Another interesting observation by these authors[32] is the growth of the Ti_3Al layer in accordance with $d^n=kt$, in

which n is 3.3 in all the couples they investigated, independent of the starting materials. Table 3 shows their results of the layer growth in various diffusion couples. The value of n for the other layers such as TiAl, $TiAl_2$ etc are smaller. Their explanation for the high value of n for the Ti_3Al layer was that there was a considerable contribution of grain boundary diffusion in the material transport through the Ti Al layer. This gave rise to enhanced growth in the first stage of annealing since the grains in the layer are small. When the diffusion duration increased the grains grew, leading to a reduced contribution of grain boundary diffusion, which eventually became negligible after very long annealing times. This model indeed implies a time-dependence and was observed by these authors, in the various couples they had studied.

Van Loo and Rieck[32] could not obtain volume diffusion data because of the non-parabolic layer growth. The dimensions of the penetration constant K are cm^n /sec instead of the customary cm^2/sec. When writing the relation between layer thickness and time in the form $d = K't^{1/n}$ (where $K'=K^{1/n}$) and, consequently, $K' = K'_0 e^{-Q'/RT}$, it is clear that $Q'=Q/n$. As may be seen from table 3, their value of Q was variable between 65.5 and 49.0 K cal/mole. On the other hand, the value of Q/n was the same for all the couples they studied, within experimental error.

TABLE 3

Results of the Layer growth in various diffusion couples[32]

Note: The layer width d follows the relation $d^n = Kt$; the penetration constant can be described as $K_o \exp(-Q/RT)$.

Couple	Temp. Range(°C)	Layer	n	10log K (cm /sec)	Q(Kcal)	Q/n(Kcal)
Ti-TiAl	768-880	Ti_3Al	3.3±0.3	-1.9±1.1	65.5±5.2	19.7±2.6
Ti-$TiAl_2$	768-880	Ti_3Al	3.3±0.3	-	-	-
Ti_3Al-$TiAl_2$	784-972	TiAl	2.7±0.3	-2.2±0.9	56.0±4.5	20.6±3.1
TiAl-$TiAl_3$	784-958	$TiAl_2$	2.4±0.3	-0.8±0.5	57.0±2.6	23.4±3.1
Ti_3Al-$TiAl_3$	800-958	$TiAl_2$	2.4±0.3	-	-	-
Ti-$TiAl_3$	700-875	Ti_3Al+ TiAl+ $TiAl_2$	2.5±0.3	-21±0.4	49.0±2.0	19.6±2.6

Figure 5 shows the results of van Loo and Rieck's[32] diffusion experiment above 700°C (973°K) in terms of a phase diagram. They showed that in the composition range ≤ 25 at.% Al, Ti is the faster diffusing component. Their phase diagram in this region is found to agree with the work of Blackburn[56], Clark et.al[49], Kornilov et.al[50], and Tsujimoto et.al[52] (see Figure 3). The Al compositions for the alpha and alpha' phase fields, however, are very slightly different in these cases. Table 4 gives the summary of the structure of phases occuring in the Ti-Al system.

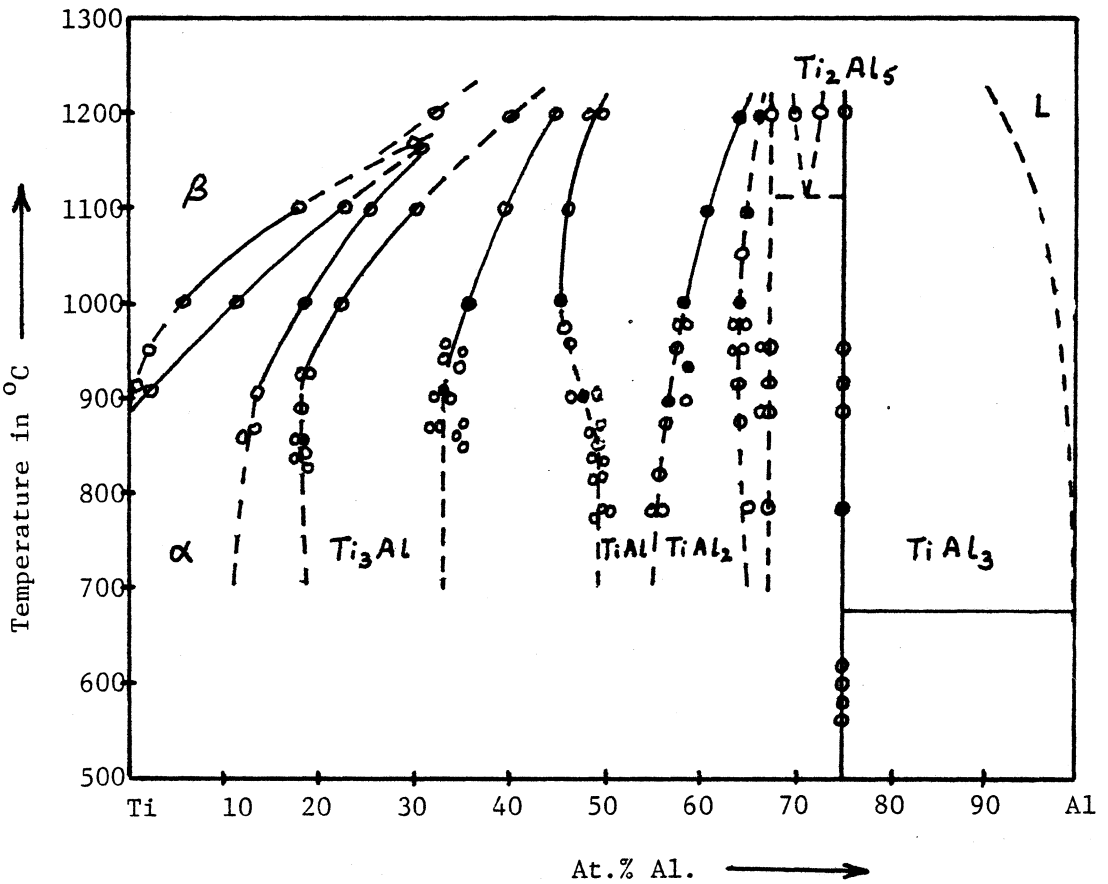


Figure 5. Phase diagram of the Ti-Al system, determined by means of the diffusion couple technique by van Loo and Rieck [32]. Black dots denote concentration measurements at phase boundaries in couples in which no new phase has been formed. Open circles denote concentration measurements at phase boundaries in couples in which one or both phases in question were formed during diffusion annealing.

TABLE 4

Summary of the structures of the phases occuring in the Ti-Al System

Phase	Structure	Lattice parameters (Å)	Hardness V.H.100[32]	Source
Ti	<882.5°C hcp >882.5°C bcc	a=2.950 c=4.683	81-143	Clark[100]
Ti_3Al	hex.Mg_3Cd type	a=5.765 c=4.625	260-380	Blackburn[56]
TiAl	Tetr.CuAu type	a=3.998 c=4.076	240-260	Dagerhamn[99]
$TiAl_2$	Tetr.$HfGa_2$ type	a=3.976 c=6x4.060	478	Potz.-Schub.[30]
Ti_5Al_{11}	Tetr.	a=3.917 c=4x4.131	-	Schubert et al[31]
Ti_9Al_{23}	Tetr.	a=3.843 c=8x4.183	-	Schubert et al[31]
$TiAl_3$	Tetr.>630°C	a=3.849 c=2x4.305	660-750	van Loo[25]
	Tetr.<600°C	a=3.875 c=8x4.23	660-750	van Loo[25]
Al	fcc	a=4.0494	19-22	ASTM 4-0787[95]

Chapter III

THEORY

In this chapter the theory required to study the inter-diffusion in the Ti-Al system shall be discussed. The necessary theory was developed by Unnam[78] and Houska for the study of bi-metallic, two phase, diffusion zones. The first part will be concerned with analyzing X-ray diffraction profiles produced by diffused metallic specimens (in this case Al thin films on Ti substrates), in order to determine the composition profiles. These composition profiles can be used to determine composition dependent diffusion coefficients (for Al diffusion in alpha-Ti). Therefore, the second part of this chapter will deal with developing solutions to the diffusion equation applicable to a two-phase, semi-infinite system, allowing for a concentration variation of diffusion coefficient.

3.1 BASIC DIFFRACTION EQUATIONS FOR DETERMINING COMPOSITION PROFILES.

The diffraction equations were originally written for an epitaxial deposition on a planar single-crystal substrate[78]. However, since we are concerned with poly-crystalline thin films on a polycrystalline substrate, the

equations have to be modified slightly[79]. Conventional reflection geometry is assumed with the angle of incidence of the X-ray beam equal to the angle of reflection as an average condition. An X-ray beam of cross-sectional area A with an angle of incidence 2θ irradiates a surface area given by:

$$A_m = A_o/\sin \theta_m \qquad (1)$$

and continues into the sample forming an oblique column. Figure 6[78] shows the cross-sectional view of a specimen. The plane 2-3 represents a limit such that material situated below this plane does not contribute a detectable signal. The maximum path length 1-2-5 depends upon the average linear absorption coefficient as well as on θ. The cross-section shown is divided into a number of thin sections with each having a slightly different average composition**.

** The distance between a pair of sampling planes, ΔY_m, which is observable at a single $2\theta_m$ setting of a diffractometer depends upon the resolution of the instrument and the spacing gradient through composition 'm'. In other words, an element of thickness ΔY_m and nearly uniform composition 'm' is related to the spacing gradient by:

$$\Delta Y_m = \Delta d \, [dY/dd]_m \qquad (2)$$

This stepped approximation to the spacing gradient is one of two approximations for a continuously varying composition profile (see ref. 80). A second considers a system of connecting elements with a linear spacing increase[82] and will not be discussed here.

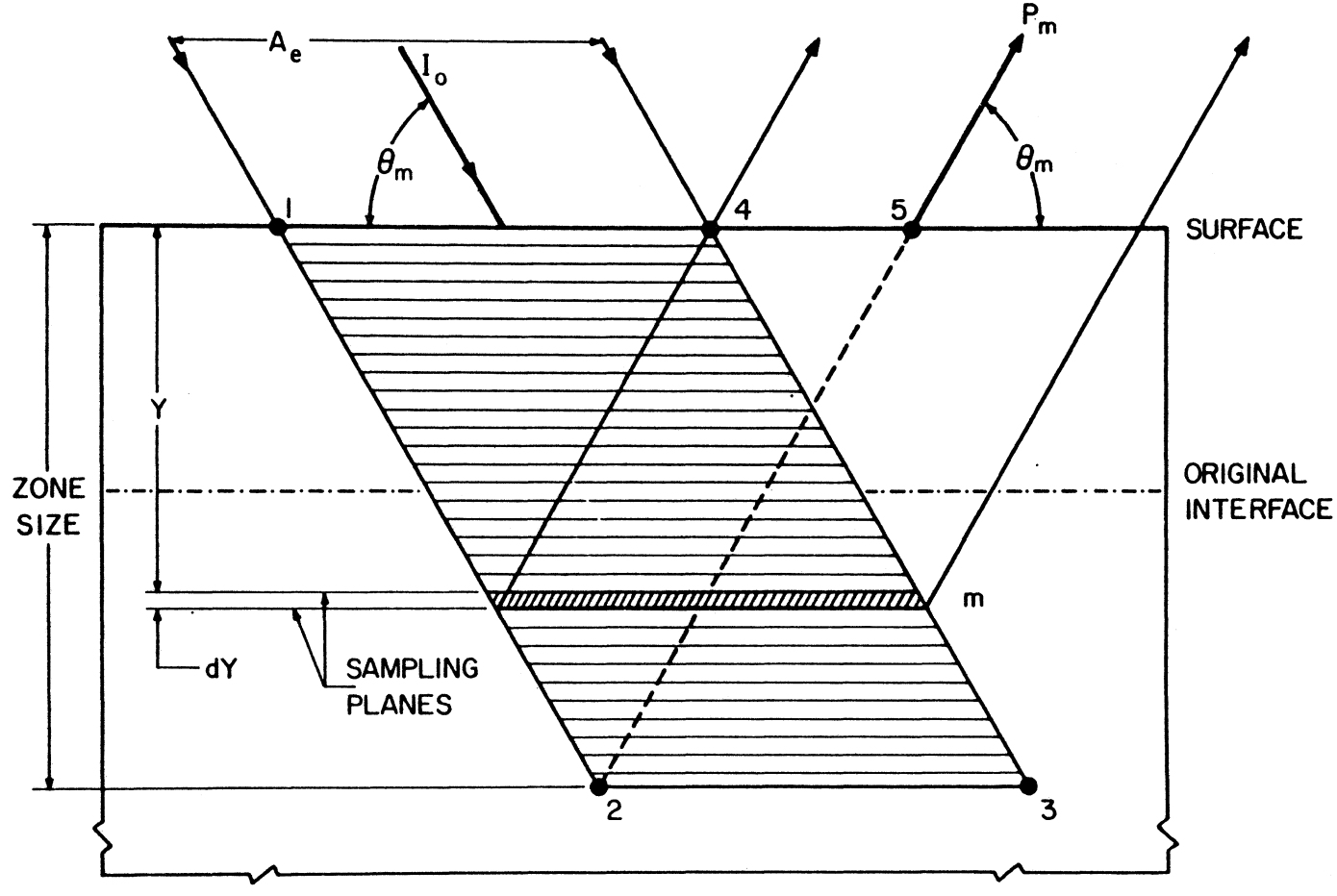


Figure 6. Cross-section of specimen, illustrating irradiated region.

Figure 6 also shows a pair of sampling planes seperated by a distance dY and at a depth Y, with an average composition "m". Let a function $H_m(Y)$ represent the fraction of the sampling plane of composition "m" (see ref. 81). For one-dimensional volume diffusion, the sampling plane will pass through regions of uniform composition with $H_m = 1$ in the range Y_m to $Y_m + \Delta Y_m$ and $H_m = 0$ elsewhere. However, if high diffusivity paths intersect the sampling plane, a range of compositions may be expected at a fixed position Y. In either case, the total volume of material of composition "m" is given by the integral

$$V_m = A_e \int_0^\infty H_m(Y)dY \tag{3}$$

The integral is usually carried out over the thickness of the specimen, but has been extended to infinety since the integrand vanishes for the specimen thicknesses considered.

Absorption of the incident and diffracted beams within the sample is given by:

$$\exp\left[\frac{-2\langle\mu(Y)\rangle_m Y_m}{\sin\theta_m}\right] \tag{4}$$

where $\langle \mu(Y) \rangle_m$ is the average linear absorption coefficient for all material between the free surface and a plane at a depth Y_m. Equations (3) and (4) are combined into a single expression defined as the effective volume:

$$V^g_{me} = gA_e \int_0^\infty H_m(Y) \exp\left(\frac{-2\langle\mu(Y)\rangle_m Y_m}{\sin\theta_m}\right) \tag{5}$$

A factor "g" has been introduced to allow for large misorientations in thick films. It designates the volume fraction of deposit within the measurement range (± 4°) for a specific (hkl) plane, and it is assumed that "g" does not vary with Y within the surface deposit or substrate. In many cases, "g" can be assumed to be 1 if we are dealing with randomly oriented deposits over randomly oriented substrates. In some cases, polycrystalline materials with strong textures may require accurate texture information to obtain quantitative results[81]. Also, further complications may result due to statistical sampling problems due to grain growth at elevated diffusion temperatures. In these cases, quantitative results can be obtained, but the technique is more laborious (see ref. 79 for more exact equations).

The kinematic integrated intensity can be written simply in terms of the effective volume as :

$$P_m = I_o Q_m V_{me}^g \qquad (6)$$

where I_0 is the intensity of the incident beam and Q_m the reflectivity per volume applicable to polycrystalline materials is given by:

$$Q_m = A \frac{\lambda^3}{v_i} \left[\frac{1 + \cos^2 2\theta \cos^2 2\theta'}{\sin \theta \sin 2\theta \, (1 + \cos^2 2\theta')} \right] j F_{i,T}^2 \qquad (7)$$

Here, A is a constant, λ is the X-ray wave length, v_i is the volume of unit cell, θ and θ' are the Bragg angles for the specimen and monochromator, j is the multiplicity, and $F^2_{i,T}$ is the structure factor containing the thermal term(83). If a monochromator (a monochromator diffracting only the K_{α_1} component of the incident X-radiation is assumed), is not used, $2\theta' = 0$. For diffused specimens having only a one-dimensional variation in composition, equation (6) is summed over all sections m, i.e.;

$$P_m = I_o A_o g \Delta Y \sum_m Q_m \left[\exp \left(\frac{-2\langle \mu(Y) \rangle_m Y_m}{\sin \theta_m} \right) \right] (\sin \theta_m)^{-1} \qquad (8)$$

Summing leads to a range of intensity over 2θ since there is a different Bragg angle for each composition. The overall distribution is defined as an intensity band(78) and a schematic of this is illustrated in Figure 7.

Equation (8) can be readily summed by integrating, provided both the initial plating and substrate are homogeneous phases parallel to the free surface, giving

$$P_f = I_o A_o Q_f \frac{g_f}{2\mu_f} \left[1 - \exp \left(\frac{-2\mu_f G_t}{\sin \theta_f} \right) \right] \qquad (9)$$

where P_f is the integrated intensity of the surface film or plating, and G_t is its thickness. Similarly, the integrated intensity of the substrate is given by:

$$P_s = I_o A_o Q_s \frac{g_s}{2\mu_s} \exp \left(\frac{-2\mu_f G_t}{\sin \theta_s} \right) \qquad (10)$$

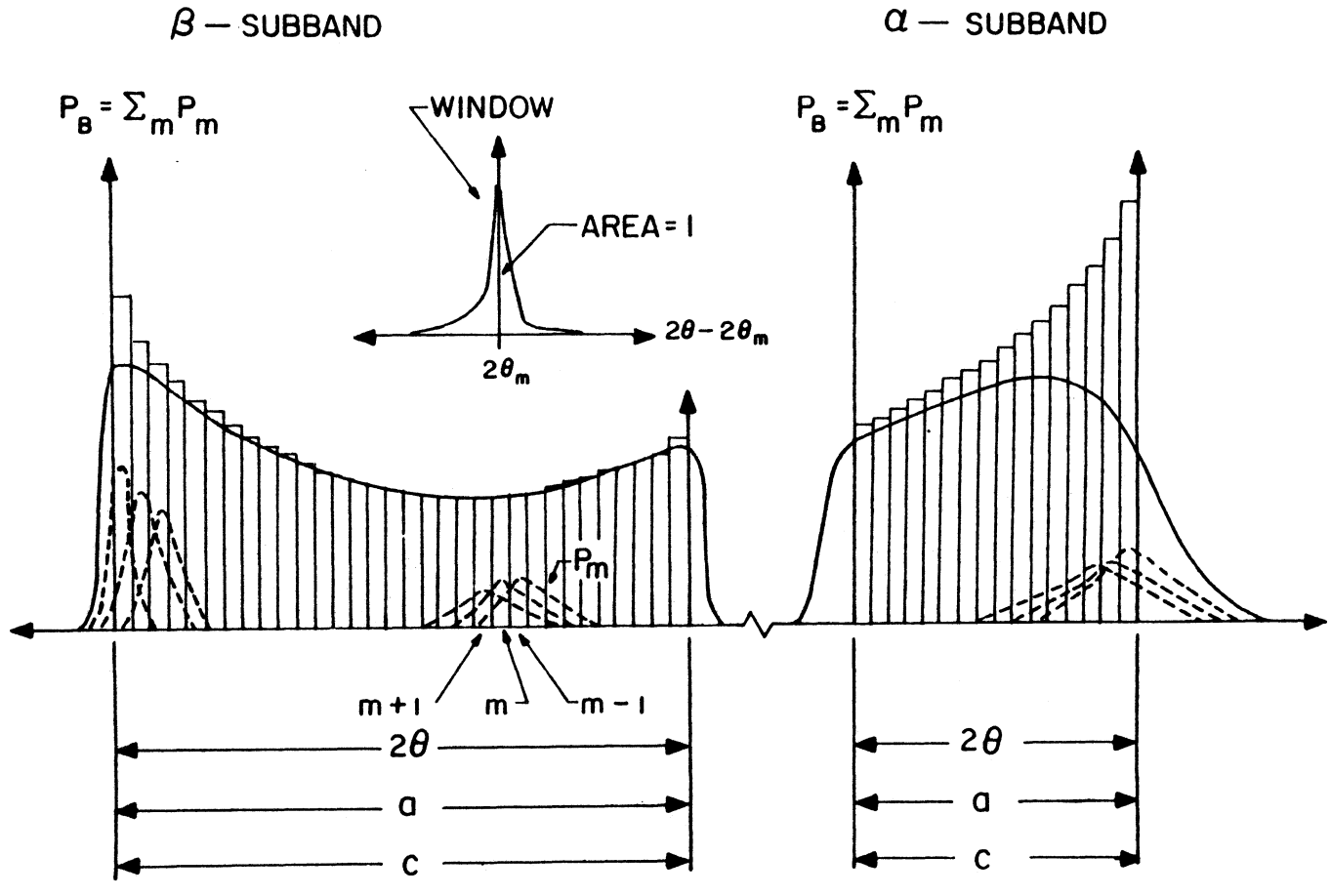


Figure 7. Schematic of the intensity band for a single phase system.

The last term allows for absorption of the incident and diffracted beams within the plating. Use of equations (9) and (10) can be made, to calculate the plating thickness, G_t, provided the ratio of g_f/g_s is either known or is assumed.

3.1.1 Computer Simulation of Intensity Bands:

If the composition profile for Al diffusion in alpha-titanium is known, an intensity band[78] can be readily computed using equation (8). The schematic of a stepped intensity band as illustrated in Figure 7 is an example of the direct application of equation 8, where the height of each step is given by a single term in the summation. The two-theta position is easily calculated by using Bragg's Law as well as data relating lattice parameter with composition. This data may be available in the literature and for the Ti-Al system, this data can be obtained from Figure 4.

Because of a spectral distribution of wavelengths and also because of sample and instrumental broadening, the stepped envelope for the intensity band is not equal to the measured curve. Instrumental factors smear the band noticably, especially at the tail portions of the band. If a central region has a slowly varying intensity, it remains unaffected by instrumental broadening. The inset of Figure 7 illustrates the normalized form for the pure instrumental

broadening with only the K_{α_1} component of the $K_{\alpha_1}-K_{\alpha_2}$ doublet. A Cauchy form with an assymmetry fits the broadening function provided it is due mainly to the spectral distribution of the emission line[84]. If a high resolution diffractometer is used for data collection and if the crystal structure of the specimen is relatively perfect, a Cauchy form would be ideal in the early stages of diffusion. Then equation 8 has to be modified to include the Cauchy instrumental broadening as :

$$P_B(2\theta) = I_o g \Delta V \sum_m Q_m \left\{ \exp \frac{(-2<\mu(Y)>_m Y_m)/\sin\theta_m}{\pi \Delta 2\theta'_m \sin\theta_m} \right\} \chi \left[1 + \left(\frac{2\theta - 2\theta_m}{\Delta 2\theta'_m} \right) \right]^{-1} \quad (11)$$

where $\Delta V = A_o \Delta Y$. The semi-half-widths $\Delta 2\theta'_m$ (in radians) can usually be obtained at the sharp tail portions of the curve where the broadening significantly influences the data[78]. Consequently, only two Cauchy functions are neccessary for each band that are charateristic of the extreme compositions. If the instrumental curves are assymmetric (which is most often true), then a pair of semi-half-widths ($\Delta 2\theta'_{mu}$ and $\Delta 2\theta'_{mL}$) are required corresponding to each extreme composition.

It was found that the broadening function can become Gaussian after longer diffusion treatments. This is related to the formation of a substructure associated with diffusion

damage. Thus far, a significant strain term has not been observed, probably because of high dislocation mobility at the diffusion temperatures[78,81]. Therefore, all of the broadening can be described largely by a Gaussian distribution of subgrain tilts and particle size broadening.

The intensity expression, equation (8), can be modified to include this effect

$$P_B(2\theta) = I_o g \Delta V \sum_m Q_m \left\{ \frac{\exp\left(-2\langle \mu(Y) \rangle_m Y_m\right)/\sin\theta_m}{\beta_m \sin\theta_m} \right\} \chi \exp\left\{ \frac{-\pi(2\theta - 2\theta_m)^2}{\beta_m^2} \right\} \quad (12)$$

where

$$\beta_m^2 = \frac{\lambda^2}{L_{3m}^2 \cos^2\theta_m} + \beta_{om}^2 \quad (13)$$

L_{3m} is the subgrain size perpendicular to the reflecting planes, and β_{om} is the instrumental parameter obtained before the diffusion anneals. The Gaussian broadening functions are symmetrical and β_m can be measured from the semi-half widths, $1/2\ B_m(2\theta)$, at the extremity of each intensity band using:

$$\beta_m = \tfrac{1}{2} (\pi/\ln 2)^{\frac{1}{2}} B_m(2\theta) \quad (14)$$

For some purposes representation of an X-ray diffraction peak with a simple mathematical function is convenient even though there are no direct physical interpretations of the parameters[85]. Functions proportional to a Gaussian

distribution are commonly too broad near the peak and too narrow at the tails. Functions proportional to a Cauchy distribution are usually unsatisfactory in the opposite way. Therefore, one requires a distribution which can be varied from Gaussian to Cauchy and which passes through the modified Lorentzian by the selection of a parameter, such as the Pearson type VII distribution.

The Pearson type VII distribution[86] is:

$$y(x) = y_o \left[1 + (x-\bar{x})^2/(ma^2)\right]^{-m} \tag{15}$$

$$y(\bar{x}) = y_o \tag{16}$$

Normalizing, such that:

$$\int_{-\infty}^{\infty} y(x)dx = 1 \tag{17}$$

sets the scaling parameter, y_o as:

$$y_o = \frac{1}{a\sqrt{\pi m}} \frac{\Gamma(m)}{\Gamma(m-\frac{1}{2})} \qquad \text{where, } \Gamma(p)=\int_0^{\infty} x^{p-1} e^{-x} dx \; ; \; p>0 \tag{18}$$

Also, the shape factor "m" and the related peak width parameter "a" are determinable from the instrumental diffraction peak. They are related to the full peak width at 1/pth maximum as:[85]

$$w(y_o/p) = 2a\sqrt{\left[m(p^{1/m}-1)\right]} \tag{19}$$

In its limiting form, the Pearson type VII function will tend towards the Cauchy or Gaussion form as indicated by the equation:

$$m = 1, \; y(x) = y_o \left[1 + (x-\bar{x})^2/a^2\right]^{-1}, \text{ Cauchy} \tag{20}$$

$$y_o = I/(a\pi) \tag{21}$$

where I is the peak intensity and,

$$m = \infty,\ y(x) = y_o \exp\left[-(x-\bar{x})^2/a^2\right],\ \text{Gaussian} \tag{23}$$

$$y_o = I/(a\sqrt{\pi}) \tag{24}$$

Therefore, instead of using the modified equations (11) and (12) separately for the Cauchy and Gaussion forms respectively, equation (8) can be modified to include a Pearson type VII distribution. This would enable one to fit the Cauchy or Gaussion peak shapes in the limiting cases, or even obtain any intermediate distributions by simply varying the three parameters y_o, a and m. This modification is given by:

$$P_B(2\theta) = I_o g \Delta V \sum_m Q_m \left\{\frac{\exp\left(-2\langle\mu(Y)\rangle_m Y_m\right)}{\sin\theta_m}\right\} \chi\ y_o\left[1 + (x-\bar{x})^{-2}/(ma^2)\right] \tag{24}$$

If the composition profile is known, the intensity bands can be simulated by using equations (11) or (12) or simply equation (24). Alternately, the composition profile can be determined from an intensity band by matching the simulated intensity (obtained from equations 11, 12 or 24) with the experimentally obtained one. This is carried out by trial and error estimates of the composition profile. The composition versus distance (Y_m) profile is used as input to a computer program[87]. Recalling from equations 11, 12 or 24, if the spacing ΔY is made smaller, the accu-

racy of the simulated intensity band is improved. This would mean that a large number of C versus Y_m input data points may have to be varied in a trial and error routine and this proves to be extremely cumbersome.

If the composition profile could be expressed by a simple function with only a few parameters that need to be adjusted, the problem becomes greatly simplified. This can be carried out using a sum of two error functions given by

$$C(Y_m) = \sum_{i=1}^{i=2} a_i \operatorname{erfc}\left(\frac{Y_m}{b_i} - d_i\right) \qquad (25)$$

The parmeters a_i, b_i and d_i need not have any theoretical significance. They are used to define $C(Y_m)$ at a given instant of time. Details on the computer technique used to simulate intensity profiles from Equation (25) may be found in Chapter 5.

3.2 DIFFUSION EQUATIONS:

Atomic diffusion is related to the transport of atoms through matter[77]. It occurs by approximately random motions of the atoms in a crystal lattice. The net result of many such random movements of a large number of atoms is diffusion, the movement being activated by the thermal energy of the crystal. In a pure material any particular atom is continually moving from one position to another in the material. This is called self-diffusion and can be studied experimentally by the use of radioactive tracers.

There is a clear analogy between heat transfer in a material by conduction and material transport in an element or alloy. This fact was recognized by Fick[88] in 1855 who first put diffusion on a quantitative basis. The mathematical theory of diffusion in isotropic substances is based on the hypothesis that the rate of transfer of the diffusing substance through unit area of cross section is proportional to the concentration gradient measured normal to the section, i.e.:

$$J = -D \frac{\partial C}{\partial x} \tag{26}$$

where D is a constant of proportionality called the diffusion coefficient. In many cases, D is treated as a constant but in general it may vary with composition. The negative sign in equation (26) indicates that diffusion should occur in a direction opposite to that of increasing concentration. Equation (26) is called Ficks First Law.

The fundamental differential equation for one-dimensional diffusion in an isotropic medium can be derived from Ficks First Law as:

$$\frac{\partial C}{\partial t} = \frac{\partial}{\partial x} \left[D \frac{\partial C}{\partial x} \right] \tag{27}$$

and is referred to as Ficks Second Law.

If the diffusion coefficient is constant, then the solutions of the diffusion equations can be obtained for a

number of initial and boundary conditions. Many solutions are presented in Crank[89], and also in Carslaw and Jaeger[90]. However, if the diffusion coefficient varies as a function of concentration, the solutions to Ficks second law are difficult to obtain. For a planar diffusion geometry and a doubly infinite system, Tenney et.al[91], obtained a one-dimensional solution which gives the concentration distribution for any continuous variation of the diffusion coefficient. The final form was obtained by integrating Ficks second law after applying the Boltzman transformation. Houska and Unnam[92] extended this solution for a finite plating allowing for an inherent time-varying surface concentration*.

3.2.1 Two-Phase Plating Problem with Constant D:

Tanzilla and Heckel[94] developed approximate solutions for finite two-phase systems. Houska and Unnam[92] extended the solution to a case where one of the phases is a finite plating and using an iterative approach obtained a closed form solution.

---

* Fogelson[93] has shown that in the customary diffusion equation, volume fraction can be used as the concentration unit. Hence, from now on 'C' in the equations (26) and (27) will be treated as the volume fraction of the diffusing components.

They[92] found Wagners' closed form solution for a doubly infinite system, useful for short times wherein the surface concentration remains at its initial value**. To extend Wagner's solution to the case where the β phase is finite, they[92] assumed a solution for the concentration as a function of position and time in each phase, with the interface between the phases free to move. The concentration within the β phase is of the form given in Crank[89],

$$C_B = C_\beta - (C_\beta - C_{\beta\alpha}) \frac{2 - \operatorname{erf} \frac{\xi + x}{2\sqrt{D_\beta t}} - \operatorname{erf} \frac{\xi - x}{2\sqrt{D_\beta t}}}{2 - \operatorname{erf} \frac{\xi}{\sqrt{D_\beta t}}} \qquad (28)$$

Equation (28) satisfies the initial and boundary conditions at the free surface and at the moving interface. For the alpha phase or $X \geq \xi$,

$$C_B = C_\beta - (C_\beta - C_{\beta\alpha}) \left[1 - \operatorname{erf} \frac{\xi - x}{2\sqrt{D_\beta t}} \right] \qquad (29)$$

which also satisfies the required initial and boundary conditions. Equations (28) and (29) are approximate equations obtained by modifying the exact single phase solutions so as to satisfy the boundary conditions for the two-phase system. X and ξ are both measured with the free surface as the origin.

** Note: These equations may be found in ref. 77 and are beyond the scope of this chapter.

For short times, by setting erf [$(x+\xi)/2\sqrt{D_\beta t}$] and erf [$\xi/\sqrt{D_\beta t}$] equal to unity, equation (28) simplifies to :

$$C_B = C_\alpha + (C_{\alpha\beta} - C_\alpha)\left[1 - \text{erf}\,\frac{x-\xi}{2\sqrt{D_\alpha t}}\right] \tag{30}$$

This implies that in the earliest stage of diffusion, the system behaves like two infinite solids with the beta and alpha fluxes given by:

$$J_\beta = (C_\beta - C_{\beta\alpha})\sqrt{D_\beta/\pi t} \tag{31}$$

$$J_\alpha = (C_{\alpha\beta} - C_\alpha)\sqrt{D_\alpha/\pi t} \tag{32}$$

An integration of the interface mass balance equation:

$$(C_{\beta\alpha} - C_{\alpha\beta})\frac{d\xi}{dt} = J_\beta - J_\alpha \tag{33}$$

gives a simple parabolic form

$$\xi = h + 2b_1\sqrt{D_\alpha t} \tag{34}$$

where

$$b_1 = \frac{1}{\pi^{\frac{1}{2}}}\left\{\frac{C_\beta - C_{\beta\alpha}}{C_{\beta\alpha} - C_{\alpha\beta}}\sqrt{\frac{D_\beta}{D_\alpha}} - \frac{C_{\alpha\beta} - C_\alpha}{C_{\beta\alpha} - C_{\alpha\beta}}\right\} \tag{35}$$

An intermediate stage is defined to include that interval of time during which the surface composition, C_β (X=0,t) varies over the full range $C_\beta > C_B > C_{\beta\alpha}$. This stage is complicated by an interface flux, J_β, which depends both on t and ξ. In stage III, the beta phase has a uniform compos-

ition and therefore does not contribute a flux for interface motion. As in stage I, the interface moves parabolically with time. To evaluate C_β from equations (28) and (29) one needs to know the interface position ξ . This can be determined from a conventional mass balance equation or by a conservation principle. Unnam and Houska[96,97] developed and used both methods and concluded that the conservation principle (the total amount of component B is conserved) was better. Hence using equations (28) and (29) a time dependent expression for the total amount of component B in the entire specimen, was developed. This was then equated to the initial amount of B. This results in a transcendental equation from which the interface position, ξ , can be solved by trial and error.

Consider a phase with thickness 1/2 and composition C_β, plated over a substrate with composition C_α, and thickness L/2[77](see Figure 8). Then the total amount of component B expressed as the equivalent thickness of pure B is given by $C_\beta(1/2)+C_\alpha(L/2)$, where C_β and C_α are the volume fractions of component B. After diffusion, this amount of B originally present in the sample should remain constant.

With diffusion, the component B gets redistributed in the alpha and beta phases according to equations (26) and (27). Integrating equations (26) and (27) over the alpha

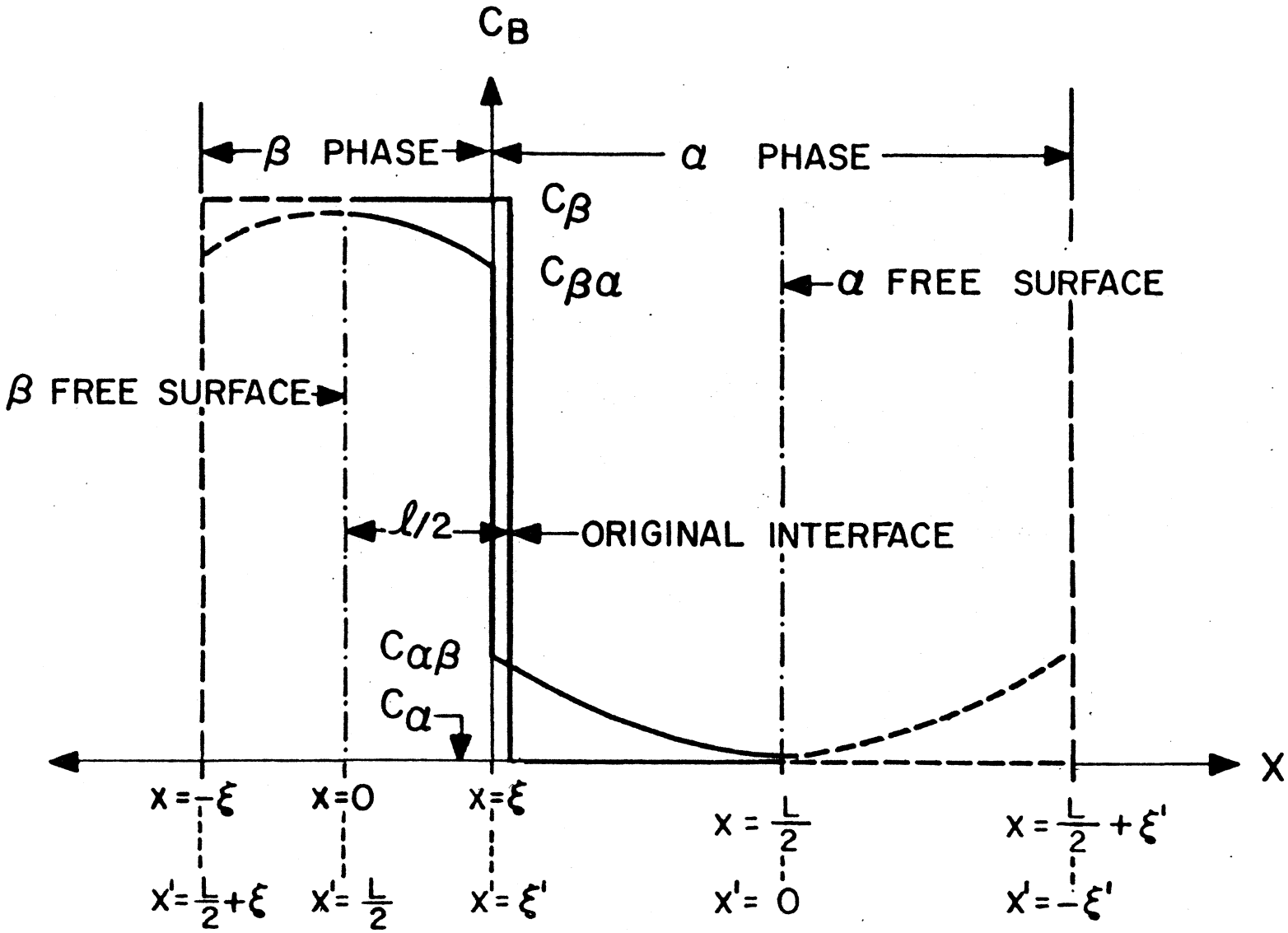


Figure 8. Schematic representation of composition profile for finite two-phase system (solid line) with image spaces (dashed lines). (from reference 98).

and beta phases gives an equivalent thickness of component B at any time t. An integration over the alpha phase yields,

$$(\ell/2)_\alpha = C_\alpha \{(L/2) + (\ell/2) - \xi\} + \frac{2}{\sqrt{\pi}} (C_{\alpha\beta} - C_\alpha) \sqrt{D_\alpha t} \tag{36}$$

and over the beta phase yields,

$$(\ell/2)_\beta = \xi C_\beta - \left[\frac{C_\beta - C_{\beta\alpha}}{2-\text{erf } r} \right] \frac{2}{\sqrt{\pi}} \frac{\xi}{r} (1-e^{-r^2} + \sqrt{\pi}\, r \text{ erfc } r) \tag{37}$$

where $r = \xi/\sqrt{D_\beta t}$ is written for convenience. Also, for the following equation[89] was made use for the integrations:

$$\int_z^\infty \text{erfc } z dz = \frac{e^{-z^2}}{\sqrt{\pi}} - z \text{ erfc } z \tag{38}$$

Two limiting cases, namely $(1/2)_\beta = C_\beta (1/2)$ for t=o, and $(1/2)_\beta = C_{\beta\alpha}$ for stage III are got from equation (37). Also, $(1/2)_\alpha + (1/2)_\beta$ gives the equivalent thickness of pure B at time t, and this should equal $C_\beta (1/2) + C_\alpha (1/2)$. Therefore,

$$(\ell/2)C_\beta = C_\alpha(\ell/2-\xi) + \frac{2}{\sqrt{\pi}} (C_{\alpha\beta}-C_\alpha) \sqrt{D_\alpha t} + \xi C_\beta - (\ell/2)_\beta \tag{39}$$

Equation (39) is the conservation equation and it may be noticed that it does not involve "H", the substrate thickness.

3.2.2 Two-Phase Plating Problem with Variable D:

If D is a function of concentration equations (26) and (27) can be generalized to give[98]:

$$C_B = C_\beta - \frac{C_\beta - C_{\beta\alpha}}{2-\text{erf } \nu_\xi/\sqrt{D_{\beta\alpha}}} [2-\{I_\beta(\nu_1/0) + I_\beta(\nu_2/0)\}\text{erf } \nu_\xi/\sqrt{D_{\beta\alpha}}] \tag{40}$$

for the beta-phase, and for the alpha phase

$$C_B = C_\alpha - \frac{C_\alpha - C_{\alpha\beta}}{2-\text{erf } \nu'_{\xi'}/\sqrt{D_{\alpha\beta}}} \left[2-\{I_\alpha(\nu'_1/0) + I_\alpha(\nu'_2/0)\} \text{ erf } \nu'_{\xi'}/\sqrt{D_{\alpha\beta}}\right] \quad (41)$$

where

$$\nu_1 = (\xi-x)/2\sqrt{t},\ \nu_2 = (\xi+x)/2\sqrt{t},\ \nu_\xi = \xi/\sqrt{t}$$

$$\nu'_1 = (\xi'-x')/2\sqrt{t},\ \nu'_2 = (\xi'+x')/2\sqrt{t},\ \nu'_{\xi'} = \xi'/\sqrt{t}$$

and

$$x' = (\ell/2)L - x$$

and

$$I_\beta(s/o) = \frac{I_{o\beta}(s/o)}{I_{o\beta}(\nu_\xi/o)},\ I_\alpha(s'/o) = \frac{I_{o\alpha}(s'/o)}{I_{o\alpha}(\nu'_{\xi'}/o)} \quad (42)$$

The integrals may be written as

$$I_{o\beta}(s/o) = \int_o^s \frac{1}{D_\beta} \exp\left(-\int_o^s (2s/D_\beta)ds\right)ds \quad (43)$$

where S is either γ_1 or γ_2. Also,

$$I_{o\alpha}(s'/o) = \int_o^{s'} \frac{1}{D_\alpha} \exp\left(-\int_o^{s'} (2s'/D_\alpha)ds'\right) \quad (44)$$

where S' is either γ_1 or γ_2. In equations (43) and (44), both D_β and D_α are functions of C.

Chapter IV

EXPERIMENTAL PROCEDURES

This chapter describes the procedures employed in the preparation, reaction and X-ray measurements on the various planar composites. A detailed description of the experimental equipment is given for completeness.

4.1 SAMPLE PREPARATION

4.1.1 Planar Composites for Studying Control of Interfacial Reactions:

SiC/Ti composites containing a Mo_5Si_3 barrier film were investigated relative to the SiC/Ti interface without a barrier. Samples containing Al films sandwiched between SiC and Ti were used to investigate the effectiveness of Al as an exchange atom in controlling silicide growth. The following planar composite systems were used for these studies.

a. SiC (2.175 Microns) / Ti Used as a standard for all systems.

b. SiC(1.825 Microns)/Al(0.800 Microns)/Ti To study the rejection mechanism.

c. SiC(2.0 Microns)/Mo_5Si_3 (1.0 Microns)/Ti Used to study the effectiveness of the barrier mechanism.

d. In addition to the above, samples of Mo_5Si_3 (1.813 microns)/Ti were used as standards for the SiC/Mo_5Si_3 / Ti system.

e. SiC (2.16 Microns) /Ti_3Al/Ti - To study the effectiveness of the two mechanisms combined with Ti_3Al acting as a barrier and with α-Ti(Al) retarding the reaction by rejection.

The substrates for all of the above composite systems were 7/8 inch diameter and 0.11 inch thick discs. These were cut from a 99.5% purity alpha-Titanium sheet obtained from Semi-alloys Inc[101]. These discs were coarse polished on SiC wet or dry abrasive papers through 600 grit. They were then fine polished on a lapping wheel using Alumina powders of 1, 0.3, and 0.05 micron sizes.

Samples in parts a through d were sputter-deposited by Perkin-Elmer-Ultek-Inc. [102]. Immediately before sputtering, the Ti wafers were sprayed with methol ethol ketone and dried with a blower. The sputtering conditions are listed in Tables 5-8 and the target purities for each of the coating materials are listed in Tables 9-11.

The SiC films on the Ti_3Al substrates (part e) were prepared in our laboratory. An attempt was made to duplicate the conditions used by Perkin Elmer for the SiC/Al/Ti system. However, due to differences in the base pressures used, it was necessary to obtain a new set of conditions to obtain the desired thickness. Details of the method of preparation of the substrates in this case are given in the

TABLE 5

Specimen Data Sheet for SiC/Ti Planar Composites

Conditions		
Thickness Required	20,000 (SiC)	Å
Initial Press.	2.8×10^{-7}	Torr
Argon Press.	10	m Torr
Sputter Etch		
Time	30	min.
Substrate Bias	375	volts
Forward Power	1000	watts
Reflected Power	5-10	watts
Deposition		
Mode	RF Diode-Static	
Time	200	min.
Target Bias	1900	volts
Substrate Bias	0	volts
Forward Power	500	watts
Reflected Power	15-20	watts
Anode Spacing	2.5	inches
Deposition Rate	217.5	Å/1kw-min.
Substrate Temp.	250-300	° C
Actual Thickness	21,750	Å (± 10%)

TABLE 6

Specimen Data Sheet for SiC/Al/Ti Planar Composites

Conditions

First Thickness Req.	10,000 (Al)	Å
Second Thickness Req.	20,000 (SiC)	Å
Initial Press.	6.5×10^{-7}	Torr
Argon Press.	10	m Torr

Sputter etch

Time	30	min.
Substrate Bias	290	volts
Forward Power	1000	watts
Reflected Power	5-10	watts

Sputter Deposition Al (8" target)

Mode	D.C. Magnetron-Rotation	
Time	21	min.
Target Bias	360	volts
Substrate Bias	0	volts
Forward power	3816	watts
Reflected power	0	watts
Anode Spacing	2.5	inches
Deposition Rate	100.2	A/1kw-min.
Substrate Temp.	<200	°C
Actual Thickness	8,000	Å (± 10%)

Sputter Deposition SiC (6" target)

Mode	RF Diode Static	
Time	200	min.
Target Bias	1750	volts
Substrate Bias	0	watts
Forward Power	500	watts
Reflected Power	5	watts
Anode Spacing	2.5	inches
Deposition Rate	217.5	Å/1kw-min.
Substrate Temp.	250-300	° C
Actual Thickness	18,250	Å (± 10%)

TABLE 7

Specimen Data Sheet for The SiC/Mo_5Si_3/Ti Planar Composites

Conditions

First Thickness Req.	10,000 (Mo_5Si_3)	Å
Second Thickness Req.	20,000 (SiC)	Å
Initial Press.	3.7×10^{-7}	Å
Argon Press.	10	m Torr

Sputter Etch

Time	30	min.
Substrate Bias	0	volts
Forward Power	1000	watts
Reflected Power	10	watts

Sputter Deposition Mo_5Si_3 (6" target)

Mode	RF Diode-Static	
Time	40.7	min.
Target Bias	1800	volts
Substrate Bias	0	volts
Forward Power	500	watts
Reflected Power	5	watts
Anode spacing	2.5	inches
Deposition Rate	491.1	Å/1kw/min.
Substrate Temp.	250-300	°C
Actual Thickness	10,000	Å (± 10%)

Sputter Deposition SiC (6" target)

Mode	RF Diode-Static	
Time	183.9	min.
Target Bias	1750	volts
Substrate Bias	0	volts
Forward Power	500	watts
Reflected Power	5	watts
Anode Spacing	2.5	inches
Deposition Rate	217.5	Å/1kw/min.
Substrate Temp.	250-300	°C
Actual Thickness	20,000	Å (± 10%)

section on annealing procedure in this chapter. Prior to sputter deposition, the samples were thoroughly cleaned. The cleaning procedure included heating the samples in the following solvents:

Solvent	Max. Temp.	Time of Immersion
Trichloroethylene	73°C	30 min.
Acetone	56°C	30 min.
Alcohol	65°C	30 min.

After cleaning, the samples were thoroughly dried and carefully weighed using a Mettler[106] scientific balance accurate up to 10^{-6} gms. The surface was sprayed with Dust-off[107] to remove dust particles before loading them into the specimen, chamber of the sputtering system. For details on the "operating instructions" of the Perkin Elmer[102] 2400 RJ system, see Appendix 4.

The sputter conditions for the SiC/Ti Al/Ti samples are given in Table 12 and the target purity is listed in Table 11. After sputtering for the desired length of time, the samples were cooled and carefully weighed again. From a difference in weight, density of the coated material and

TABLE 8

Specimen Data Sheet for Mo_5Si_3 /Ti Planar Composites

Conditions		
Thickness Req.	20,000	Å
Initial Press.	2.8×10^{-7}	Torr
Argon Press	10	m Torr
Sputter Etch		
Time	30	min.
Substrate Bias	340	volts
Forward Power	1000	watts
Reflected Power	20-25	watts
Sputter Deposition		
Mode	RF Diode-Static	
Time	73.8	min.
Target Bias	1700	volts
Substrate Bias	0	volts
Forward Power	500	watts
Reflected Power	5	watts
Anode spacing	2.5	inches
Deposition Rate	491.1	Å/1kw/min.
Substrate Temp.	250-300	°C
Actual Thickness	18,125	Å (± 10%)

TABLE 9

Spectrographic Analysis of The Aluminum Target

Ultra High Purity Aluminum Target (99.999%) from Specialty Metals and Alloys Co. Inc. [103]

Impurity Levels (in parts per million)	
Ca	< 0.5
Cr	< 1.0
Cu	1.0
Fe	2.0
Mg	2.0
Na	< 1.0
Sn	0.2
Ti	0.2
Zn	2.0
Mn	0.3
Si	1.5

TABLE 10

Spectrographic Analysis for the Mo_5Si_3 Target

Molybdenum Silicide Target
from Metron Inc. (104).

Impurity Levels in Wt.%

Al	0.35%
Fe	0.25%
W	< 0.1%
Ti	< 0.1%
As	< 0.1%

TABLE 11

Spectrographic Analysis of the SiC Target

Silicon Carbide Target
from Haseldon Company Inc. (105)

Impurity Levels in Wt.%

Free C	0.09
SiO2	0.41
Surface Si	0.02
Al	0.06
Fe	0.03

specimen dimensions, the thickness ΔY was calculated according to the formula:

$$\left[\frac{\pi}{4}\left(\frac{7}{8} \times 2.54\right)^2\right] \text{cm}^2 \left[\rho_{SiC}\right] \frac{\text{gm}}{\text{cm}^3} \left[\Delta Y_{SiC}\right] \text{cms} = \left[W_{final} - W_{initial}\right] \text{gms} \quad (45)$$

4.1.2 Planar Composites for Diffusion Studies:

A number of thin films of aluminum on alpha-titanium substrates were prepared. These samples served a dual role: first, they were used to provide additional information on the effectiveness of Al as an exchange atom to reduce silicide growth. In other words these samples could be used as internal standards for the SiC/Al/Ti planar composites. Also, information such as thickness of the Aluminum coating neccessary for delaying silicide growth could also be used to design an optimum hot-pressing cycle for the fabrication of actual fiber reinforced composites. The second important use for these samples was to investigate the Ti-Al system and obtain diffusion data such as composition dependent diffusion coefficients. The following thin-film samples were prepared for this purpose:

f. Al (1.0 microns)/Ti - Prepared by Perkin Elmer Ultek[102].

g. Al (0.4, 0.5 & 0.64 microns)/Ti - Sputter-deposited in our laboratory.

TABLE 12

Specimen Data Sheet for SiC/Ti_3Al/Ti Planar Composites

Conditions		
Thickness Required	20,000 (SiC)	Å
Initial Press.	3.5×10^{-6}	Torr
Argon Press.	10	mTorr
Clean Target		
Time	15	min
Substrate Bias	0	volts
Forward Power	500	watts
Reflected Power	approx. 0	watts
Target Bias	1650	volts
Deposition		
Mode	RF Diode Static	
Time	130	min
Target Bias	1850	volts
Substrate Bias	approx. 0	volts
Forward Power	625 to 650	watts
Reflected Power	approx. 0	watts
Anode Spacing	1.5"	inches
Deposition Rate	-	Å/1kw-min.
Substrate Temp.	Not known	°C
Actual Thickness	21,600	Å (± 10%)

The sputtering conditions for the 1 micron Al films on Ti are shown in Table 13 and that for the 0.5 micron Al films on Ti is shown in Table 14.

4.2 ANNEALING PROCEDURE:

4.2.1 Planar Composite Samples for Control of Interface Reactions

The planar samples in parts a thru e in the previous section intended for study of the control of interface reactions were vacuum annealed at 875°C for 1/2 hr,1hr,2hrs,4hrs. These heat treatments were carried out in oil free, high vacuum furnace which incorporated sorption and ion (20 liter/sec) pumps obtained from Perkin Elmer Ultek[102]. Using both control and specimen thermo- couples made of chromel-alumel, temperature measurements were within ±2°C. This was also cross-checked against a Leeds and Northrup[108] potentiometer as well as a National Bureau of Standards[109] thermocouple. Interlocks in the furnace did not permit operation unless a vacuum of 10^{-4} torr or better was maintained.

The samples were enclosed in a one-inch diameter fused quartz tube and evacuated to $3x10^{-6}$ torr. The specimens were suspended in the tube on a horizontal alumina platform

TABLE 13

Specimen Data Sheet for Al(1 micron)/Ti Planar Composites

Conditions		
Thickness Required	10,000	Å
Initial Press	3×10^{-7}	Torr
Ar Press	7	mTorr
Sputter Etch		
Time	5	min.
Substrate Bias	Unknown	volts
Forward Power	1000	watts
Reflected Power	5	watts
Deposition		
Mode	RF Diode - Static	-
Time	21.3	min.
Target Bias	1700	volts
Substrate Bias	0	volts
Forward Power	1000	watts
Reflected Power	5	watts
Anode Spacing	1.5	inches
Deposition Rate	470	Å/1kw-min.
Substrate Temp.	254 to 300	°C
Actual Thickness	10,000	Å (± 10%)

TABLE 14

Specimen Data Sheet for Al(0.5 microns)/Ti Planar Composites

Conditions		
Thickness Required	5000	Å
Initial Press	1.5×10^{-6}	Torr
Argon Press	10	m Torr
Sputter Etch		
Time	5	min.
Substrate Bias	1800	volts
Forward Power	1000	watts
Reflected Power	approx.0	watts
Deposition		
Mode	Static	-
Time	12.68	min.
Target Bias	1900	volts
Substrate Bias	0	volts
Forward Power	1000	watts
Reflected Power	approx.0	watts
Deposition Rate	-	Å /1kw-min.
Substrate Temp.	Not Known	°C
Actual Thickness	4800	Å (± 10%)

which eliminated contact of the specimen with the quartz. The end of the tube was sealed to the pumping system by tightening two flanges against a high vacuum seal. A water cooled, open coil furnace was positioned around the sample tube to produce a one-inch constant temperature zone at 650°C.

The following recommended start-up procedures are employed to reduce the inefficient pumping of samples at the reaction temperature. The ion pump is isolated from the rest of the system during an exposure to atmosphere. Dry nitrogen is bled into the chamber for 5 minutes to reduce oxygen contamination. A roughing vacuum is obtained by filling the sorption pump with liquid nitrogen. After about 30 minutes the valve between the ion pump and the remainder of the system may be opened after valving off the sorption pump. The vacuum should quickly attain 5×10^{-5} torr and sufficient time must be allowed to pump below this level.

The initial anneal at 600°C produces a large amount of gases at the reaction temperature and is easily handled by the sorption pump. During this anneal it is necessary to supply liquid nitrogen to the sorption pump so that the roughing vacuum is not lost. This is neccessary for 1 to 2 hours at which time the ion pump may be introduced into the system. All subsequent anneals were done at 10^{-6} torr using the ion pump.

The planar composite samples were heat treated at a heating rate of 10°C per minute. Because of rapid degassing at around 600°C possibly due to the release of hydrogen from the samples, they were held at 600°C for two hours before continuing the heat up to the reaction temperature (675°C). After annealing at this temperature for the desired length of time they are air cooled by retracting the furnace. The final cooling to room temperature was about 30°C/min to 300°C and 10°C/min. to 150°C where it was opened to the air.

4.2.2 Planar Composites for Diffusion and Reaction Studies:

The samples intended for Ti-Al diffusion studies (parts g and f) were, on the other hand, held at 635°C for one hour and then annealed at 900°C 1/2hr, 1hr, 2hrs and 4 hrs. These anneals shall henceforth be referred to as high temperature diffusion studies. The hold at 635°C instead of 600°C, for degassing, was carried out to ensure that the samples were in a two-phase condition viz. $TiAl_3$ and alpha-Ti. As it was pointed out in chapter 2, at temperatures around 580°C, we have an additional phase (Ti_8Al_{24}) coexisting with $TiAl_3$ and alpha-Ti. Also, the hold at 635°C ensures that Al quickly reacts with the alpha-titanium to form $TiAl_3$ before continuing on to the reaction temperature, through the melting temperature of Al (660°C). Since a low thermal mass, fast rise

furnace was used for these anneals, the rise time to reach the diffusion temperature (900°C) from 635°C was usually 2-3 mins. This is fairly small when compared to the shortest anealing time of a half hour and may be neglected.

In order to understand the diffusion processes occuring during the hold at 635°C to allow the samples to react and degas, three anneals were performed at 635°C for 1/2hr, 1hr and 2 hrs, using Al(1 micron) thin films on Ti substrates. These anneals shall henceforth be referred to as low temperature studies. Since the annealing times in this case were comparable to the time neccessary to degas the samples, it was not possible to introduce the ion pump into the system. However, this did not produce any oxidation of the samples as will be described in Chapter 6. After annealing, using only the sorption pump, for the described length of time the samples were cooled as described previously. These anneals at 635°C shall henceforth be referred to as low temperature diffusion studies.

The Ti_3Al/Ti substrates that were to be sputter-deposited with SiC were prepared in the following manner. It will be shown in chapter 6 that annealing thin films of Al(0.5 microns) on Ti substrates at 900°C for one hour results in a certain thickness of the Ti_3Al phase and a certain amount of Al goes into solid solution in the alpha-

titanium. Since it was intended to sputter SiC on substrates that had this predetermined amount of Ti_3Al and Al solid solution, several samples were prepared according to the above condition. A hold at 635°c for 1 hour was again necessary for the reasons mentioned earlier before annealing all these samples individually but identically at 900°C for 1 hour. The samples were cleaned and prepared for sputtering as described previously. It is evident from table 12 that the Ti_3Al surface was not sputter-etched, so as to avoid any loss of Ti_3Al before deposition. To aid better sticking of the SiC film, a thorough clean up procedure prior to sputtering is essential.

4.3 X-RAY MEASUREMENTS

The X-ray diffractometer that is used to collect all data on planar composites as well as the Al thin film samples will be briefly described in this section. Figure 9 shows the schematic of the pertinent X-ray diffraction geometry.

Distinct advantages obtained through the use of this equipment are emphasized.

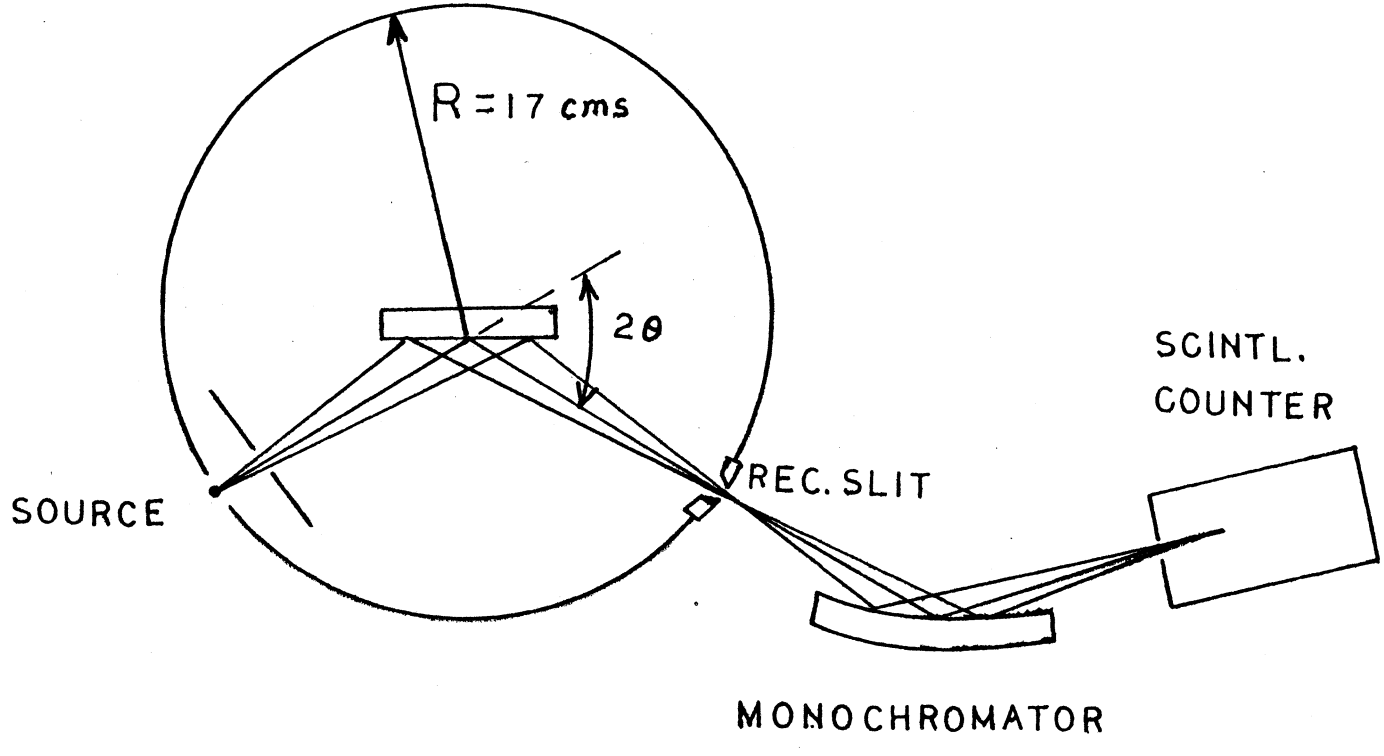


Figure 9. Schematic of the X-ray diffraction geometry.

4.3.1 X-ray Measurements on Planar Composites

A Siemens [110] diffractometer with a high intensity, fine focus copper tube was used to collect all data. This diffractometer was equipped with a specimen spinner and oscillator which allows the specimen to be rotated about the phi axis and oscillated about the ω axis (see Figure 10) independently of the detector carriage. Spinning and oscillating the specimen helps to minimize any fluctuations in intensity which may result due to the presence of large grains within the sample. The data was collected with a scintillation counter, a pulse height analyzer, and a ES Industries[111] diffracted beam graphite monochromator. Coarse scans were made at 1° per minute. Although the diffractometer was aligned to within 0.02 degree two theta, small corrections were made on all line positions using a silicon powder** standard. Integrated intensities were measured using a Numonics[112] electronic planimeter after subtracting background.

A diffracted beam graphite monochromator greatly reduces the background contributions from the continuous radiation as well as fluorescence from the titanium-base substrates. The peak to background ratio was considerably improved with the use of this monochromator. This

** Supplied by the National Bureau of Standards[109]. Standard reference material 640.

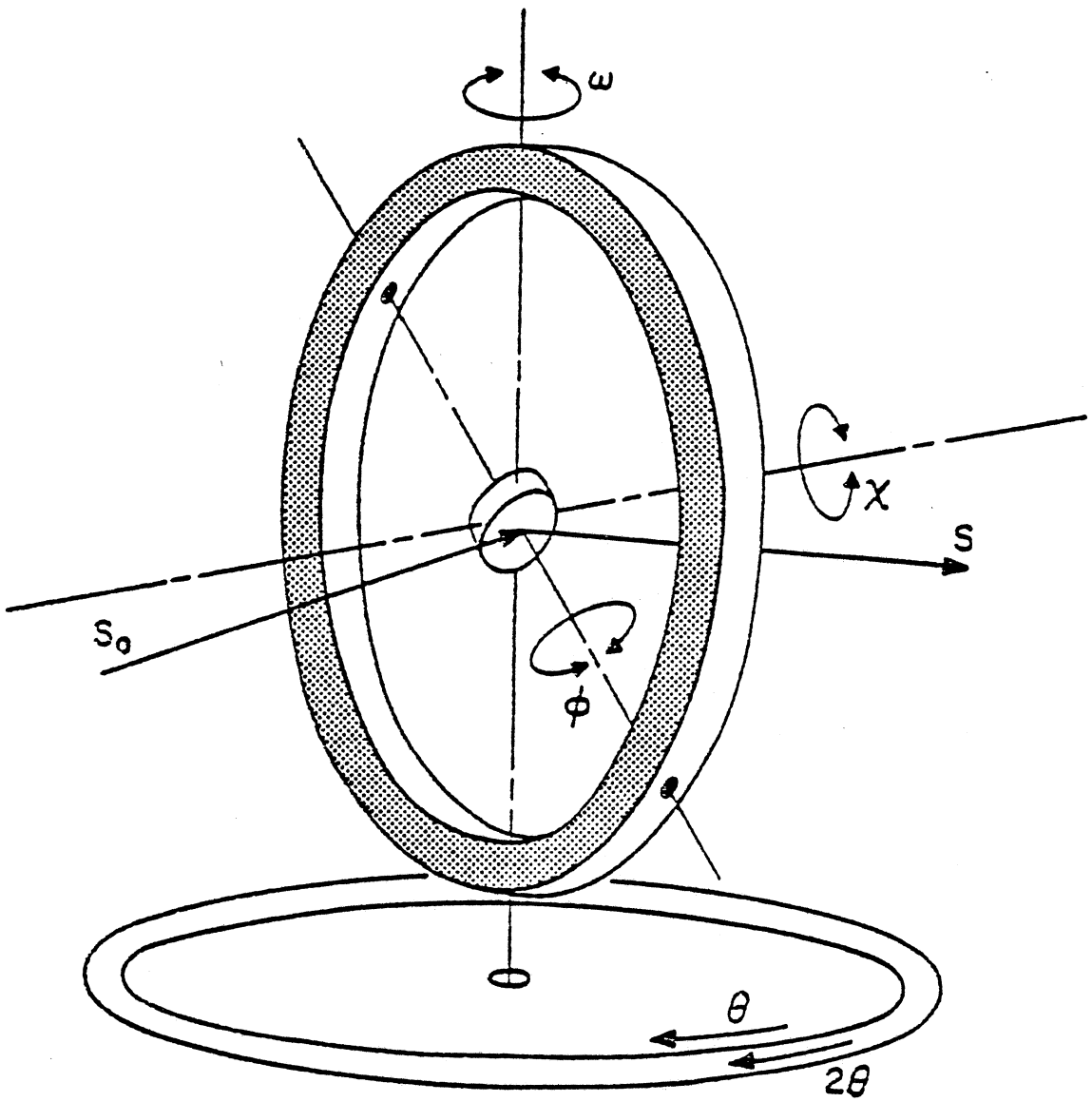


Figure 10. Illustration of four rotational axes 2θ, ω, χ, and φ relative to the incident beam, S_o, and the diffracted beam S.

diffractometer set-up allowed relatively low intensity lines to be measured.

Use of the Diffractometer:

The high voltage generator was warmed up at the operating voltage for several hours prior to data collection. The generator and diffractometer settings were:

Voltage	50 KV
Current	20 ma
Entrance Slit	1°
Receiver Slit	0.2 mm

The detector panel (Tennelec)[112] settings were:

Detector Voltage	1200V
Pulse Height Analyzer	2.0V (base)
	2.5V (window)
Linear Amplifier Gain	4 x 64

4.3.2 X-ray Measurements on Planar Composites for Diffusion Studies

The various Al thin films samples annealed for low and high temperature studies were examined by X-ray diffraction. For obtaining general diffraction patterns for iden-

tifying the various phases, the X-ray set up is similar to that described for the other planar composites. Integrated intensities obtained after subtracting background, were obtained as before. These were useful in quantifying the kinetics of the diffusion process as well as to calculate the thickness of $TiAl_3$ (low temperature studies) and Ti_3Al (high temperature studies).

The X-ray diffraction measurements used to obtain composition profiles were made on the (101) alpha-titanium intensity bands. The samples used for low temperature studies were those annealed at 635°C for 1/2 hr and 1hr. Also, the samples chosen for high temperature studies were Al(0.5 micron) thin films on titanium substrates annealed at 900°C for 1/2 hr, 1hr and 4 hours.

The (experimental) intensities were carefully determined by point counting using the usual diffractometer set-up and the timer-scaler combination on the Tennelac detecter panel. The diffractometer was equipped with a curved crystal quartz monochromator tuned only to the K_{α_1} component of the K_{α_1} - K_{α_2} doublet. The specimen omega position was set using a silicon single crystal, to give maximum intensity at the Si(111) two-theta peak position and the sample was only allowed to spin about the phi axis. The point counting was done at 0.01° two-theta intervals around

the peak position and 0.05° two-theta intervals at the tails. The time for each counting was predetermined such that the maximum statistical error for each count (±1%) was held nearly constant throughout the measurement of each intensity band.

The instrumental broadening was determined by point counting using a National Bureau of Standards Silicon powder standard, for the Si(220) reflection*. The instrumental curve was also used to correct for any peak shifts of the alpha-titanium intensity band. The generator and detector panel settings for the line profile measurements were similar to those described in the previous section. However, a narrower receiver slit (0.05mm) was used to keep the instrumental broadening small. To compensate for the loss of intensity due to the narrow receiver slit, a wider entrance slit (2°) was used.

4.4 MICROSCOPY

After diffraction studies, the samples were examined using a Reichert optical microscope[113]. It was not neccessary to etch the samples used to study the control of interface reactions as will be described in chapter 6. How-

---

* Note: The two-theta position for the Si(220) reflection is 47.303°. This is close to the two-theta position for the (101) alpha-titanium intensity band which is around 40.15°.

ever, the samples used for diffusion studies were examined in the etched and unetched condition. The latter samples were swab etched for 3-10 seconds using Krolls reagent, which does not stain but brings out the grain boundaries.

Kroll's reagent:	HF (48%)	1-3 ml.
	HNO (conc)	2-6 ml.
	Water	to 100 ml.

In certain cases they were also studied using a scanning electron microscope.

4.5 PREPARATION OF THE TIAL POWDER STANDARDS

4.5.1 Annealing Procedure

For the preparation of $TiAl_3$ standards, pure Ti and Al powders (both - 325 mesh) obtained from Venton Corp., Alpha Division[117] were used. Titanium and Aluminum were mixed in the stochiometer ratio of:

11.1534 grams of Ti

18.8467 grams of Al

for the preparation of 30 gms of the sample. The two powders were suspended in acetone and mixed thoroughly to obtain a homogenous mixture. The acetone was allowed to evaporate by using a low heat. A certain amount of powder was weighed out in a aluminum boat and the weight of powder used was found to be 5.0250 gms.

The powder sample was reached at 635°C in a horizontal tube furnace positioned around a quartz tube which contained the boat and powder. The quartz tube was kept under a constant vacuum of better than 10^{-5} torr. A West furnace controller provided many different constant rise and fall times, ranging from 20°F/hr to 300°F/min. Temperature was measured on a Brown electronic recorder with a chromel - alumel thermocouple which was in contact with the boat containing the powder. The temperature was also checked against a Leeds-Northrup potentiometer. The furnace control thermocouple was platinum-10% rhodium. A three-inch constant temperature zone was obtained. Prior to heat treatments of the powder, the aluminum boat was air-baked at 1000°C.

During the heat-up to 635°C, care was taken to ensure that the sample remained in the 500 to 600°C temperature range for the shortest possible time to avoid formation of the Ti_8Al_{24} phase. The powder sample was annealed at 635°C for 28 hours and removed. The powder was weighed and crushed and an X-ray diffraction sample was prepared. The initial diffraction pattern indicated that some aluminum was still remaining. The weight loss was around 0.11%. The powder was reannealed at 635°C for a total of 369 hours and at 650°C for an additional 118 hours (a total of 487 hours

at both temperatures) until there was no trace of Al left. The final weight loss was less than 0.2%.

The powder was sieved through a 325 mesh and filled into the cavity of an aluminum sample holder. Acetone and Duco cement (10 parts to 1) was used as a binder after the powder was settled with acetone. This produced a sample with limited surface roughness.

4.5.2 X-ray Diffraction Measurements

The $TiAl_3$ powder standard was examined by X-ray diffraction in a manner similar to that described earlier. A 1/2° entrance slit was used in this case to ensure that the beam did not strike the aluminum sample holder at the lowest angle line ($2\theta = 20^{\circ}$). A rough scan at 1 degree per minute scanning speed indicated that all reflections were from the $TiAl_3$ phase only. Only one weak low angle line was identified to be due to aluminum oxide, but the integrated intensity from this line is less than 1/250 of the strongest $TiAl_3$ peak. Detailed scans were obtained by using a 0.1° per minute scanning speed. The areas were by an electronic planimeter after subtracting background.

Chapter V

COMPUTER SIMULATION TECHNIQUES

5.1 SIMULATION OF DIFFRACTED INTENSITY BANDS

In this section the procedure employed to simulate diffracted intensity bands in an effort to obtain composition profiles, shall be discussed. It was shown in Chapter 3 that if a sample cross-section was divided into slabs of uniform thickness ΔY, (Figure 6), the diffracted intensity due to one such slab with an average composition "m" is given by:

$$P_m = I_o Q_m g \frac{A_o}{\sin \theta_m} \exp\left[\frac{-2\langle\mu(Y)\rangle_m Y_m}{\sin \theta_m}\right] \Delta Y \qquad (46)$$

Therefore, the simulation technique consists of calculating the diffracted intensity for an assumed concentration profile and matching the simulated intensity band with the experimentally obtained one. This is carried out by a trial and error estimate of the concentration profile. To carry out this simulation a previously developed[87] computer program (DXIS) was modified as shown in Appendix 1, and used. As it is evident from equation (46), the linear absorption coefficient as well as the reflectivity per unit volume are both functions of composition. Therefore another computer program (QMAC), shown in Appendix 2, was used to obtain this data. Table 15 shows the absorption and reflectivity data

for the Ti-Al system with Cu K_{α_1} radiation. As can be seen, the linear absorption coefficient varies appreciably with aluminum concentration and this variation is taken into account in the program DXIS.

Equation (46) was used to calculate the integrated intensity due to all slabs, and a schematic plot of this stepped intensity distribution is shown in Figure 7. The envelope formed by the stepped distribution will not be the measured curve because instrumental conditions have not yet been considered. The inset in Figure 7 schematically illustrates the normalized form of the pure instrumental broadening curve for an arrangement with only the K_{α_1} component of the K_{α_1}-K_{α_2} doublet. For the present discussion, it may be considered as a window, which provides a view of neighbouring composition elements as well as the one that it is peaked on. If either the instrumental curve is relatively broad or the specimen intensity distribution is narrow, a considerable range of compositions will be observed at a fixed two-theta position[77].

In addition to the pure instrumental effect, there could be broadening due to particle size, composition etc. Consequently, the experimental curve that is obtained by point counting on a diffractometer is a convolution of the intensity band from the specimen and the instrumental curve.

TABLE 15

Lattice Parameter, Absorption and Reflectivity Data* for the Ti-Al system with CuK_{α_1} radiation

Two-theta	Atom Frac.Al	Lattice Par. a (A)	Lattice Par. C (A)	Q (101) x10^{-3}	M per cm.
40.17830	0.0	2.94815	4.69061	0.76989	911.196
40.23244	0.025	2.94401	4.68635	0.75536	899.173
40.28671	0.050	2.93988	4.68208	0.73702	886.833
40.34114	0.075	2.93575	4.67782	0.72087	874.170
40.39574	0.100	2.93161	4.67355	0.70491	861.178
40.45049	0.125	2.92748	4.66929	0.68912	847.849
40.50539	0.150	2.92334	4.66502	0.67353	834.177
40.56044	0.175	2.91921	4.66075	0.65812	820.157
40.61568	0.200	2.91508	4.65649	0.64290	805.783
40.67107	0.225	2.91094	4.65222	0.62786	791.047
40.72661	0.250	2.90681	4.64796	0.61301	775.944
40.78232	0.275	2.90267	4.64369	0.59834	760.469
40.83817	0.300	2.89854	4.63943	0.58386	744.614
40.89420	0.325	2.89441	4.63516	0.56956	728.375
40.95039	0.350	2.89027	4.63089	0.55544	711.747

* This is only a partial data at 0.025 atom fraction Al intervals. In the actual computer program, data for 0.0025 at. fraction Al was used.

The form of the broadening curve could be Cauchy or Gaussian but in many cases it could be intermediate between these two extremes. It was shown in Chapter 3 that a Pearson type VII distribution could be used in place of these two extreme cases*.

The net broadening can be obtained from the experimental intensity curve by the following procedure. It is evident from Table 15 that the two theta position for the (111) pure titanium peak is 40.1783. All the intensity for $2\theta<40.1783$ would be due to the net broadening (pure instrumental, particle size etc.). On the other hand, the intensity on the high angle side of this peak ($2\theta>40.1783$) could involve significant composition broadening. Thus to assess the net broadening (all except composition broadening), one can measure the semi-half width of the pure Ti peak on the low angle side and multiply by 2. This could be used equation in (19) to determine the value of "a" for any "m" and these values could be used for the simulations. These values for various times at the low and high temperatures are presented in Table 16.

---

*Note: Although the limiting cases of the Pearson type VII distribution are the Cauchy and Gaussian forms, these forms have been left unaltered in the original computer program[87]. Any form can be conveniently used by selecting a certain parameter and this is documented, as shown in Appendix 1.

TABLE 16

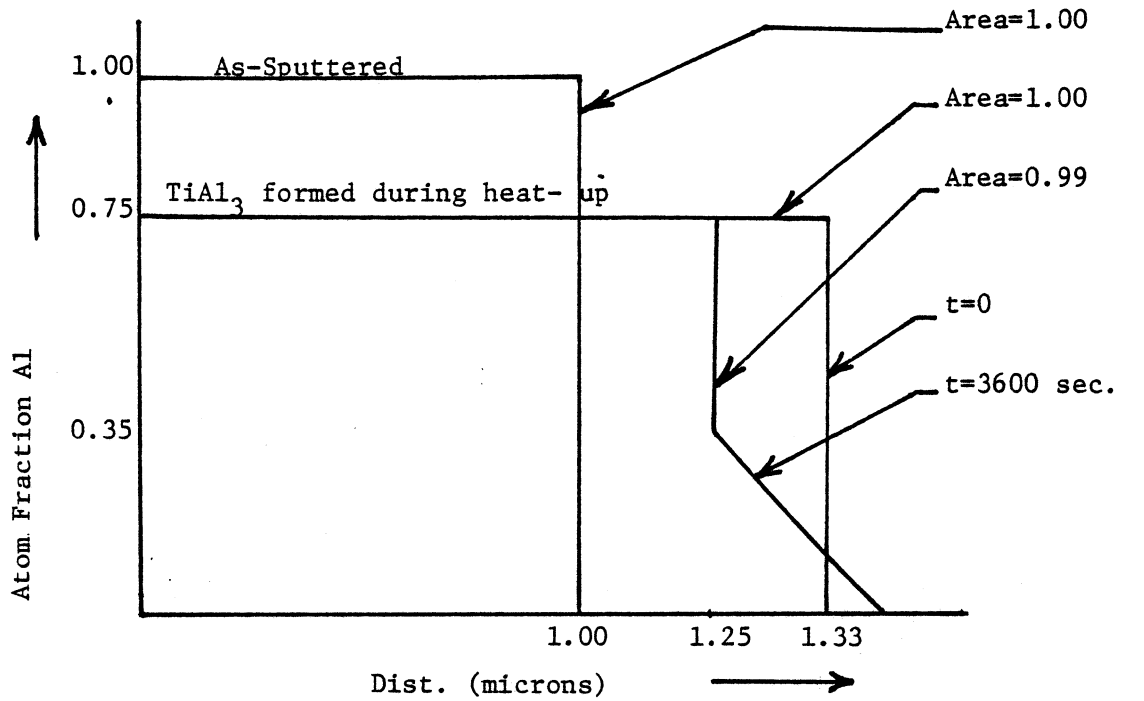
Table showing the Half-Width values* used in the Computer Simulations

t (hours) T in°C	Low Angle side		High Angle side	
	Expt.	Used	Expt.	Used
0.5 at 635	0.150	0.150	0.110	0.105
1.0 at 635	0.110	0.105	0.100	0.102
0.5 at 900	0.110	0.105	0.110	0.105
1.0 at 900	0.120	0.120	-	0.126
4.0 at 900	0.120	0.126	-	0.126

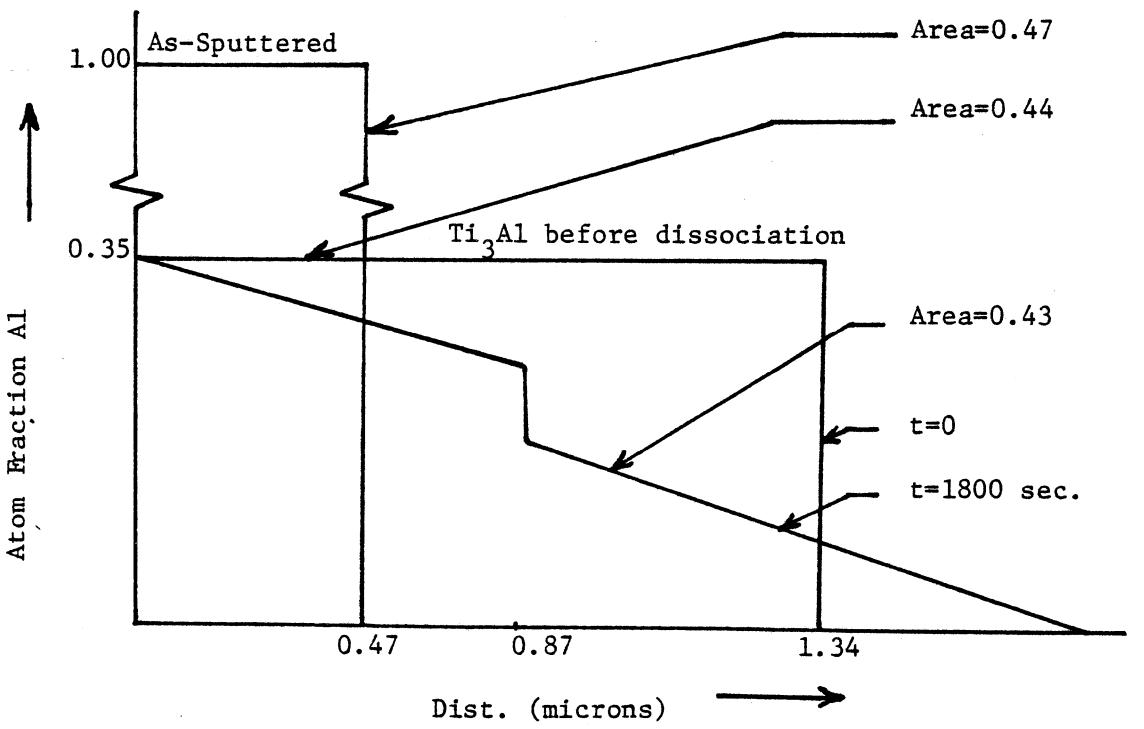
* The semi-half width values on the low and high angle side of the peak were obtained and multiplied by 2.

Recalling, for the Ti-Al system, we will have the $TiAl_3$ and alpha-titanium phase for diffusion at the low temperature (635°C). Also, at the higher temperature, we will have the Ti_3Al and alpha-titanium phase. It was mentioned in Chapter 4 that the thickness of these layers could be determined from integrated intensity measurements. The computer program sets up equidistant stations or distance grid points within the sample. For simulation of the low temperature data, the interface position has been set equal to the thickness of the $TiAl_3$ layer as an initial estimate. No diffraction peak was simulated in the $TiAl_3$ region above the interface for reasons to be discussed in Chapter 6. Instead, the thickness of the the $TiAl_3$ layer was used to calculate the absorption of the X-ray beam diffracted from the alpha- titanium below the interface. For the high temperature case simulation of the Ti_3Al diffraction peak as well as the alpha-titanium intensity band was made. In both cases, the final interface position was determined by conservation of aluminum atoms and is illustrated in figure 11. For determining the conservation of Al atoms, the area under the composition profiles was obtained using a three-point Simpson's numerical integration.

Corresponding to each station at any depth Y_m and interval Δy, an assumed composition (C_m) in terms of atom



(a)



(b)

Figure 11. Initial conditions and conservation of Al atoms for a) 635°C and b) 900°C diffusion studies.

fraction of aluminum must be introduced to the program. It was shown in Chapter 3 that this can be carried out using a sum of two error functions given by equation (25). This assumed profile has to be varied by trial and error until the simulated intensity according to equation (24) matches the experimental curve. It is helpful to recognize that reducing the slope of the composition profile at a given composition results in an increase in the intensity at a two-theta value corresponding to that composition. In other words, there is a reciprocal relationship between the slope of the composition profile and the intensity. Figure 12 illustrates how the parameters a_i, b_i and d_i in equation (25) can be adjusted to obtain the desired shape of the composition profile used to simulate the low temperature data. It is evident that the sum of the a_i parameters equals the surface composition, i.e. for two error functions*,

$$C\,(Y = o) = a_1 + a_2 \qquad (47)$$

Also, the slope of the composition profile can be varied by adjusting the b_i parameters realizing that larger values for b_i result in a shallower slope and vice versa (see curve a and b in figure 12). If the composition profile does not

*Note: Provision for up to three error functions was made in the computer program although only two error functions were adequate for the present case. If the third error function is not used a and d must be set equl to 0 and b equal to 1.

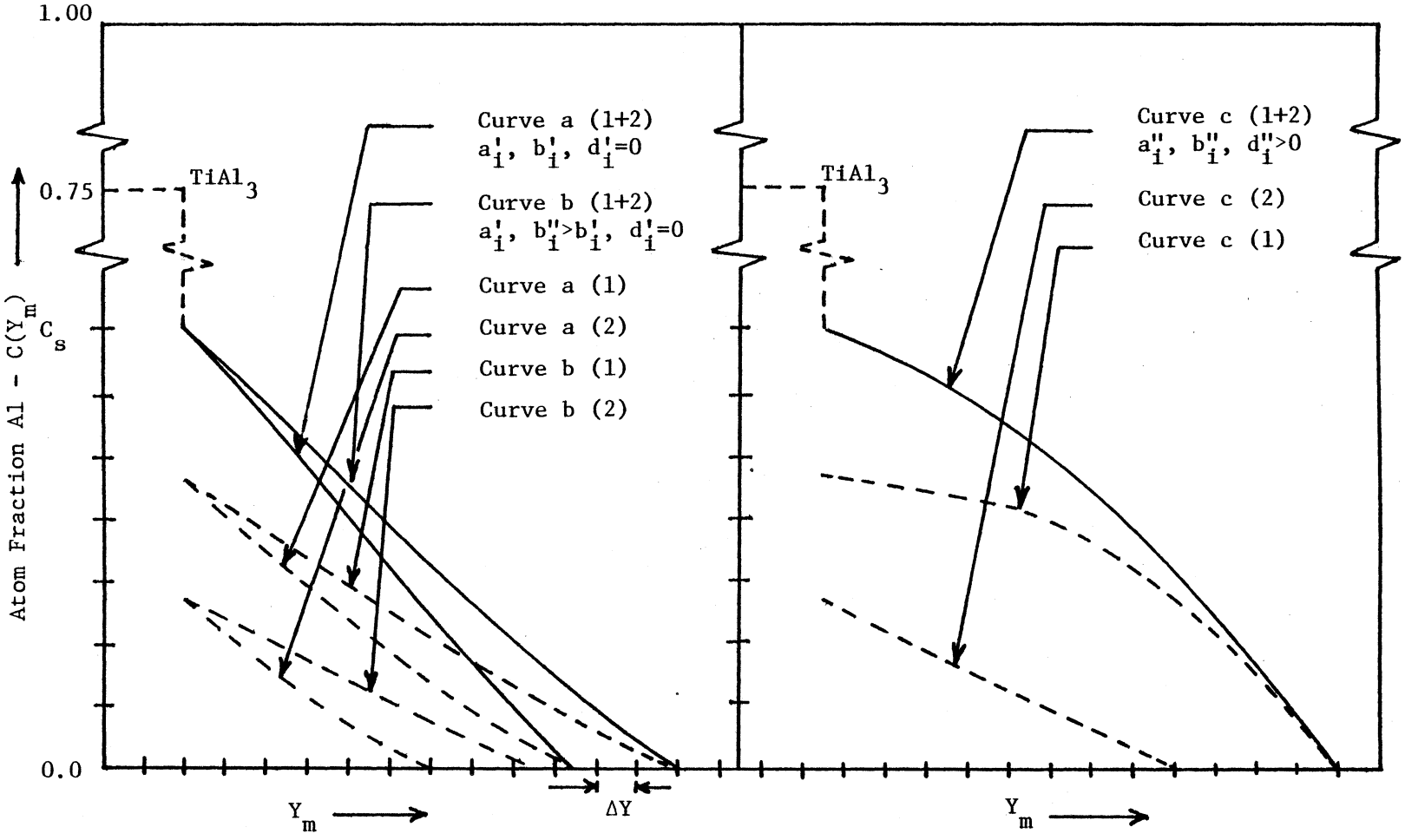


Figure 12. Schematic representation of the composition profiles that can be determined from equation (25), for the low temperature diffusion studies in the Ti-Al system.

have an inflexion point in it, the values for d_i can be set equal to 0. However, to produce an inflexion point, positive values for d_i must be used such that d_i is $\leq Y/b_i$ (curve c). The actual values that were used to simulate the diffracted intensity band will be given in Chapter 6.

Figure 13, illustrates the method to simulate the high temperature data. As before, only two error functions are required to obtain the composition profile for the alpha-titanium intensity band. The Ti_3Al diffraction peak requires only a linear variation in composition, or,

$$C(Y_m) = b''Y_m + a' \qquad (48)$$

Again, a' is the surface composition and b' is the slope. It is seen from figure 13 that a "composition gap" between the Ti_3Al region and alpha-titanium, can be introduced and varied by adjusting these parameters. This has the effect of using a lattice parameter vs. composition profile that becomes discontinuous where the two phases meet as shown in Figure 4 (for further details see Chapter 6).

5.2 TWO-PHASE ITERATIVE SOLUTION TO OBTAIN DIFFUSION COEFFICIENTS

A method of obtaining diffusion coefficients will be discussed in this section. The method consists of a simulation of the composition profiles (that are obtained from

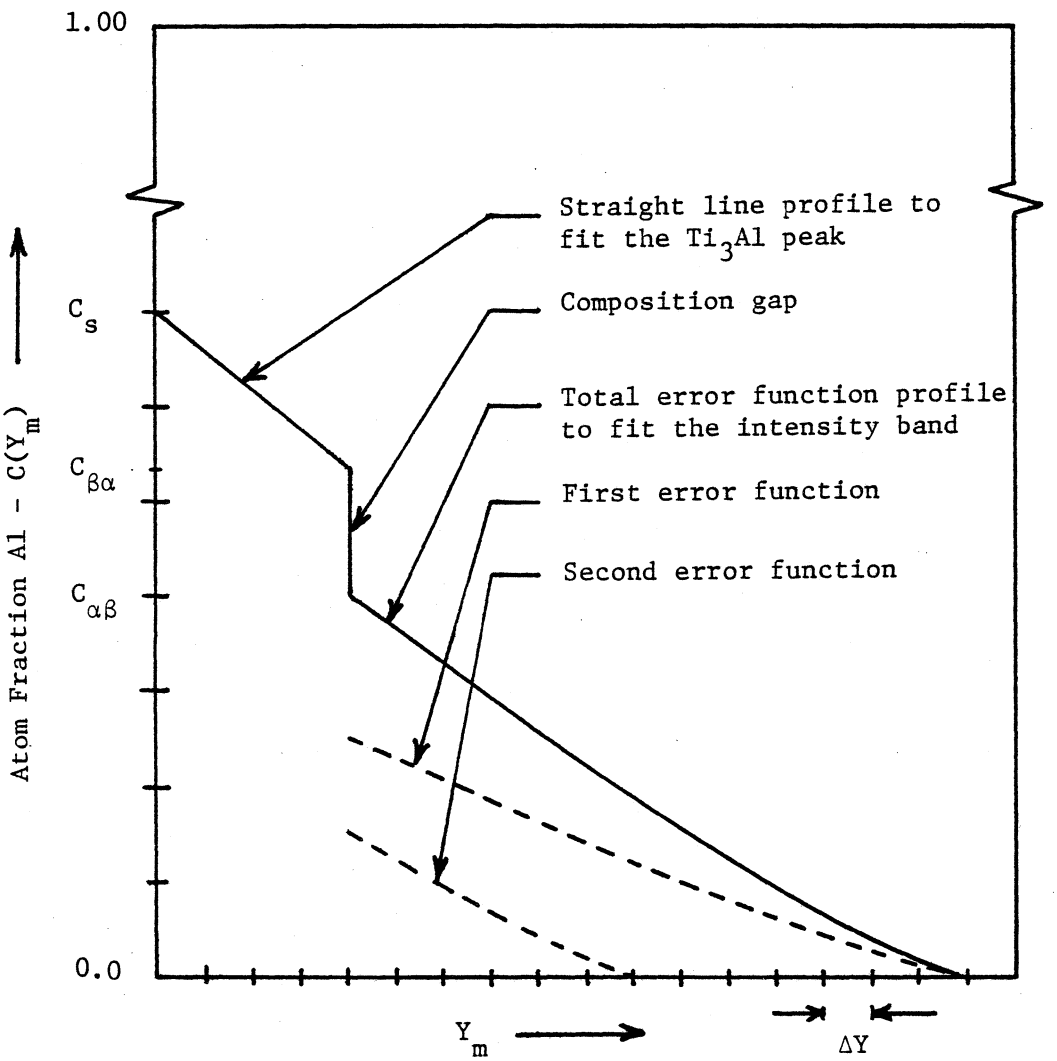


Figure 13. Schematic representation of the composition profile that can be determined from equation (25), to simulate the high temperature diffusion data.

intensity bands), by using the computer program (ITR2) shown in Appendix 3. This program provides numerical solutions to equations (40) and (41) by using an iterative scheme, allowing for a variation of D with concentration in each phase.

For the low and high temperature cases, the initial conditions are shown by curve b in figures 11a and 11b. These are obtained by a conservation of Al atoms and from a known thickness of the Al thin film on the titanium substrate. Therefore, a first estimate is made using $\xi = 1/2$ (see Figure 8), where 1/2 is the starting thickness of the layer of the Ti-Al compound which may be either $TiAl_3$ or Ti_3Al in this study. After diffusion for a certain period of time has taken place, the composition profiles would be similar to curve C in figures 11a and 11b. The program sets up equidistant grid stations in the region $x=-\xi$ to $x=L/2+\xi$ (see figure 8).

A starting concentration profile is determined by using equations (28) and (29) and an average value for D_α and D_β. The diffusion coefficients corresponding to each point in the starting concentration profile are calculated by logarithmic interpolation using a subroutine (COEF) in the computer program (ITR2). There starting concentrations and D values are then used in equations (40) and (41) to obtain a first refinement of the concentration profile. Since the

initial concentrations C_β and C_α in atom fraction B are known in every case, the following conservation is used,

$$\int_0^{L/2} C_\beta \, dx = C_\beta\left(\frac{\ell}{2}\right) + C_\alpha\left(\frac{L-\ell}{2}\right) \qquad (49)$$

If the quantity on the left hand side is less than 1/2, ξ is increased and vice versa. Therefore, a new estimate for ξ is made on this basis and the above computations are repeated to obtain a second and higher refinements on the concentration profile and ξ .

It takes about 5 iterations to give concentrations within 1% of the final solution[98]. To be on the safe side, the program makes 20 iteratives, and at the end of the 20th iteration, lists the differences in concentration between the 20th and 19th iteration. The experimental as well as the simulated composition profiles are plotted on a Tektronix[115] graphic terminal, for visual comparisons. If the two profiles do not match, the input diffusion coefficient data would have to be varied by trial and error until a good match is obtained. It is helpful to recognize that the slope of the composition profile is inversely proportional to the diffusion coefficient. Also, the interface position either moves towards the free surface or away from it, depending on the net flux of Al atoms, as given by Ficks first law.

5.3 COMPUTER SIMULATION OF INTEGRATED INTENSITIES OF THE TI-AL COMPOUNDS

5.3.1 Simulation of $TiAl_3$ Integrated Intensities

In the reaction studies on Al/Ti standards, the $TiAl_3$ phase was observed. To confirm that a layer of $TiAl_3$ was formed and to determine its thickness, the integrated intensities from $TiAl_3$ powder standards was essential. It was mentioned in Chapter 2 that van Loo and Rieck[25] first identified the $TiAl_3$ structure (b.c. tetragonal, Ga_2Hf type) and assigned it to the space group I4/mmm. However, in the determination of relative intensities of the various hkl planes, they used visual estimates of the integrated intensities. Usually, visual comparisons can tend to be linear instead of logarithmic and may be in error. Also, their data in the card files does not give reflections beyond two-theta= 85.0°. Therefore, the one of the purposes of this section is to describe the computer calculation of integrated intensities and compare these with the more complete experimental data obtained on $TiAl_3$ powder samples using a diffractometer.

Figure 55 (Appendix 6) shows the $TiAl_3$ unit cell, along with the atom positions. These atomic positions for both Ti and Al are used in a computer program (INTCLASS) shown in Appendix 5 in order to calculate the integrated intensities for random powders,

$$I = |F|^2_j \left[\frac{1+\cos^2 2\theta \cos^2 2\theta'}{\sin\theta \sin 2\theta (1+\cos^2 2\theta')} \right] \qquad (50)$$

While the various terms have their usual meaning (Chapter 3), the structure factor is used without a correction for Temperature Diffused Scattering. The angle of the monochromator used was $2\theta^{\circ} = 26.4^{\circ}$. The structure factor can be calculated from the atomic positions according to the equation.

$$F_{hkl} = \sum_{1}^{N} f_n \, e^{2\pi i (hu_n + kv_n + lw_n)} \qquad (51)$$

where the summation extends over all the N atoms of the unit cell. The atomic scattering factors for the elements are also calculated within the program.

5.3.2 Simulation of the Ti_2Al and Ti_3Al Phases

Ence and Margolin[74] and Goldak and Parr[47] had determined the structures for Ti_2Al and Ti_3Al respectively. Both phases are hexagonal and are known to have a $D0_{19}$ type structure and were assigned to the P63/mmc space group. The atomic positions for the Ti_3Al unit cell are given in Appendix 6. In this section, the integrated intensities from the disordered Ti_3Al and Ti_2Al phase will be obtained by computer simulations similar to those described in the previous section.

The structure factors were calculated from equation (51). For a disordered structure, the atoms of each type occupy all positions at random without any preference for a sublattice. For the disordered Ti_2Al and Ti_3Al phases, an equivalent atomic scattering factor can be calculated as

$$f(\text{equivalent}) = (1-x)f_{Ti} + xf_{Al}$$

where x is the composition of the phase in atom fraction Al.

Chapter VI

RESULTS AND DISCUSSION

In this chapter, the results on the control of interface reactions in planar composites, diffusion studies in the Ti-Al system, as well as computer simulations of integrated intensities for a few Ti-Al compounds will be presented. One of the major objectives of this study is to design an optimum hot-pressing cycle, for fiber reinforced SiC/Ti composites with a protective coating to delay silicide formation. Wherever pertinent, the results from the three sections will be compared.

6.1 CONTROL OF INTERFACE REACTIONS IN PLANAR COMPOSITES

The various SiC/Ti planar composites with and without the protective coatings (Al and Mo_5Si_3) were carefully characterized by X-ray diffraction in the as-received condition. This was done so as to determine the effects of subsequent heat-treatments on these composites. In all the composites which had a SiC coating the SiC appeared to be amorphous. This conclusion was based on the absence of crystalline reflections as well as a fairly high background due to diffused scattering. Also, the Mo_5Si_3 coatings in the as-sputtered condition were amorphous while the Al and

alpha-titanium were crystalline. From these initial diffraction patterns, there was no indication of any silicide formation during the sputter-deposition and also no beta-titanium reflections were observed.

The SiC/Ti system was investigated, both as a system in itself, as well as a standard for comparison with the other systems because of the possible complexities in reaction products involved with these systems. As described in Chapter 4, this involved an initial 2 hour hold at 600°C before annealing at 875°C for 1/2hr., 1hr., 2hrs. and 4hrs. During the hold at 600°C, there was no silicide formation.

An X-ray examination of the reacted samples was made. A 1/2 hour anneal at 875°C on the SiC/Ti samples yielded significant amount of reaction products. At least thirteen Ti_5Si_3 lines were positively identified giving a considerable amount of integrated intensity. At this early stage, 5 lines from TiC and a couple of weak reflections from TiSi and $TiSi_2$ were observed. The SiC film did not stay intact even with slow furnace cooling. The possible reasons for the flaking of the film are discused in a later section. After annealing for longer times (1hr., 2hrs., 4hrs.), it was observed that the film stayed intact. A one hour anneal at 875°C appears to be the threshhold for flaking.

X-ray studies on the samples annealed for 1hr., 2hrs., and 4hrs., indicated that Ti_5Si_3 continued to form in sizeable amounts over the 4 hour period. On the 4 hour anneal, at least twenty-three Ti_5Si_3 lines were positively identified. The amounts of TiC, TiSi and $TiSi_2$ also increased consistently from the half hour to the 4 hour anneal. The largest total intensity was from TiC and the smallest was from $TiSi_2$. The matrix was entirely alpha and twenty alpha-titanium lines were observed. The X-ray diffraction results on the SiC/Ti system annealed for the various times, is presented in Table 17. The integrated intensity values were obtained by measuring areas after subtracting background, and the two-theta positions were corrected using a silicon powder standard. It should be noted that even after annealing at 875°C for the various times, the SiC phase did not crystallize. This is discussed later with reference to the determination of relative reaction rates.

When a SiC/Al/Ti sample was annealed at 875°C for 1/2 hour, some Ti_5Si_3 was formed. Although only 10 Ti_5Si_3 lines were identified, the integrated intensity from Ti_5Si_3 appeared to be comparable with that obtained from the SiC/Ti sample annealed for 1/2 hour. However, for increasing annealing times, the amount of Ti_5Si_3 as well as the number of lines observed increased only slightly, suggesting a sat-

TABLE 17

Integrated intensities and two theta positions for the SiC/Ti system annealed at 875°C for various times.

	1/2 hour		1 hour		2 hours		4 hours	
Identification	Int.	2θ	Int	2θ	Int	2θ	Int	2θ
Ti_5Si_3 (200)	6.0	27.648	11.9	27.658	33.5	27.658	35.1	27.671
Ti_5Si_3 (111)	6.3	29.561	12.1	29.558	10.8	29.558	11.1	29.571
TiSi (201)	-	-	4.2	31.808	6.1	31.883	3.5	31.838
TiSi (111)	-	-	-	-	9.8	33.132	7.2	33.132
Ti_5Si_3 (002)	14.6	34.723	19.3	34.732	4.9	34.745	7.3	34.770
α-Ti (100)	84.0	35.161	86.1	35.157	79.6	35.170	40.9	35.195
TiC (111)	74.9	36.021	87.7	36.027	115.2	36.045	147.7	36.070
TiSi (210)	22.5	36.348	30.3	36.532	25.4	36.632	22.6	36.620
Ti_5Si_3 (210)	30.9	36.873	35.3	36.882	100.4	36.870	108.9	36.895
Ti_5Si_3 (102)	40.9	37.461	52.5	37.587	13.9	37.507	14.8	37.507
TiSi (102)	-	-	-	-	37.6	37.695	47.5	37.695
α-Ti (002)	469.8	38.411	403.4	38.419	146.3	38.419	173.3	38.431
$TiSi_2$ (311)	13.3	39.598	27.9	39.754	26.8	39.869	34.3	39.831
α-Ti (101)	685.5	40.221	669.9	40.219	503.2	40.231	393.9	40.244
Ti_5Si_3 (211)	74.9	40.923	121.3	40.919	192.2	40.919	234.0	40.944
TiC (200)	99.9	41.836	151.6	41.831	139.4	41.844	165.4	41.869
Ti_5Si_3 (300) / $TiSi_2$ (004)	-	-	-	-	136.8	41.996	168.8	42.006
Ti_5Si_3 (112)	53.3	42.561	71.4	42.581	52.1	42.594	62.2	42.606
TiSi (301) / $TiSi_2$ (022)	5.5	43.473	8.9	43.684	11.2	43.781	9.8	43.769
$TiSi_2$ (112)	7.2	45.361	14.3	45.58	16.5	45.718	17.8	45.694
TiSi (020)	-	-	-	-	5.1	51.055	6.7	51.068
Ti_5Si_3 (221)	-	-	2.5	52.204	7.4	52.217	8.2	52.230
α-Ti (102)	184.6	53.023	133.5	53.029	131.6	53.029	107.3	53.067
Ti_5Si_3 (311)	3.2	54.223	5.0	54.227	10.7	54.267	14.1	54.267
Ti_5Si_3 (400)	-	-	-	-	4.5	57.116	6.6	57.128
TiC (220)	25.7	60.611	40.8	60.604	68.1	60.666	77.9	60.690
Ti_5Si_3 (222)	10.2	61.348	14.3	61.350	17.9	6.1352	23.7	61.365
α-Ti (110)	81.1	63.011	61.7	63.027	60.5	63.040	63.5	63.077
TiSi (112,411)	-	-	-	-	3.2	65.190	5.9	65.177
Ti_5Si_3 (321)	5.4	65.685	6.6	65.690	15.4	65.590	16.2	65.627
Ti_5Si_3 (410)	14.8	66.438	21.4	66.427	28.1	66.427	21.1	66.415
Ti_5Si_3 (112)	-	-	-	-	-	-	15.4	66.588
Ti_5Si_3 (402)	5.7	68.547	8.1	68.602	9.9	68.577	14.2	68.590
α-Ti (103)	239.6	70.634	185.8	70.652	145.6	70.665	177.8	70.690
TiC (113)	10.4	72.559	21.7	72.552	28.3	72.627	38.9	72.640
Ti_5Si_3 (500,004)	-	-	6.8	73.502	4.2	73.390	9.9	73.402
$TiSi_2$ (602)	-	-	-	-	3.8	73.652	-	-
α-Ti (200)	9.5	74.259	8.9	74.227	4.8	74.252	5.3	74.265
α-Ti (112)	150.1	76.245	115.4	76.265	153.1	76.265	88.2	76.315

Table 17 Continued

	1/2 hour		1 hour		2 hours		4 hours	
Identification	Int	2θ	Int	2θ	Int	2θ	Int	2θ
α-Ti (201)	75.9	77.408	59.2	77.427	69.3	77.440	72.1	77.477
Ti_5Si_3 (420)	-	-	-	-	4.9	78.405	10.4	78.427
Ti_5Si_3 (331)	-	-	1.8	79.381	6.8	79.352	9.0	79.365
α-Ti (004)	49.8	82.207	29.2	82.226	24.7	82.239	11.9	82.251
TiSi (114, 131)	-	-	-	-	2.7	83.351	3.0	83.414
Ti_5Si_3 (502)	4.0	83.750	6.2	83.801	13.3	83.751	12.3	83.763
Ti_5Si_3 (511)	-	-	1.2	86.001	4.6	86.001	6.3	85.938
α-Ti (202)	23.1	86.780	31.2	86.801	28.0	86.838	26.2	83.838
TiC (400)	2.3	91.125	2.6	91.050	4.7	91.122	8.2	91.060
α-Ti (104)	50.8	29.650	38.8	92.673	29.0	92.672	21.3	92.697
α-Ti (203)	66.9	102.336	76.6	102.370	82.7	102.395	84.9	102.433
TiC (420)	15.5	105.823	21.4	105.860	25.0	105.919	43.2	105.971
α-Ti (211)	55.9	109.085	66.5	109.138	56.0	109.169	52.5	109.207
α-Ti (114)	110.7	114.175	110.0	114.210	120.0	114.230	102.7	114.280
α-Ti (212)	43.4	119.250	30.0	119.325	34.0	119.340	16.2	119.415
α-Ti (105)	145.6	122.103	134.8	122.190	84.4	122.190	107.0	122.215
Ti_5Si_3 (532)	-	-	3.5	125.160	9.7	125.200	11.9	125.214
α-Ti (204)	28.4	126.250	25.2	126.310	23.1	126.327	13.6	126.377
Ti_5Si_3 (206) / TiC (511)	-	-	-	-	5.7	136.100	14.6	136.100
α-Ti (213)	144.3	139.345	143.3	139.362	147.8	139.448	131.8	139.400
α-Ti (302)	138.2	148.470	87.0	148.480	128.7	148.635	70.2	148.698

uration of silicide growth after 4 hours. No lines from TiSi and $TiSi_2$ were observed even up to the longest anneal (4 hours). During the early stages, no TiC reflections were noticed. However, after the 2 hour anneal, at least two TiC lines were positively identified. There was also some evidence of Ti_3AlC being formed, although overlapping lines prevented an unambiguous identification. Only one separated high angle line was found, and this remained constant up to the 4 hour anneal. If this is due to Ti_3AlC, the amount of this phase remains constant.

In the shorter time anneals (1/2 hour and 1 hour), at least 6 lines from the tetragonal TiAl phase (a=4.015Å, c=4.062Å) were observed. These lines decreased in intensity consistently from the 1/2 hour to the 1 hour anneal and disappeared after 2 hours. Also, the lattice tended to become more and more cubic before the TiAl lines disappeared.

Starting from 1/2 hour and up to 4 hours, a number of diffraction peaks from the Ti_3Al (disordered) phase were positively identified. The amount of Ti_3Al increased systematically from 1/2 hour to 4 hours and at least 20 lines were observed. The lines from the matrix were entirely from the alpha-phase as expected since Al would tend to stabilize this phase. As noted in the SiC/Ti system, the SiC phase did not crystallize upon annealing. The integrated intensi-

ties as well as two-theta positions for the various phases discussed, are presented in Table 18.

The Mo_5Si_3 /Ti system was used as a standard for comparison with the SiC/Mo_5Si_3 /Ti planar composites. These standards were annealed at 875°C for 1/2 hr, 1 hr, 2 hrs and 4 hours. X-ray diffraction analysis on these standard samples revealed at least 25 lines from the Ti_5Si_3 phase. This would appear surprising at first, since one would expect that without a SiC coating, no silicide should form. The diffraction pattern after the 1/2 hour anneal on this sample revealed a number of lines from Mo_5Si_3 and a few from Mo_3Si although the Mo_5Si_3 layer appeared amorphous in the as-sputtered state. A very broad and diffuse peak was observed in the latter case, that indicates an amorphous mixture of Mo and Si atoms having some degree of short range ordering. This reasoning is supported by the results of a recent thesis[116] which was concerned with studies on Mo_5Si_3 thin films on Si single crystal substrates. It appears that the Mo_3Si phase near the interface dissociates such that

$Mo_3Si \longrightarrow 3Mo + Si$

Free Mo $\longrightarrow$ Ti(Mo)

Free Si forms Ti Si in the crystalline state.

This observation is consistent with a decrease in the intensity of the Mo Si diffraction lines for longer annealing times.

TABLE 18

Integrated intensities and two theta positions for the SiC/Al/Ti system annealed at 875°C for various times.

	1/2 hour		1 hour		2 hours		4 hours	
Identification	Int	2θ	Int	2θ	Int	2θ	Int	2θ
Ti_3Al (101)	33.4	26.196	41.5	26.196	49.0	26.171	44.0	26.096
Ti_5Si_3 (200)	7.8	27.646	6.7	27.571	6.6	27.521	6.1	27.608
Ti_2Al (110)	6.7	30.933	11.1	30.971	10.8	30.946	11.3	30.883
TiAl (110)	22.8	31.658	6.9	31.632	-	-	-	-
Ti_5Si_3 (002)	10.9	34.708	9.7	34.708	13.2	34.608	8.7	34.688
α-Ti (100)	49.6	35.171	38.1	35.157	28.1	35.157	29.4	35.195
Ti_3Al (200)	160.2	35.907	189.9	35.907	213.7	35.895	262.5	35.807
Ti_5Si_3 (210)	28.8	36.832	28.5	36.782	25.5	36.770	37.5	36.820
Ti_5Si_3 (102)	15.7	37.557	26.1	37.332	52.4	37.357	34.6	37.595
α-Ti (002)	152.1	38.470	132.6	38.457	116.8	38.495	187.0	38.500
Ti_3Al (002)	466.9	38.795	355.2	38.832	290.9	38.782	203.9	38.720
TiAl (111)	-	-	-	-	-	-	-	-
α-Ti (101)	312.6	40.232	302.8	40.231	207.8	40.244	238.0	40.256
Ti_3Al (201)	414.3	40.969	560.9	40.981	635.5	40.944	723.8	40.869
Ti_5Si_3 (300)	41.6	41.806	59.9	41.781	68.7	41.831	91.9	41.944
Ti_5Si_3 (112)	37.9	42.606	33.7	42.444	42.2	42.481	35.2	42.531
Ti_3AlC (200)	-	-	-	-	20.4	43.381	4.9	43.469
TiAl (002)	35.6	44.554	10.5	44.593	-	-	-	-
TiAl (200)	79.1	45.404	23.4	45.343	-	-	-	-
Ti_3Al (112)	5.6	50.494	8.1	50.505	8.3	50.417	6.1	50.317
Ti_2Al (201)	7.2	50.917	-	-	-	-	-	-
Ti_5Si_3 (221)	-	-	3.6	52.217	4.3	52.192	8.4	52.092
α-Ti (102)	84.9	53.043	80.2	53.044	66.8	53.053	55.5	53.041
Ti_3Al (202)	69.0	53.867	99.7	53.917	117.5	53.842	111.3	53.767
TiC (220)	16.6	60.534	16.7	60.528	23.4	60.330	37.8	60.850
Ti_5Si_3 (222)	7.3	61.378	5.7	61.378	7.8	61.264		
α-Ti (110)	61.5	63.015	43.8	63.016	55.7	63.027	46.7	63.040
Ti_3Al (220)	41.9	64.402	59.5	64.440	70.3	64.440	87.3	64.340
TiAl (202)	39.9	65.402	11.5	65.415	-	-	-	-
Ti_5Si_3 (410)	19.4	66.127	11.7	66.150	11.3	66.252	7.4	66.352
α-Ti (103)	149.4	70.677	144.7	70.692	124.2	70.690	120.5	70.677
Ti_3Al (203)	86.9	71.652	117.3	71.790	128.4	71.665	99.3	71.565
α-Ti (200)	-	-	-	-	-	-	6.1	74.277
Ti_3Al (400) / Ti_3AlC (311)	-	-	-	-	16.0	75.821	10.5	75.852
α-Ti (112)	110.0	76.272	74.2	76.265	68.8	76.290	66.1	76.277
α-Ti (201)	101.9	77.452	86.2	77.422	23.7	77.465	145.4	77.477
Ti_3Al (222)		77.752	116.7	77.817	117.7	77.790		77.715
Ti_3Al (401)	62.4	79.352	52.1	79.227	52.3	79.227	55.9	79.115
α-Ti (004)	41.0	82.277	22.8	82.314	21.0	82.314	27.7	82.314

Table 18 Continued

	1/2 hour		1 hour		2 hours		4 hours	
Identification	Int	2θ	Int	2θ	Int	2θ	Int	2θ
Ti_3Al (004)	28.9	83.151	22.1	83.377	22.8	38.201	16.4	83.063
α-Ti (202)	14.2	86.825	11.9	86.828	10.6	86.825	20.1	86.838
Ti_3Al (402)	-	-	-	-	9.7	88.750	12.6	88.600
α-Ti (104)	29.7	92.722	25.5	92.759	26.5	92.772	20.8	92.736
Ti_3Al (204)	8.4	94.171	13.3	94.184	20.1	94.071	14.5	93.934
α-Ti (203)	41.8	102.405	20.4	102.420	56.1	102.420	56.1	102.408
Ti_3Al (403)	15.4	104.695	25.2	104.732	27.9	104.683	30.2	104.533
α-Ti (210)	8.4	105.919	6.6	105.932	7.0	105.932	9.6	105.908
α-Ti (211)	50.0	109.143	52.3	109.143	41.6	109.156	35.5	109.168
Ti_3Al (421)	31.9	112.268	36.4	112.380	39.9	112.393	49.5	112.206
α-Ti (114)	79.3	114.268	68.1	114.305	63.5	114.317	66.7	114.305
Ti_3Al (224)	20.4	116.672	33.1	116.780	47.2	116.730	39.0	116.517
α-Ti (212)	22.9	119.342	17.4	119.355	11.8	119.366	15.7	119.329
α-Ti (105)	77.1	122.291	81.3	122.315	84.6	122.328	106.2	122.290
Ti_3Al (205)	14.2	124.450	30.0	124.615	42.2	124.514	28.6	124.327
α-Ti (204)	18.3	126.240	18.6	126.377	17.4	126.402	10.2	126.414
αTic (422)	18.4	129.340	16.4	129.602	18.9	129.638	16.7	129.676
α-Ti (213)	114.7	139.413	89.6	139.498	73.6	139.523	61.8	139.560
Ti_3Al (423)	26.9	145.050	-	-	64.4	145.210	71.6	144.963
α-Ti (302)	59.9	148.660	86.9	148.350	51.2	148.635	55.2	148.660

The integrated intensity of Ti_5Si_3 (hexagonal) from the 1/2 hr anneal at 875°C was appreciable and corresponded roughly to that obtained in the SiC/Ti sample annealed for 1/2 hour. The Ti_5Si_3 phase formed with a strong preferred orientation for the basal plane. It was also found that the matrix was mainly beta titanium since Mo stabilizes the beta phase. The few alpha reflections observed were weak.

The behavior of the $SiC/Mo_5Si_3/Ti$ samples was similar to that of the Mo_5Si_3/Ti standard. The amount of Ti_5Si_3 formed, increased consistently with increasing time and was greater than that observed in the standard. The number of Mo_5Si_3 lines were fewer than those from the standard, but possible overlapping of these with the Ti_5Si_3 lines makes the interpretations difficult. Again, the matrix tended to be mainly beta-titanium. The X-ray diffraction data for the $SiC/Mo_5Si_3/Ti$ planar composites are presented in Table 19.

6.1.1 Lattice Parameters

Systematic changes in lattice parameters were observed in all the systems, throughout the annealing procedure. This may result from local composition changes due to either interstitial or substitutional atoms, or to a lesser extent due to differential thermal contractions between the various phases. The latter will generate residual stresses on cool-

TABLE 19

Integrated intensities and two-theta positions for the SiC/Mo_5Si_3/Ti planar composites

SiC/Mo_5Si_3/Ti	1/2 hour		1 hour		2 hours		4 hours	
Identification	Int	2θ	Int	2θ	Int	2θ	Int	2θ
Ti_5Si_3 (200)	11.49	27.670	11.89	27.713	21.95	27.658	28.97	27.671
Ti_5Si_3 (111)	15.07	29.633	15.90	29.646	19.85	29.583	18.14	29.583
Ti_5Si_3 (002)	59.52	34.858	50.95	34.871	59.59	34.796	54.61	34.796
TiC (111)	-	-	32.85	36.058	134.35	36.046	148.11	36.083
Mo_5Si_3 (002)	16.89	36.607	-	-	-	-	-	-
Ti_5Si_3 (210)	47.01	36.919	39.03	36.957	75.58	36.899	74.99	36.895
Ti_5Si_3 (102)	65.45	37.644	56.96	37.645	84.70	37.595	70.79	37.595
α-Ti (002)	39.05	38.544	21.84	38.570	-	-	-	-
β-Ti (110)	387.69	39.132	292.43	39.132	893.11	39.132	750.64	39.170
Mo_5Si_3 (330)	903.73	39.532	887.07	39.382	4.62	39.782	-	-
α-Ti (101)	281.68	40.168	40.83	40.256	16.43	40.181	20.07	40.094
Ti_5Si_3 (211)	147.19	40.981	144.23	41.019	212.23	40.964	229.68	40.970
Ti_5Si_3 (300)	24.44	42.056	53.45	42.056	115.22	42.006	125.08	42.019
Ti_5Si_3 (112)	243.59	42.706	198.66	42.719	236.48	42.656	231.64	42.681
Ti_5Si_3 (202)	13.13	45.105	9.16	45.080	8.98	44.994	9.87	45.030
Mo_5Si_3 (222)	17.90	45.430	3.21	45.480	-	-	-	-
Ti_5Si_3 (221)	-	-	-	-	5.26	52.243	7.24	52.293
α-Ti (102)	27.65	53.054	10.39	53.092	9.65	53.092	4.89	52.779
Ti_5Si_3 (311)	2.90	54.328	4.11	54.341	15.37	54.304	13.33	54.292
β-Ti (200)	23.33	56.503	31.24	56.511	223.92	56.515	219.26	56.578
Ti_5Si_3 (400)	257.12	57.09	259.19	56.891	-	-	-	-
TiC (220)	-	-	11.09	60.702	42.41	60.664	58.52	60.740
Ti_5Si_3 (222)	9.70	61.515	33.34	61.502	39.49	61.402	40.57	61.427
α-Ti (110)	9.03	63.015	4.83	63.066	-	-	-	-
Ti_5Si_3 (312)	11.76	63.278	4.74	63.415	14.68	63.302	7.88	63.277
Ti_5Si_3 (321)	6.82	65.727	7.72	65.765	14.13	65.665	16.62	65.665
Ti_5Si_3 (213)	22.28	66.739	46.94}	66.653}	63.09	66.565	61.70	66.566
Mo_5Si_3 (442)	19.11	66.632			-	-	-	-
Ti_5Si_3 (402)	13.12	68.779	15.17	68.752	20.15	68.653	23.86	68.663
β-Ti (211) α-Ti (103)	140.99	70.814	105.11	70.863	236.48	70.877	200.80	70.940
TiC (113)	-	-	-	-	13.82	72.627	18.04	72.777
Ti_5Si_3 (004, 500)	53.59	73.538	37.16	73.539	25.96	73.512	26.82	73.502
α-Ti (112)	32.10	76.327	17.31	76.377	-	-	-	-
TiC (222)	-	-	-	-	28.83	76.412	13.44	76.490
α-Ti (201)	25.63	77.427	16.39	77.365	23.68	77.277	9.86	77.115
Ti_5Si_3 (420)	-	-	-	-	8.34	78.502	3.77	78.502
Ti_5Si_3 (331)	-	-	-	-	5.24	79.427	4.44	79.465

Table 19 Continued

SiC/Mo_5Si_3.Ti	1/2 hours		1 hour		2 hours		4 hours	
Identification	Int	2θ	Int	2θ	Int	2θ	Int	2θ
α-Ti (004)	11.02	82.501	7.39	82.439	-	-	-	-
Ti_5Si_3 (502)	34.82	84.076	51.07	84.062	75.87	84.051	82.39	84.026
Ti_5Si_3 (214)	58.83	85.188	31.25	85.133	10.65	85.126	10.83	85.189
Ti_5Si_3 (511)	-	-	-	-	4.01	86.026	4.92	86.064
α-Ti (202) Mo_5Si_3 (750)	17.85	87.038	13.93	87.000	19.07	87.050	19.92	87.038
Ti_5Si_3 (304)	10.59	88.505	12.14	88.525	16.80	88.462	19.80	88.475
α-Ti (104)	16.60	92.822	-	-	--	-	-	-
Mo_5Si_3 (514, 662)	23.93	96.996	27.36	96.960	75.14	96.922	75.95	96.922
Mo_5Si_3 (930)	87.90	98.171	68.98	97.696	-	-	-	-
Mo_5Si_3 (851)	4.36	100.033	-	-	-	-	-	-
α-Ti (203)	23.16	102.270	19.20	102.408	20.47	102.333	18.48	102.000
TiC (420)	-	-	-	-	4.74	105.920	13.86	105.120
Ti_5Si_3 (215)	9.55	108.619	20.18	108.970	24.51	108.594	23.39	108.632
β-Ti (222)	-	-	-	-	21.37	110.206	14.90	110.382
α-Ti (114)	18.02	114.567	13.45	114.604	22.67	114.506	-	-
α-Ti (212)	6.90	119.290	6.30	119.490	3.00	119.140	-	-
Ti_5Si_3 (621)	15.40	122.040	12.36	122.030	25.06	121.940	13.71	121.960
α-Ti (105)	26.40	122.565	28.52	122.565	-	-	-	-

ing to room temperature. Intrinsic stresses are also known to develop during sputtering.

The lattice parameter data for Ti and Ti_5Si_3 phases, for the SiC/Ti system, is presented in Table 20. The a and c parameters were calculated using Cohen's least squares analysis[119], with at least 18 lines for the titanium phase and at least 16 lines for the Ti_5Si_3 phase. The accuracy of the calculated lattice parameters was typically around ±0.001A. Comparisons of the volume of the titanium unit cell for the various times of exposure relative to the as-received condition shows that there was a very small change. Although Ti can accomodate upto 0.2wt% carbon[13], the volume changes in the present case are within experimental error. On the other hand, the volume of the Ti_5Si_3 phase increases systematically up to the 4 hour anneal (Table 20). The total change in the volume of the unit cell between the 4 hour anneal and the data in the card files for Ti_5Si_3 powders, is about 1.08%. This expansion could be due to interstitial carbon (from the SiC layer) entering the Ti_5Si_3 unit cell. This type of behaviour was also observed in a previous study[4] which showed that the X-ray line positions from Ti_5Si_3 were very close to the ternary Ti-Si-C phase[13]. This ternary phase can accommodate roughly up to 10 wt.%C. Table 20 also shows the total TiC integrated

intensity (for 6 lines) which increases upto the 4 hour anneal.

Similar lattice parameter data for the Ti reflections were also obtained for the SiC/Al/Ti and SiC/Mo_5Si_3 /Ti planar composites but are not reported because the changes were too small to be significant.

6.1.2 Optical Microscopy

Unetched samples from the various systems were examined under a Reichert[113] microscope using polarized light and an oblique illuminator. The SiC/Ti samples showed a reaction zone, even after a half hour anneal. The reaction zone for all the samples is very regular and appeared to be largely along grain boundaries. Figure 14 shows the general surface showing this structure, for a SiC/Ti sample that was annealed for 2 hrs. The sample that flaked after a half hour clearly shows cracks as well as a reaction zone that is at the Ti grain boundaries (figures 15 and 16). This suggests that the reaction could be nucleated at grain boundary sites with Si atoms diffusing preferentially along the Ti boundaries. Figure 15 also shows that the underlying Ti surface in the region where the film flaked is rough indicating that a significant part of the reaction also takes place at the SiC-Ti interface. The width of the reaction

TABLE 20

Lattice Parameter Data for the SiC/Ti System

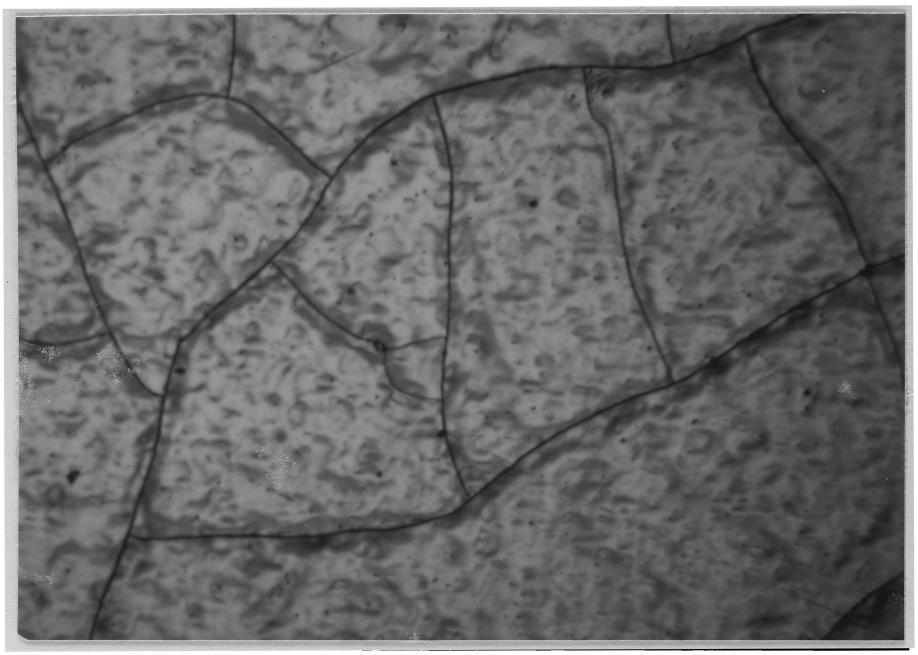
Lattice Parameters (A)

		Card file data	1/2 hr	1 hr	2 hrs	4 hrs
Ti.	a	2.950	2.950	2.950	2.949	2.949
	c	4.686	4.689	4.688	4.688	4.688
vol. (A^3)		35.32	35.34	35.32	35.30	35.30
Ti_5Si_3	a	7.429	7.446	7.446	7.448	7.453
	c	5.139	5.162	5.162	5.160	5.162
vol. (A^3)		245.63	247.82	247.84	247.86	248.29
Int. of TiC (6 lines)		-	228.91	325.88	380.85	481.50

zone increases with increasing annealing times as seen from figures 17-19, and this seems to correlate well with the increase in the amount of reaction products. The photomicrograph for the 4 hour anneal also shows the presence of a depletion zone alongside the reaction zones (Figure 18). Figures 19 and 20 show the photomicrographs for the SiC/Al/Ti system. The sample that was annealed for 1/2 hour shows large regions of discontinuous reaction zones. The widths of the reaction zones for this system are smaller than for the SiC/Ti system. This seems to correlate with the lower amounts of reaction in these samples. A similar behavior is observed for the SiC/Mo_5Si_3/Ti samples as seen from figures 22 and 23.

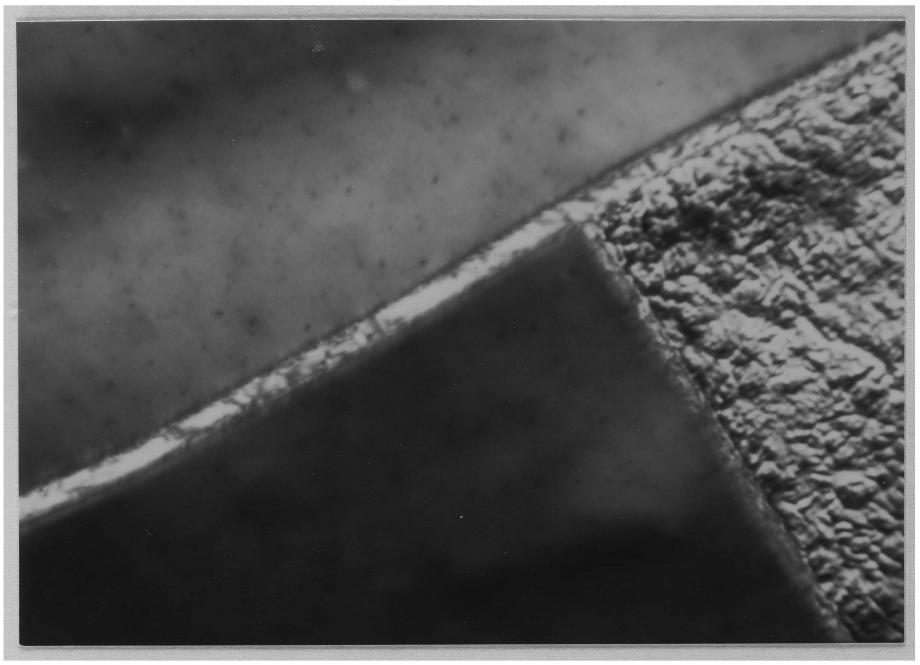
6.1.3 Relative Reaction Rates

Several X-ray methods were examined in order to arrive at a quantitative method that inter-relates the rate of silicide formation. The most obvious method would have been to follow the rate of decrease of SiC. However, the lack of crystalline reflections of SiC made this task difficult. A background intensity scan was also made to obtain a rate of decrease of SiC, but this did not give meaningful results. However, one method gave systematic results that could be used to evaluate the effectiveness of Mo_5Si_3 and Al films in



Magfn. 40X

Fig. 14 Photomicrograph of the SiC/Ti sample annealed at 875^{o}C for 2 hours.



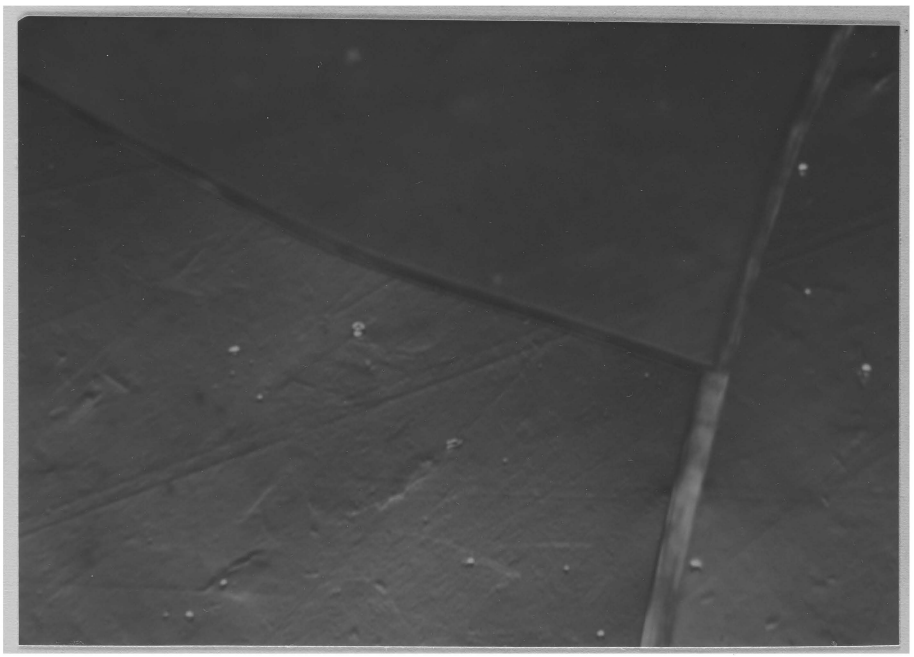
Magfn. 630X

Fig. 15 Photomicrograph of the SiC/Ti sample annealed at 875^{o}C for 1/2 hr., showing flaking.



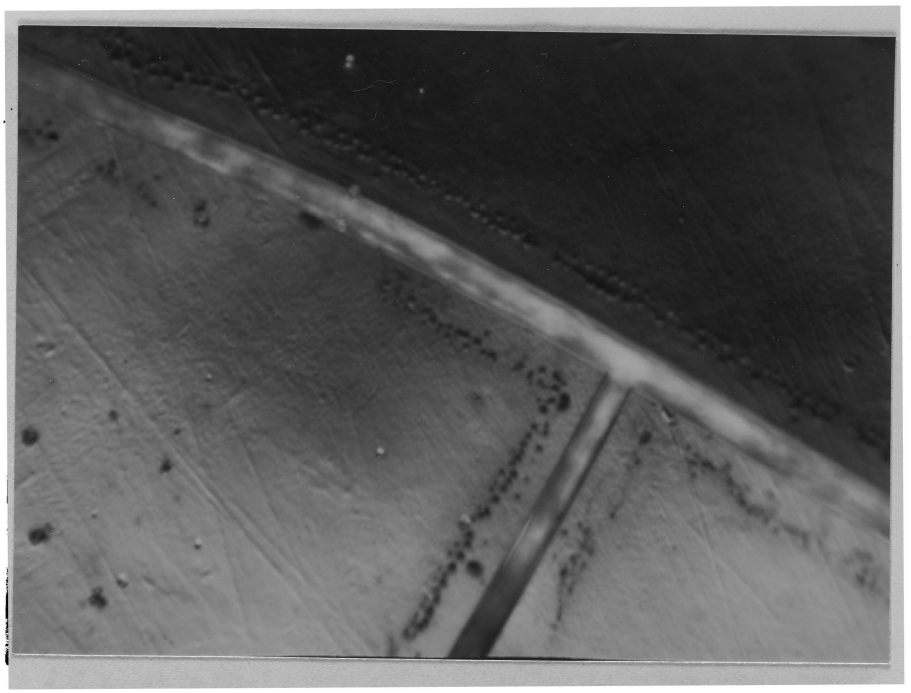
Magfn. 630X

Fig. 16 Photomicrograph of the SiC/Ti sample annealed at 875^{o}C for 1/2 hr. (polarized light).



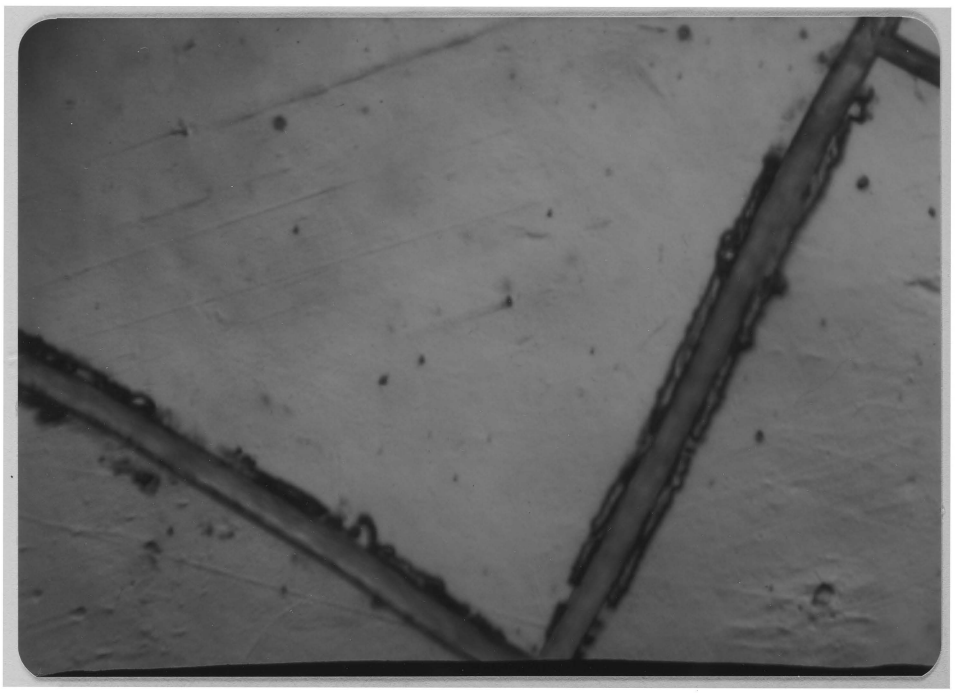
Magfn. 630X

Fig. 17 Photomicrograph of the SiC/Ti sample annealed at 875^{o}C for 1 hr., showing widening of the reaction zone.



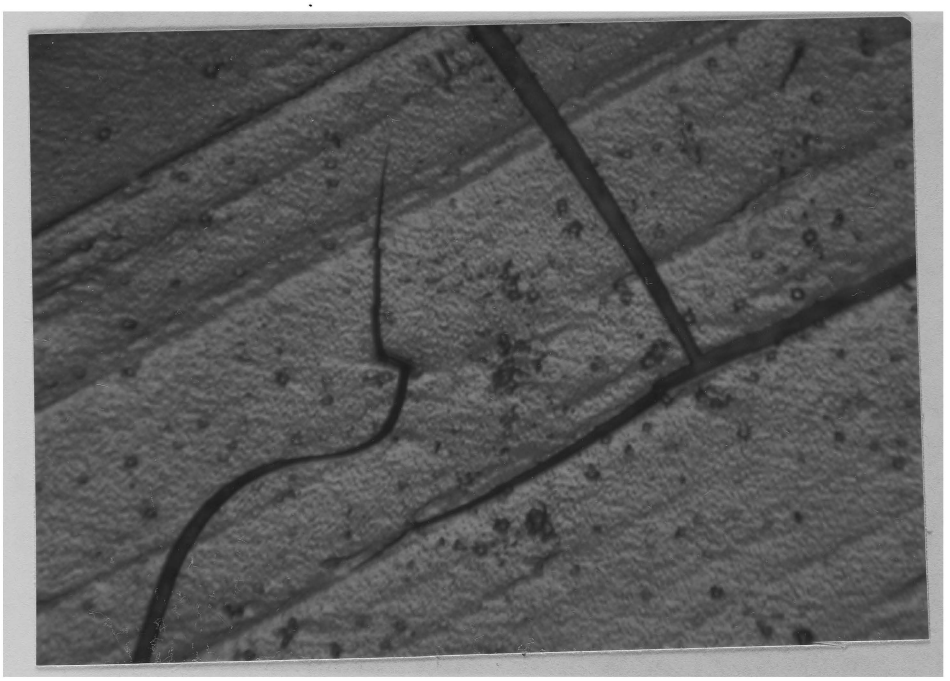
Magfn. 630X

Fig. 18 Photomicrograph of the SiC/Ti sample annealed at 875^{o}C for 4 hrs., showing a depletion zone alongside the reaction zone.



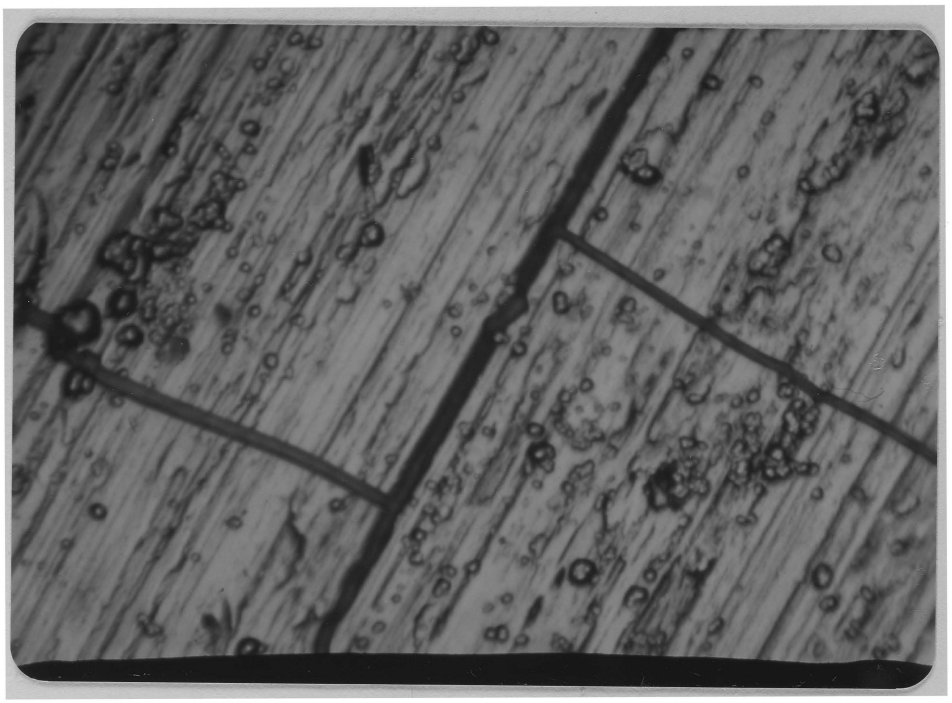
Magfn. 630X

Fig. 19 Photomicrograph of the SiC/Ti sample annealed at 875^{o}C for 6 hours.



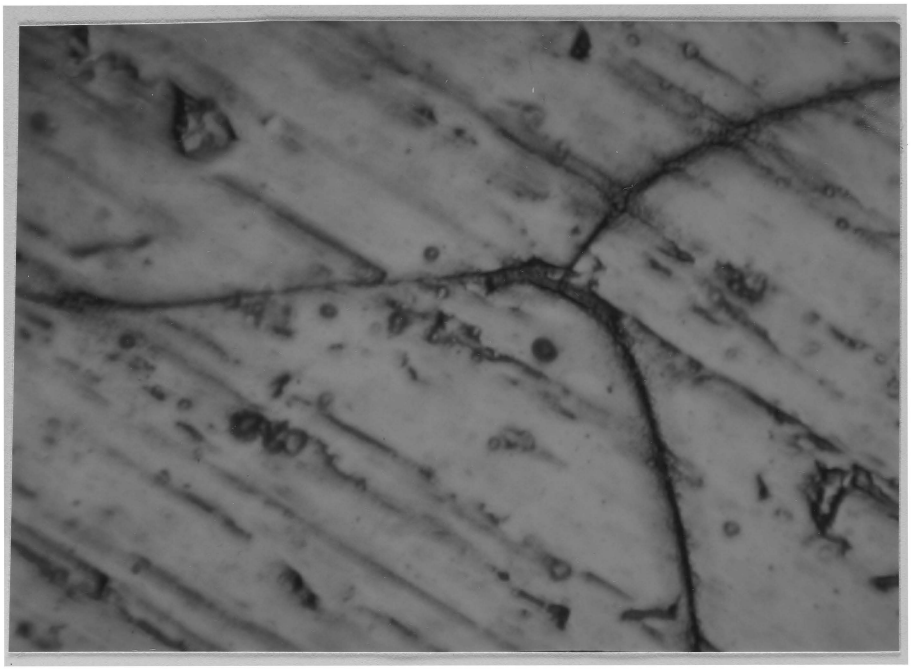
Magfn. 630X

Fig. 20 Photomicrograph of the SiC/Al/Ti sample annealed at 875^{o}C for 1/2 hr., showing discontinuous reaction zones.



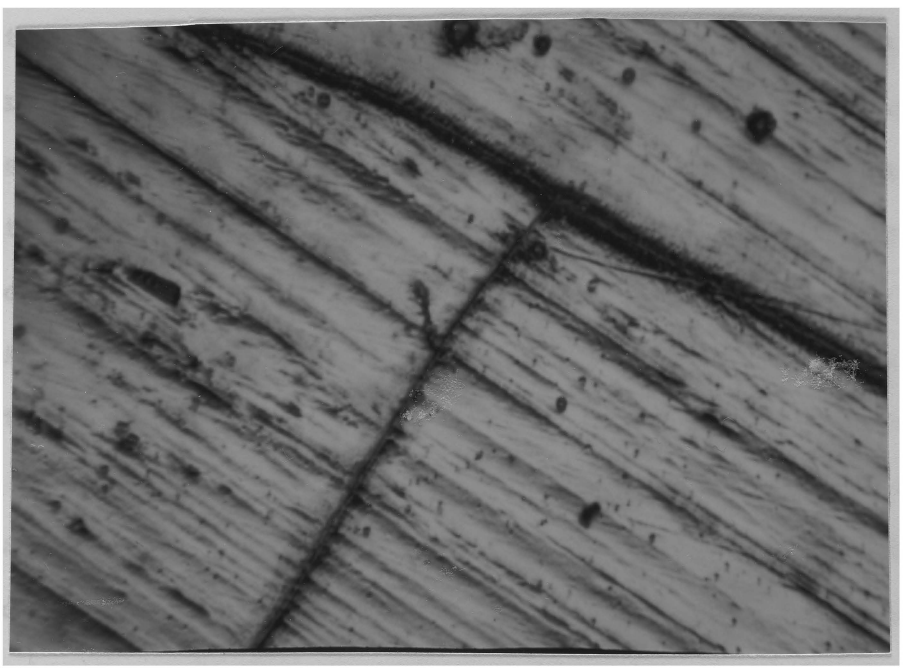
Magfn. 630X

Fig. 21 Photomicrograph of the SiC/Al/Ti sample annealed at 875^{o}C for 2 hours.



Magfn. 630X

Fig. 22 Photomicrograph of the SiC/Mo_5Si_3/Ti sample annealed at 875^{o}C for 1/2 hour.



Magfn. 630X

Fig. 23 Photomicrograph of the SiC/Mo_5Si_3/Ti sample annealed at 875^{o}C for 2 hours.

suppressing interface silicide formation. These results will be of considerable value in selecting the best interface film and also in designing a suitable procedure for hot-pressing composite panels.

The major silicide product associated with SiC/Ti matrix reactions has been Ti_5Si_3 . This phase also gives a large number of diffraction lines in this investigation. In previous studies(4), one finds that the initial stage of interface reaction is of importance in determining the mechanical properties of composites. Ideally, one would like to obtain as-pressed composites that are in the earliest stage of this interface reaction. If one concentrates on this stage, it is possible to make certain simplifying assumptions that enable x-ray data to be interpreted without a detailed model of the morphology of the various reaction products. It may be assumed that the rate limiting step is the diffusion of Si from the SiC filament to the alpha (or beta) titanium substrate producing mainly Ti_5Si_3 . Also, the absorption of the incident and diffracted beams for both Ti_5Si_3 and Ti diffraction lines is the same. This assumption is most easily visualized for SiC/Ti samples without an intermediate film (figure 24). With intermediate reaction products such as certain Ti-Al compounds, one must assume that these act as equivalent absorbers for diffraction lines

from the Ti substrate and Ti_5Si_3 (see figures 25 and 26). If the Si atoms are transported primarly along grain boundaries of the Ti substrate to "feed" silicide nuclei for further growth, the assumption of equi-absorption is reasonable. Even if a layer is present and the thickness of this layer is small, absorption through the layer may be neglected.

Ten pairs of lines, with a Ti_5Si_3 line and an alpha-titanium line to a pair, were selected such that each pair had Bragg angles that are nearly the same (see tables 21 - 23). The pairing in terms of Bragg angle gives nearly equivalent absorption path lengths. By summing all ten ratios, a set of internally consistent plots are obtained for all annealed samples.

The Mo_5Si_3 barrier film presented special problems because the dominant substrate phase was beta titanium and not alpha titanium. To overcome this difficulty, the total beta integrated intensity was redistributed into the ten alpha titanium lines according to the theoretical distribution as obtained from the integrated intensity for random powders. It was found that the Mo_5Si_3/Ti standards also give the Ti_5Si_3 phase and a beta titanium matrix. In fact, this amount of Ti_5Si_3 accounts for about 50% of the Ti_5Si_3 intensity from SiC/Mo_5Si_3/Ti samples. In order to relate all results to Ti_5Si_3 formation which is associated with Si

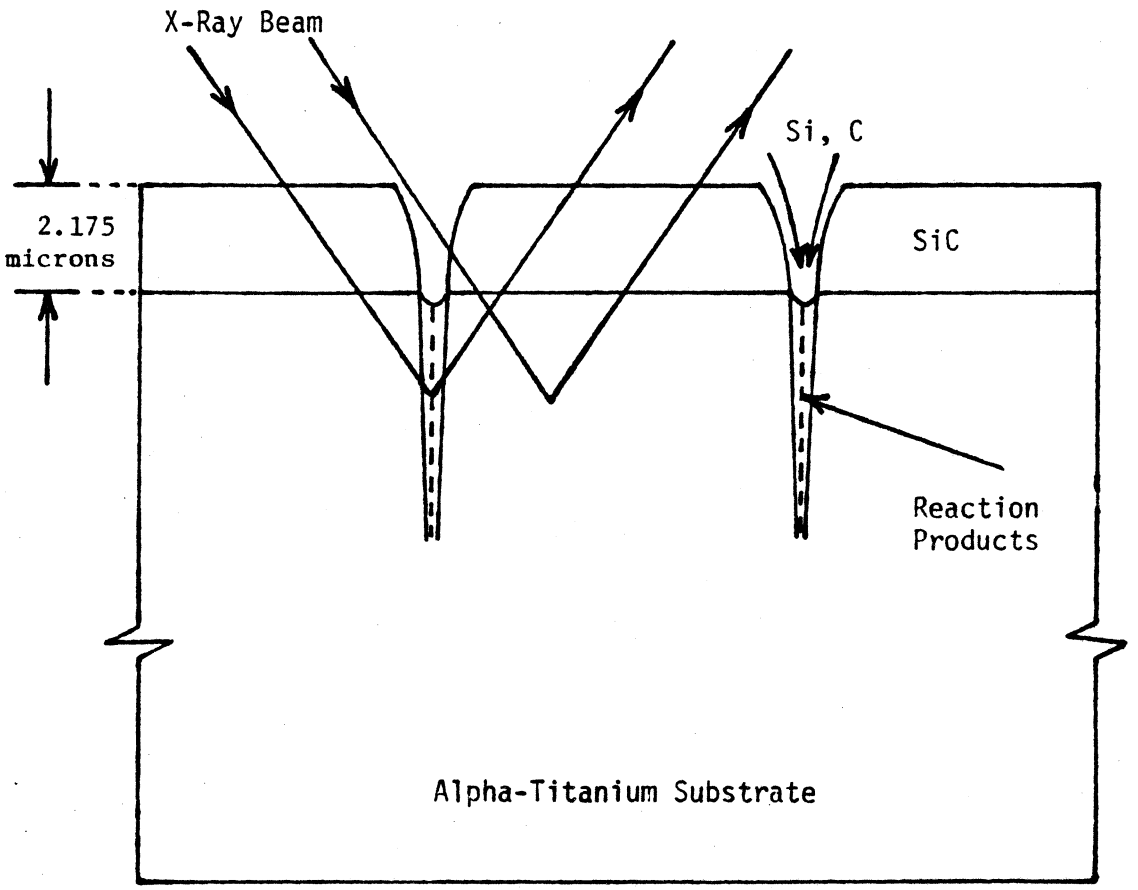


Figure 24: Schematic of a SiC/Ti planar composite used to illustrate equivalent absorption path lengths.

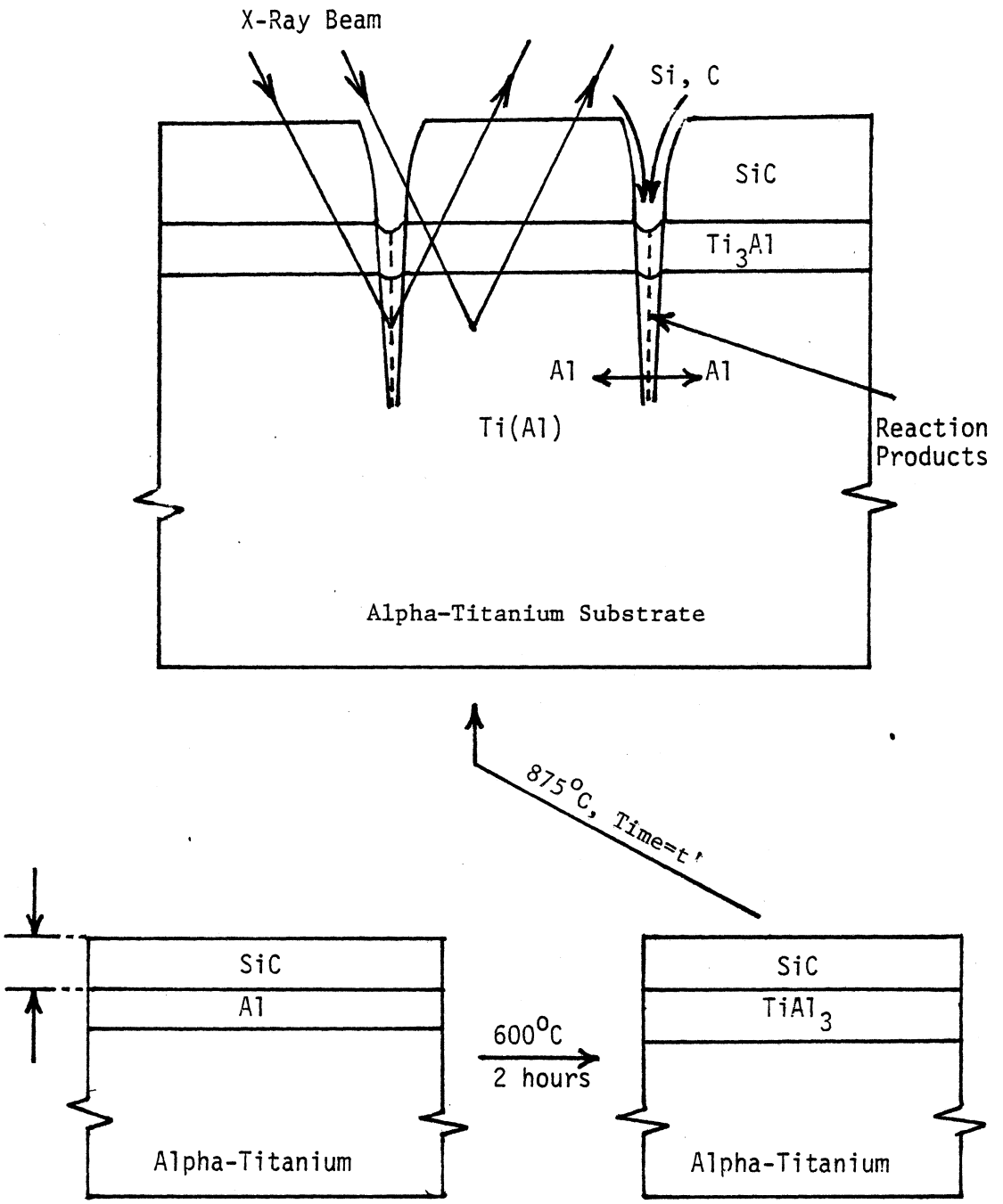


Figure 25: Schematic of a SiC/Al/Ti planar composite used to illustrate equivalent absorption path lengths.

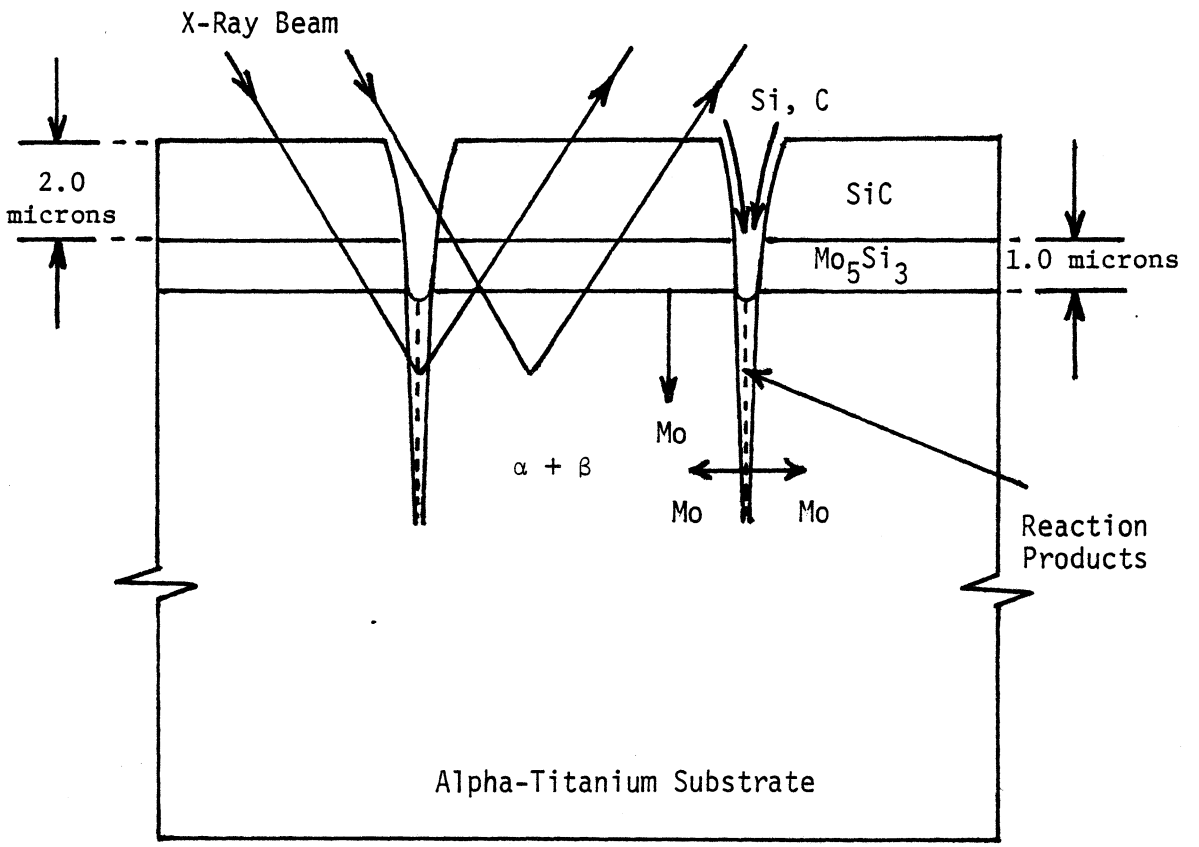


Figure 26: Schematic of a SiC/Mo Si /Ti planar composite used to illustrate equivalent absorption path lengths.

TABLE 21

Table showing the ratios for Ti_5Si_3/Ti reflection pairs for the SiC/Ti system

Reflection Pair	Ratio for 1/2 hr	Ratio for 1 hr	Ratio for 2 hrs	Ratio for 4 hrs
Ti_5Si_3 (200) α-Ti (100)	0.13	0.13	0.36	0.78
Ti_5Si_3 (210) α-Ti (002)	0.12	0.29	0.60	0.64
Ti_5Si_3 (211) α-Ti	0.20	0.19	0.38	0.60
Ti_5Si_3 (221) α-Ti (102)	0.00	0.02	0.06	0.08
Ti_5Si_3 (222) α-Ti (110)	0.22	0.23	0.30	0.38
Ti_5Si_3 (420) α-Ti (201)	0.00	0.03	0.07	0.15
Ti_5Si_3 (331) α-Ti (004)	0.00	0.07	0.28	0.77
Ti_5Si_3 (511) α-Ti (202)	0.00	0.04	0.16	0.25
Ti_5Si_3 (521) α-Ti (203)	0.00	0.00	0.04	0.00
Ti_5Si_3 (532) α-Ti (204)	0.00	0.14	0.42	0.78

TABLE 22

Table showing the ratios for Ti_5Si_3/Ti reflection pairs for the SiC/Al/Ti system

Reflection Pair	Ratio for 1/2 hr	Ratio for 1 hr	Ratio for 2 hrs	Ratio for 4 hrs
Ti_5Si_3 (200) α-Ti (100)	0.214	0.226	0.310	0.209
Ti_5Si_3 (210) α-Ti (002)	0.186	0.219	0.217	0.201
Ti_5Si_3 (211) α-Ti (101)	0.266	0.198	0.425	0.434
Ti_5Si_3 (221) α-Ti (102)	0.0	0.046	0.121	0.266
Ti_5Si_3 (222) α-Ti (110)	0.133	0.145	0.157	0.000
Ti_5Si_3 (420) α-Ti (201)	0.0	0.193	0.0	0.0
Ti_5Si_3 (331) α-Ti (004)	0.0	0.0	0.0	0.0
Ti_5Si_3 (511) α-Ti (202)	0.0	0.0	0.0	0.0
Ti_5Si_3 (521) α-Ti (203)	0.0	0.0	0.0	0.0
Ti_5Si_3 (532) α-Ti (204)	0.0	0.0	0.0	0.0

TABLE 23

Table showing the ratios for Ti_5Si_3/Ti reflection pairs for the SiC/Mo_5Si_3/Ti system

Reflection Pair	Ratio for 1/2 hr	Ratio for 1 hr	Ratio for 2 hrs	Ratio for 4 hrs
Ti_5Si_3 (200) α-Ti (100)	0.856	0.791	0.409	0.458
Ti_5Si_3 (210) α-Ti (002)	0.0	0.044	0.248	0.258
Ti_5Si_3 (211) α-Ti (101)	0.035	0.088	0.241	0.311
Ti_5Si_3 (221) α-Ti (102)	0.0	0.0	0.049	0.075
Ti_5Si_3 (222) α-Ti (110)	0.157	0.176	0.102	0.134
Ti_5Si_3 (420) α-Ti (201)	0.0	0.05	0.065	0.038
Ti_5Si_3 (331) α-Ti (004)	0.0	0.152	0.271	0.272
Ti_5Si_3 (511) α-Ti (202)	0.0	0.0	0.164	0.249
Ti_5Si_3 (521) α-Ti (203)	0.0	0.0	0.0	0.0
Ti_5Si_3 (532) α-Ti (204)	0.0	0.0	0.0	0.0

coming only from the SiC, a correction was necessary for the SiC/Mo_5Si_3/Ti samples. The intensity for each Ti_5Si_3 line from the corresponding Mo_5Si_3 sample was corrected for suitable absorption if a SiC film was present, and subtracted. The intensity ratios were then calculated and summed over pairs (see solid curve in figure 27). The dashed curve illustrates the uncorrected results for SiC/Mo_5Si_3 /Ti samples.

The data for SiC/Ti samples that flaked after a half hour anneal also had to be corrected slightly. This was done by obtaining the area fraction of flaked film from a photomicrograph taken before X-ray studies. The Ti intensities were decreased in proportion to the amount of absorption that would have resulted if the SiC film was intact. The Ti_5Si_3 intensities were increased based on the area fraction of flaked film.

Figure 27 shows the sum of the ratios of the integrated intensities from Ti_5Si_3 and alpha titanium, versus annealing time. It is seen that for the SiC/Ti system, the ratio increases continuously with increasing annealing times. This rate curve can be compared with those for the SiC/Al/Ti and SiC/Mo_5Si_3/Ti planar composites to determine the effectiveness of either coatings in retarding silicide formation.

The SiC/Mo_5Si_3/Ti composites that have not been corrected for Ti_5Si_3 formation at the Mo_5Si_3 interfaces have a high rate of silicide formation during the initial stages at 675°C. The ratios of Ti_5Si_3 to alpha titanium are larger than those for the samples without a barrier film. For longer annealing times there appears to be a saturation of the silicide formation. It was mentioned earlier that Mo_3Si dissociation at the interface was probably responsible for silicide formation during the early stages. When all of the Mo_3Si phase is consumed, silicide formation could continue with Si transfer from the SiC film along Ti grain boundaries. Thus, if the Mo_5Si_3 film is 'broken' in these regions, the barrier film will not be effective. Instead, as more Mo enters the Ti substrate, the formation of additional Ti_5Si_3 is reduced by the presence of a Mo saturated beta-Ti phase.

The rate curve for the SiC/Mo_5Si_3/Ti planar composites which has been corrected against the Mo_5Si_3 standards is also shown in Figure 27. Although it may appear from the corrected values that Mo_5Si_3 is an effective barrier, the high overall rate is important in the design of these composites. If the Mo_5Si_3 phase can be sputter-deposited without any Mo_3Si at the interface, this barrier film may be useful. However, if stoichiometric Mo_5Si_3 targets are used,

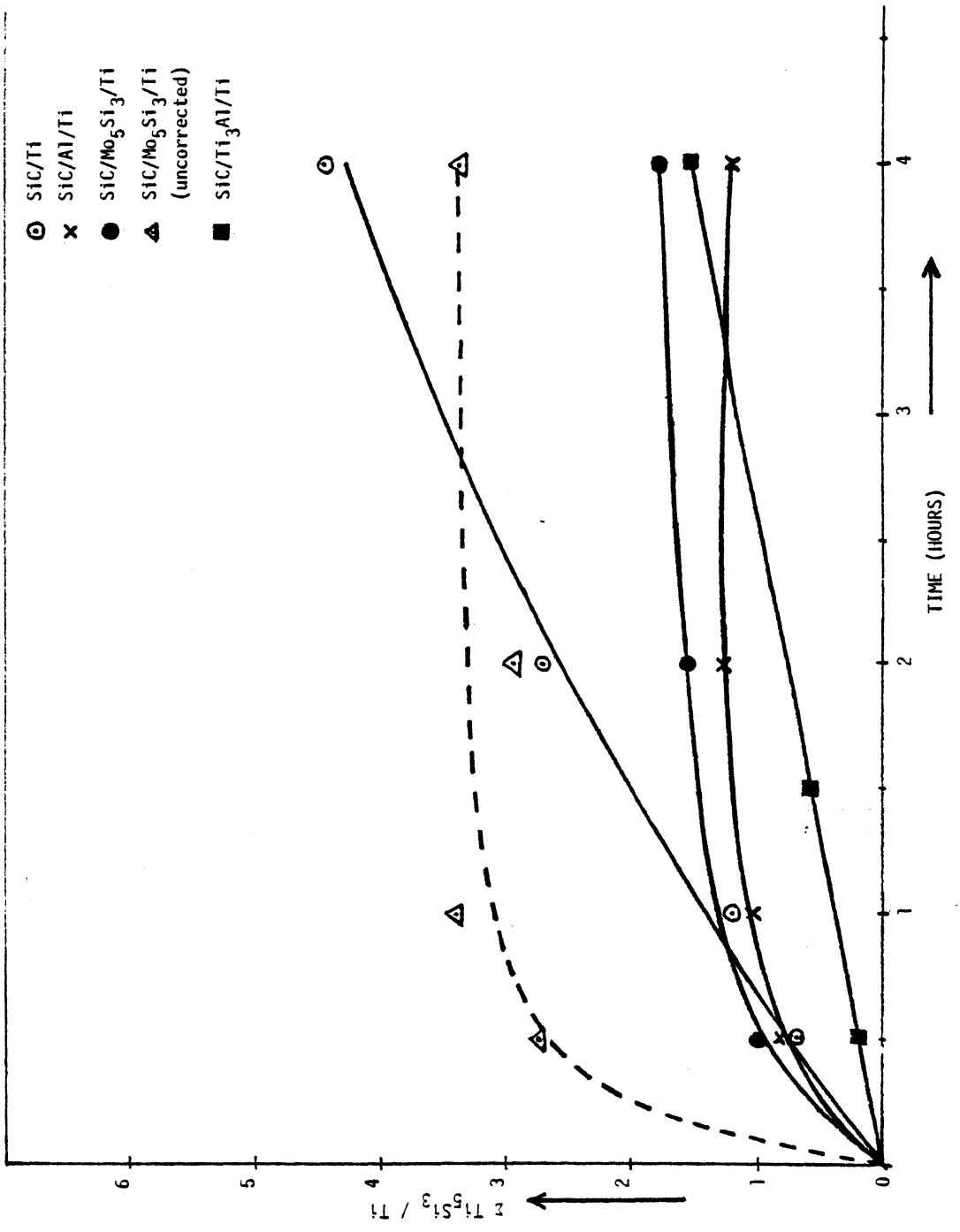


Figure 27: Reaction rate curves for the various planar composite systems.

there is a tendency for silicon to resputter, resulting in nonstoichiometric films. Another reason for a lack of stoichiometry is a non-equilibrium situation in the initial stages of sputter-deposition.

The rate curve for SiC/Al/Ti planar composites shows a trend similar to the SiC/Mo_5Si_3/Ti composites. During the first hour at 875°C, it is evident that the Al film is not very effective in reducing silicide formation. This is due to a lack of an Al saturated matrix (as will be described in a later section) initially. Data for samples annealed at 600°C for 2 hours shows that there is a small amount of Al solid solubility. This remains nearly constant up to the 1 hour anneal at 875°C during which time Ti-Al compounds continue to form and dissolve. For longer times the only Ti-Al compound is Ti_3Al and when this dissolves, the Al solid solution increases. This gives a low reaction rate by the rejection mechanism.

It may be useful to obtain reaction rates from the curves in Figure 27. The initial reaction occuring up to 1 hour is nearly the same for the SiC/Ti standards and for samples with Al and Mo_5Si_3 films. Consequently, the amount of reaction that took place in 1 hour can be ignored in calculating the rates for longer times. A least squares fit was used to fit the three points at 1,2 and 4 hours. This gave the following slopes (intensity/hour).

Sample	Reaction Rate (Int./hour)
SiC/Ti	1.660
SiC/Mo_5Si_3/Ti	0.248
SiC/Al/Ti	0.057

If the integrated intensities are taken to be proportional to the volume fraction of Ti_5Si_3, the tabulated values can be related to the relative volume of Ti_5Si_3 formed per hour. When normalized one obtains:

$$\frac{R\ (SiC/Al/Ti)}{R\ (SiC/Ti)} \simeq \frac{1}{29}$$

and

$$\frac{R\ (SiC/Mo_5Si_3/Ti)}{R\ (SiC/Ti)} \simeq \frac{1}{7}$$

These results strongly support the use of Al films on Ti foils in the preparation of SiC/Ti matrix composites. Moreover, Al films are more desirable compared, to the brittle Mo_5Si_3 films and can also be deposited with ease.

6.2 INTERFACE REACTIONS IN AL THIN FILMS ON TITANIUM SUBSTRATES

In the previous section, the use of Al films on Ti foils in the preparation of SiC/Ti matrix composites appeared to have advantages in controlling interface reac-

tions over the Mo_5Si_3 films. However, many open ended questions remained such as the optimum thickness of Al films as well as the optimum thermal cycle for hot-pressing. Therefore, it was essential to study the behavior of the Al/Ti planar standards in greater depth.

These standards were investigated after thermal exposures similar to those for the SiC/Al/Ti system. A hold at 600°C was required before proceeding to the higher temperature (close to the hot-pressing temperature), so that Ti-Al compounds form before heating through the melting temperature for Al (660°C). Al (1 Micron)/titanium samples were studied at 600°C as well at 900°C for various times. X-ray diffraction analysis on the samples reacted at 600°C showed the presence of alpha titanium and $TiAl_3$ as well as a few extra lines from the Ti_8Al_{24} phase. This seems to be consistent with the reported[25] existence of two crystallographic modifications of $TiAl_3$, below 600°C. However, in order to study the interdiffusion of Al and Ti without unnecessary complications, samples were reacted so as to form only the TiAl phase. To achieve this, the samples were quickly taken to 635°C, for 1/2 hour, 1 hour and 2 hours.

It was essential to know whether the $TiAl_3$ was randomly dispersed near the interface or whether it was in the form

of a uniform layer. An absorption analysis was performed based on two models - one assuming a layer and the other assuming random distribution. If a layer was present, the reduced* integrated intensity from the $TiAl_3$ diffraction lines would be proportional to $[1-\exp(-2\mu G_t/\sin\theta)]$, where G_t is the layer thickness. On the other hand, the intensities from a random assumption would be independent of the diffraction angle. It was found that the experimental intensities from $TiAl_3$ could be best related to the theoretically obtained ones based on a layer assumption. Table 24 gives the data for the sample that was annealed for 1/2 hour in addition to calculation based on these models.

The $TiAl_3$ layer thickness was determined in each case from the attenuation of the integrated intensities of 14 well separated alpha-titanium lines. The intensity from the alpha-titanium phase below the $TiAl_3$ layer is proportional to $\exp(-2\mu G_t/\sin\theta)$. The average thickness for the 1/2 hour anneal was found to be 1.08 microns while for the 1 hour anneal it was 0.93 microns. A theoretical calculation for the thickness of $TiAl_3$ was also performed based on the mass

---

* note: If a layer is present, the reduced intensity is given by

$$\frac{I}{I_0 Q\, p\, |F|^2} = \left[1-\exp\left(\frac{2\,\mu G_t}{\sin\theta}\right)\right]$$

where the terms have their usual meaning (see Chapter 5). For a random assumption the right side of the above equation would be equal to 1.

TABLE 24

Comparison of the layer or random assumption for $TiAl_3$ at 635°C , 1/2 hour.

hkl	Random	Observed	Film
002	3.71	5.91	6.41
101	8.69	14.68	12.65
110	2.08	1.70	2.45
112,103	100.00	100.00	100.00
004	20.45	19.36	19.24
200	28.45	25.53	24.17
114,211	2.19	1.54	1.65
204,006	21.00	13.67	13.57
220	8.67	5.61	5.32
116,301	13.70	8.22	7.86
224,206	10.00	4.74	5.24

conservation of Al atoms using the following relations:

$$n_{Al}\ (t=0) = n_{Al}\ (t=1/2 \text{ hour or } 1 \text{ hour})$$

$$G_{Al}{}^{A}\rho_{Al} = G_{TiAl_3}{}^{A}\rho_{TiAl_3}$$

where

n is the total number of Al atoms

A is the area of cross section of the sample

Y is the thickness of the layer and

ρ is the atom density (no. of atoms/unit cell)

The calculated thickness was 1.33 microns. The difference between this thickness and the measured values is due to a local decomposition of $TiAl_3$ at the interface with Al going into the alpha-titanium lattice. Diffraction lines showed a broadening on the high two-theta side indicative of a range of compositions. This type of composition broadening is known as an intensity band[92] and the related theoretical aspects were discussed in Chapter 3. The intensity bands can be used to determine composition profiles and hence diffusion coefficients. This will be discussed in a later section on 'Diffusion studies in Al/Ti thin films' .

A comparison of the integrated intensities for the TiAl diffraction lines was made for the 1/2 hour and 1 hour anneal. This was done after allowing for a small correction due to the absorption of the X-ray beam within the TiAl

layer according to the relation $[1-\exp(-2\mu G_t/\sin\theta)]$. There was a 10% average decrease in the integrated intensity of six corresponding diffraction lines from $TiAl_3$, between the 1/2 hour and 1 hour anneal. This seems to be in reasonable agreement with the decrease of the $TiAl_3$ layer thickness (14%) between the two anneals. The diffraction lines from a sample annealed for 2 hours at 635°C showed that the TiAl phase was just beginning to form.

The Al(1 micron)/Ti samples that were annealed at 900°C for 15 min, 30 min, 1 hr, 2 hrs, 4 hrs, 8 hrs and 16 hrs, were examined by X-ray diffraction. In the shorter time anneals (upto 4 hours), a number of reflections from the tetragonal TiAl phase (a= 4.015A and c= 4.062A) were observed. The integrated intensities from these lines decreased consistently from the 15 min. anneal upto 4 hours and the lines disappeared after 8 hours. Also, the two-theta positions from these TiAl reflections indicated that the lattice tended to become more and more cubic before the TiAl phase disappeared.

Diffraction lines from Ti_3Al (nearly the same two-theta positions as Ti_2Al) appeared even from the 15 min anneal and remained upto the 16 hr anneal. Integrated intensities from 7 strong Ti_3Al lines were obtained and summed for each anneal. This sum showed a systematic increase for increas-

ing annealing times as shown in Figure 28. After a 4 hour anneal there is a trend showing a nearly constant or small decrease in Ti_3Al intensity. Also plotted in Figure 28 are the peak heights of the intensity bands that correspond to Al-rich alpha-titanium.

This shows that initially while the other Ti-Al compounds such as TiAl, etc, form and dissolve, the peak heights of the intensity band is more or less constant. During this time, the Al that is released in the dissociation of the TiAl compounds is being used to form more Ti_3Al. For longer annealing times (when Ti_3Al is the only phase), the Ti_3Al partially dissociates and the Al released goes into the alpha-titanium solid solution. The peak heights of the intensity bands increase significantly, until after the 16 hour anneal, the matrix contains more Aluminum. This is observed by a total peak shift towards the higher two-theta positions.

The object of this part of the study was to determine the optimum thickness of the Al films that were necessary to yield the lowest amount of silicide formation and hence better mechanical properties of the composite. Clearly, if a 1 Micron film of Al was to be used, then at least a 4 to 8 hour pre-anneal on the Al/Ti panels may be necessary before the SiC/Al/Ti composites can be hot-pressed. This condition is necessary to ensure that enough Al is introduced into the

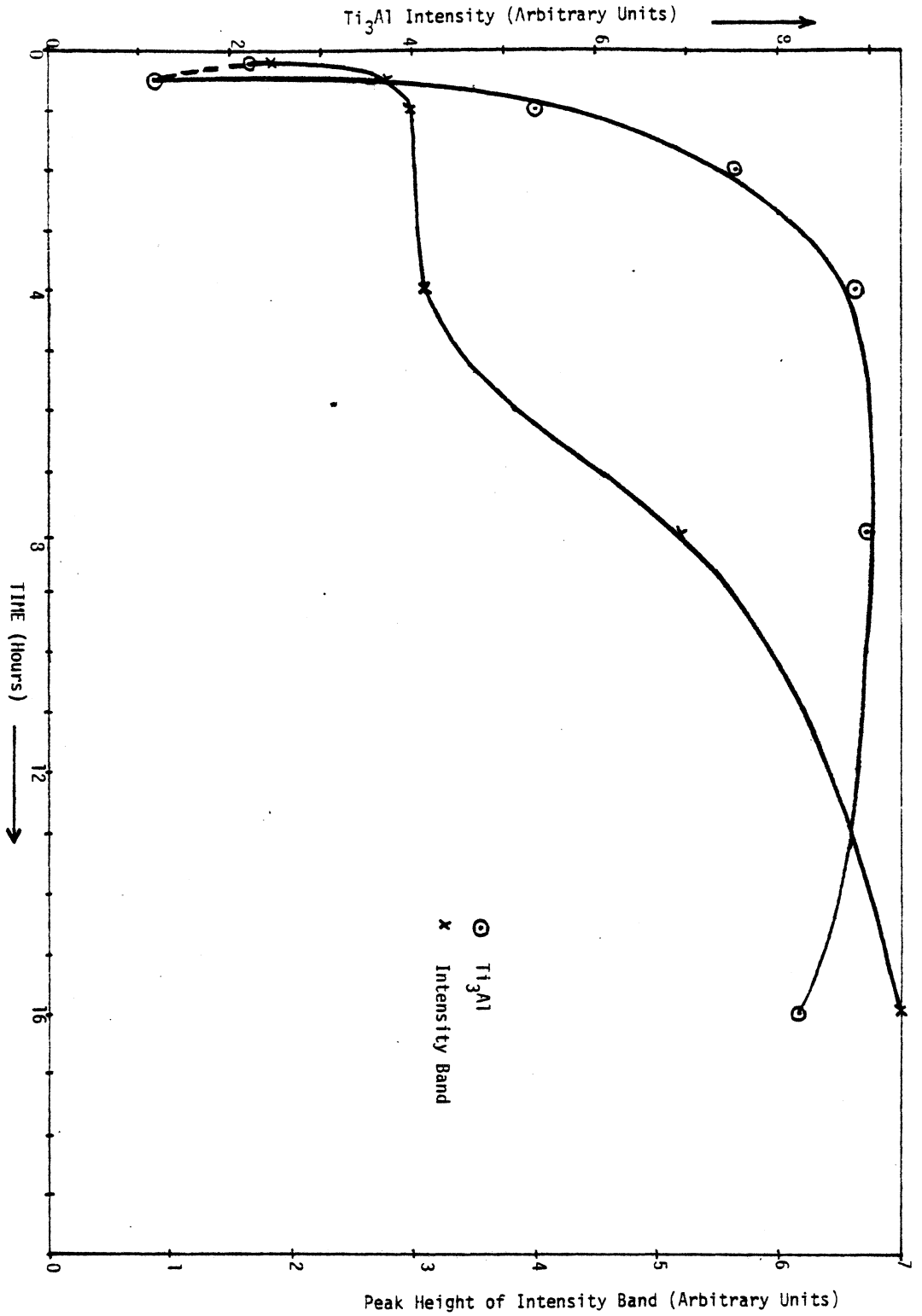


Figure 28 : Reaction kinetics for the 1 micron Al film samples.

alpha-titanium matrix so that silicide formation by the rejection mechanism, is minimized. It may help to recall that a lack of Al in the matrix for the SiC/Al/Ti planar composites, is the reason for the high rate of silicide formation for the early annealing times in figure 27. Therefore, it was neccessary to experiment with smaller Al thicknesses, so that the early stages of the reaction kinetics is completed even before the shortest annealing time (1/2 hr).

Therefore, 0.4, 0.5 and 0.64 micron Al thin films on Ti were annealed for 1/2hr, 1hr, 2hrs and 4hrs and examined by X-ray diffraction. A preliminary study on the 0.64 micron thin films indicated a behavior somewhat similar to the 1 micron samples, although to a lesser extent. In this case a 2 to 4 hour preanneal would be necessary before fabrication, to ensure adequate intensity band formation.

For the 0.4 and 0.5 micron thin films, integrated intensity measurements on a few reflections from Ti_3Al and the intensity band were obtained. The results are shown in Figure 29. For the 0.4 micron samples, it is seen that between a 1/2 hr and 1hr anneal, Ti_3Al is continuing to form. At this time, the intensity band increases only slightly. After 2 hours, Ti_3Al dissociates and the solid solution increases and the overall increase in intensity is 33%. In the 0.5 micron samples however, intensity band for-

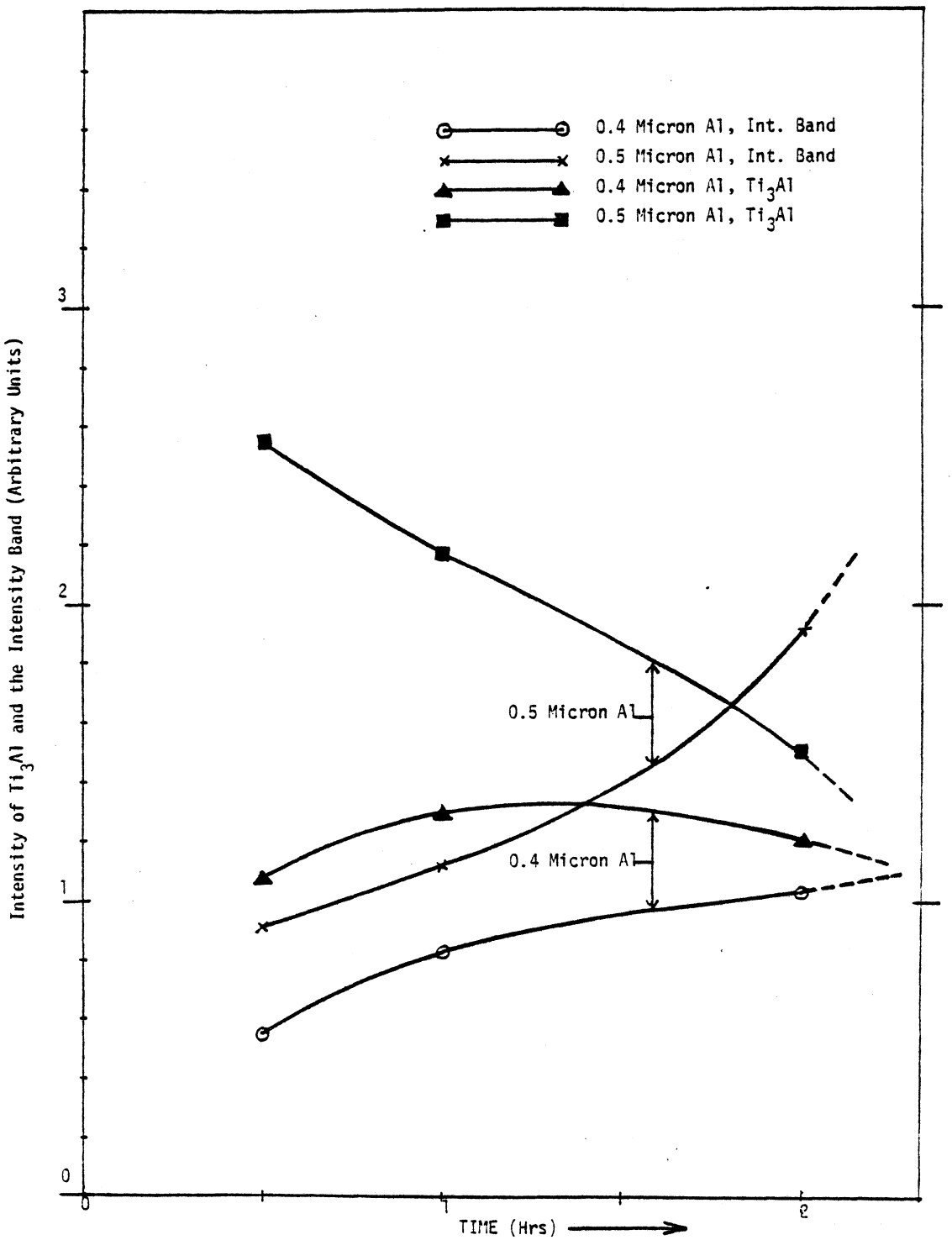


Figure 29: Reaction kinetics for the 0.4 and 0.5 micron Al film samples.

mation increases continuously from the 1/2 hr up to the 4 hr anneal (53% increase). Also, the amount of Ti Al in these samples is larger and this could act as the source of Al atoms for saturation of the alpha titanium matrix. With reference to figure 29, if 0.5 micron Al thin films are used and a 1 hour pre-anneal was given to the panels, silicide formation during the composite fabrication cycle could be greatly minimized. Also, the choice of a 0.5 micron Al film would ensure that approximately 85% of the Ti Al layer would remain and act as a source of Al atoms during fabrication and during service.

In the various Al/Ti thin films discussed until now, no mention was made of a possible occurence of the Ti Al phase. This phase was observed by Ence and Margolin[74] who proposed that below 700°C, the Ti_3Al phase dissociates to yield Ti_2Al and alpha-titanium. Many authors[50-60] have not observed this phase. In the present investigation, the Ti_3Al was the predominant phase in all the diffusion anneals. It is likely that Ti_2Al is an extension of the Ti_3Al phase with nearly similar lattice parameters.

6.3 CONTROL OF INTERFACE REACTIONS IN SIC/TI_3AL/TI PLANAR COMPOSITES.

The SiC/Ti_3 Al/Ti planar composites that were annealed at 875°C for 1/2 hr, 1.5hrs and 4hrs were studied using

X-ray diffraction. As with the SiC/Al/Ti composites, the SiC phase was amorphous both in the as-sputtered condition as well as after thermal treatments. A 1/2 hour anneal at 875°C gave only 5 weak Ti_5Si_3 reflections. A number of reflections from Ti_3Al were observed. Because of the nature of preparation of these planar composites (1 hour preanneal of Al(0.5 microns)/Ti before SiC deposition), there was appreciable intensity band formation. Compared to a 1/2 hour anneal of the SiC/Al/Ti composites, the integrated intensities as well as the number of Ti_5Si_3 lines was considerably lower. No lines from TiSi and $TiSi_2$ were observed even upto the longest anneal (4 hours). No other Ti-Al compounds were observed.

For longer annealing times (1.5hr and 4 hrs) a few more Ti Si reflections were noticed and the integrated intensities from Ti_5Si_3 increased consistently. The intensity band formation increased systematically upto the 4 hour anneal during which time the Ti_3Al intensities decreased. The overall decrease in Ti_3Al integrated intensity was nearly 11%. Again, no other silicides or Ti-Al compounds were observed. The lines from the matrix were entirely from the alpha-phase since Al tends to stabilize it. In all the anneals, there was some evidence of Ti_3AlC being formed, although overlapping lines from the Ti_3Al phase prevented an

unambiguous identification. The integrated intensities as well as two-theta positions for the various phases discussed are given in Table 25.

6.3.1 Relative Reaction Rates

The procedures employed in the determination of the relative reaction rates for the SiC/Ti_3Al/Ti system were the same as those discussed for the other systems. Table 26 shows the ten pairs of lines, from which the total ratio of the integrated intensity from Ti_5Si_3 with respect to alpha-titanium, was calculated. The integrated intensity from alpha-titanium lines was taken to be that from the entire intensity band. The relative reaction rates are shown in figure 27 along with the data for the other systems.

It is evident from figure 27 that for early reaction times (1/2 hr) the amount of reaction and the rate for SiC/Ti Al/Ti is considerably lower than the SiC/Al/Ti composites (about 83% lower). After 1 hour however, the reaction rate increases linearly and when compared to the SiC/Al/Ti composites, the reduction in silicide formation is about 55%. Comparison of the reaction rates for the two 4 hour anneals shows that the SiC/Ti_3Al/Ti composite has nearly the same (or sligthly greater) amount of silicide formation. These results do indicate that the Al rejection

TABLE 25

Integrated intensities and two theta positions for the SiC/Ti_3Al/Ti samples annealed at 875°C for various times.

	1/2 hour		1 1/2 hours		4 hours	
Identification	**Int**	**2θ**	**Int**	**2θ**	**Int**	**2θ**
Ti_3Al (101)	26.37	26.125	25.06	26.138	19.45	26.125
Ti_5Si_3 (200)	-	-	5.86	27.675	21.09	27.675
Ti_5Si_3 (111)	-	-	5.24	29.575	7.85	29.563
Ti_3Al (110)	-	-	6.09	30.963	-	-
Ti_5Si_3 (002)	8.82	34.675	10.41	34.725	19.20	34.738
α-Ti (100)	32.21	35.20	32.50	35.188	50.37	35.238
Ti_3Al (200)	57.58	35.813	36.58	35.813	28.32	35.815
Ti_5Si_3 (210)	7.91	36.838	26.42	36.888	83.48	36.888
Ti_5Si_3 (102)	24.15	37.475	32.82	37.488	30.42	37.500
α-Ti (002)	385.60	38.488	341.97	38.463	244.19	38.513
Ti_3Al (002)	382.70	38.663	379.67	38.675	315.75	38.688
α-Ti (101)	534.0	40.263	449.62	40.288	449.51	40.300
Ti_3Al (201)	325.13	40.875	295.24	40.888	309.80	40.888
Ti_5Si_3 (300)	18.97	41.975	62.11	41.938	171.72	42.000
Ti_5Si_3 (112)	33.68	42.538	56.17	42.575	66.49	42.575
Ti_5Si_3 (210)	5.53	43.538	5.22	43.525	4.30	43.525
Ti_3Al (112)	2.59	50.288	2.59	50.288	1.41	50.325
Ti_3Al (201)	-	-	-	-	1.69	51.063
Ti_5Si_3 (221)	-	-	1.71	52.188	4.94	52.213
α-Ti (102)	185.28	53.000	164.73	53.288	140.28	53.038
Ti_3Al (202)	39.24	53.713	56.85	53.988	49.93	53.738
TiC (220)	6.52	60.875	13.19	60.800	33.24	60.800
Ti_5Si_3 (222)	4.52	61.313	8.45	61.750	14.92	61.313
α-Ti (110)	56.30	62.975	61.99	62.975	72.39	63.038
Ti_3Al (220)	21.32	64.325	19.57	64.325	17.99	64.338
Ti_5Si_3 (321)	-	-	-	-	12.44	65.613
Ti_5Si_3 (410)	6.52	66.388	12.04	66.413	26.54	66.388
Ti_5Si_3 (402)	-	-	4.16	68.563	8.71	68.550
α-Ti (103)	285.88	70.600	266.56	70.613	243.16	70.625
Ti_3Al (203)	83.64	71.425	85.73	71.463	88.39	71.470
TiC (113)	-	-	8.32	72.713	26.67	72.750
Ti_3Al (400)	2.40	76.000	1.86	76.000	1.44	75.950
α-Ti (112)	85.44	76.213	86.68	76.200	49.30	76.500
α-Ti (201)	50.75	Inseperable}	65.67	Inseperable}	44.53	77.450
Ti_3Al (222)					12.09	77.875
Ti_5Si_3 (420)					10.10	78.388
Ti_3Al (401)	8.38	79.20	14.14	79.15	17.22	79.200
α-Ti (004)	56.58	82.162	47.16	82.163	24.15	82.213
	8.29	83.163	5.51	83.225	31.98	82.938
α-Ti (202)	13.47	86.750	12.80	86.800	-	-
Ti_3Al (402)	2.87	88.600	3.45	88.600	v-weak	88.600

Table 25 Continued

	1/2 hour		1 1/2 hours		4 hours	
Identification	Int	2θ	Int	2θ	Int	2θ
α-Ti (104)	56.15	92.600	42.75	92.588	28.58	92.638
Ti_3Al (204)	5.08	94.075	10.71	93.725	12.92	93.788
α-Ti (203)	60.51	102.400	69.69	102.300	67.60	102.338
Ti_3Al (403)	5.97	104.626	13.01	104.400	11.03	104.350
TiC (420)	-	-	12.45	105.850	21.71	106.325
α-Ti (211)	29.83	109.188	36.48	109.050	43.56	109.088
Ti_3Al (421)	10.71	112.250	9.20	112.125	11.48	112.100
α-Ti (114)	104.57	114.263	100.95	114.138	95.06	114.200
Ti_3Al (224)	21.42	116.375	24.14	116.300	17.59	116.300
α-Ti (212)	12.72	119.388	20.16	119.250	15.99	119.313
α-Ti (105)	135.71	122.163	120.94	122.063	92.58	122.063
Ti_3Al (205	28.66	123.880	26.44	123.881	24.12	123.963
α-Ti (204)	27.55	126.325	25.31	126.313	17.67	126.238
α-Ti (213)	105.64	139.400	104.79	139.300	103.68	139.325
Ti_3Al (423)	8.42	144.750	13.51	144.750	11.80	144.625
α-Ti (302)	60.29	148.538	72.21	148.388	77.91	148.380

TABLE 26

Table showing the ratios for Ti_5Si_3/Ti reflection pairs for the SiC/Ti_3Al/Ti system

Reflection Pair	Ratio for 1/2 hr	Ratio for 1.5 hr	Ratio for 4 hrs
Ti_5Si_3 (200) α-Ti (100)	0.00	0.18	0.42
Ti_5Si_3 (210) α-Ti (002)	0.02	0.07	0.34
Ti_5Si_3 (300) α-Ti (101)	0.04	0.13	0.38
Ti_5Si_3 (221) α-Ti (102)	0.00	0.01	0.04
Ti_5Si_3 (222) α-Ti (110)	0.08	0.14	0.21
Ti_5Si_3 (420) α-Ti (201)	0.00	0.12	0.22
Ti_5Si_3 (331) α-Ti (004)	0.00	0.00	0.00
Ti_5Si_3 (511) α-Ti (202)	0.00	0.00	0.00
Ti_5Si_3 (521) α-Ti (203)	0.00	0.00	0.00
Ti_5Si_3 (532) α-Ti (204)	0.00	0.00	0.00

mechanism is effective in the early stages in minimizing silicide formation. If this was the only mechanism operative, then silicide formation should be further reduced after the 4 hour anneal, since more Al was rejected into the matrix (this was observed by an increase in the intensity band formation). However, the increase in silicide formation for longer times indicates that the Ti_3Al layer was acting as an effective barrier to silicide formation. Its depletion for longer times (indicated by a 11% decrease in integrated intensity) renders the planar composite susceptible to silicide formation.

In the SiC/Al/Ti composites, a 1 micron Al film was used. Recalling from the reaction kinetics discussed for 1 micron Al standards, Ti_3Al continues to form up to the 4 hour anneal. Also, intensity band formation is limited. This accounts for the higher rate of silicide formation for shorter times due to the limited rejection mechanism. For longer times (upto 4 hours) there is a saturation in silicide formation due to the effective Ti_3Al barrier. In the present case, since only a 0.5 micron Al film was used, we do not observe saturation probably because of a discontinuous Ti_3Al layer.

It was mentioned earlier, that the silicide formation during the early stages (especially during fabrication) is

very detrimental to mechanical properties. If this stage is to be avoided, it would be useful to use composites similar to the SiC/Ti_3Al/Ti system. The amount of silicide formation during actual service is much smaller due to the lower temperatures encountered. In any case, however, it would be necessary to ensure that the critical reaction zone thickness is not exceeded. If composites with reaction zones beyond the critical value are being dealt with, then reducing the silicide formation by any mechanism (if the zone thickness is still beyond the critical value) would not improve the mechanical properties.

6.4 DIFFUSION STUDIES ON THE AL/TI THIN FILMS

6.4.1 Low Temperature Diffusion Studies

It was seen earlier that for 1 micron thick samples annealed at 635°C for 1/2hr, 1hr and 2 hrs, $TiAl_3$ partially decomposed and provided a source of Al atoms for diffusion into the alpha-titanium matrix. This produces an Al composition gradient within the substrate. In this section, the method of determining this composition profile will be discussed.

The diffraction lines from $TiAl_3$ did not show any appreciable broadening between the two annealing times. Hence, the only variation in Al composition is one that

starts at the interface and penetrates into the alpha-titanium substrate resulting in an alpha-titanium intensity band. The experimental intensities for the (101) alpha-titanium intensity band (for 1/2 hr and 1 hr) was determined by point counting as described in Chapter 4 and these data sets are shown in Tables 27 and 28.

The simulated intensity band was obtained by using parameters tending towards Cauchy (m=2.5) for the low angle side and Gaussian parameters for the high angle side (Table 29), using the procedures outlined in Chapter 5. An initial calculation of the area under the curve (figure 11 a) showed that the simulations departed from the conservation of Al atoms. The discrepancy was as large as 15% and this meant that the calculated thickness (from integrated intensities) for the $TiAl_3$ layer was slightly in error. This thickness was increased and the simulations were carried out. This adjustment did not alter the composition profile in the titanium region appreciably, because of a small difference in absorption. Instead, it helped to maintain the conservation of Al atoms.

Figure 30 shows the simulated and experimental intensity bands for the Ti(101) reflections after the 1/2 hour anneal. The sharp peak corresponds to the "hkl" reflection from essentially pure titanium and the small "hump" on the

TABLE 27

Diffraction data for Al/Ti standards for 635°C, 1/2 hr

Two-theta	Intensity (C/S)
39.50	1.10
39.60	0.78
39.70	1.03
39.80	1.04
39.90	4.46
39.95	8.84
39.98	17.50
40.00	26.64
40.02	41.49
40.04	60.94
40.05	73.80
40.06	82.30
40.07	96.30
40.08	106.95
40.09	121.21
40.10	134.77
40.11	150.83
40.12	165.56
40.14	179.53
40.15	183.73
40.16	178.57
40.17	168.92
40.18	149.25
40.19	121.36
40.195	103.41
40.20	84.64
40.21	56.56
40.22	38.84
40.24	20.47
40.27	10.40
40.35	4.80
40.45	4.02
40.50	4.05
40.55	4.12
40.60	4.43
40.65	4.81
40.70	4.80
40.75	4.21
40.80	3.23
40.85	3.00
40.90	1.59
41.00	0.97
41.10	0.93

41.20	0.84
41.30	0.82
41.40	0.76
41.50	0.80

TABLE 28

Diffraction data for Al/Ti standards for 635°C, 1 hr

Two-theta	Intensity (C/S)
39.40	1.06
39.50	0.90
39.60	0.95
39.70	0.98
39.80	0.96
39.90	0.99
39.95	2.04
39.98	5.18
40.00	9.83
40.02	18.57
40.04	34.13
40.06	57.24
40.08	87.89
40.10	125.84
40.12	162.34
40.14	197.82
40.15	207.47
40.16	211.86
40.18	187.27
40.20	99.63
40.22	43.86
40.24	25.89
40.26	17.75
40.28	12.20
40.30	7.49
40.35	5.70
40.40	5.90
40.45	6.02
40.50	6.54
40.55	6.40
40.60	6.53
40.65	7.75
40.70	9.24
40.75	9.95
40.80	9.28
40.85	7.85
40.90	5.68
41.00	1.48
41.10	0.75
41.20	0.70
41.30	0.70
41.40	0.65
41.50	0.65

TABLE 29

Pearson Parameters and Error Function Coefficients for 635°C

Parameters		635°C (1/2 hr)	635°C (1 hr)
Pearson			
Low angle;	a	0.0839	0.0570
	m	2.5	2.5
High angle;	a	0.0625	0.0625
	m	20.0	20.0
Half-Widths			
Low angle;	w	0.150	0.105
High angle;	w	0.105	0.102
Error function (ERFC)			
	a_1	0.15	0.15
	a_2	0.095	0.10
	a_3	0.0	0.0
	b_1	0.000017	0.0000254
	b_2	0.000012	0.0000122
	b_3	1.0	1.0
	d_1	0.0	0.0
	d_2	0.8	2.49
	d_3	0.0	0.0
Background counts (c/s)		0.80	0.70

high two-theta side is due to Al solid solution in alpha-titanium. During the simulations, the intensity axis was expanded 5 times so as to ensure that the fit in the region of this "hump" was perfect and this is also shown in Figure 30. The Al composition profile that was used in the simulations is shown in Figure 31. The $TiAl_3$ interface is taken as the zero along the y-axis. The Al profile in the TiAl layer is constant. However, the Al profile in the alpha phase has a fairly steep gradient and extends to a depth of only 0.5 microns from the interface position.

Figure 32 shows the simulations for the sample annealed for 1 hour. Here again parameters tending towards Cauchy (m=2.5) for the low angle side, and Gaussian parameters (a=0.0625, m=20.0) for the high angle side were used for the instrumental and particle size broadening. The composition profile for these simulations is shown in Figure 33. The profiles show that the composition gradient is slightly smaller compared to the 1/2 hour case. Also, with the longer diffusion time, the profiles have extended out to about 0.8 microns from the interface, as one would expect. Although the modulation on the experimental intensity band was larger, no gap in the composition profiles was neces-

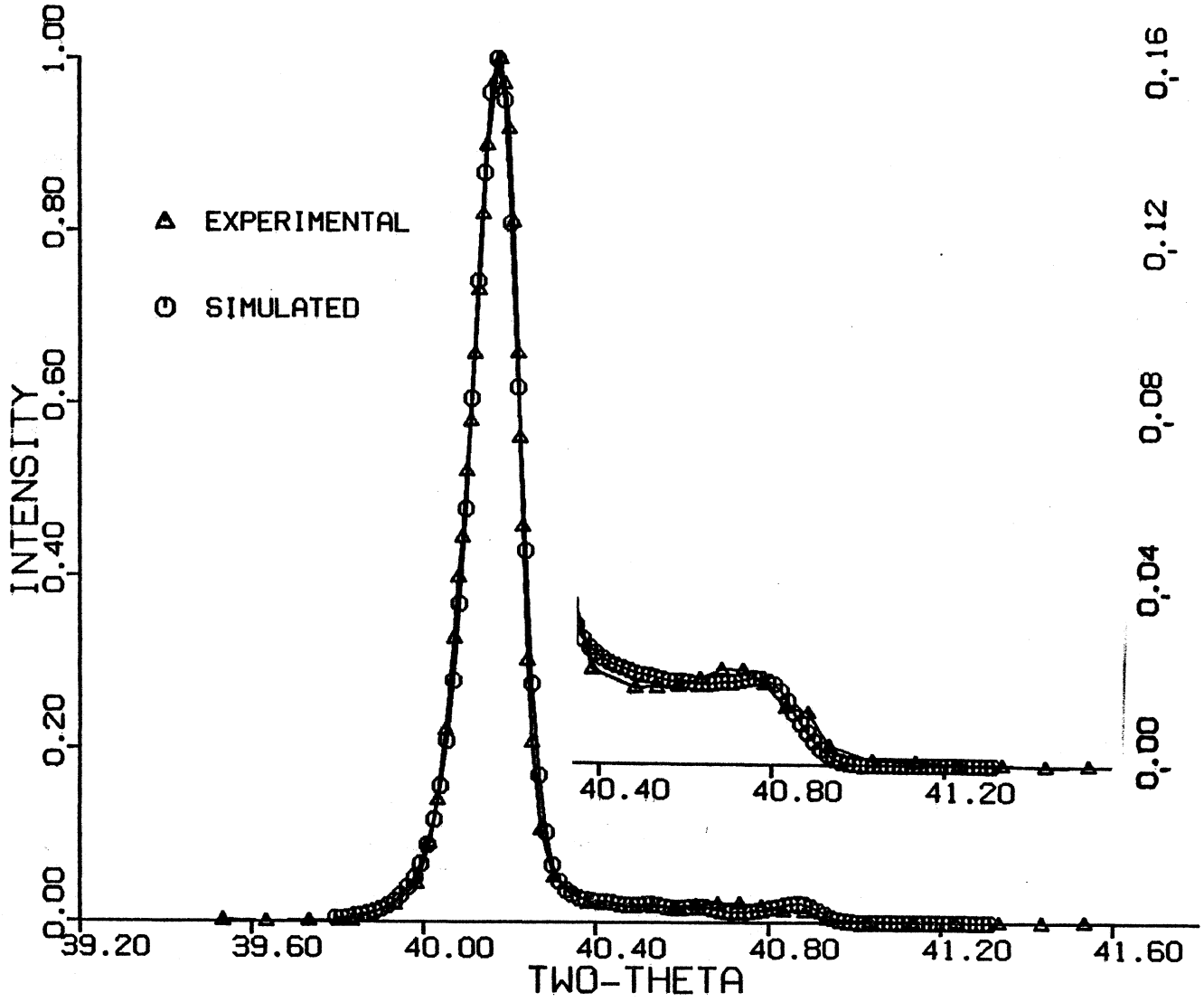


Fig. 30 Computer simulations of the (101) intensity band, 635°C (1/2 hr).

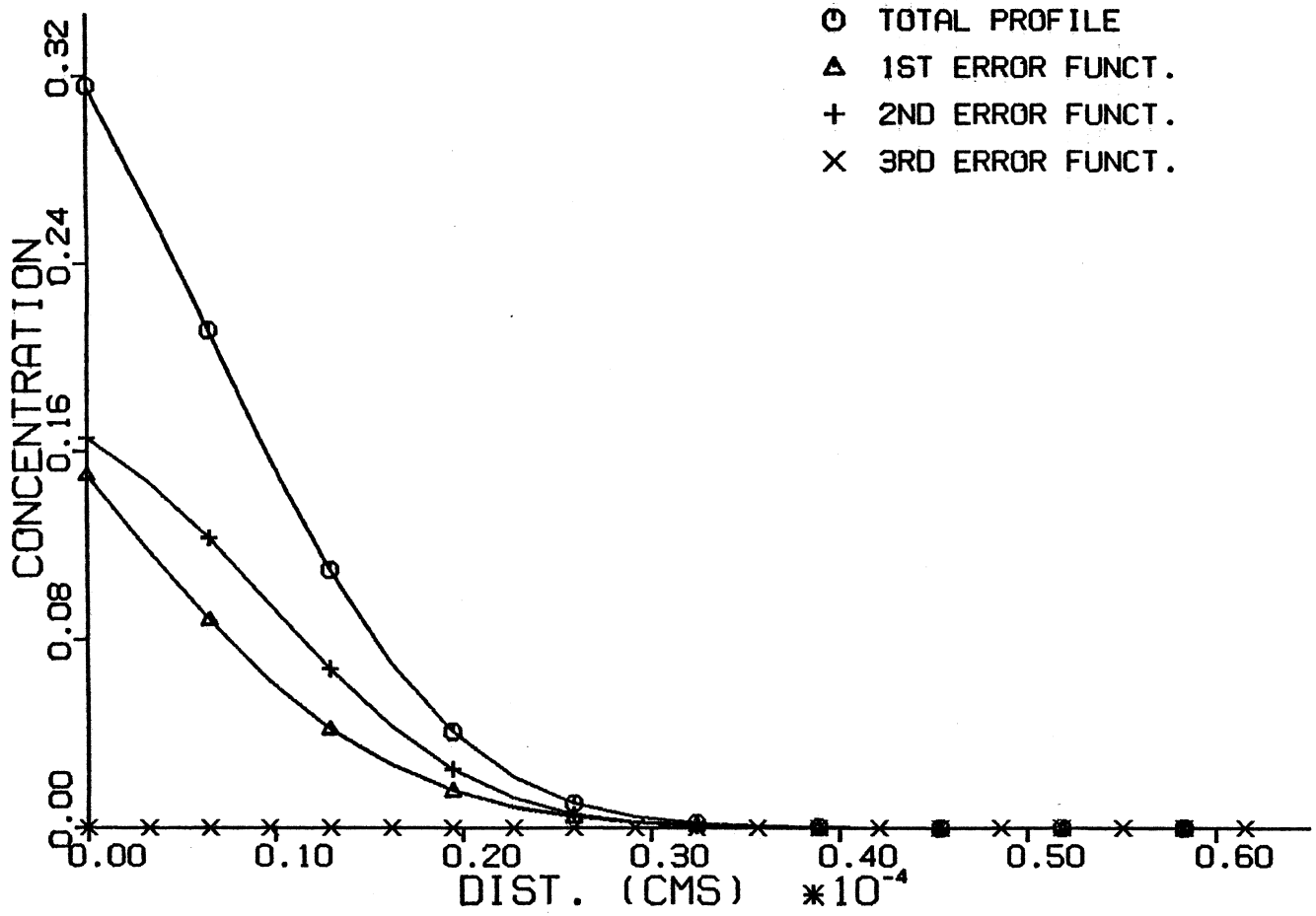


Fig. 31 Composition profiles for the simulations of the (101) intensity band, 635°C (1/2 hr).

sary. However, the profiles do indicate a change in slope around 22 %Al. The parameters that were used in the above simulations are presented in Table 29.

The intensity band for the sample annealed for 2 hours shows a significant modulation on the high two-theta side. This band was simulated by using a profile with a small composition gap and the simulation is shown in Figure 34. A linear profile was adequate to simulate the peak on the high two-theta side of the modulation. On the other hand, a sum of two error functions was neccessary for the simulation of the low two-theta side. The composition profile used for the above simulations is shown in Figure 35. Although the gap is fairly small, this data shows a definite tendency for the formation of the Ti_3Al (disordered) phase for longer annealing times. Also, for shorter times the assumption of a continuous extension of the alpha phase is justified.

6.4.2 High Temperature Diffusion Studies

The Al (0.5 microns)/Ti samples that were annealed at 900°C for 1/2 hr, 1 hr and 4 hrs were analyzed in order to determine composition profiles.* As before, the experimental data is obtained by point counting and is presented in

* Note: There was only a small difference in the intensity bands from samples annealed for 1 hr and 2 hrs. Consequently, the 2 hr anneal was not used for the analysis.

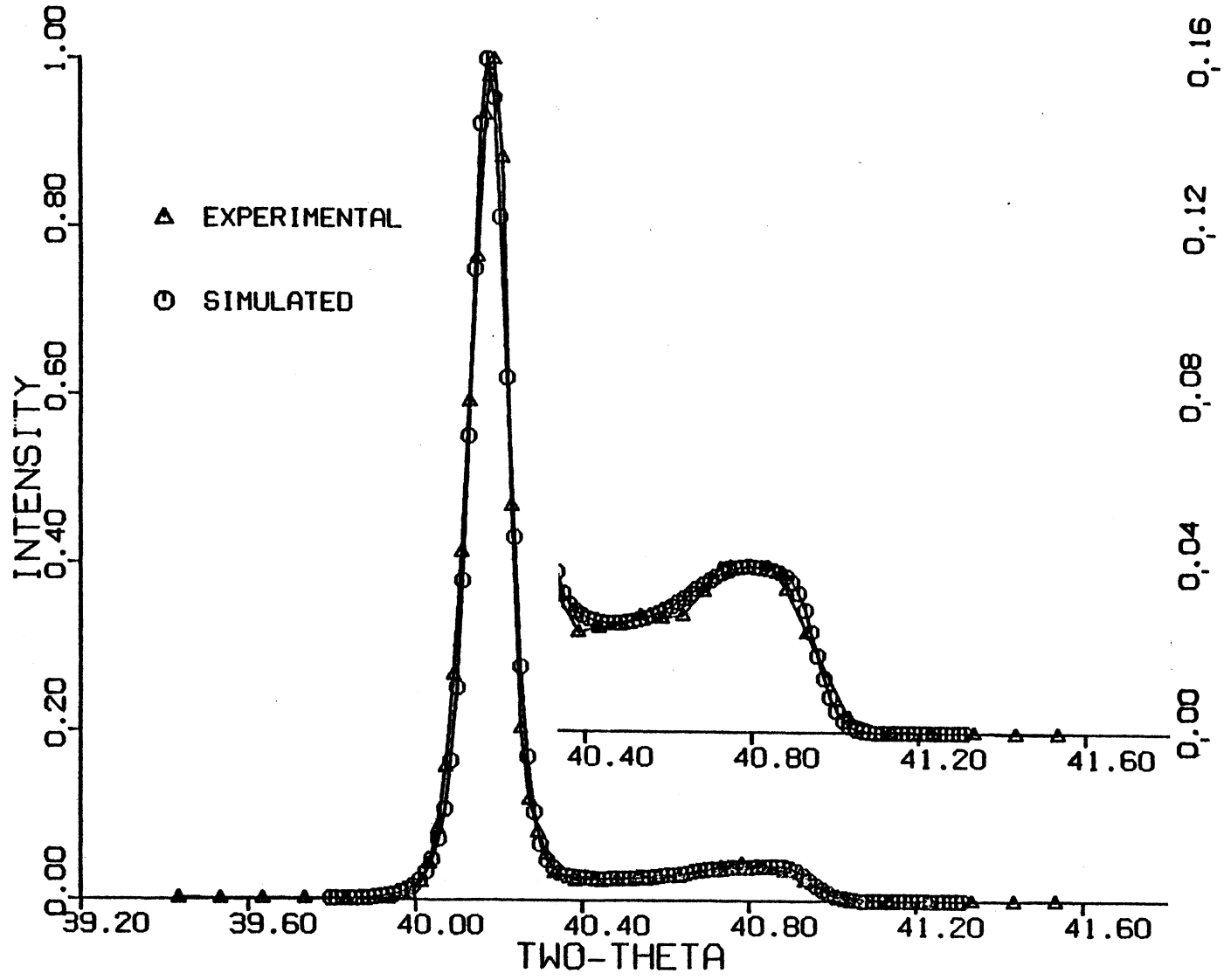


Fig. 32 Computer simulation of the (101) intensity band, 635°C (1hr).

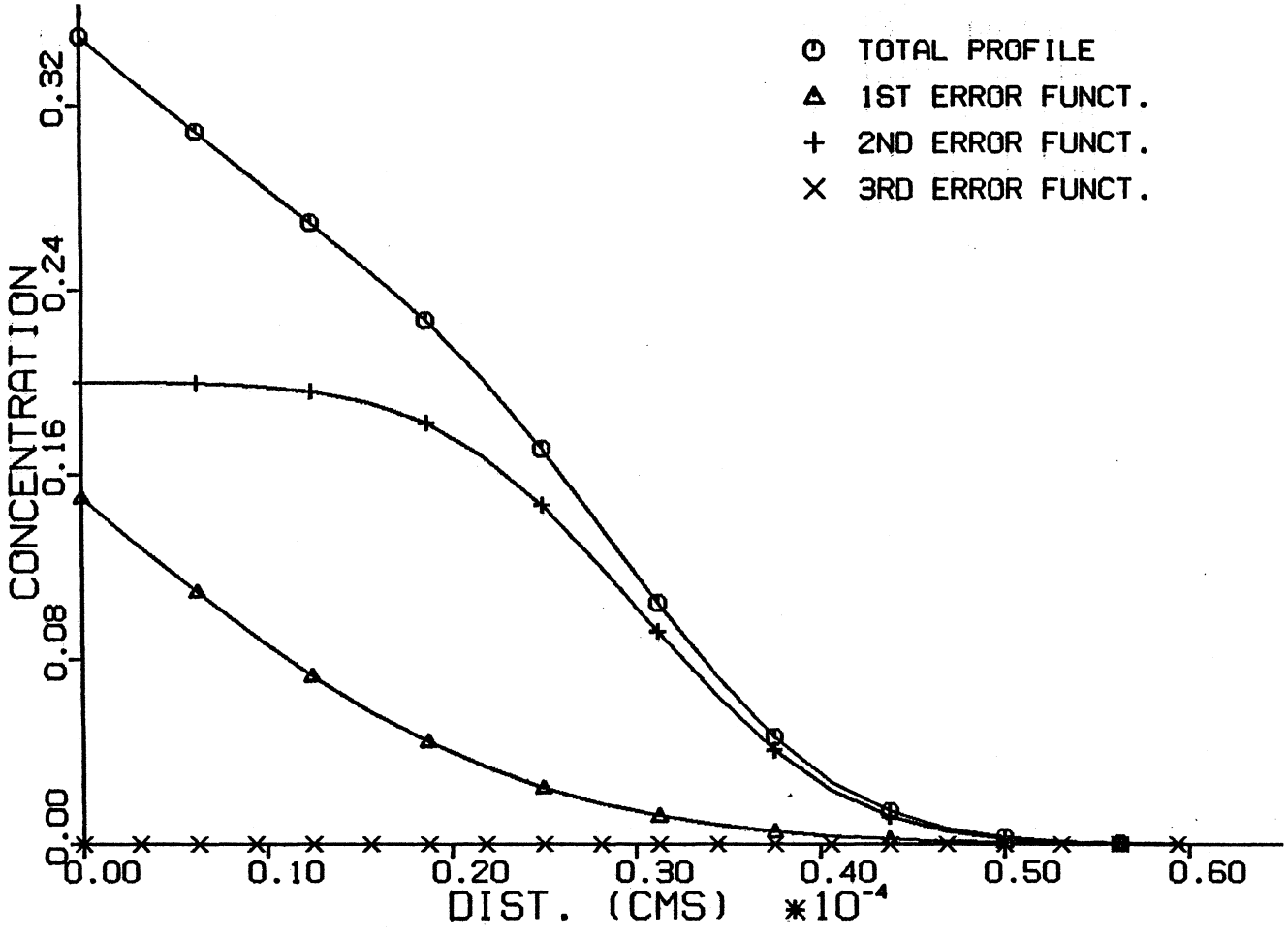


Fig. 33 Composition Profiles for the simulations of the (101) intensity band, 635^{0}C (1hr).

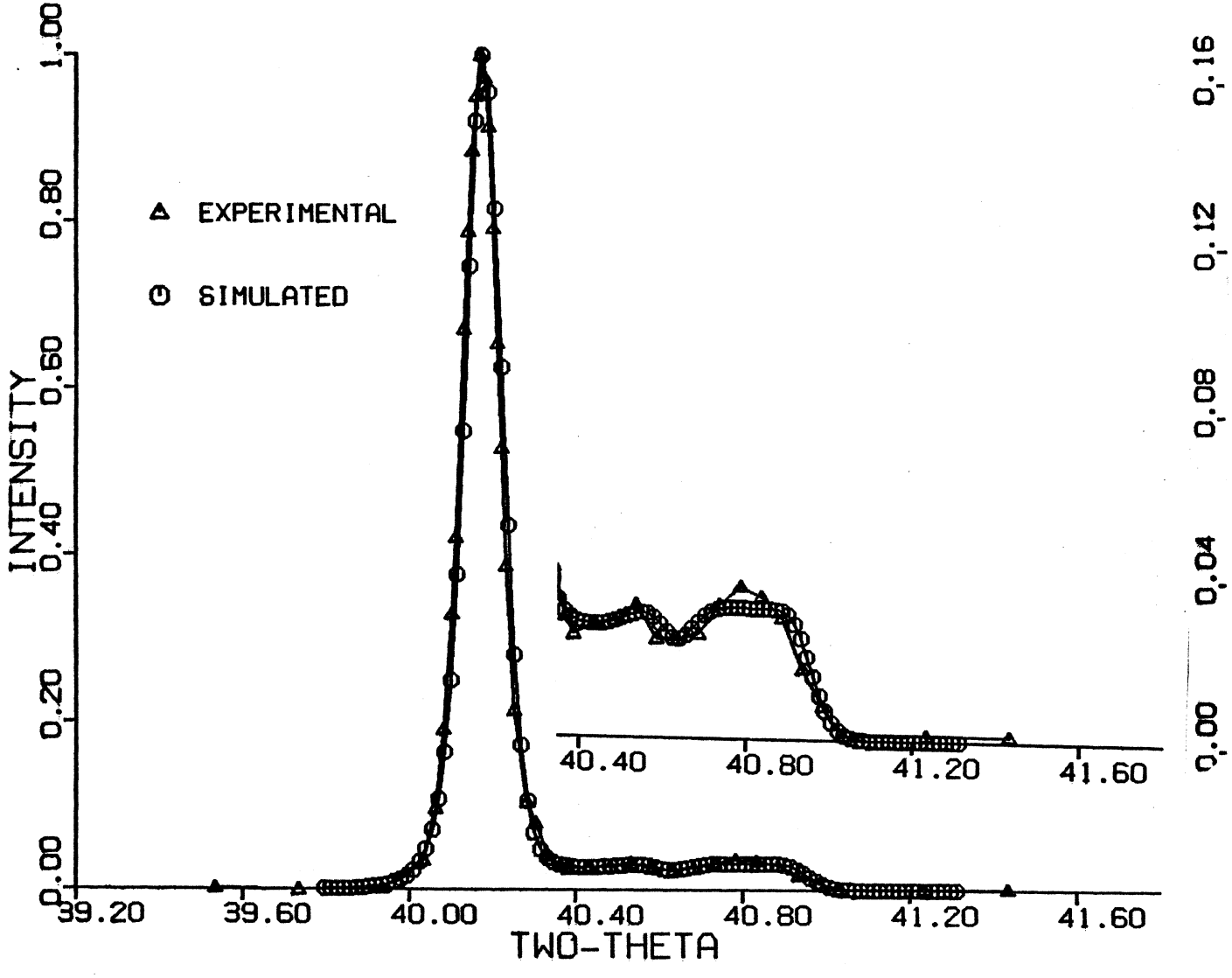


Figure 34. Computer simulation of the (101) intensity band, 635°C (2 hours).

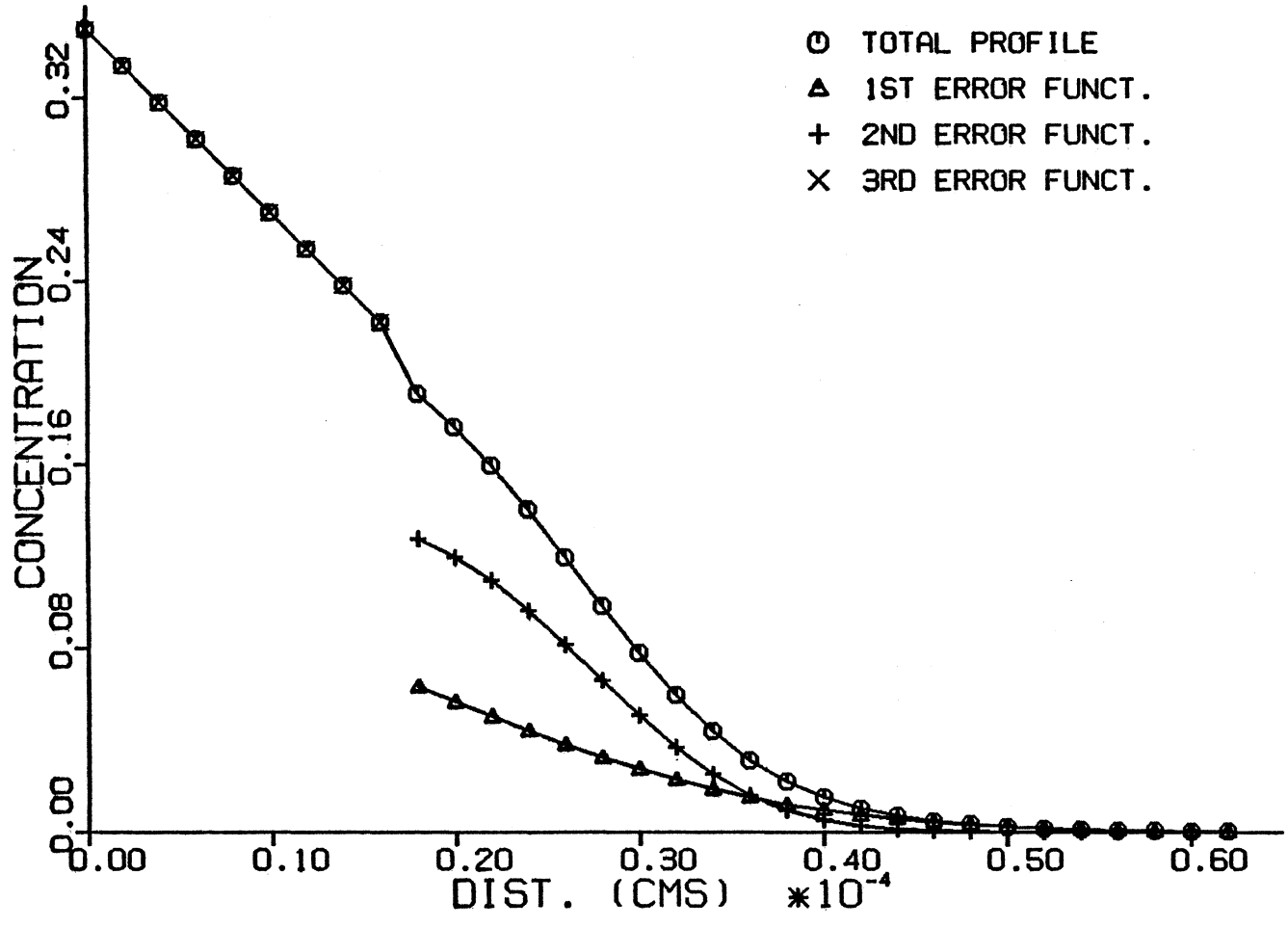


Figure 35. Composition profile used to simulate the (101) intensity band, 635°C (2 hrs).

Tables 30, 31 and 32 for the 1/2 hr, 1 hr and 4 hr anneals, respectively. In this case, both the alpha-titanium intensity band as well as the Ti_3Al diffraction peak were simulated by the procedures outlined in Chapter 5 because in this case the Ti_3Al lines displayed composition broadening.

The Ti_3Al layer thickness was obtained in each case by the attenuation of the integrated intensity of alpha-titanium diffraction lines from the Ti_3Al side, relative to the back-side. Because of problems with preferred orientation layer thicknesses ranging from 0.5 to 1.5 microns (depending upon which reflections are selected), were obtained. However, the thickness of the Ti_3Al layer is not needed for the analysis. Instead, the thickness (interface position) can be obtained from the profile analysis and the X-ray thicknesses can be merely used to check for internal consistency.

The simulated and experimental intensity bands for the 1/2 hr, 1 hr and 4 hr anneals are shown in figures 36, 37 and 38 respectively. In all cases, the Gaussian extreme of the Pearson VII distribution for the instrumental and particle size broadening, gave the best simulations. The half-widths that were neccessary, were larger for the longer annealing times.

Previous investigations[92] have showed that with longer diffusion treatments, the broadening function becomes

TABLE 30

Diffraction data for Al/Ti standards for 900°C, 1/2 hr

Two-theta	Intensity (C/S)
39.50	0.49
39.70	0.56
39.90	0.72
40.00	1.64
40.03	4.33
40.05	8.27
40.06	12.87
40.07	18.10
40.08	26.75
40.09	35.36
40.10	44.59
40.11	54.82
40.12	68.29
40.13	78.82
40.14	88.45
40.15	93.67
40.16	93.46
40.17	88.25
40.18	79.97
40.19	74.50
40.20	64.18
40.21	56.30
40.22	48.65
40.23	41.27
40.24	33.52
40.25	28.79
40.26	25.26
40.27	22.09
40.28	21.78
40.30	19.96
40.32	18.70
40.35	18.00
40.38	18.75
40.40	19.20
40.41	20.41
40.42	21.03
40.43	22.13
40.45	22.83
40.46	23.96
40.48	25.35
40.50	27.18
40.52	28.61
40.54	27.83

40.55	27.34
40.56	26.69
40.57	25.88
40.58	23.55
40.59	21.71
40.60	20.66
40.61	18.36
40.62	16.18
40.63	14.49
40.65	11.48
40.67	10.63
40.70	12.57

TABLE 31

Diffraction data for Al/Ti standards for 900°C, 1 hour.

2	Int (C/S)
39.50	0.48
39.70	0.61
40.00	1.09
40.04	6.16
40.06	11.62
40.07	19.17
40.085	26.53
40.10	32.48
40.11	40.11
40.12	48.26
40.13	57.18
40.14	63.19
40.15	67.10
40.16	69.06
40.17	68.36
40.18	68.29
40.19	65.92
40.20	59.51
40.21	57.57
40.22	53.54
40.23	49.79
40.24	45.15
40.25	42.89
40.27	39.33
40.29	37.02
40.32	37.28
40.35	39.71
40.38	44.45
40.40	48.30
40.41	51.16
40.42	54.12
40.43	56.94
40.45	62.88
40.46	65.49
40.48	69.62
40.50	71.94
40.52	73.42
40.54	70.44
40.55	65.86
40.56	62.84
40.57	56.69
40.58	51.29
40.59	44.31

40.60	37.89
40.61	30.87
40.62	26.37
40.63	21.54
40.64	17.25
40.65	14.46
40.67	9.40
40.70	8.45
40.73	10.53
40.75	13.42
40.77	15.83
40.79	19.92
40.81	22.59
40.83	24.19
40.85	22.86
40.87	20.31
40.89	18.21
40.91	15.31
40.93	10.47
40.95	8.09
40.97	6.02
40.99	3.61
41.05	1.17
41.15	0.87
41.25	0.67
41.40	0.48

TABLE 32

Diffraction data for Al/Ti standards for 900°C,4hrs

2	Int (C/S)
39.50	0.530
39.70	0.59
39.90	0.73
40.00	1.29
40.03	2.88
40.05	6.33
40.06	8.70
40.07	12.39
40.08	17.50
40.09	22.10
40.10	28.19
40.11	31.16
40.12	36.96
40.13	41.25
40.14	46.34
40.15	48.84
40.16	50.44
40.17	52.00
40.18	51.79
40.19	51.18
40.20	50.78
40.21	47.99
40.22	46.43
40.23	44.42
40.24	42.05
40.25	42.15
40.26	42.47
40.27	43.18
40.28	45.45
40.29	48.79
40.30	51.16
40.31	52.16
40.32	55.30
40.33	56.27
40.34	59.40
40.35	62.76
40.36	66.06
40.37	69.92
40.38	72.07
40.39	75.07
40.40	77.64
40.41	81.10
40.42	83.04

40.43	84.64
40.44	84.66
40.45	84.75
40.46	84.70
40.47	84.37
40.48	83.66
40.49	81.95
40.50	81.50
40.51	80.39
40.52	78.58
40.53	74.29
40.54	72.80
40.55	69.51
40.56	65.11
40.57	61.01
40.58	55.18
40.59	49.11
40.60	42.55
40.61	35.87
40.62	30.35
40.63	24.07
40.64	19.45
40.65	14.26
40.66	11.23
40.67	8.37
40.68	6.83
40.70	4.61
40.73	4.67
40.75	5.35
40.77	6.41
40.79	7.58
40.81	9.12
40.83	9.26
40.85	8.31
40.87	7.17
40.89	5.65
40.91	3.92
40.93	2.63
40.95	1.80
40.97	1.14
40.99	0.80
41.15	0.46
41.25	0.35
41.40	0.40

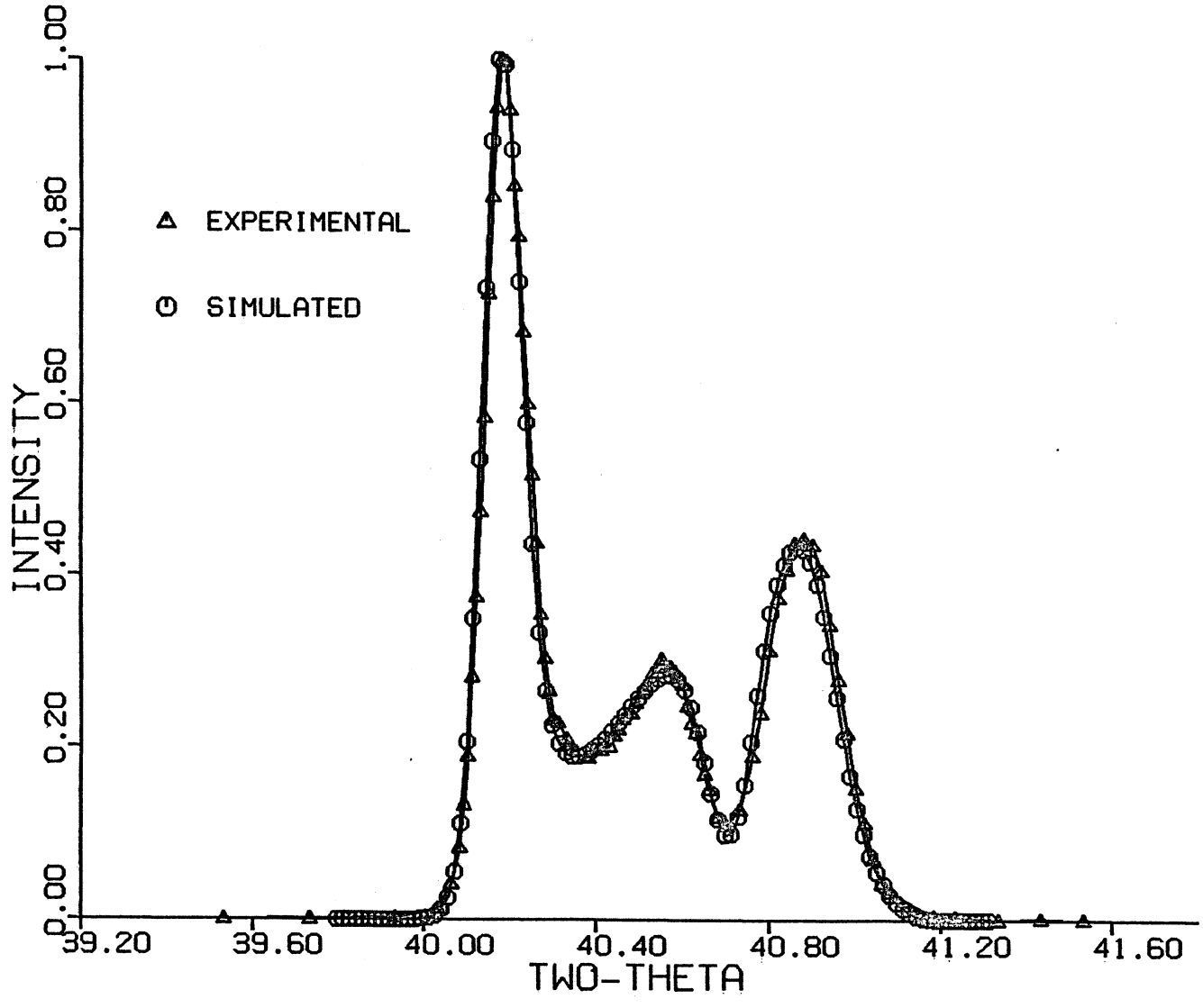


Fig. 36 Computer simulations of the (101) intensity band, 900°C (1/2 hr).

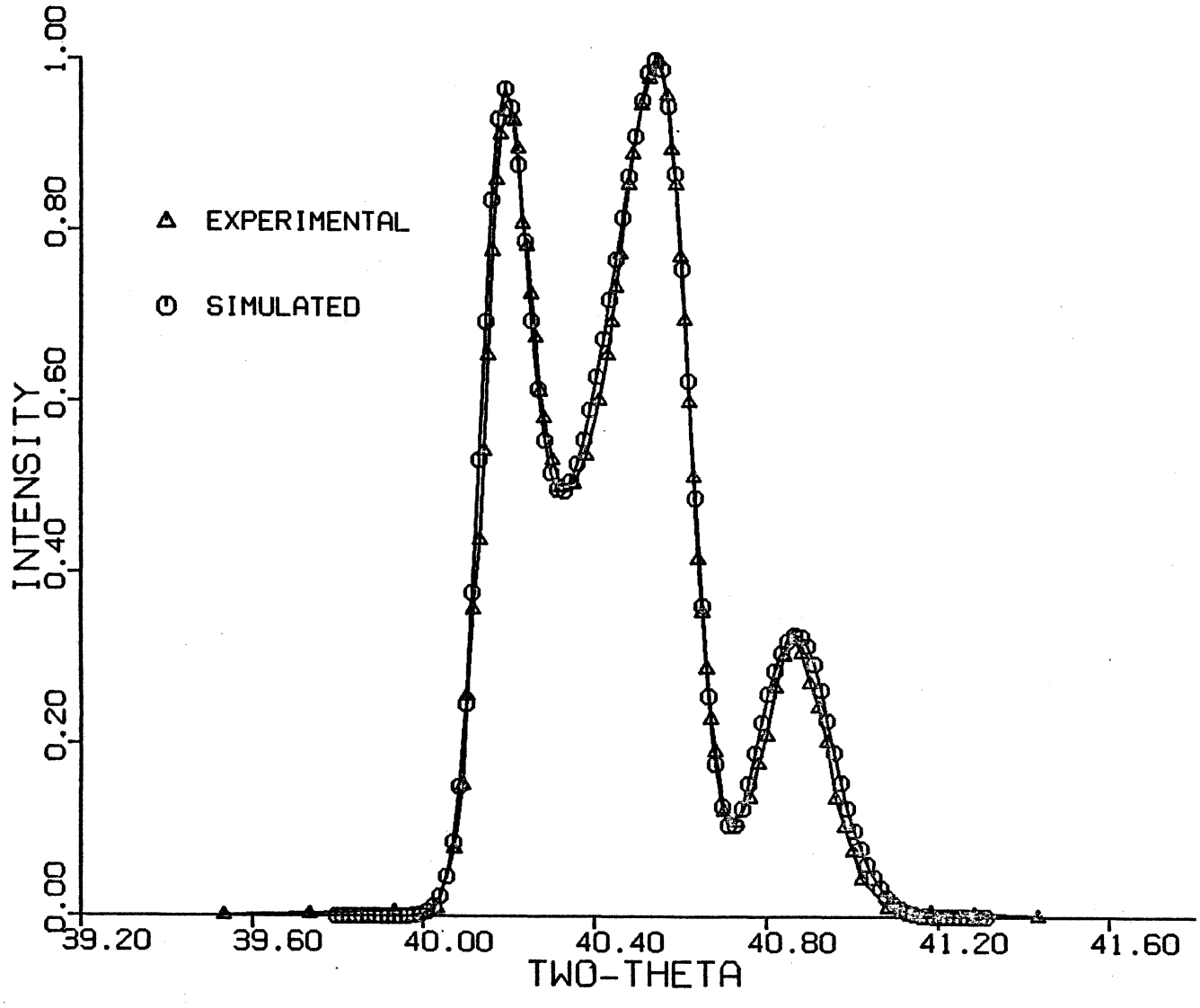


Fig. 37 Computer simulation of the (101) intensity band, 900°C (1hr).

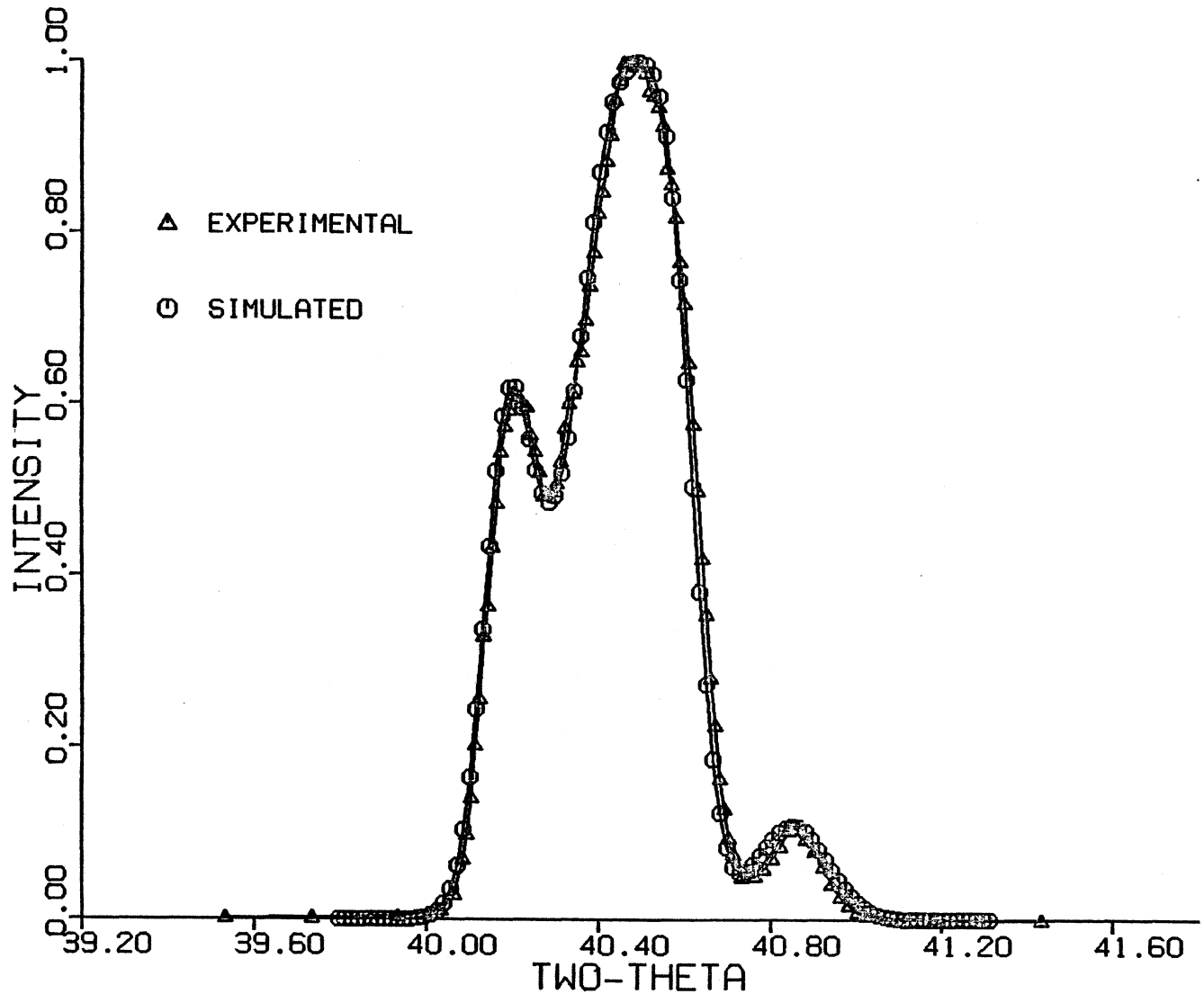


Fig. 36 Computer simulation of the (101) intensity band, 900°C (4hrs).

Gaussian and is related to the formation of a substructure associated with diffusion damage. Also, the broadening is described by a particle size broadening. The parameters that were used for these simulations are shown in Table 33. Figures 39, 40 and 41 show the composition profiles that were used for the 1/2 hr, 1 hr and 4 hr simulations respectively. It is seen from these figures that the Al compositions at the Ti_3Al/Ti interface is almost constant for the 3 annealing times. However, with longer diffusion times, the Al profiles in the alpha-titanium have extended deeper into the substrate. The interface is tending to move towards the free surface with longer diffusion times.

The Al composition at the free surface is fairly constant in the three cases. This lack of a time dependence at the free surface makes it possible to use a previously developed computer program[77] to determine diffusion coefficients as will be discussed in the next section. In all the cases, a straight line profile was used to simulate the intensity for the Ti_3Al reflections. Although the profile could have been defined by an error function, a straight line was chosen for convenience. This choice, however, makes the Al compositions meet the free surface with a finite slope and the result is a finite Al flux, from Ficks first law. The compositions could as well meet the free

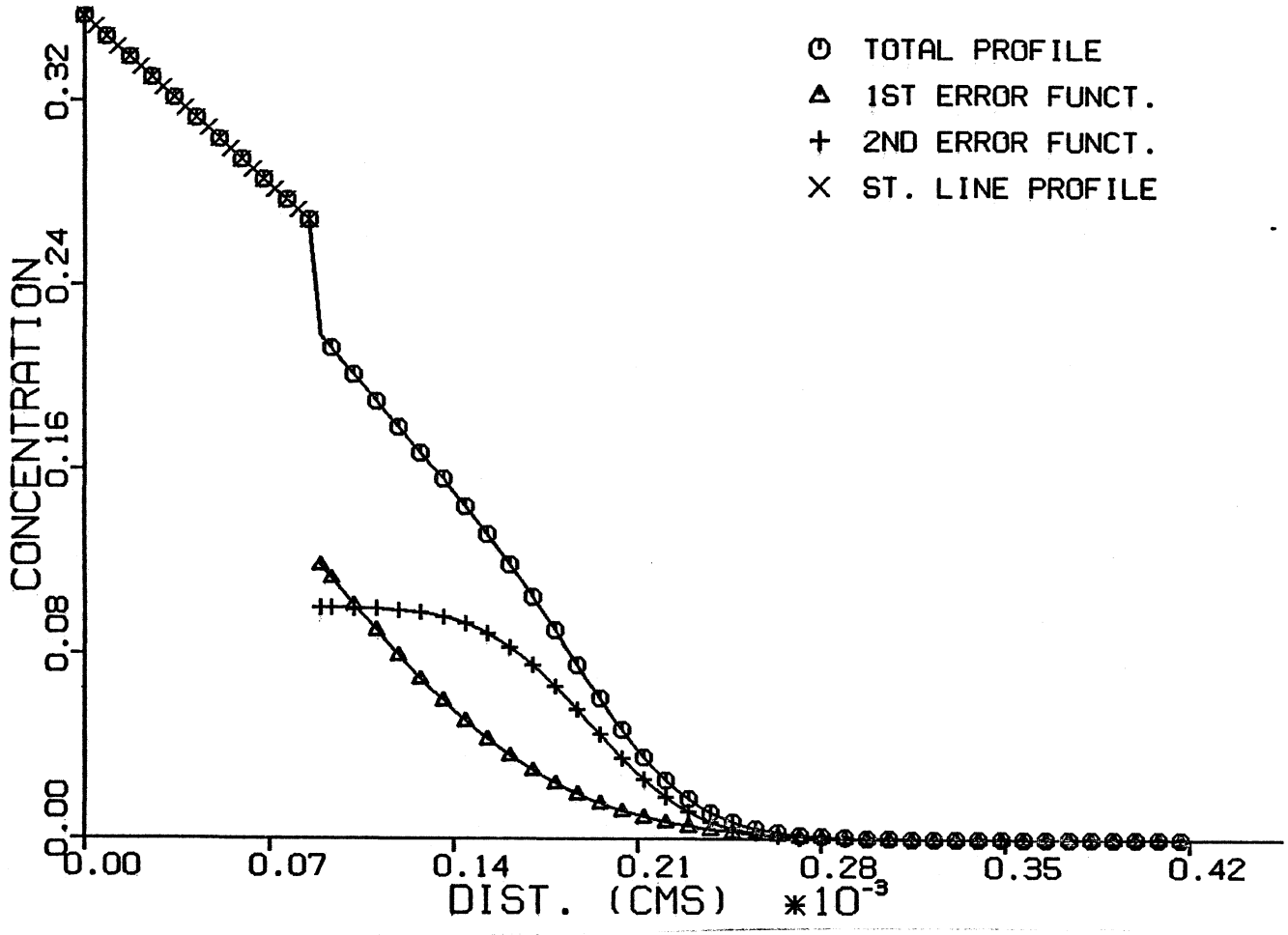


Fig. 39 Composition Profiles for the simulations of the (101) intensity band, 900°C (1/2hr).

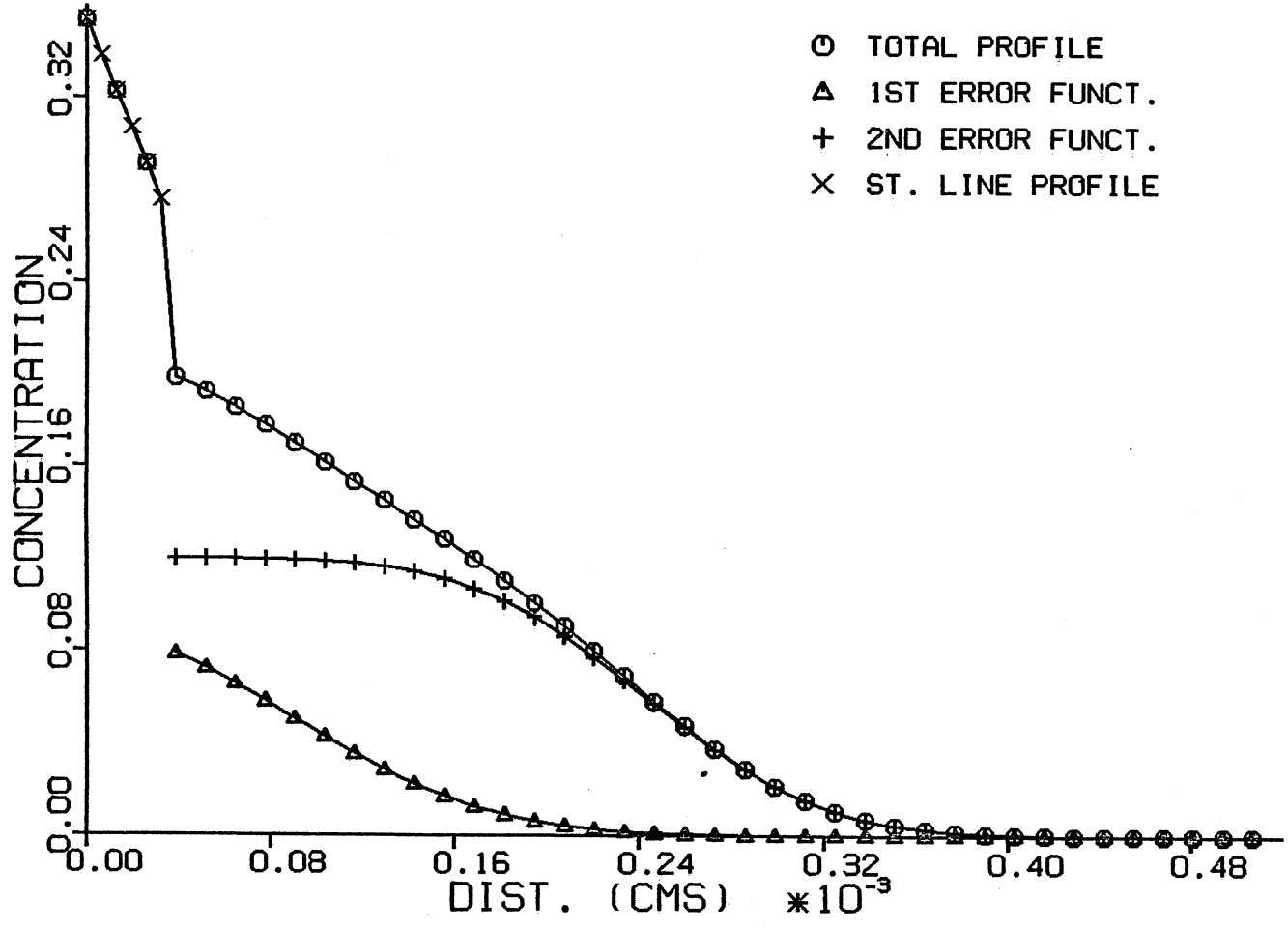


Fig. 40 Composition profiles for the simulations of the (101) intensity band , 900°C (1hr).

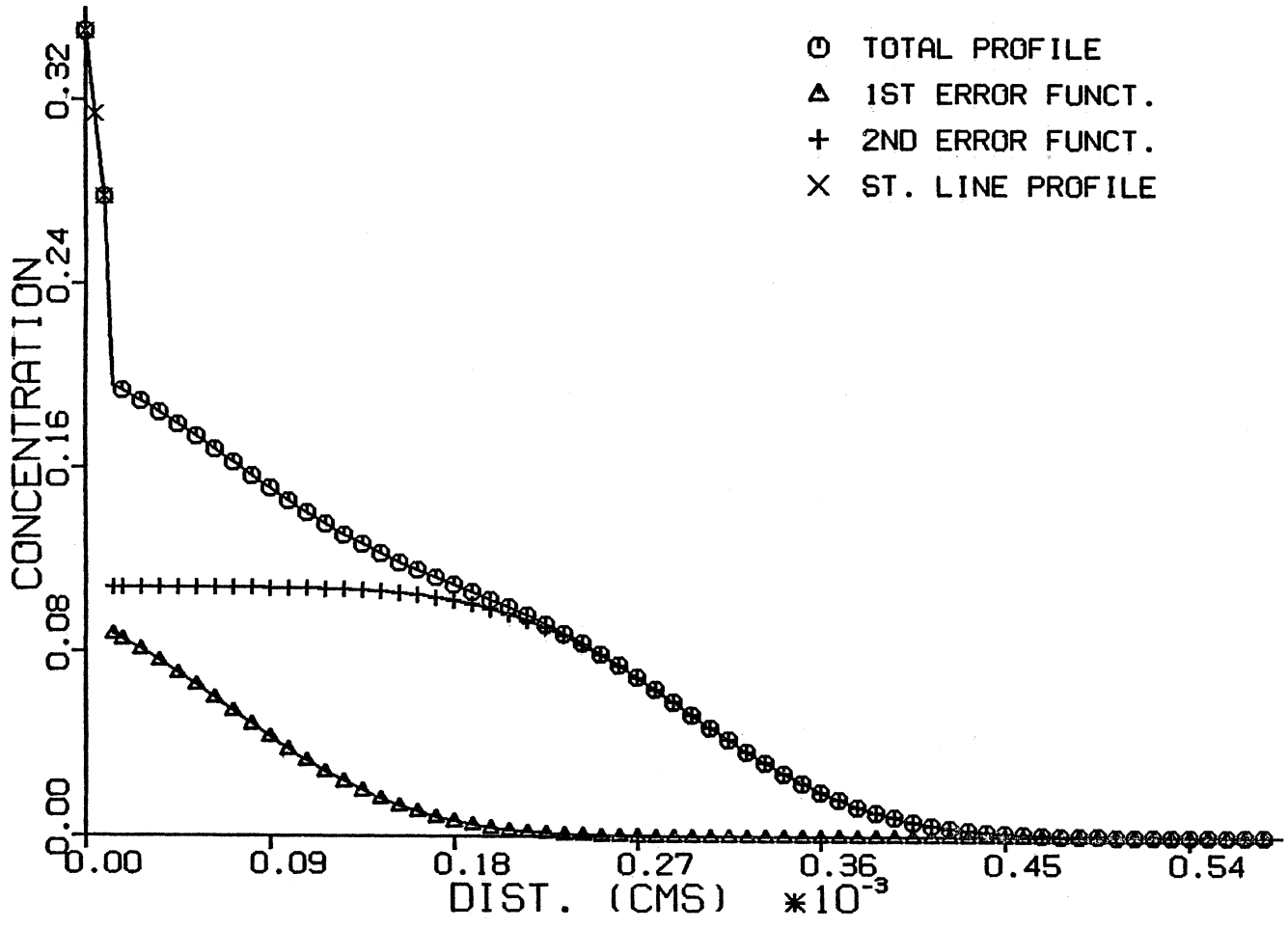


Fig. 41 Composition Profiles for the simulation of the (101) intensity band, 900°C (4hrs).

TABLE 33

Pearson parameters and the Error function coefficients for (900°C)

Parameters		(1/2 hr)	1 hr	4 hrs
Pearson				
Low angle;	a	0.0625	0.0714	0.0750
	m	20.000	20.000	20.000
High angle;	a	0.0625	0.0750	0.0750
	m	20.000	20.000	20.000
Half-widths				
Low angle;	w	0.105	0.120	0.126
High angle;	w	0.105	0.126	0.126
Error funct. (ERFC)				
a_1		0.1200	0.0500	0.0556
a_2		0.0500	0.0600	0.0540
a_3*		0.3570	0.3540	0.3500
b_1		0.0001	0.000095	0.0001
b_2		0.000045	0.000085	0.0001
b_3*		-0.0009583	-0.0004167	-0.000125
d_1		0.0000	0.6000	0.6000
d_2		2.3000	2.4500	2.8500
d_3*		0.2650	0.2700	0.2700
Background counts(c/s)		0.49	0.40	0.45

* Note: The a_i,b_i, and d_i parameters are used to fit the straight line profile for the Ti_3Al phase. Details on this may be found in the computer program (ITR2).

surface with a zero slope with essentially no change in the simulated Ti_3Al reflection. This would then be consistent with the existance of a zero flux at the free surface.

The area under each composition profile was determined by a 3 point Simpson's integration. The areas were fairly constant for the 3 diffusion times (0.445, 0.425, 0.415 for 1/2 hr, 1 hr and 4 hrs respectively). These areas should equal the initial thickness of pure Al in the as-sputterd samples. This thickness was determined from the attenuation of several alpha-titanium reflections from the coated side relative to the uncoated side. The coating thickness was found to be 0.47 microns indicating a discrepancy between 5 and 11% between the two extreme diffusion times. This systematic decrease in Al thickness from the as-sputterd samples to the 4 hr anneal could be due to a small amount of surface diffusion of Al atoms around the edges of the titanium disc. However, X-ray diffraction did not reveal any aluminum, Ti-Al compounds or aluminum solid solution on the reverse side of the samples.

6.5 DETERMINATION OF DIFFUSION COEFFICIENTS

6.5.1 Low Temperature Case

In Chapter 5, the procedures used to determine diffusion coefficients by an iterative method, were discussed.

The initial conditions (C(x) at t=0) for the samples that were annealed at 635°C, are shown in figure 11a. The simulations required use of a constant value of 0.75 atom fraction Al in the $TiAl_3$ region, up to a distance equal to the thickness of the $TiAl_3$ layer. In order to be able to use the computer program (ITR2) for two-phase systems, very small diffusion coefficients (less than 10^{-17} cm^2/sec) had to be used in the $TiAl_3$ region, although they do not have any physical significance. Figures 42 and 43 show the experimental and simulated profiles for the samples annealed at 635°C for 1/2 hr and 1 hr respectively. Although a composition profile for the 2 hour anneal was obtained, it was not analyzed for diffusion coefficients due to the occurance of the TiAl phase. In both cases, the departure from conservation of Al atoms according to equation (49) was less than 1 atomic %. The diffusion coefficient versus composition data that was used for the above simulations is presented by a semi-log plot in Figure 47. An ideal situation would require that the simulations for various times at any given temperature would yield diffusion coefficients that are nearly the same for these times. However, the results (for 635°C) in Figure 47 show a small time dependence. Since different samples were used for these anneals, there could be differences in the initial thickness of the Al film.

Also, problems associated with surface diffusion of Al atoms, (around corners) could result in differences in the thickness of the $TiAl_3$ layer. Therefore, for the above reasons, the initial conditions used may not be exact but the discrepancies in the diffusion coefficients can be treated as being within experimental error.

6.5.2 High Temperature Case

In order to obtain the initial conditions (C(x) at t=0), the areas under the experimental profiles (Figures 39 - 41) were obtained. This area was redistributed into an "equivalent thickness" of an "initial Ti_3Al layer" (before dissociation) according to the equilibrium solid solubility limit in Ti_3Al. This is shown schematically in Figure 11b.

Figures 44-46 show the simulated and experimental profiles for the 900°C samples annealed for 1/2hr, 1hr, and 4hrs respectively. In this case diffusion coefficients in Ti_3Al and alpha-titanium were obtained. These are shown in figure 47. It is observed that the diffusion coefficients obtained for the various times, in the alpha-titanium phase are nearly the same. The small differences are clearly within experimental error.

In the Ti_3Al phase however, there appears to be a definite time dependence. Again, there could be discrepancies

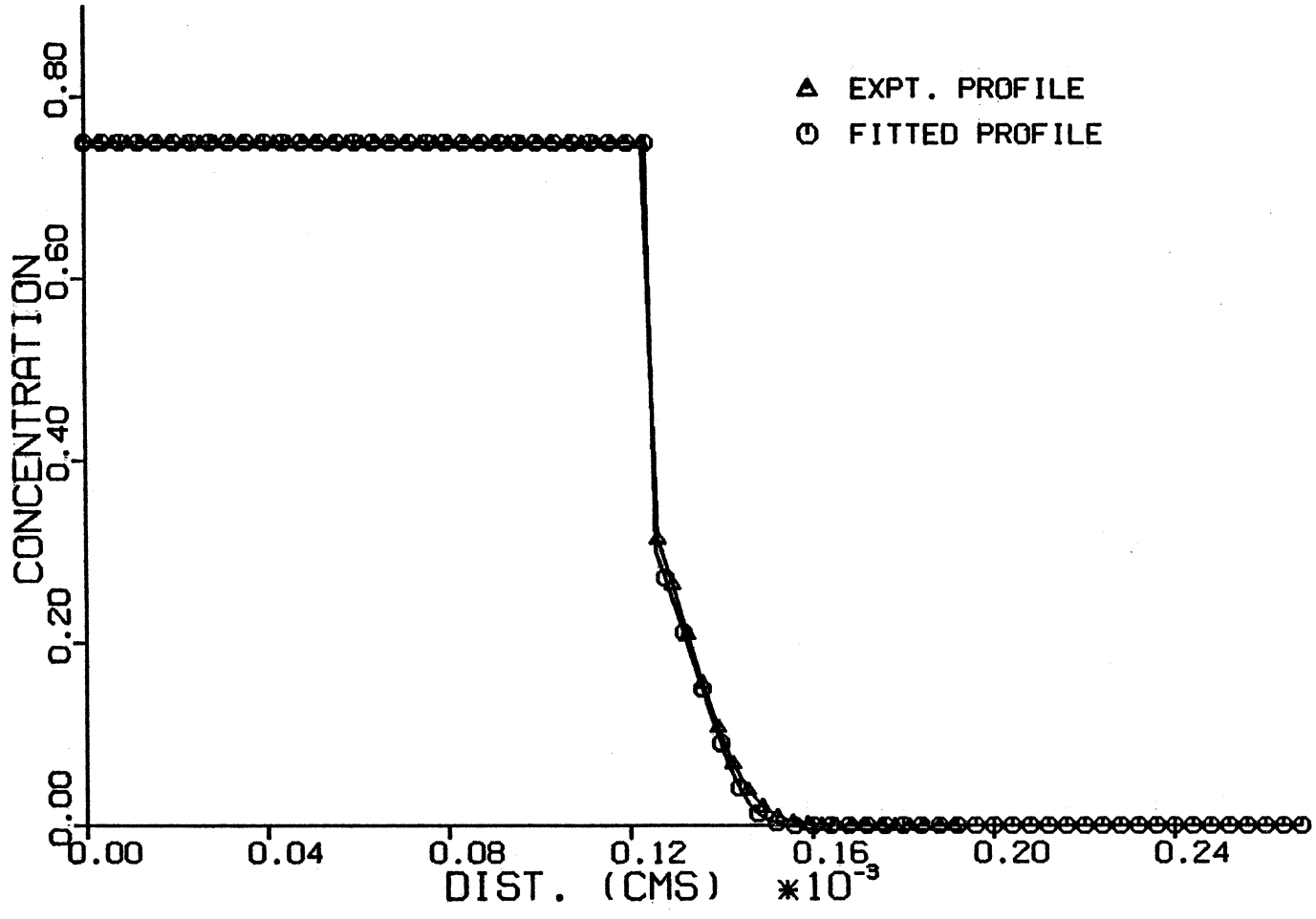


Fig. 42 Simulation of the Composition profiles, 635°C (1/2hr), to obtain diffusion coefficients.

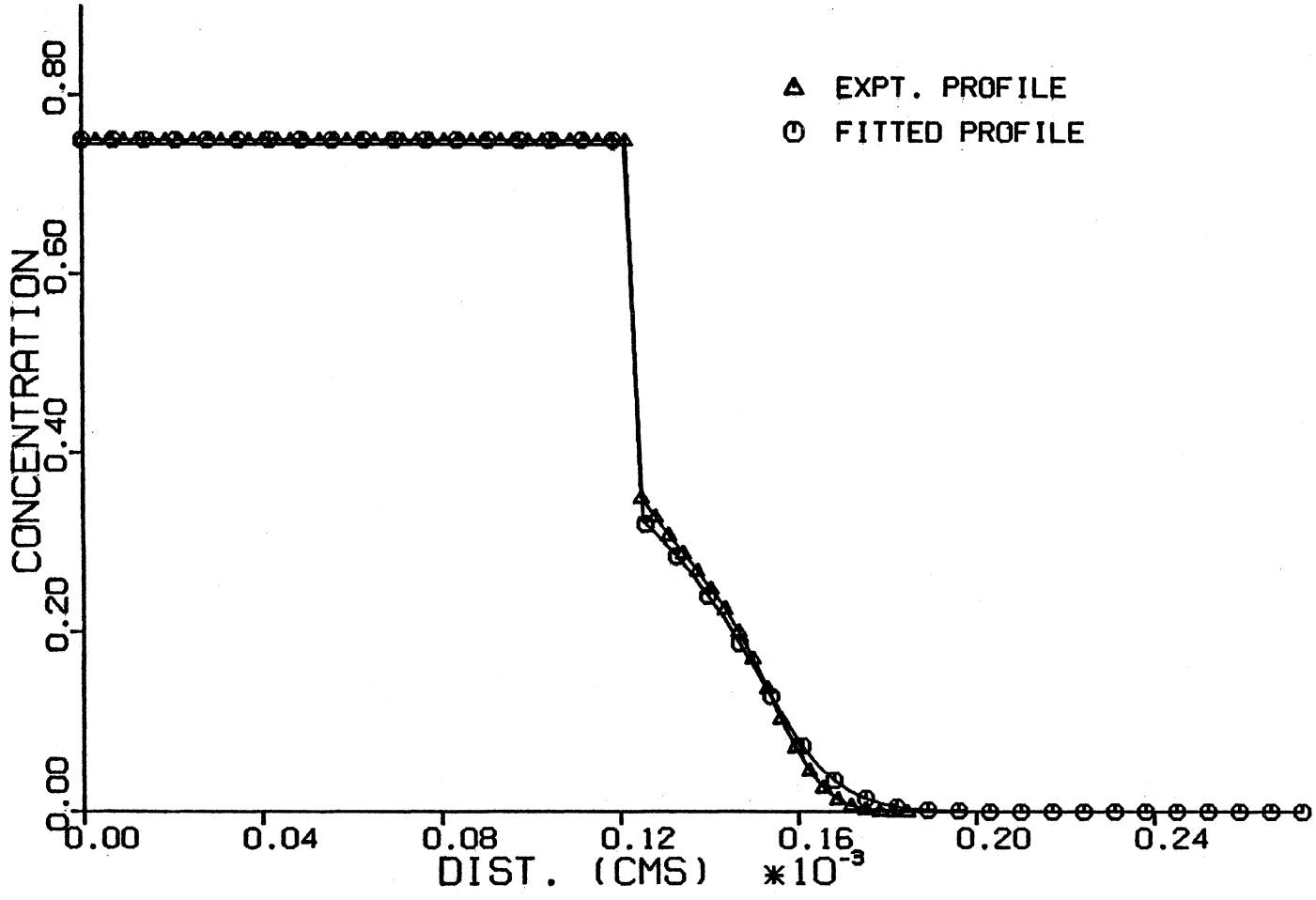


Fig. 43 Simulations of the composition profiles, 635°C (1hr) to obtain diffusion coefficients.

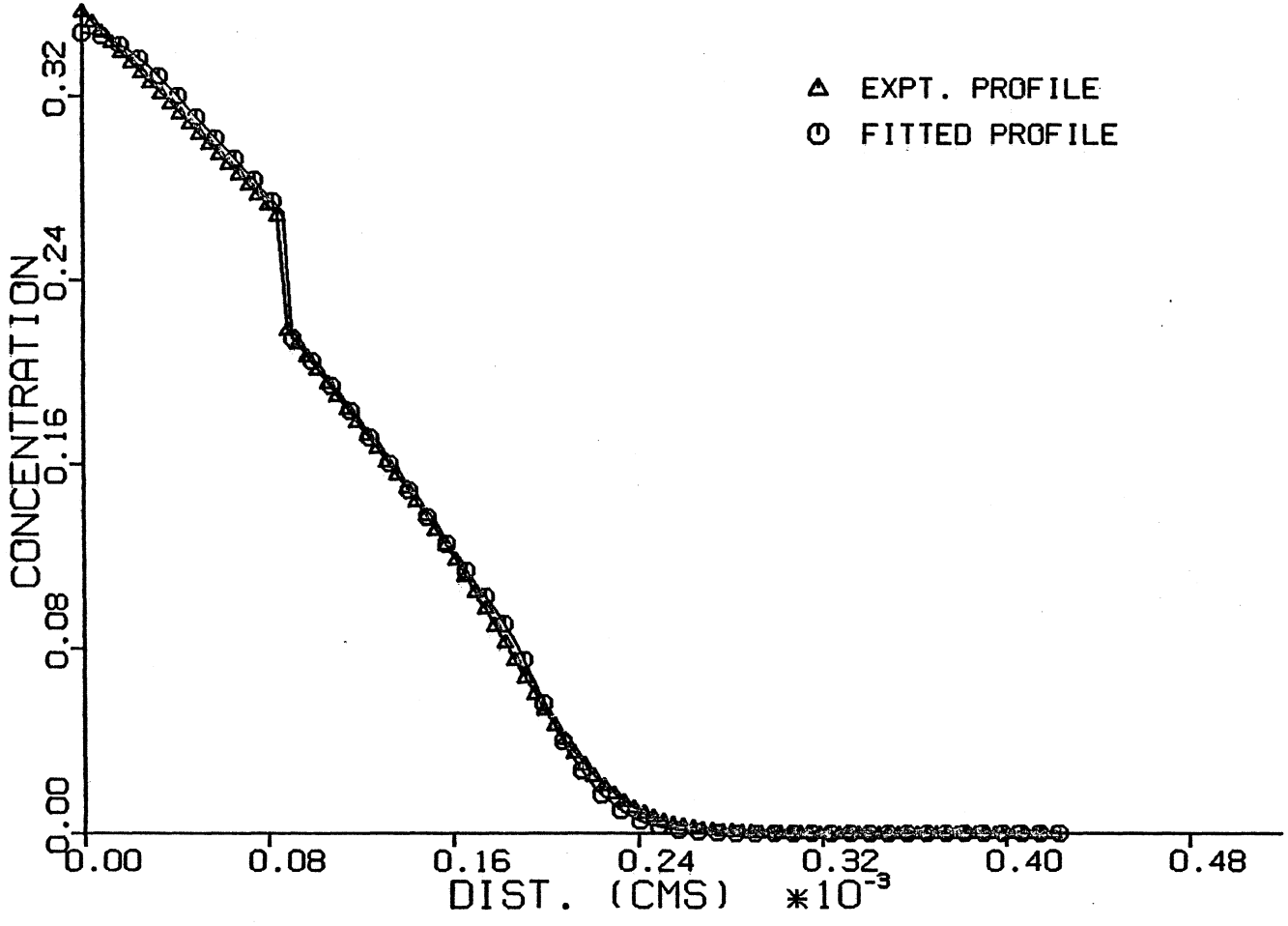


Fig. 44 Simulations of the composition profiles 900°C (1/2hr), to obtain diffusion coefficients.

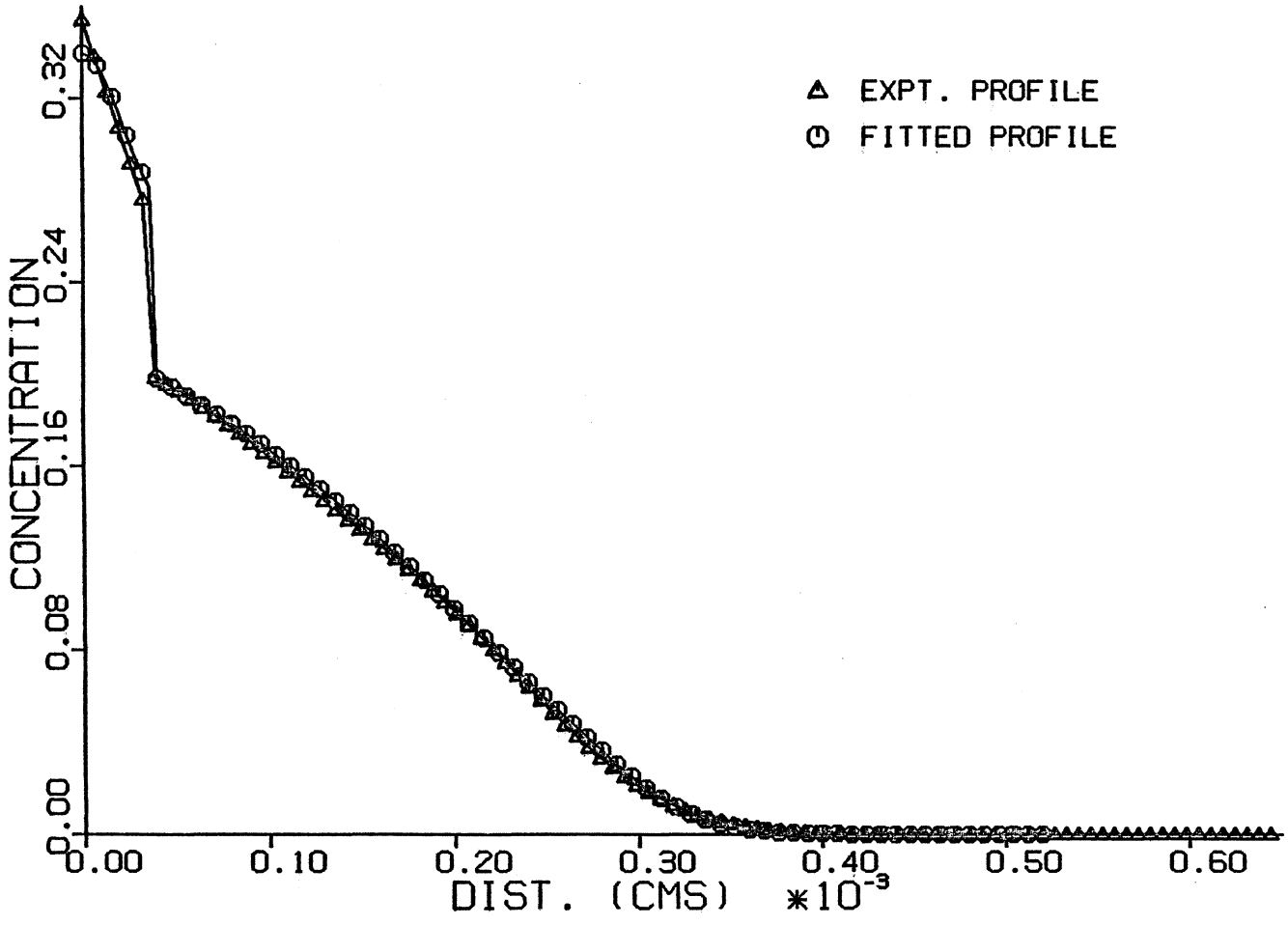


Fig. 45 Simulations of the composition profiles, 900°C (1hr) to obtain diffusion coefficients.

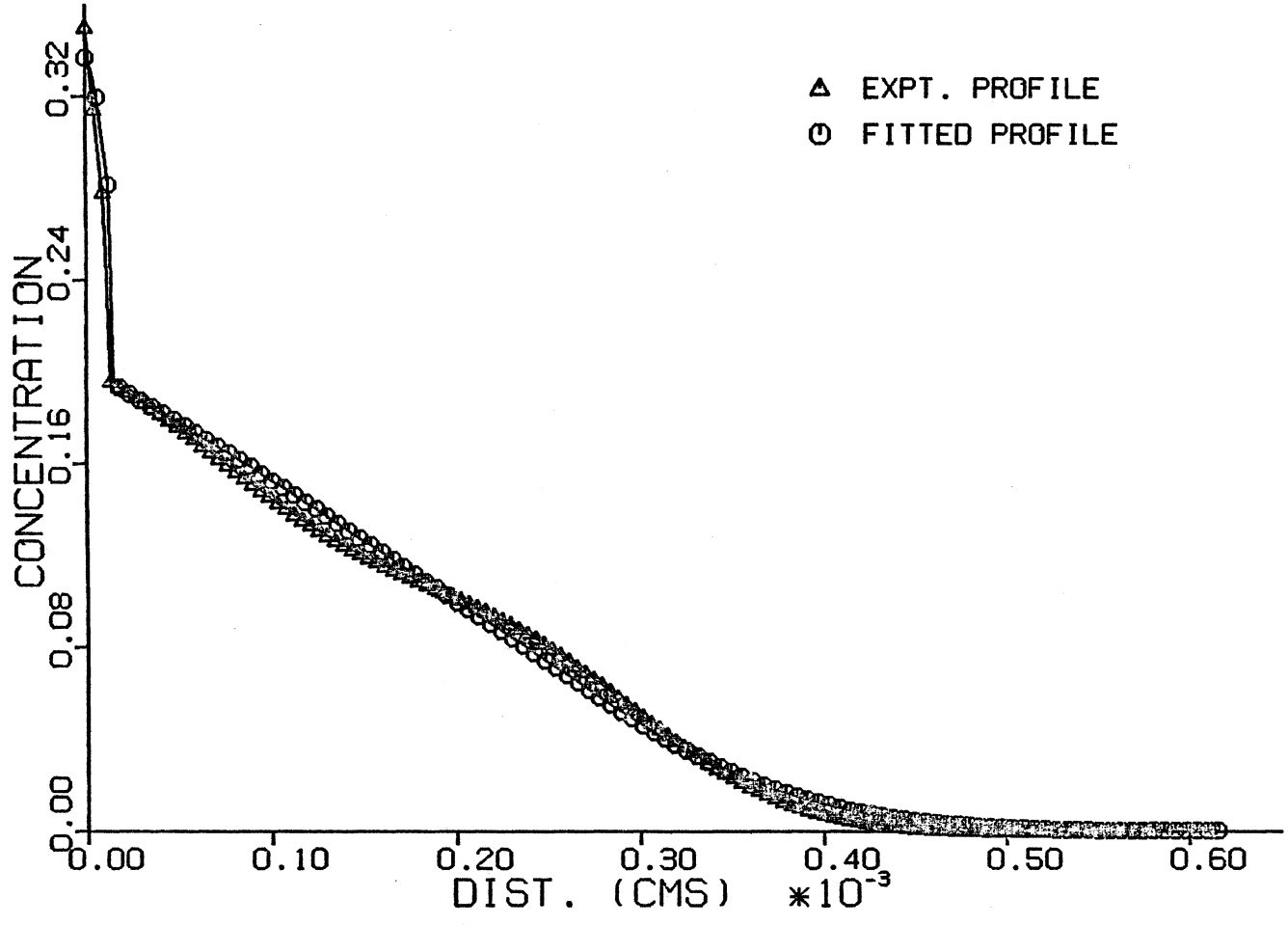


Fig. 46 Simulations of the composition profiles, 900°C (4hrs), to obtain diffusion coefficients.

due to differences in the initial thickness of the Al films, since different samples were used for the various anneals. The maximum error associated with up to a 10% discrepancy in Al thickness was estimated by making use of the data shown in Figure 29. This data shows the integrated intensity of Ti_3Al as well the intensity band for 0.4 and 0.5 micron Al films. It was found that for a ±10% discrepancy in Al thickness, there is a ±14% variation in the slope of the straight line needed to simulate the Ti_3Al reflection. However, there is a very small change in the profile within the alpha-titanium region. Based on this, the range of diffusion coefficients for each time of anneal was determined. This is shown by the error band in Figure 47.

In spite of these corrections it is evident from Figure 47, that the diffusion coefficients for Ti_3Al do have a definite dependence. van Loo and Rieck[32] observed that in the Ti_3Al layer, there was a considerable contribution from grain boundary diffusion. They also observed appreciable growth for longer times. In the present investigations, the differences in diffusion coefficients could be due to enhanced diffusion along grain boundaries. It is seen from Figure 47 that for longer diffusion times, there is reduced contribution of grain boundary diffusion due to grain growth.

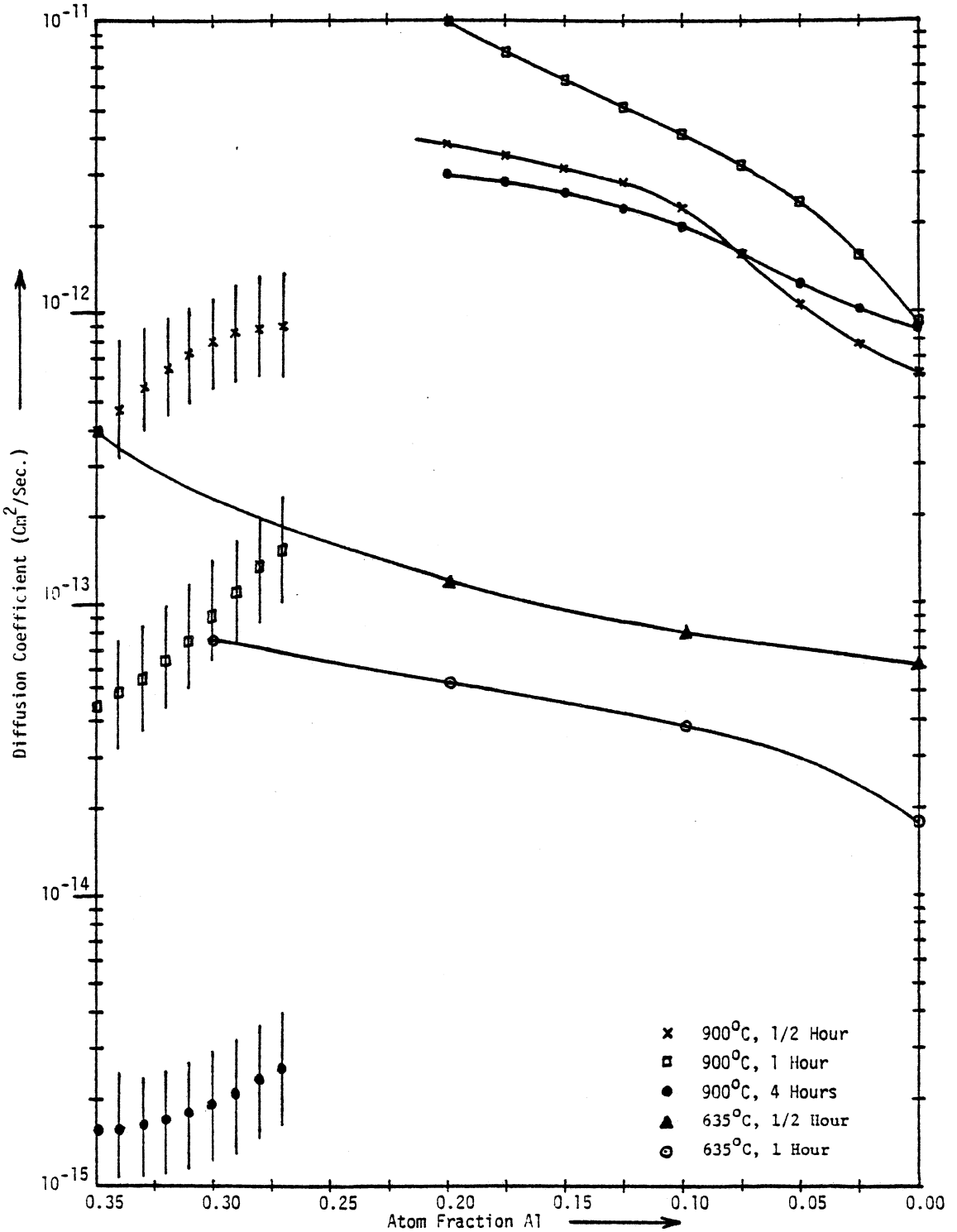


Figure 47. Diffusion coefficient data from the present investigation.

To confirm this, optical microscopy studies was performed on the 1/2hr, 1hr and 4hr samples. Since the samples could not be etched (to avoid etching the Ti_3Al layer away) the grains were not clearly discernable. However, there was some indication of differences in grain growth between the various samples. Attempts to perform scanning electron microscopy studies failed due to lack of contrast. A few photomicrographs using a Reichert optical microscope were obtained, but due to lack of resolution in these pictures they are not included.

Figure 48 shows the arithmetic average of the diffusion coefficients for various times at both 900°C and 635°C, from the present investigation. For 900°C, 2 literature data due to Goold[76] and van Loo and Rieck[32] are also included. The latter data was obtained by electron microprobe studies. It is seen that the average D versus C curve from the present studies is in reasonable agreement with the literature values. However, the present results are the first to show a concentration dependence for the diffusion coefficients. This data shows an increase in diffusion coefficient as the interface is approached. For the low temperature (635°C), the data by van Loo and Rieck[32] is shown along with the averaged data from the present studies. Again, there is reasonable agreement in the diffusion coefficients.

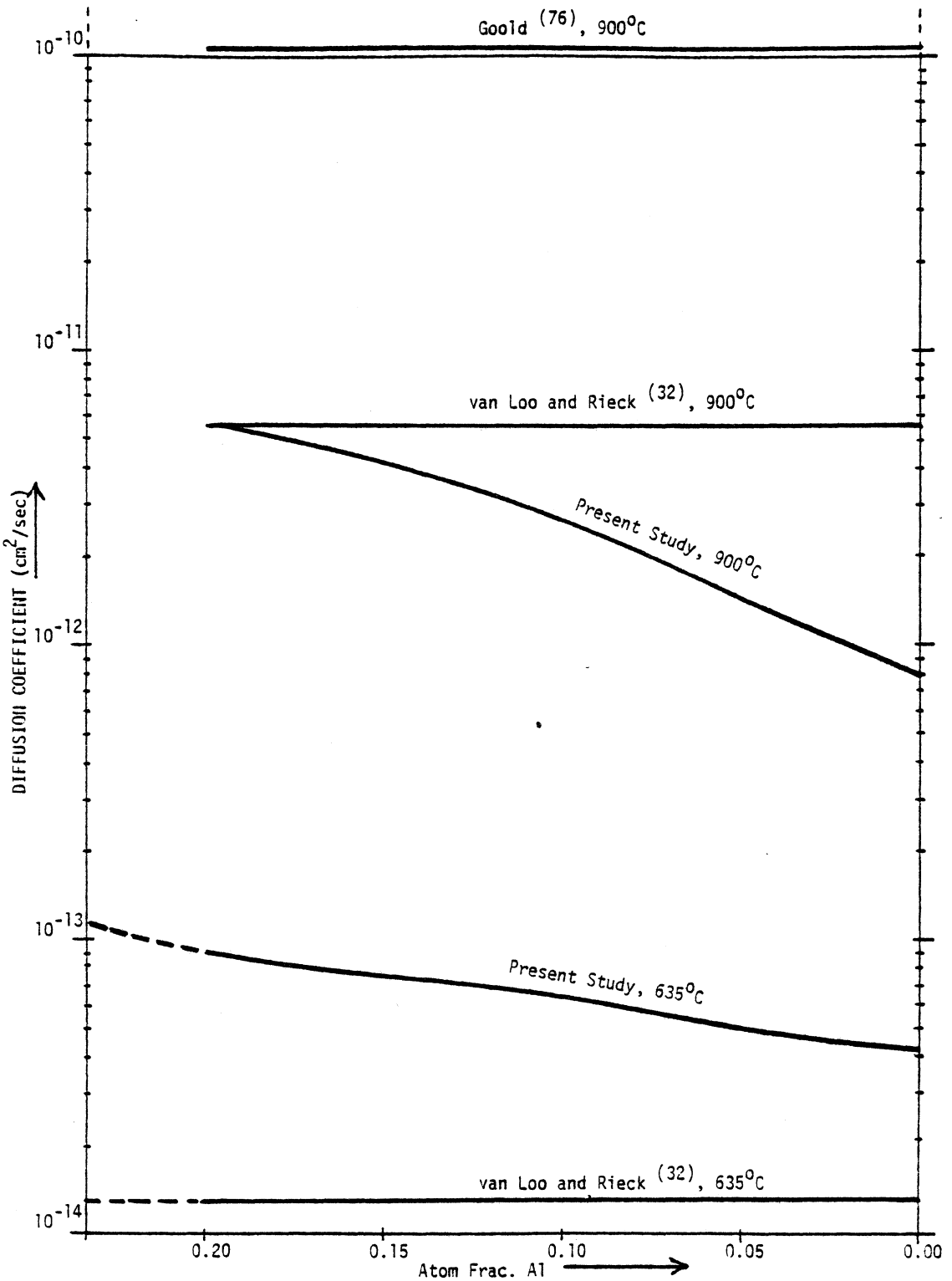


Figure 48. Comparisons of the diffusion coefficients from the present study with those in the literature.

An attempt was made to calculate the diffusion coefficients that can be obtained from a melting point correlation[118]. For this, the following equation is valid: $Q = (K_o + V)RT$ where $K_o = 17$ for FCC and HCP metals $K_o = 14$ for BCC metals $K_o = 21$ for Diamond cubic and $V = 1.5$ for Group IVB metals (Ti, Zr, etc). The melting temperatures can be taken as the average between the solidus and liquidus points in the phase diagram. Using a melting temperature of 1945°K (for 0 at.% Al) a value of 71,487 cals/mole was calculated for Q. For Tm equal to 1873°K (for 30 at.% Al), the value of Q was 68850 cals/mole. The value for D can be calculated from the relation $D_o = 1.04 \times 10^{-3}\ Qa^2$ (ref 118), where a is the lattice constant. Using these extreme values for Q the following diffusion coefficients were calculated.

D (at 900°C) for T_m = 1945°K is 2.97×10^{-14} cm²/sec

D (at 900°C) for T_m = 1873°K is 9.19×10^{-14} cm²/sec

D (at 635°C) for T_m = 1945°K is 3.84×10^{-18} cm²/sec

D (at 635°C) for T_m = 1873°K is 1.66×10^{-17} cm²/sec

It is evident that at 900°C, the diffusion coefficients calculated from a melting point correlation are nearly two orders of magnitude lower that the data from the present study. At the lower temperature (635°C) the deviation is even larger. The diffusion coefficients obtained from a

melting point correlation represent volume diffusion only. With grain boundary diffusion, the observed diffusion coefficients would tend to be higher. This indicates that in the present study, there was a significant contribution from grain boundary diffusion at 635°C and this became smaller at the higher temperature. However, the present diffusion coefficient data is closer to the data from a melting point correlation when compared with other literature data.

Using the relationship between D_o and Q described earlier and the relation $D=D_o \exp(-Q/RT)$, composition dependent activation energies were calculated from the 635 and 900°C data. These values along with the activation energies from the melting point correlation are shown in Figure 49. If only volume diffusion were present, the activation energies from the 900°C and 635°C data should be the same. However, the activation energy for 635°C is lower because of enhanced grain boundary diffusion. For the higher temperature, the activation energies approach those predicted from a melting point correlation.

6.6 COMPUTER SIMULATIONS OF THE INTEGRATED INTENSITIES OF TI-AL COMPOUNDS

The results of the computer calculation of integrated intensities for the $TiAl_3$ compound are shown in Table 34. The two-theta positions calculated by using the lattice par-

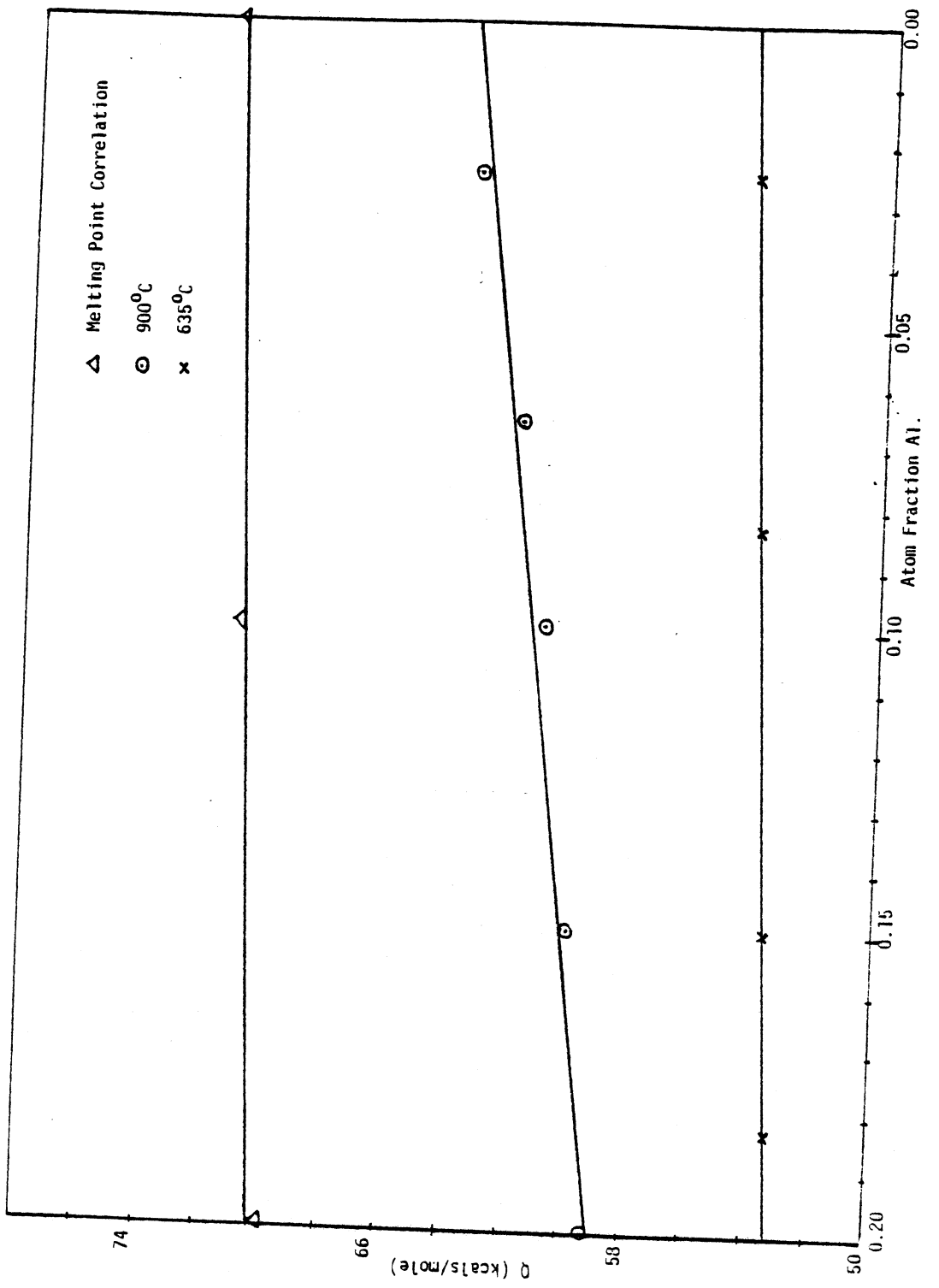


Figure 49. Activation energies plotted against composition, for Al diffusion in alpha-titanium.

ameters from the van Loo and Rieck[25] study are also shown. The corresponding data obtained by using the TiAl standard prepared in the present study is also included. Both sets of results are those obtained if a graphite monochromator (2 = 26.40) is used. It can be seen from Table 34 that there is excellent agreement between the integrated intensity results of the present study and the theoretical (computer) calculations. The "card file" values obtained by van Loo and Rieck[25] are also shown alongside for comparison. It can also be seen that the card file data is incomplete and approximate.

Table 35 shows the computer calculated relative intensities for the disordered Ti_3Al and Ti_2Al phases based on a random occupation of all sites (see Appendix 6). The relative intensities from the corresponding powder diffraction data is also shown alongside. A comparison of this data with the computer calculations shows that Ence and Margolin[74] observed several diffraction lines from the Ti_2Al superlattice. These are easily distinguished from the fundamental lines since the computer values are entirely for the disordered phase (having fundamental lines only). Also, there are significant discrepancies between the theoretical relative intensities and those obtained by Ence and Margolin, for the Ti_2Al phase. On the other hand, Goldak and

TABLE 34

Integrated intensities and two-theta positions for $TiAl_3$

hkl	$TiAl_3$ 2θ	Std.(present) Rel.Int.	Computer Calc. 2θ	Computer Calc. Rel.Int.	van Loo (25) 2θ	van Loo (25) Rel.Int.
002	20.585	3.49	20.61	3.36	20.59	60.00
101	25.305	10.10	25.32	8.11	25.28	40.00
110	32.875	1.74	32.88	2.02	32.90	20.00
112	39.100	100.00	39.12	100.00	39.08	100.00
103	39.200					
004	41.910	21.14	41.94	19.95	41.92	100.00
200	47.155	25.29	47.19	28.15	47.14	80.00
202	51.975	0.97	52.00	0.91	-	-
114	54.265	2.60	54.29	2.33	54.26	20.00
211						
105	58.655	0.39	58.68	0.58	58.64	10.00
213	62.875	0.89	62.90	0.90	62.86	10.00
006	64.915	24.79	64.93	21.24	64.88	60.00
204						
220	68.910	7.90	68.95	8.80	68.88	40.00
222	-	-	72.83	0.27	-	-
116	74.685	13.96	74.73	14.16	74.68	60.00
301						
215	78.470	0.57	78.50	0.62	78.46	10.00
310						
312						
303	82.205	22.71	82.23	21.83	82.18	60.00
107						
224	84.045	11.13	84.05	10.33	84.09	40.00
206						
008	91.365	1.73	91.40	2.12	-	-
314	93.235	0.41	93.28	0.55	-	-
321						
305	-	-	96.95	0.13	-	-
118	100.620	0.70	100.65	0.50	-	-
217						
323						
226	-	-	102.53	0.13	-	-
400	106.320	3.01	106.35	3.45	-	-
208						
402	110.135	7.10	110.19	7.00	-	-
316						
411	112.130	15.32	112.17	13.88	-	-
325	-	-	116.19	0.33	-	-
330						
307						
413	120.350	7.47	120.36	7.38	-	-

332						
404	122.500	5.72	122.52	7.07	-	-
420	126.985	6.79	127.01	7.36	-	-
228	131.665	8.86	131.73	8.14	-	-
422						
334	-	-	134.25	0.18	-	-
415	139.645	8.70	139.62	0.40	-	-
318						
327	-	-	145.63	0.97	-	-
406						
424	149.075	21.51	149.07	22.89	-	-

Parr[47] observed fewer superlattice lines for the Ti_3Al phase. Also, the relative intensities obtained by Goldak and Parr are in reasonable agreement with the theoretically predicted ones.

A Ti_2Al powder standard was prepared by mixing stoichiometric amounts of pure Ti and Al powders. This was reacted at 900°C for 71 hours and an X-ray diffraction sample was prepared as described in Chapter 4. The relative intensities from the Ti_2Al standard are also included in Table 35. It is seen that there is reasonable agreement between these intensities when compared with the computer values. No superlattice lines from the Ti_2Al phase were observed. The 'a' and 'c' lattice parameters obtained from two 'hk0' and '00k' type reflections were obtained. The 'a' lattice parameter was found to be 2.891 A. By an examination of Figure 4, it is seen that this value would be obtained if the 'a' parameter curve (<13%Al) is extrapolated into the region corresponding to the Ti_2Al composition. This proves that in the presence of the disordered Ti_2Al (or Ti Al) phases, an extension of the alpha-titanium compositions is valid. For superlattice Ti_2Al (or Ti_3Al), the lower branch of the 'a' parameter curve should be used.

TABLE 35

Table showing the Integrated Intensities of Ti_2Al and Ti_3Al from several investigations.

hkl	Ti_2Al			Ti_3Al	
	Std. (present)	Computer Calc. Disordered	Ence and Margolin	Computer Calc. Disordered	Goldak and Parr
100	-	0.0	10.0	0.0	-
101	-	0.0	20.0	0.0	4.0
110	-	0.0	5.0	0.0	2.0
200	27.3	24.8	50.0	24.8	20.0
002	23.7	26.0	70.0	26.0	25.0
201	100.0	100.0	100.0	100.0	100.0
210	-	0.0	5.0	-	-
112	-	0.0	10.0	-	-
211	-	0.0	5.0	-	-
202	15.1	13.9	60.0	13.9	18.0
103	-	0.0	5.0	-	-
220	13.6	15.4	50.0	15.3	18.0
302	-	0.0	5.0	-	-
203	23.5	16.2	50.0	16.1	30.0
400	2.8	2.3	10.0	2.3	2.0
222	20.4	16.9	40.0	16.8	30.0
401	15.3	12.1	30.0	12.0	18.0
004	2.5	2.3	20.0	2.3	2.0
402	2.3	3.0	20.0	3.0	4.0
204	3.2	2.7	20.0	2.7	4.0
403	11.1	7.3	30.0	7.2	10.0
420	1.1	2.4	10.0	2.4	-
421	12.6	14.5	40.0	14.4	18.0
224	12.2	9.9	40.0	9.8	18.0
422	4.8	5.2	10.0	5.2	4.0
205	7.9	8.1	40.0	8.0	10.0
404	-	2.9	10.0	2.9	-
215	14.3	6.3	20.0	6.3	25.0
423	21.2	24.6	50.0	24.6	40.0
602	27.8	26.2	40.0	26.3	18.0

Chapter VII

CONCLUSIONS

1. Aluminum and Mo_5Si_3 films were investigated to study the use of coatings for the control of interface reactions in SiC/Ti planar composites.

2. X-ray diffraction analysis on samples vacuum annealed at 875°C for various times indicated that Ti_5Si_3 was the major silicide product.

3. For the SiC/Mo_5Si_3/Ti composites, a large amount of Ti_5Si_3 was formed. Most of this silicide formation was due to the presence of free silicon from the dissociation of Mo Si at the interface.

4. Reaction rate curves were obtained for the SiC/Mo_5Si_3/Ti, SiC/Al/Ti and SiC/Ti_3Al/Ti systems. It was found that aluminum films were effective in reducing silicide formation. Also, the results indicated that Ti_3Al acts as an effective barrier.

5. In order to determine the optimum thickness of aluminum films for fabrication of SiC/Ti composites, reaction studies on Al/Ti standards were performed.

6. It was found that a 0.5 micron aluminum film would be used. A 1 hour preanneal at 900°C is necessary before fabrication of the panels. A hold at 635°C for 1 hour ensures that a Ti-Al intermetallic compound forms before the Al melts during the heat-up to 900°C.

7. The decomposition of the $TiAl_3$ phase at 635°C and the Ti_3Al phase at 900°C results in a solid-solution of Al in alpha-titanium. When examined by X-ray diffraction, this appears as an intensity band.

8. Using a computer simulation technique, composition profiles for aluminum diffusion in alpha-titanium, were obtained.

9. For the simulations, an extension of the 'a' parameter curve into the disordered Ti_3Al and Ti_2Al regions, was used.

10. A composition gap was used in the profiles to simulate the Ti_3Al diffraction peak. The size of the gap increased for longer annealing times. The equilibrium limit and the compositions at the gap are in accord with the equilibrium phase diagram,

although there is no certainty that an equilibrium situation existed.

11. Composition profiles were analyzed and composition dependent diffusion coefficients in Ti_3Al and alpha-titanium were obtained.

12. At 900°C, the diffusion coefficients in Ti_3Al ranged between 10^{-13} and 10^{-15} cm^2/sec. There was a significant contribution from grain boundary diffusion in the Ti_3Al phase. For longer annealing times, there was grain growth and smaller diffusion coefficients were obtained.

13. For alpha-titanium, diffusion coefficients in the 10^{-12} cm^2/sec range at 900°C were obtained. Activation energies were calculated from the data at 635°C and 900°C. These values were compared with the activation energies calculated from a melting point correlation. The activation energies at 635°C(0.5 T) and 900°C(0.6 T) were lower, indicating that there was diffusion along high diffusivity paths.

REFERENCES

1. Prewo, K.M. and Kreider, K.G., 'Deformation and Fracture of Borsic Reinforced Composites', Titanium Science and Technology, ed. Jaffee, R.I. and Burte, H.M., Plenum Press, 1973, p.2333-2345.

2. Brentnal, W.D. and Toth, I.J., 'High Temperature Composites', AFML-TR-73-223, Sept. 1973.

3. Doble, G. S., Melnyk, K. P., Toth, I.J., 'Manufacturing methods for Filamentary Reinforced Titanium Monotapes', AFML-TR-74-14, Jan. 1974.

4. Rao, V.B., Houska, C.R., Unnam, J., Brewer, W.D. , and Tenney, D.R., 'Interfacial Reactions in Borsic/Ti-3Al-2.5V Composites', Proceedings of the TMS-AIME Fall Meeting, Oct., 1978.

5. Schob, O., Nowotny, H. and Benesovsky, F., 'The Ternary System (Ti, Zr, Hf)-Al-Si', Planseeber., Pulvermetall, vol. 10, 1962, p. 65-71.

6. Paillier, R., Lahaye, M., Thebault, J., and Naslain, R., 'Chemical Interaction Phenomena at High Temperature between Boron Fibers and Ti Metal (or TA6V alloy)', Fall Meeting of TMS-AIME, Chicago, Oct. 1977.

7. 'High Temperature Ti Composites', Air Force Materials Lab., Wright Patterson Air Force Base, Ohio, AFML-TR-73-223, Sept., 1973.

8. Metcalfe, A.G. , 'Interfaces in Metal Matrix Composites (Academic Press, N.Y., 1974).

9. Schmitz, G. K., and Metcalfe, A. G., 'Development of Continuous Filament Reinforced Metal Tape', AFML-TR-68-41, Feb. 1968.

10. Snide, J.A. , 'Compatibility of Vapor Deposited B, SiC, and TiB2, Filaments with Several Ti Matrices', AFML-TR-67-354, Feb. 1968.

11. Ashdown, K.C., and Chang, W.H., Trans. A.S.M., vol. 61, 1968, p.550-556.

12. Rudy, E. , 'A Compendium of Phase Diagrams', AFML-TR-65-2, Part V, 1969.

13. Ratliff, J.C., and Powell, G.W., 'Research on Diffusion Multiphase Systems, Reaction Diffusion in Ti/SiC and Ti-6Al-4V/SiC Systems' AFML-TR-70-42, Mar. 1970.

14. Brukl, C., Nowotny, H., Schob, O., and Benesovsky, F., Monatsh. Chem., vol. 92, 1961, p.781-788.

15. Elliot, R. P., 'Constitution of Binary Alloys', McGraw Hill Book Co., N.Y., 1965.

16. Moffat, W.G., 'Binary Phase Diagrams Handbook', General Electric co. Schenectady, 1976.

17. Dietrich, F. E., 'An X-Ray Study of the Behavior of Ti Films on Si Substrates', M.S.Thesis,VPI&SU, June, 1977.

18. Orszagh, J. , and van der Poorten, H., Rev. Int. Hautes Temper. et Refract., vol. 11 (2), 1974, p.109-112.

19. Fitzer, E., and Schmidt, F.K., High-Temp.-High Press., vol. 3, No.4, 1971, p.445-460. In german.

20. Gehman, V. H. Jr,.'An X-Ray Method for the Kinetic Analysis of Ti on Si Thin Films', Masters Thesis, VPI& SU, Oct., 1979.

21. Zemskov, G. V. , and Shulenok, P. F. , Prot. Metals 2, vol. 83, 1966.

22. Mackowiak, J., and Shreir, L.L., J. Less Common Metals, vol. 1, 1959, p.456.

23. Mackowiak, J., and Shreir, L.L., J. Less Common Metals, vol. 15, 1968, p.341.

24. Slama, G. , and Vignes, A. , J. Less Common Metals, vol. 24, 1971, p.1.

25. van Loo, F. J. J., and Rieck, G. D. , 'Diffusion in the Ti-Al system-Interdiffusion between solid Al and Ti or Ti-Al alloys', Acta Met., vol. 21, Jan. 1973.

26. Raman, A., and Schubert, K. , Z.Metallk, vol. 56, 1965, p.44.

27. Kidson, G . V. , J. Nucl. Mater, vol. 3 , 1961 p. 21.

28. Heumann, Th. , La diffusion dans les Mitaux , Comptes Rendus du colloque a Eindhoven, 1956 p. 59-75.

29. Baird , J. D . , J. Nucl. Energy vol. A11, 1960 p. 81.

30. Potzechke, M. , and Schubert, K. , Z. Metallk, vol. 53, 1962 p.548.

31. Schubert , K. , Meissnev , H. G. , Raman , A. , and Rosstentscher, W., Naturwissenschaften, vol.51 , 1964, p.287.

32. van Loo, F. J. J., and Rieck, G. D., Acta Metallurgica, vol.21, Jan.1973.

33. Wagner, C. , Acta Metallurgica., vol. 17, 1969, p. 99.

34. Kidson, G.V., and Miller, G.D., J.nucl. Mater, vol. 12, 1964, p. 61.

35. Heumann, Th. , and Dittrich, S. , Z. Metallk., vol. 50, 1959, p.617.

36. Heumann, Th. , Z. Metallk, vol. 58 , 1969, p. 168.

37. Heumann, Th. , Z. Metallk, vol. 59, 1968 , p. 455.

38. Pouliquen, J., Offret, S., and deFouquet, J., C.R.Acad. Sci., Ser.C, vol. 274., No.22, 1972, p.1760-3.

39. Pokcev, A. V., Mironov, V. M., Kudryavtseva,L. K., Izv. Vyssh. Uchebn. Zaved. Tsvetn. Metall. , vol. 2, 1976 , p.130-132.

40. Hansen, M.,'Constitution of Binary Alloys', McGraw-Hill Book Co., 1958.

41. Sagel, K. , Schultz, E. , and Zwicker, U., Z. Metallk, vol. 47, 1956, p.529.

42. Anderko, K. , Sagel, K., and Zwicker, U., Z. Metallk, vol. 48, 1957, p.57.

43. Ence, E., and Margolin, H., Trans.Metall.Soc. A.I.M.E., vol. 221, 1961, p.151.

44. Glazova, V. V. , Dokl. Chem. , vol. 160, 1965, p.11.

45. Yao, Y.L., Trans. Am. soc. Metals, vol. 54, 1961,p.241.

46. Pietrokowsky , P . , Nature, vol. 190. , 1961, p. 77.

47. Goldak,A.J., and Parr,J.G., Trans.Metall.Soc. A.I.M.E., vo. 221, 1961, p.639.

48. Clark, D., and Terry, J.C., Bull. Inst. Metals, vol. 3, 1955-57, p.116.

49. Clark, D., Jepson,K.S., and Lewis,G.I, J. Inst, Metals, vol. 91, p.1962-63, p.91.

50. Kornilov, I. I., Pylaeva, E.N., Volkova, M.A., Kripya kevich, P.I., and Markiv, V. Ya., Dokl. Chem. vol.161, 1965, p.332.

51. Kornilov, I.I., and Volkova, M.A., Russ. Metall., 1968, p. 105.

52. Tsujomoto, T., and Adachi, M., J.Inst. Metals, vol. 94, 1966, p.358.

53. Crossley, F.A., Trans. Metall. Soc., A.I.M.E., vol.236, 1966, p.1174.

54. Crossley, F. A., Trans. Am. Soc. Metals, vol. 60, 1976, p.714.

55. Crossley, F.A., Trans. Metall. Soc., A.I.M.E., vol.245, 1969, p.1963.

56. Blackburn, M.J., Trans.Metall.Soc., A.I.M.E., vol. 239, 1967, p.1200.

57. Crossley, F.A., Trans. Metall. Soc., A.I.M.E., vol.242, 1968, p.726.

58. Blackburn, M.J., Trans. Metall. Soc.,A.I.M.E., vol.242, 1968, p.728.

59. Margolin, H., Trans. Metall. Soc., A.I.M.E., vol. 242, 1968, p.742.

60. Blackburn, M.J., Trans. Metall. Soc.,A.I.M.E., vol.242, 1968, p.743.

61. Ogden, H.R., Maykuth, D. J., Finlay, W. L., and Jaffee, R. I., 'Constitution of Titanium - Aluminum Alloys', AIME Trans., vol. 191, 1951, p.1150.

62. Bumps, E.S., Kessler, H.D., and Hansen, M. , 'Titanium Aluminum System', AIME Trans., vol. 194, 1952, p.609.

63. Kornilov, I. I., Pilajewa, E. N., and Volkova, M. H., 'Diagramma Sostojania Dvoinoi Sistemi Titan-Aluminia', Izves. Akad. Nauk SSSR, 1956, No. 7, p.2.

64. Ence, E. , and Margolin, H., 'Preliminary Report on Ti-Al-O and Ti-Al Phase Diagrams', Physical Metallurgy Symposium, Watertown Arsenal , Watertown, Mass. , Sept.1955

65. Ence, E., and Margolin, H., 'Research and Development with Respect to the Ti-Al-O System', Summary Report to Watertown Arsenal, July 1956, Contract No. DA-069-ORD -1481,Wal No. 40/214-3.

66. Ence, E., and Margolin, H., 'Compounds in the Titanium Rich Region of the Ti-Al System', AIME Trans. , vol. 209,1957, p.464.

67. Pietrokowsky, P. , 'Crystal Structure of Ti3Sn', Trans. AIME, vol. 194, 1952, p.211.

68. Clark, D., and Terry, J. C., 'Superlattice Formation in Alpha-Titanium-Aluminum Solid Solutions', Bull. Inst. Metals.,vol. 3, pt. 13, 1956, p. 116, letter to the editor.

69. Anderko, K., Sagel, K., and Zwicker, U., 'Hexagonale Ordnungsphasen in den Systemen Ti-Al und Ti-In ', Z.Metallk,vol. 48, 1957, p.57.

70. Saulnier, A., and Croutzelles, M.,'Surstructure dans un alliage Ti-Al 15 Pct.', Academie des Sciences, Compt. rend.des Sciences, vol. 246(26), 1958, p. 3622-3625.

71. Crossley, F.A., and Carew, W.F.,'Embrittlement of Ti-Al Alloys in the 6 to 10 Percent Al Range', Trans AIME, vol.209, 1957, p.43.

72. Sagel, K., Schulz, E., and Zwicker, U., 'Untersuchungen am System Titan-Aluminum', Z. Metallk, vol. 46, 1956, p.529.

73. Ence, E. and Margolin, H., Final Report to Watertown Arsenal, June 1957, Contract No. DA-30-069-505-ORD1781, WAL No. 401/214-4.

74. Ence, E. , and Margolin, H. ,' Phase Relations in the Titanium-Aluminum System', Trans.AIME, vol.221,Feb.1961 p.151.

75. Jepson, K.S. , Lewis, G.I., Clark, D., unpublished work

76. Goold, J. Inst. Metals, vol. 88 , 1959-60, p. 444

77. Unnam,J., 'X-ray diffraction technique for the study of bi-mettalic, two phase, diffusion zones', Ph.D Thesis, V.P.I and S.U, May 1975.

78. Unnam, J., and Houska, C. R., Journal of Appl. Phys., vol.47, No.10, Oct.1976, p.4336.

79. Houska, C.R., and Rao, V.B., Met.Trans. A., vol9A, Oct. p.1483.

80. Houska, C. R. , J. Appl. Phys., vol. 41 p. 69, 1970.

81. Houska, C.R., Thin Solid films, vol.25,1975, p.451-464.

82. Houska, C.R., "Investigation of Composition Variation by diffraction", Review article, V.P.I and S.U.

83. Warren, B.E., X-ray Diffraction, p.49 and volume. 171, Addison-Wesley Publishing Co. Inc. , Reading, Mass., 1968.

84. Pike, E.R., Acta Crystallographica, vol.12, 1959, p.87.

85. Hall ,M. M. Jr., Veeraraghavan, V. G., Rubin, H. , and Winchell, P.G., J. Appl. Crystallography, vol.10, 1977, p.66-68

86. Elderton, W.D., and Johnson,N.L., 'Systems of Frequency Curves', New York: Cambridge Press, 1969, p.77-78.

87. Unnam, J., Tenney, D. R., Carpenter, J.A., and Houska, C. R., College of Engr., VPI&SU, Technical Report No. VPI-E76.9, 1976.

88. Fick, A., Ann. Phys. Lpz., vol. 94, 1855, p.59.

89. Crank, J., 'The Mathematics of Diffusion', Oxford Univ. Press, London, 1964.

90. Carslaw, H.S., and Jaeger, J.C., 'Conduction of Heat in Solids', Oxford, 1947.

91. Tenney, D. R., Carpenter, J. A., and Houska, C. R., J. Appl. Phys., vol. 41, 1970, p4485.

92. Houska, C. R., and Unnam, J., J. Appl. Phys., vol. 47, No. 10, Oct.1976, p.4325.

93. Fogelson, R. L., and Heckel, R. W., AIME, Trans., vol. 19, 1965, p.212.

94. Tanzilli, R. A., and Heckel, R. W., AIME, Trans., Vol. 242, 1968, p.2313.

95. Swanson, H.E., and Tatge, E., JC Fel.Reports, NBS 1950, (ASTM 4-0787).

96. Unnam, J., and Houska, C. R., Scripta Met., vol.8,1974, p. 61.

97. Unnam, J., and Houska, C. R., Scripta Met, vol.8, 1974, p. 801.

98. Unnam, J., and Houska, C. R., College of Engr., VPI&SU, Technical Report, No. VPI-E76.3, 1976.

99. Dagernann, T, in 'Constitution of binary alloys', 2nd Suppl., McGraw Hill, 1969, p.45

100. Clark, H. T., Trans. Metall. Soc., AIME, vol.185, 1949, p.588.

101. Semi-alloys Inc., 888 S. Columbus Ave., Mount Vernon, New York 10550.

102. Perkin Elmer Ultek Inc., P.O. Box 10920, Palo Alto, California 94303.

103. Specialty Metals and Alloys Co., Inc., 75 Grove City Rd., Grove City, Ohio 43123.

104. Metron Inc., P.O. Box 147-Allamuchy, New Jersey 07820.

105. Haseldon Company Inc., P.O. Box 1436, San Jose, Calif. 95109.

106. Mettler Instr. Corp., Hightstown, N.J., Made in Switz.

107. Dustoff, Manostat, 519, 8th Ave., N.Y., N.Y. 10018.

108. Leeds and Northrup Co., Philadelphia, Pa.

109. National Bureau of Standards.

110. Siemens America, Inc., N.Y., N.Y.

111. ES Industries , 8S Maple Ave., Marlton, N.Jersey.

112. Tennelec, Oak Ridge, Tennessee.

113. Riechert, Optiche Werke, Austria.

114. Perkin Elmer Ultek Inc., Instruction Manual for the Kandex 2400 Series Sputtering Systems, P/N 112128100.

115. Tektronix Inc., P.O. Box 500, Beaverton, Oregon 97077.

116. Smith, T. M., Masters Thesis, VPI&SU, Aug. 1980.

117. Ventron Corp, Alpha Division, 152 Andover St., Danvers, Ma. 01923.

118. Sherby, O. and Simnad, M.T., Trans. ASM, Vol. 54, 1961, p.227.

119. Cullity. B. ,'Elements of X-ray diffraction', Addison Wesley Publishing Co., Inc., Reading, Mass.

```
C                              APPENDIX 1
C
C
C
C
C
C    DIFFRACTED X-RAY INTENSITY SIMULATION,  PROGRAM DXIS.
C
C    MODIFIED ON JAN 25,1979 FOR K-ALPHA-1 K-ALPHA-2 SIMULATION.
C    CHOOSE NBANDS=2 AND IAL12=1 FOR THIS SIMULATION.
C    K-ALPHA-1 DATA SHOULD BE INPUT FIRST, THEN K-ALPHA-2 DATA.
C    THE COMPO ARRAY SHOULD BE SAME FOR BOTH ALPHA1 AND ALPHA2.
C    THE FINAL INTENSITY (AINTEN) IS COMPUTED AS ALPHA1 + 0.5 ALPHA2.
C    ONLY ONE BAND CAN BE SIMULATED AT A TIME.
C
C   THIS PROGRAM SIMULATES THE DIFFRACTED X-RAY INTENSITY FOR A GIVEN
C   CONCENTRATION PROFILE OF A SINGLE OR TWO-PHASE BINARY SYSTEM ALLOWING
C   FOR VARIATION OF LINEAR ABSORPTION COEFFICIENT WITH CONCENTRATION.
C   ALL CONCENTRATIONS SHOULD BE INPUT IN ATOM FRACTION OF PLATING ELEMENT B.
C
      DIMENSION COMPO(160), TT(160), Q(160), ALU(160),C(500),P(500),
     1 IDEN4(20)  , EFA(500),TG(500), QG(500), ALUG(500), ALG(500),
     2  IDEN2(10), FI(20), PLA(2), SUB(2),T2V(200),AEXP(150),
     3 AINTEN(200),UBP(200),EFV(200),DIST(500),NPTS(10),AINT12(200)
      DIMENSION T2X(100),AINTX(100),AP(10),BP(10),DP(10),SDIST(500)
      DIMENSION SUM(200,3),ICOEFF(150)
C
C   THE ABOVE FORTRAN STATEMENT SETS ALL UNDERFLOWS TO ZERO. THE CORRESPONDING
C   WATFIV STATEMENT IS   CALL TRAPS (0,5,999999,3,1)
C
    3 FORMAT(1H1, //////)
    6 FORMAT(E12.5,E12.5,4I4,E12.5)
    9 FORMAT(F5.3,5I5)
```

```
   11 FORMAT( 2F13.9, 4I5 ,F8.5)
   13 FORMAT(  2F12.5,  36X,  E12.5  )
   18 FORMAT( 15X,'TWO-THETA  UB INTEN.  BROAD.INTEN  EFF.VOLUME'/)
   19 FORMAT(10X,I5, F8.4, E11.3, E13.3,E12.3)
   40 FORMAT(8F8.5)
   41 FORMAT(20A4)
   52 FORMAT(51X, F12.5)
   53 FORMAT(2I5)
  304 FORMAT(15X, 'SINGLE PHASE BINARY SYSTEM.')
  305 FORMAT(15X, 'TWO-PHASE BINARY SYSTEM.')
  306 FORMAT(15X, 'PLATING THICKNESS',T35, '=',E12.4, ' CMS.')
  307 FORMAT(15X, 'SUBSTRATE THICKNESS', T35, '=', E12.4, ' CMS.')
  308 FORMAT(15X, 'SUBSTRATE THICKNESS', T35, '=', 4X, 'INFINITE')
  309 FORMAT(15X, 'INTERFACE POSITION', T35, '=', E12.4, ' CMS.')
  310 FORMAT(15X, 'G FACTOR', T40,'=', F15.4)
  311 FORMAT(//15X,'CAUCHY FUNCTION IS USED FOR INTENSITY BROADENING.'/
     1  15X, 'FOLLOWING ARE THE SEMI-HALFWIDTHS IN DEGREES.')
  312 FORMAT(//15X,'GAUSSIAN FUNCTION IS USED FOR INTENSITY BROADENING.'
     1 /15X, 'FOLLOWING ARE THE HALFWIDTHS IN DEGREES.')
  313 FORMAT(15X, 'NO.   DISTANCE   CONCN.'/)
  314 FORMAT(15X, I3, 2X,E10.4,2X,F8.5)
  315 FORMAT( 15X,20A4)
  316 FORMAT(15X, 'PLA(1) = ', F8.5/15X,'PLA(2) = ', F8.5/
     1       15X, 'SUB(1) = ', F8.5/15X,'SUB(2) = ', F8.5/ )
C
      ICOUNT=  1
      READ(5,41) IDEN4
      READ(5,11)  H, YH,NY, NPHASE,NSUB,NSTR
C     NSTR=1 FOR CUBIC MATERIALS.
C     NSTR=2 FOR HEXAGONAL MATERIALS.
      IF (NPHASE.EQ.2)READ(5,11)CPLT
      IF(NPHASE.EQ.2)  READ(5,11) ZI
```

```
      IF(NPHASE.EQ.2)  READ(5,13) CAB,CBA
      READ(5,9)  GFA,IOPC, NBANDS
C
C IDEN4     / INFOMATION TO BE WRITTEN.
C H         / PLATING THICKNESS IN CENTIMETERS.
C YH        / DISTANCE GRID SIZE IN CENTIMETERS.
C NY        / NUMBER OF STATIONS IN THE DISTANCE GRID.
C NPHASE    / NUMBER OF PHASES
C             1, SINGLE PHASE BINARY SYSTEM
C             2, TWO-PHASE BINARY SYSTEM.
C NSUB      / OPTION FOR INFINITE SUBSTRATE
C             1, SUBSTRATE THICKNESS EQUALS  (NY-1)/YH-H
C             2, TREAT THE SUBSTRATE TO BE INFINITE
C C         / CONCENTRATION IN ATOM FRACTION B . FIRST CONCENTRATION VALUE
C             SHOULD CORRESPOND TO THE FREE SURFACE OF THE PLATING.
C ZI        / INTERFACE POSITION FROM FREE SURFACE, CENTIMETERS.
C CAB       / C ALPHA BETA IN ATOM FRACTION B.
C CBA       / C BETA ALPHA IN ATOM FRACTION B.
C GFA       / VOLUME FRACTION OF ORIENTED PLATING OVER VOLUME FRACTION
C             OF ORIENTED SUBSTRATE.
C IOPC      / TYPE OF BROADENING.
C           /  +1 , CAUCHY
C           /  -1 , GAUSSIAN.
C NBANDS    / NUMBER OF BANDS FOR WHICH THE INTENSITY IS TO BE SIMULATED.
C              SPECIFY NBANDS=2 & IAL12=1 FOR K-ALPHA-1-2 SIMULATION.
C
      WRITE(6,3)
      IF( NPHASE.EQ.1)  WRITE(6,304)
      IF( NPHASE.EQ.2)  WRITE(6,305)
      WRITE(6,315) IDEN4
      WRITE(6,306) H
      SUBT= FLOAT(NY-1) *YH-H
```

```
      NINP=(IFIX(H/YH)+1)
      NINS=NY-NINP
      NINPM=NINP-1
      NINSP=NINS+1
  457 FORMAT(4I5)
      DO 740 J=1,NINPM
  740 C(J)=CPLT
      WRITE(7,741)
  741 FORMAT('ENTER THE A,B AND D PARAMETERS ONE SET BELOW THE OTHER')
      WRITE(7,742)
  742 FORMAT('XX.XXX X.XXXXXX XX.XXX')
      DO 743 K=1,3
      READ(7,744)AP(K),BP(K),DP(K)
  743 WRITE(7,744)AP(K),BP(K),DP(K)
  744 FORMAT(F7.4,F9.7,F7.4)
  444 FORMAT(2I3)
      IF (NSUB.EQ.1)  WRITE(6,307) SUBT
      IF (NSUB.EQ.2)  WRITE(6,308)
      IF (NPHASE.EQ.2)  WRITE(6,309) ZI
      WRITE(6,310) GFA
      DO 320 J=1,NY
  320 DIST(J)= FLOAT(J-1) *YH
      DO 756 JK=NINP,NY
  756 SDIST(JK)=DIST(JK)-DIST(NINP)
      DO 746 L=NINP,NY
      DO 745 KL=1,2
      TDIST=BP(3)*(DP(3)-AP(3))
      STDIFF=SDIST(L)-TDIST
      IF(STDIFF.LT.0.)TFACT=0.0
      IF(STDIFF.GE.0.)TFACT=1.0
      SFACT=1.0-TFACT
      ARGUM=(STDIFF/BP(KL))-DP(KL)
```

```
745 SUM(L,KL)=TFACT*AP(KL)*ERFC(ARGUM)
    SUM(L,3)=SFACT*(AP(3)+SDIST(L)/BP(3))
746 C(L)=SUM(L,1)+SUM(L,2)+SUM(L,3)
    WRITE(7,598)
598 FORMAT('ENTER NO. OF PTS. FOR SIMPSON INTEGRATION-ODD NOS. ONLY')
    WRITE(7,597)
597 FORMAT('XXX')
    READ(7,444)NSIMP
    ICOEFF(1)=1
    ICOEFF(NSIMP)=1
    DO 77 I=2,NSIMP,2
 77 ICOEFF(I)=4
    NSIMP2=NSIMP-2
    DO 78 J=3,NSIMP2,2
 78 ICOEFF(J)=2
    AREA=0.0
    HSIMP=YH/3.0
    DO 79 K=1,NSIMP
 79 AREA=AREA+ICOEFF(K)*C(K+NINPM)
    AREA=AREA*HSIMP
    WRITE(7,76)AREA
 76 FORMAT('AREA UNDER CURVE=',E15.7)
    VOL= YH
    GIY= YH
    ID2= NY
    NJTOW= H/YH +1
    NZI= ZI/YH +1
    SU= (ZI - FLOAT(NZI-1) *YH )
    BFA= (0.5 *YH+ SU) /YH
    AFA= (0.5 *YH+ (YH-SU))/ YH
    IID2= ID2
 20 READ(5,41) IDEN2
```

```
      IF( ICOUNT.GT.1)  GO TO 377
      READ(5,53) NQ,IAL12
  377 CONTINUE
      DO 650 JJJ=1,NQ
      I=NQ-JJJ+1
      READ(5,13)TT(I),COMPO(I),Q(I)
  650 WRITE(6,13)TT(I),COMPO(I),Q(I)
      IF( ICOUNT.GT.1)  GO TO 378
      DO 660 KKK=1,NQ
      I=NQ-KKK+1
      READ(5,52) ALU(I)
  660 WRITE(6,52)ALU(I)
  378 CONTINUE
      READ(5,40) PLA(1), PLA(2), SUB(1), SUB(2)
      IF(ICOUNT.EQ.2 .AND. IAL12.EQ.1) GO TO 379
      IF( NSUB.EQ.2.AND.NSTR.EQ.1)  READ(5,6) ALAMDA, ASPACE, NORDER,IH,
     1IK,IL
      IF(NSUB.EQ.2.AND.NSTR.EQ.2) READ(5,6)ALAMDA,ASPACE,NORDER,IH,IK,IL
     1,CSPACE
C
C  THE ABOVE IS THE LAST READ STATEMENT IN THE PROGRAM.
C
C
C IDEN2     / IDENTIFICATION FOR THE FOLLOWING TABLE.
C NQ        / NUMBER OF SETS IN THE FOLLOWING TABLE.
C IAL12     / OPTION FOR K-ALPHA-1-2 SIMULATION.
C               0 , NO.
C               1 , YES. (NBANDS SHOULD BE 2 WITH IAL12=1).
C COMPO,TT,Q  / COMPOSITION-TWOTHETA-REFLECTIVITY TABLE.
C ***************************************************************************
C             'COMPO' ARRAY SHOULD BE INPUT IN DESCENDING ORDER OF AT. FR. B.
C ***************************************************************************
```

```
C             TT SHOULD BE IN DEGREES.
C             Q SHOULD BE IN UNITS OF PER CENTIMETER CUBED.
C ALU       / LINEAR ABSORPTION COEFFICIENT ARRAY CORRESPONDING TO THE
C             ABOVE 'COMPO' ARRAY. UNITS= PER CENTIMETER.
C PLA(1),PLA(2) / BROADENING PARAMETERS FOR PLATING. FOR CAUCHY THESE
C             SHOULD BE SEMIHALFWIDTHS DUE TO LOW AND HIGH ANGLE SIDES.
C             FOR GAUSSIAN THESE SHOULD BE SAME AND = HALFWIDTH.
C SUB(1),SUB(2) / BROADENING PARAMETERS FOR SUBSTRATE. FOR CAUCHY THESE
C             SHOULD BE SEMIHALFWIDTHS DUE TO LOW AND HIGH ANGLE SIDES.
C             FOR GAUSSIAN THESE SHOULD BE SAME AND = HALFWIDTH.
C ***************************************************************************
C IF NSUB IS CHOSEN AS 2, READ THE FOLLOWING PARAMETERS.
C ALAMDA    / X-RAY WAVELENGTH IN CENTIMETERS.
C ASPACE    / LATTICE PARAMETER IN CENTIMETERS FOR THE SUBSTRATE ELEMENT.
C NORDER    / ORDER OF REFLECTION.
C IH,IK,IL / H,K,L VALUES FOR THE BAND UNDER CONSIDERATION.
C ***************************************************************************
C ORIGINAL INTERFACE LIES IN BETWEEN (NJTOW) TH & (NJTOW+1) TH STATION
C PRESENT  INTERFACE LIES IN BETWEEN ( NZI ) TH & ( NZI +1) TH STATION
C
      IF( NSUB.EQ.1)  GO TO 322
      IF(NSTR.EQ.2)GO TO 500
      DSPACE= ASPACE/SQRT(FLOAT(IH**2+IK**2+IL**2))
      GO TO 510
  500 DTEMP=(4./3.)*FLOAT(IH**2+IK**2+IH*IK)/(ASPACE**2)+(FLOAT(IL**2)
     1/(CSPACE**2))
      DSPACE=SQRT(1./DTEMP)
  510 AMUMIN= ALU(1)
      DO 35 I=1,NQ
      IF( ALU(I).LT.AMUMIN ) AMUMIN= ALU(I)
   35 CONTINUE
      CVOL= FLOAT(NORDER) *ALAMDA/(8.*DSPACE*AMUMIN)
```

```
      IID2= ID2+ 20
      DO 50 J= ID2,IID2
      DIST(J)= DIST(NY) + FLOAT( J -NY) * CVOL
  322 IF( ICOUNT.GT.1)  GO TO 379
   50 CONTINUE
      IID1=IID2-1
      DUM=C(ID2)/20.0
      DO 777 KIK=ID2,IID1
      C(KIK+1)=C(KIK)-DUM
      C(IID2)=0.0
  777 CONTINUE
      WRITE(6,3)
      WRITE(6,313)
      DO 321 J=1,IID2
      IHF=IID2-20
  321 IF(J.GT.NINPM.AND.J.LE.NY)WRITE(2,747)SDIST(J),C(J),SUM(J,1),SUM(J
     1,2),SUM(J,3)
  747 FORMAT(5E15.7)
      C(1)=(3.*C(1) + C(2)) /4.
  379 CONTINUE
      WRITE(6,3)
      WRITE(6,315)  IDEN2
      IF(IOPC .EQ. 1)  WRITE(6,311)
      IF(IOPC .LT. 1)  WRITE(6,312)
      WRITE(6,316)  PLA(1), PLA(2), SUB(1), SUB(2)
C
C CALCULATING UNBROADENED INTENSITY(UBP),EFFECTIVE VOLUME(EFV),
C AND INTENSITY CORRECTED FOR INSTRUMENTAL BROADENING (AINTEN).
C
      NNQ=NQ-1
      DO 55 J= 1,IID2
      CC= C(J)
```

```
      DO 57 K=2, NQ
      IF(  .NOT. ( CC.GE. COMPO(K) .AND. CC.LE.COMPO(K-1)))
     1GO TO 57
      DC= (CC -COMPO(K)) /(COMPO(K-1)-COMPO(K))
      ALUG(J)= ALU(K)+ (ALU(K-1)- ALU(K)) *DC
      TG(J)=  TT(K)+ (TT(K-1)- TT(K)) *DC
      QG(J)= Q(K)+ (Q(K-1)- Q(K)) *DC
   57 CONTINUE
   55 CONTINUE
      ALG(1)= 0.0
      DO 56 J= 2,ID2
   56 ALG(J)= ALG(J-1) +( ALUG(J)+ ALUG(J-1))/2.
      ALG(1)=  ALUG(1)/4.
      DO 25 J=1,IID2
      TIR= 3.1415 /180.* TG(J)/2.
      IF(J.LE.ID2)  GO TO 43
      CDY= GIY*ALG(ID2) + ( CVOL  * (FLOAT(J-ID2)-0.5)*ALUG(ID2))
      P(J)= QG(J)*CVOL*EXP(-2./SIN(TIR)* CDY)/ SIN(TIR)
      GO TO 44
   43 P(J)= QG(J) * VOL* EXP(- ALG(J)* 2./SIN(TIR) *GIY) / SIN(TIR)
   44 CONTINUE
      IF( J.EQ.NZI)  P(J)= P(J)* BFA
      IF( J.EQ.(NZI+1) ) P(J)= P(J) *AFA
      IF(J.LE.NJTOW )  P(J)= P(J) *GFA
      IF(J.EQ.1)  P(J)= P(J)/2.
      EFA(J)= P(J)/ QG(J)
   25 CONTINUE
      WRITE(6,965)
  965 FORMAT('THESE ARE THE QG(J) ,TG(J),ALUG(J)VALUES')
      DO 755 J=1,IID2
  755 WRITE(6,788)QG(J),TG(J),ALUG(J)
  788 FORMAT(3F13.8)
```

```
      NR=200
      RP=200.
      DO 61 I= 1,NR
      UBP(I)=0.
      EFV(I)=0.
   61 AINTEN(I)= 0.
      IF(ICOUNT.EQ.2 .AND. IAL12.EQ.1) GO TO 381
      NR2= NR/2
      FNR2= NR2
      NNR2= NR2+1
      IF(NPHASE .EQ.1)  GO TO 326
      DO 323 I=2,NNQ
      IF(CBA .LE.COMPO(I) .AND. CBA.GT. COMPO(I+1))  IBA=I-1
      IF(CAB .LE.COMPO(I) .AND. CAB.GT. COMPO(I+1))  IAB= I+1
  323 CONTINUE
      T2INI= TT(NQ)
      T2RANG= (TT(IAB)- TT(NQ)) *2.
      T2INC=  T2RANG/FNR2
      START= T2INI- T2RANG * 0.25
      DO 26 I=1,NR2
   26 T2V(I)=   START  + T2INC *FLOAT(I-1)
      T2INI= TT(IBA)
      T2RANG=  ( TT(1)- TT(IBA)) *2.
      T2INC=  T2RANG/FNR2
      START= T2INI- T2RANG * 0.25
      DO 60 I= NNR2,NR
      J= I-NR2
      T2V(I)=   START  + T2INC *FLOAT(J-1)
   60 CONTINUE
      GO TO 325
  326 T2INI= TT(NQ)
      T2RANG=(TT(1)- TT(NQ)) *2.
```

```
      T2INC= T2RANG/NR
      START= T2INI - T2RANG* 0.25
      DO 324 I=1,NR
  324 T2V(I)= START+ T2INC * FLOAT(I-1)
  325 MP=0
      IF( T2V(1).GT.T2V(2))  MP=1
  381 DO301 K=1,NR
      IF( K.EQ.1.OR.K.EQ.NR)  GO TO 16
      ALI=  (T2V(K) + T2V(K-1)) /2.
      ULI=  (T2V(K) + T2V(K+1)) /2.
   16 CONTINUE
      IF( IOPC.GT.0)  GO TO 303
      AKP= 0.93944
      AKDP= 2.7726
      DO 302 J=1,IID2
      TOWARY= SUB(1)
      IF(J.LE.NJTOW)  TOWARY=PLA(1)
      IF( K.EQ.1.OR.K.EQ.NR)  GO TO 989
      IF(.NOT.(TG(J) . LE.ALI .AND. TG(J) .GT.ULI).AND.MP.EQ.1)GO TO 989
      IF(.NOT.(TG(J) . GE.ALI .AND. TG(J) .LT.ULI).AND.MP.EQ.0)GO TO 989
      UBP(K)=  UBP(K)+  P(J)
      EFV(K)=  EFV(K)+  EFA(J)
  989 ARG=AKDP*(T2V(K)-TG(J))**2/TOWARY**2
      IF(ARG.GE.12.0)DEC=0.0
      IF(ARG.GE.12.0)GO TO 302
      DEC=EXP(-ARG)
  302 AINTEN(K)=  AINTEN(K)+  P(J)    * AKP/TOWARY*DEC
      GO TO 301
  303 IF(IOPC.EQ.10) GO TO 402
      DO 27  J=1,IID2
      A1=1./SUB(1)
      A2=1./SUB(2)
```

```
      IF(J.LE.NJTOW) A1=1./PLA(1)
      IF(J.LE.NJTOW) A2=1./PLA(2)
      X =  T2V(K) - TG(J)
      IF(X.LT.0.) A3=A1
      IF(X.GE.0.) A3=A2
      BR=  2./( 1.+ A3**2*X**2) /3.14/(1./A1+1./A2)
      IF( K.EQ.1.OR.K.EQ.NR)  GO TO 27
      IF(.NOT.(TG(J) . LE.ALI .AND. TG(J) .GT.ULI).AND.MP.EQ.1)GO TO 27
      IF(.NOT.(TG(J) . GE.ALI .AND. TG(J) .LT.ULI).AND.MP.EQ.0)GO TO 27
      UBP(K)=  UBP(K)+  P(J)
      EFV(K)=  EFV(K)+  EFA(J)
   27 AINTEN(K)=  AINTEN(K)+  P(J) *BR
      GO TO 301
  402 IF(K.EQ.1)WRITE(7,587)
  587 FORMAT('ENTER THE B1 AND B2 PARS. FOR PEARSON 7 FOR LOW ANGLE')
      IF(K.EQ.1)WRITE(7,588)
  588 FORMAT('XX.XXXX XX.XXX')
      IF(K.EQ.1)READ(7,599)B1,B2
      B1=0.0839
      B2=2.5
      IF(K.EQ.1)WRITE(7,599)B1,B2
  599 FORMAT(F8.4,F7.3)
      IF(K.EQ.1)WRITE(7,593)
  593 FORMAT('ENTER B3 AND B4 PARS. FOR PEARSON 7 FOR HIGH ANGLE')
      IF(K.EQ.1)WRITE(7,588)
      IF(K.EQ.1)READ(7,599)B3,B4
      B3=0.0625
      B4=20.0
      IF(K.EQ.1)WRITE(7,599)B3,B4
      DO 489 J=1,IID2
      X=T2V(K)-TG(J)
      IF(X.LT.0.0)B1P=B1
```

```
      IF(X.LT.0.0)B2P=B2
      IF(X.GE.0.0)B1P=B3
      IF(X.GE.0.0)B2P=B4
      BR=1./(1.+(X**2)/(B2P*B1P**2))**B2P
      IF(K.EQ.1.OR.K.EQ.NR)GO TO 489
      IF(.NOT.(TG(J) . GE.ALI .AND. TG(J) .LT.ULI).AND.MP.EQ.0)GO TO 489
      IF(.NOT.(TG(J) . LE.ALI .AND. TG(J) .GT.ULI).AND.MP.EQ.1)GO TO 489
      UBP(K)=UBP(K)+P(J)
      EFV(K)=EFV(K)+EFA(J)
  489 AINTEN(K)=AINTEN(K)+P(J)*BR
  301 CONTINUE
      WRITE(6,3 )
      WRITE(6,18)
      DO 380 I=1,NR
      IF(I.EQ.51 .OR.I.EQ.101 .OR.I.EQ.151 ) WRITE(6,3)
      WRITE(6,19) I,T2V(I), UBP(I), AINTEN(I),EFV(I)
      IF(ICOUNT.EQ.1 .AND. IAL12.EQ.1) AINT12(I)=AINTEN(I)
      IF(ICOUNT.EQ.2 .AND. IAL12.EQ.1) AINTEN(I)=AINT12(I)+.5*AINTEN(I)
  380 CONTINUE
      AMAX=0.0
      WRITE(7,128)
  128 FORMAT('ENTER NO OF INPUT DATA POINTS'/'XXX')
      READ(7,127)NY1
  127 FORMAT(I3)
      NY1=100
      WRITE(7,892)
  892 FORMAT('ENTER THE SCALING FACTOR',/'X')
      READ(7,893)ISCL
  893 FORMAT(I1)
      XSCL=1./ISCL
      NY11=NY1-1
      DO 799 JJ=1,NY11
```

```
      IF(AINTEN(JJ+1).GE.AMAX)AMAX=AINTEN(JJ+1)
  799 CONTINUE
      DO 798 II=1,NY1
      AINTEN(II)=AINTEN(II)/AMAX
  798 IF(AINTEN(II).GE.XSCL)AINTEN(II)=XSCL
      WRITE(7,668)
  668 FORMAT('ENTER THE NUMBER OF POINTS AND ERROR FOR EXPT CURVE AS
     1WELL AS THE BACKGROUND'/'XXX XX.XXXX XX.XXX')
      READ(7,669)NPPX,ERROR,BCK
      ERROR=0.033
  669 FORMAT(I3,F9.5,F6.3)
      DO 667 KK=1,NPPX
      READ(3,666)T2X(KK),AEXP(KK)
  666 FORMAT(2F12.5)
      T2X(KK)=T2X(KK)+ERROR
  667 AEXP(KK)=AEXP(KK)-BCK
      NPPX3=NPPX-1
      EXMAX=0.0
      DO 797 LL=1,NPPX3
      IF(AEXP(LL+1).GE.EXMAX)EXMAX=AEXP(LL+1)
  797 CONTINUE
      DO 796 LIL=1,NPPX
      AEXP(LIL)=AEXP(LIL)/EXMAX
  796 IF(AEXP(LIL).GE.XSCL)AEXP(LIL)=XSCL
      IF(ICOUNT.EQ.1 .AND. IAL12.EQ.1) GO TO 333
      NPP=NY1
      CALL PLOTS(0,0,50)
      CALL PLOT (1.5,3.5,-3)
      CALL SCALE(T2X,6.5,NPPX,1)
      CALL SCALE(AEXP,5.0,NPPX,1)
      CALL NEWPEN(3)
      NPP1=NPP+1
```

```
      NPP2=NPP+2
      NPX1=NPPX+1
      NPX2=NPPX+2
      CALL AXIS(0.,0.,'TWO-THETA',-9,6.5,0.,T2X(NPX1),T2X(NPX2))
      CALL AXIS(0.,0.,'INTENSITY',9,5.0,90.,AEXP(NPX1),AEXP(NPX2))
      CALL SYMBOL(0.5,4.0500,.100,2,0.,-1)
      CALL SYMBOL(0.75,4.0,.100,'EXPERIMENTAL',0.,12)
      CALL SYMBOL(0.5,3.5500,.100,1,0.,-1)
      CALL SYMBOL(0.75,3.5,.100,'SIMULATED',0.,9)
      T2V(NPP1)=T2X(NPX1)
      T2V(NPP2)=T2X(NPX2)
      AINTEN(NPP1)=AEXP(NPX1)
      AINTEN(NPP2)=AEXP(NPX2)
      CALL LINE(T2V,AINTEN,NPP,1,1,1)
      CALL LINE(T2X,AEXP,NPPX,1,1,2)
      CALL VPISYM(1.,6.,15,KTIL,0.,80)
      CALL PLOT(12.0,0.0,999)
333   CONTINUE
      IF(  ICOUNT .EQ. NBANDS  )  GO TO 300
      ICOUNT=  ICOUNT+  1
      GO TO 20
  300 STOP
      END
```

APPENDIX 2

```
C
C
C
C
C
      DIMENSION SA(101), FA(101), SB(101), FB(101), CA(101,4), CB(101,4)
     1, A(16), B(4), ABLE(160), AFB(201), CP(201), FI(20), IH(20),
     2 IK(20), IL(20),CPC(201),SLOPE(4),CEPT(4),ALU(200),AVMAC(200)
  100 FORMAT ( 20A4 )
  501 FORMAT(F7.5,2F6.3)
  101 FORMAT(I2,2F5.2)
  102 FORMAT(2F10.0, 60X )
  103 FORMAT(F7.5,2F4.1,2I3)
  104 FORMAT(6F12.5)
  105 FORMAT (  F10.0 )
  106 FORMAT ( 5F12.5, E12.5 )
  107 FORMAT (1H1)
  108 FORMAT ( 1H , 20A4 )
  110 FORMAT(                                                          //
     1 1H , 1X, 'NO.', 4X, 'ST/W', 7X, 'FA', 7X, 'CA(1)', 5X, 'CA(2)',
     2 5X, 'CA(3)', 5X, 'CA(4)' // )
  112 FORMAT(                                                          //
     1 1H , 1X, 'NO.', 4X, 'ST/W', 7X, 'FB', 7X, 'CB(1)', 5X, 'CB(2)',
     2 5X, 'CB(3)', 5X, 'CB(4)' // )
  111 FORMAT(1H ,I5,6F10.5)
  113 FORMAT(     1H , 'W', 8X, '=', F15.5 /1H , 'TFA', 6X, '=', E15.5/
     11H , 'TFB', 6X, '=', E15.5 /1H , 'C', 8X, '=', E15.7 /1H , 'T6',
     2 7X, '=', E15.7 /1H , 'T7', 7X, '=', E15.7 )
  114 FORMAT(1H , 'AM', 7X, '=', F15.5)
  115 FORMAT(//1H ,5X,'TT',9X,'AFB',10X,'CP',10X,'CPC',9X,'AVSF',9X,'PF'
     1,10X,'ST',10X,'Q1',10X,'Q2',11X,'Q' // )
  116 FORMAT (I5, F10.0 )
```

```
  117 FORMAT( // 1H , '(', I1, I1, I1, ')', ' BAND' // )
  118 FORMAT ( 2F15.7, E15.7 )
  119 FORMAT ( 2F10.0 )
  120 FORMAT( 16(2X,3I1) )
  121 FORMAT('(',3I1,') BAND' )
      CF = 180.0/3.14159
      READ(5,101)  NSYSTM,CONSTS,XMULT
C     CONSTS IS THE CONSTANT FACTOR FOR THE STRUCTURE FACTOR,SQUARED
C     FOR BCC,FCC MATERIALS IT IS 16.00
C     FOR HEX. MATERIALS IT IS 16.00 FOR H+2K=3N AND L EVEN
C                              9.00 FOR H+2K=3N+OR- 1 AND L ODD
C                              1.00 FOR   DITTO       AND L EVEN
C     XMULT IS THE MULTIPLICITY FACTOR
C NSYSTM /NUMBER OF DIFFERENT ALLOY SYSTEMS TO BE WORKED.
      LSYSTM = 0
   40 LSYSTM = LSYSTM+1
C RETURN POINT FOR EACH NEW SYSTEM.
      READ(5,100)  ( ABLE(I), I=121,160)
      READ(5,100)  ( FI(I), I=1,20 )
      READ(5,101)  NCP
      READ(5,501)   ( AFB(I), CP(I),CPC(I), I=1,NCP )
      READ(5,104)ATWTA,ATWTB,AMAC,BMAC
C     ATWTA  IS THE ATOMIC WEIGHT OF A
C     ATWTB  IS THE ATOMIC WEIGHT OF B
C     AMAC IS THE LINEAR ABSORPTION COEFFICIENT OF A
C     BMAC IS THE LINEAR ABSORPTION COEFFICIENT OF B
C ABLE   /WRITTEN IDENTIFICATION FOR THE ALLOY SYSTEM.
C FI     /VARIABLE FORMAT FOR READING IN THE TABLE OF LATTICE PARAMETERS.
C NCP    /NUMBER OF (AT.FR.-LAT.PAR.) PAIRS IN THE TABLE
C AFB    /COMPOSITION IN ATOMIC FRACTION OF COMPONENT B
C CP     /LATTICE PARAMETER IN ANGSTROMS.
      READ (5,100)  ( ABLE(I), I=1,60)
```

```
      READ(5,100)  ( FI(I), I=1,20 )
      READ(5,101)  NFA
      READ(5,FI)   (SA(I), FA(I), I=1,NFA)
C ABLE    / WRITTEN IDENTIFICATION FOR SCATTERING FACTOR DATA.
C FI      /VARIABLE FORMAT FOR READING IN THE ATOMIC SCATTERING FACTOR TABLE.
C NFA     / NUMBER OF PAIRS IN THE ATOMIC SCATTERING FACTOR TABLE FOR COMPONENT A
C SA      / SIN(THETA)/LAMDA HAVING UNITS OF 1.0/ANGSTROMS.
C FA      / ATOMIC SCATTERING FACTOR
      READ (5,100)  ( ABLE(I), I=61,120)
      READ(5,100)  ( FI(I), I=1,20 )
      READ(5,101)  NFB
      READ(5,FI)   (SB(I), FB(I), I=1,NFB)
C NFB,SB,FB SAME AS NFA,SA,FA BUT FOR COMPONENT B.
      READ(5,103)  W, TFA, TFB, NPT, NBN
C W       / WAVELENGTH IN ANGSTROMS.
C TFA     / TEMPERATURE FUNCTION FOR A.
C TFB     / TEMPERATURE FUNCTION FOR B.
C NPT     / PARAMETER DICTATING WHICH POLARIZATION TERM IS TO BE USED.
C         / 0, IF SINGLE CRYSTAL.
C         /+1, IF DOUBLE CRYSTAL - ( REQUIRES AM INPUT - SEE BELOW )
C      99,IF WE HAVE A POWDER EXPRESSION TO WORK WITH
C NBN     /NUMBER OF BANDS TO BE WORKED.
      IF(NPT.NE.0) READ(5,104)  AM
C AM      / MONOCHROMATOR ANGLE.
      READ(5,120)  ( IH(I), IK(I), IL(I), I=1,NBN )
      IF(NPT.EQ.99)GO TO 520
      C = 0.2298057E+05
      T6 = C*TFA/W**2
      T7 = (TFB-TFA) / TFA
C C,T6,T7 ARE RECURRENT FACTORS USED IN CALCULATION OF TEMPERATURE FACTOR.
C
C DETERMINE THE CONSTANTS USED FOR INTERPOLATING IN THE SCATTERING FACTOR
```

```
C    TABLES.
C
  520 IF(NPT.EQ.99)READ(5,530)(SLOPE(NO),CEPT(NO),NO=1,3)
  530 FORMAT(2F12.8)
      AFB(1)=0.0000
      DO 550 MNM=1,141
      IF(AFB(MNM).LT.0.185)CP(MNM)=SLOPE(1)*AFB(MNM)+CEPT(1)
      IF(AFB(MNM).GE.0.185)CP(MNM)=SLOPE(2)*AFB(MNM)+CEPT(2)
      CPC(MNM)=SLOPE(3)*AFB(MNM)+CEPT(3)
  550 AFB(MNM+1)=AFB(MNM)+0.0025
      WRITE(7,333)(CP(IND),CPC(IND),AFB(IND),IND=1,15)
  333 FORMAT(T10,3F15.7)
      NFAM2 = NFA-2
      DO 3 I=2,NFAM2
      KK = 0
      DO 1 J=1,3
      ME = 4-J
      DO 1 K=1,4
      KK = KK+1
      KE = K-2
    1 A(KK) = SA(I+KE)**ME
      K = 0
      DO 2 KK=13,16
      K = K+1
      KE = 14-KK
      A(KK) = 1.0
    2 B(K ) = FA(I-KE)
      CALL SIMQ(A,B,4,KS)
      DO 3 J=1,4
    3 CA(I,J) = B(J)
      DO 4 J=1,4
      CA(1,J) = CA(2,J)
```

```
      CA(NFA-1,J) = CA(NFAM2,J)
    4 CA(NFA,J) = CA(NFAM2,J)
      NFBM2 = NFB-2
      DO 7 I=2,NFBM2
      KK = 0
      DO 5 J=1,3
      ME = 4-J
      DO 5 K=1,4
      KK = KK+1
      KE = K-2
    5 A(KK) = SB(I+KE)**ME
      K = 0
      DO 6 KK=13,16
      K = K+1
      KE = 14-KK
      A(KK) = 1.0
    6 B(K ) = FB(I-KE)
      CALL SIMQ(A,B,4,KS)
      DO 7 J=1,4
    7 CB(I,J) = B(J)
      DO 8 J=1,4
      CB(1,J) = CB(2,J)
      CB(NFB-1,J) = CB(NFBM2,J)
    8 CB(NFB,J) = CB(NFBM2,J)
C
C WRITE OUT THE TABLES OF SCATTERING FACTORS AND THE INTERPOLATION CONSTANTS.
C
      WRITE (6,107)
      WRITE(7,101)NSYSTM,CONSTS,XMULT
      WRITE (6,108)  ( ABLE(I), I=1,60 )
      WRITE(6,110)
      WRITE(6,111) (I, SA(I), FA(I), ( CA(I,J), J=1,4), I=1,NFA )
```

```
      WRITE (6,107)
      WRITE (6,108)  ( ABLE(I), I=61,120)
      WRITE(6,112)
      WRITE(6,111) (I, SB(I), FB(I), ( CB(I,J), J=1,4), I=1,NFB )
C     COMPUTE THE LINEAR AND MASS ABSORPTION COEFFICIENTS
C
      LBN = 0
   30 LBN = LBN+1
      ONE=(4./3.)*(IH(LBN)**2+IK(LBN)**2+IH(LBN)*IK(LBN))
      TWO=(IL(LBN)**2)
      CPD = 0.5 * W
      WRITE(6,107)
      WRITE(6,108)  ( ABLE(I), I=121,160)
      WRITE(7,100)  (ABLE(I),I=121,160)
      WRITE(6,117)  IH(LBN), IK(LBN), IL(LBN)
      WRITE(7,121)  IH(LBN), IK(LBN), IL(LBN)
      WRITE(6,113) W, TFA, TFB, C, T6, T7
      WRITE(7,101)  NCP
      IF ( NPT.NE.0)  WRITE(6,114) AM
      WRITE(6,115)
      N = 0
    9 N = N+1
C RETURN POINT FOR EACH NEW (AT.FR.-LAT.PARA.) PAIR.
      TTR = 2.0*ARSIN(CPD*SQRT((ONE/(CP(N)**2))+(TWO/(CPC(N)**2))))
      TT = CF * TTR
      TR  = 0.5 * TTR
      ST  = SIN(TR)
      SST = ST**2
      STT = SIN(TTR)
      CSTT= COS(TTR)**2
      IF (NPT.EQ.0 ) GO TO 10
      TAMR = 2.0 * .0174533 * AM
```

```
      CSTAMR = COS(TAMR)**2
      PF = (1.0+CSTAMR*CSTT) / (STT*(1.0+CSTAMR)*ST)
      GO TO 11
   10 PF = (1.0+CSTT) / (2.0*STT)
   11 STL  = ST/W
      STL2 = STL**2
      STL3 = STL**3
      I = 0
   12 I = I+1
      IF (I.EQ.NFA )  GO TO 13
      IF (SA(I).LE.STL ) GO TO 12
   13 SCFA = CA(I-1,1)*STL3+CA(I-1,2)*STL2+CA(I-1,3)*STL+CA(I-1,4)
      I = 0
   14 I = I+1
      IF (I.EQ.NFB)  GO TO 15
      IF (SB(I).LE.STL)  GO TO 14
   15 SCFB = CB(I-1,1)*STL3+CB(I-1,2)*STL2+CB(I-1,3)*STL+CB(I-1,4)
      AVSF = CONSTS * SCFA**2 * (1.0+((SCFB-SCFA)/SCFA*AFB(N)))**2
      IF(NPT.NE.99)TF = EXP(-T6*(1.0+AFB(N)*T7)*SST)
      IF(NPT.EQ.99)TF=1.000
      Q1 = W**3/((CP(N)**2)*CPC(N)*0.866667)*0.0793977
      Q2 = AVSF * PF * TF*XMULT
      Q  = Q1*Q2
      WRITE (6,106) TT, AFB(N), CP(N), CPC(N), AVSF, Q
      WRITE(7,118)  AFB(N), TT,  Q
      IF (N.NE.141)   GO TO 9
      WRITE(6,630)
  630 FORMAT(2X,'I',T10,'AFB',T22,'WFB',T34,'A',T46,'C',T57,'ALU',T68,'A
     1VMAC',T82,'ALDEN')
      DO 600 I=1,141
      WFB=AFB(I)*ATWTB/((1.0-AFB(I))*ATWTA+ATWTB*AFB(I))
      AVMAC(I)=AMAC+WFB*(BMAC-AMAC)
```

```
      ALDEN=2.0/((CP(I)**2)*CPC(I)*0.86667)*(ATWTA+WFB*(ATWTB-ATWTA))/0.
     1602257
      ALU(I)=AVMAC(I)*ALDEN
      WRITE(6,610)I,AFB(I),WFB,CP(I),CPC(I),ALU(I),AVMAC(I),ALDEN
  610 FORMAT(I3,7F12.5)
  600 WRITE(7,104)AFB(I),ALU(I)
      IF ( LBN.NE.NBN )  GO TO 30
      IF (LSYSTM.NE.NSYSTM)  GO TO 40
      STOP
      END
      SUBROUTINE SIMQ(A,B,N,KS)                                          SIMQ 490
      DIMENSION A(16),B(4)
C                                                                        SIMQ 510
C        FORWARD SOLUTION                                                SIMQ 520
C                                                                        SIMQ 530
      TOL=0.0                                                            SIMQ 540
      KS=0                                                               SIMQ 550
      JJ=-N                                                              SIMQ 560
      DO 65 J=1,N                                                        SIMQ 570
      JY=J+1                                                             SIMQ 580
      JJ=JJ+N+1                                                          SIMQ 590
      BIGA=0                                                             SIMQ 600
      IT=JJ-J                                                            SIMQ 610
      DO 30 I=J,N                                                        SIMQ 620
C                                                                        SIMQ 630
C        SEARCH FOR MAXIMUM COEFFICIENT IN COLUMN                        SIMQ 640
C                                                                        SIMQ 650
      IJ=IT+I                                                            SIMQ 660
      IF(ABS(BIGA)-ABS(A(IJ))) 20,30,30                                  SIMQ 670
   20 BIGA=A(IJ)                                                         SIMQ 680
      IMAX=I                                                             SIMQ 690
   30 CONTINUE                                                           SIMQ 700
```

```
C                                                                       SIMQ 710
C       TEST FOR PIVOT LESS THAN TOLERANCE (SINGULAR MATRIX)            SIMQ 720
C                                                                       SIMQ 730
      IF(ABS(BIGA)-TOL) 35,35,40                                        SIMQ 740
   35 KS=1                                                              SIMQ 750
      RETURN                                                            SIMQ 760
C                                                                       SIMQ 770
C       INTERCHANGE ROWS IF NECESSARY                                   SIMQ 780
C                                                                       SIMQ 790
   40 I1=J+N*(J-2)                                                      SIMQ 800
      IT=IMAX-J                                                         SIMQ 810
      DO 50 K=J,N                                                       SIMQ 820
      I1=I1+N                                                           SIMQ 830
      I2=I1+IT                                                          SIMQ 840
      SAVE=A(I1)                                                        SIMQ 850
      A(I1)=A(I2)                                                       SIMQ 860
      A(I2)=SAVE                                                        SIMQ 870
C                                                                       SIMQ 880
C       DIVIDE EQUATION BY LEADING COEFFICIENT                          SIMQ 890
C                                                                       SIMQ 900
   50 A(I1)=A(I1)/BIGA                                                  SIMQ 910
      SAVE=B(IMAX)                                                      SIMQ 920
      B(IMAX)=B(J)                                                      SIMQ 930
      B(J)=SAVE/BIGA                                                    SIMQ 940
C                                                                       SIMQ 950
C       ELIMINATE NEXT VARIABLE                                         SIMQ 960
C                                                                       SIMQ 970
      IF(J-N) 55,70,55                                                  SIMQ 980
   55 IQS=N*(J-1)                                                       SIMQ 990
      DO 65 IX=JY,N                                                     SIMQ1000
      IXJ=IQS+IX                                                        SIMQ1010
      IT=J-IX                                                           SIMQ1020
```

```
      DO 60 JX=JY,N                                                    SIMQ1030
      IXJX=N*(JX-1)+IX                                                 SIMQ1040
      JJX=IXJX+IT                                                      SIMQ1050
   60 A(IXJX)=A(IXJX)-(A(IXJ)*A(JJX))                                  SIMQ1060
   65 B(IX)=B(IX)-(B(J)*A(IXJ))                                        SIMQ1070
C                                                                      SIMQ1080
C        BACK SOLUTION                                                 SIMQ1090
C                                                                      SIMQ1100
   70 NY=N-1                                                           SIMQ1110
      IT=N*N                                                           SIMQ1120
      DO 80 J=1,NY                                                     SIMQ1130
      IA=IT-J                                                          SIMQ1140
      IB=N-J                                                           SIMQ1150
      IC=N                                                             SIMQ1160
      DO 80 K=1,J                                                      SIMQ1170
      B(IB)=B(IB)-A(IA)*B(IC)                                          SIMQ1180
      IA=IA-N                                                          SIMQ1190
   80 IC=IC-1                                                          SIMQ1200
      RETURN                                                           SIMQ1210
       END                                                             SIMQ122
```

```
C                              APPENDIX 3
C
C
C
C
C
C   ITERATIVE PLANAR ONE-DIMENSIONAL SOLUTION FOR TWO-PHASE SINGLY OR
C   DOUBLY FINITE BINARY SYSTEM WITH VARIABLE DIFFUSION COEFFICIENT.
C   THE FINITE LAYER INITIALLY CONTAINS PURE ELEMENT B, WHILE THE FINITE
C   OR INFINITE SUBSTRATE CONTAINS PURE ELEMENT A. ALL CONCENTRATIONS SHOULD
C   BE INPUT IN ATOM FRACTION B. THE FREE SURFACE OF THE B LAYER IS THE
C   ORIGION FOR DISTANCE. CONSERVATION CREITERIAN IS USED TO LOCATE THE
C   INTERFACE POSITION.
C
      DIMENSION  FI(20), ABLE(40), RC(20 ), RS(20 ), TRC(20 ), TRD(20 ),
     1X(1001), Z(1001), CP(1001), DI(1001), ANEW(1001), SNU(1001),TOTNEW
     2(1001),Y(1001), ANEY(1001), SNY(1001),TOTNEY(1001), TARY(1001)
     3,XP(1000), ZP(1000),YP(1000),COMPO(200),DIST(200)
      COMMON   NX, RD(20 ), CR(20 ), D(1001), C(1001),ND
      CALL ERRSET (208,256,-1)
C
C   THE ABOVE FORTAN STATEMENT SETS ALL UNDERFLOWS TO ZERO. THE EQUIVALENT
C   WATFIV STATEMENT IS   CALL TRAPS (0,5,999999,3,1)
C
C
C                              FORMAT STATEMENTS
C
  100 FORMAT ( I5 )
  101 FORMAT ( 20A4 )
  102 FORMAT ( 2I5 )
  103 FORMAT( 1H1, //////)
  104 FORMAT ( 1H , 20A4 )
  106 FORMAT ( 1H ,22X,              'COMPOSITION',
```

```
     1 10X, 'DIFFUSION COEFFICIENT' )
  107 FORMAT ( 1H ,15X, F15.4,14X,E15.4)
  108 FORMAT(10X,I5, 2E15.7)
  110 FORMAT ( 3E15.4, 7I5 )
  112 FORMAT ( 1H , 27HCP(M) IN CALCULATION NUMBER , I4, 21H IN ITERATIO
     1N NUMBER , I2, 36H WENT NEGATIVE --- SET EQUAL TO ZERO )
  113 FORMAT ( 1H , 27HCP(M) IN CALCULATION NUMBER , I4, 21H IN ITERATIO
     1N NUMBER , I2, 43H WENT GREATER THAN ONE --- SET EQUAL TO ONE )
  114 FORMAT ( 1H ,10X, 'DIFFERENCES DI(M) BETWEEN COMPOSITIONS IN LAST'
     1/11X, 'AND NEXT TO LAST PROFILES'//1H ,13X, 1HM, 12X, 4HX(M), 15X,
     2 5HDI(M) // )
  115 FORMAT ( 1H ,12X, I3, 5X, E15.8, 7X, F11.8 )
  116 FORMAT ( /  1H ,15X, 'TIME IN SECONDS',20X, '=', F15.0 / 1H ,15X,
     1 'INTEGRAL OF C OVER ALL X(INITIAL)',2X, '=', E15.5/
     2 1H ,15X,'INTEGRAL OF C OVER ALL X(FINAL)', 4X, '=', E15.5)
  120 FORMAT (    1H ,12X, 'NO.', 9X, 'DISTANCE', 10X, 'COMPOSITION'    )
  121 FORMAT (  E15.8,  E15.8 ,E15.8)
  125 FORMAT(2E15.7,2F10.7)
  136 FORMAT(//16X,'ZI = ', E15.4)
  200 FORMAT ( 11X, '  FIRST, APPROXIMATE, ERROR FUNCTION PROFILE.'
     1 // 1H ,13X, 1HM, 12X, 4HX(M), 16X,'C(M)' //)
  201 FORMAT ( 1H ,12X, I3, 5X, E15.8, 5X, E15.8 )
  202 FORMAT(8F8.2)
  312 FORMAT( 16X, 'ITERATION NUMBER = ', I2,5X,'ZI = ',E15.4/)
  313 FORMAT( //16X, 'TWO-PHASE ITERATIVE SOLUTION.' /16X,'CONSERVATION
     1CREITERIAN USED TO LOCATE INTERFACE POSITION ZI.')
  333 FORMAT(//////)
  334 FORMAT(//)
C
C READ NTDC, THE NUMBER OF TABLES OF DIFFUSION COEFFICIENTS TO BE
C CONSIDERED.
C
```

```
  304 READ (5,100)  NTDC
      LPAL=0
  305 LPAL= LPAL+1
C
C RETURN POINT FOR EACH NEW TABLE OF DIFFUSION COEFFICIENTS.
C READ IN THE TABLE OF CONCENTRATION DEPENDENT DIFFUSION COEFFICIENTS,
C REARRANGE IT IN DESCENDING ORDER OF CONCENTRATION.
C
      READ (5,101)  ( ABLE(I), I=1,40 )
      READ (5,101)  ( FI(I), I=1,20 )
      READ (5,102)  ND, NDO
      DO 777 I=1,ND
  777 READ (5,FI)  RC(I), RD(I)
      READ(5,125) DAB,DBA,CAB, CBA
      CA=0.
      CB=0.7500
C
C ABLE    / IDENTIFICATION FOR C VERSUS D TABLE.
C FI      / VARIABLE FORMAT FOR READING IN TABLE.
C ND      / NUMBER OF ( CONCENTRATION, DIFFUSION COEFFICIENT ) PAIRS
C NDO     / PARAMETER DICTATING WHETHER OR NOT THE TABLE IS TO BE WRITTEN
C         /  0, NO.
C         / +1, YES.
C RC      / CONCENTRATION IN ATOM FRACTION B.
C RD      / DIFFUSION COEFFICIENT IN CENTIMETER SQUARED PER SECOND.
C DAB     / D ALPHA BETA.
C DBA     / D BETA ALPHA.
C  DAB AND DBA SHOULD BE IN CENTIMETER SQUARED PER SECOND.
C CAB     / C ALPHA BETA.
C CBA     / C BETA ALPHA.
C  CAB AND CBA SHOULD BE IN ATOM FRACTION B.
C
```

```
      IF ( RC(1).GT.RC(ND) )  GO TO 3
      DO 1  I=1,ND
      TRC(I) = RC(I)
    1 TRD(I) = RD(I)
      DO 2  I=1,ND
      N = ND+1-I
      RC(N) = TRC(I)
    2 RD(N) = TRD(I)
    3 IF ( NDO.EQ.0 )  GO TO 80
      WRITE (6,103)
      WRITE(6,313)
      WRITE (6,104)  ( ABLE(I), I=1,40 )
      WRITE(6,334)
      WRITE (6,106)
      WRITE (6,107)  (    RC(I),         RD(I), I=1,ND )
   80 READ (5,101)  ( ABLE(I), I=1,40 )
      READ (5,110) H,HS,DX,NTE,NTO,ND,NT
      READ(5,202)  (TARY(I),I=1,NT)
      WRITE(7,202)TARY(1)
C
C  THIS IS THE LAST READ STAMENT.
      NUMB=60
      DO 505 I=1,NUMB
  505 READ(2,503)DIST(I),COMPO(I)
  503 FORMAT(2E15.7)
C
      SDTB= (RD(1) *DBA) **0.25
      SDTA= (RD(ND)* DAB)**0.25
      TOTAL= (H+HS) *1.0001
      ZIN= H*1.0001
      ZIN2= TOTAL- ZIN
C
```

```
C ABLE    / IDENTIFICATION FOR SOLUTION.
C H       / PLTING THICKNESS IN CENTIMETERS.
C HS      / SUBSTRATE THICKNESS IN CENTIMETERS.
C DX      / DISTANCE GRID SPACING IN CENTIMETERS.
C NTE     / OPTION FOR PRINTOUT OF EACH ITERATION.
C           +1, PRINT
C           -1, DO NOT PRINT.
C NTO     / PARAMETER DENOTING WHETHER OR NOT THE FIRST, APPROXIMATE,
C         / ERROR FUNCTION PROFILE AND THE DIFFERENCES BETWEEN THE
C         / LAST AND THE NEXT-TO-LAST PROFILE ARE TO BE WRITTEN OUT.
C         /  0, NO.
C         / +1, YES.
C NO      / PARAMETER DICTATING FORM OF OUTPUT.
C         / -1, IF WRITTEN ONLY.
C         /  0, IF WRITTEN AND PUNCHED.
C         / +1, IF PUNCHED ONLY.
C NT      / TOTAL NUMBER OF DIFFUSION TIMES FOR WHICH THE CALCULATIOS
C           ARE TO BE DONE.
C TARY    / DIFFUSION TIMES IN SECONDS.
C
      DO 9  I=1,ND
    9 CR(I) = RC(I)
      DO 126 K=1,NT
      T= TARY(K)
C
C THE FOLLOWING SEGMENT SETS UP THE ARRAYS OF X,Y  AND Z VALUES.  THE X
C ARE THE ACTUAL DIFFUSION ZONE DISTANCES.  THE Y VALUES ARE EQUAL TO
C (X-ZI)/(2*SQRT(T)), AND THE Z ARE EQUAL TO (X+ZI)/(2*SQRT(T)).
C
      SR2 = 2.0 * SQRT(T)
      DZ=-DX/SR2
      L=0
```

```
  131  ZIO= ZIN
       ZIO2= TOTAL-ZIO
       L= L+1
       J = 0
       NNP= ZIO/ DX
       NX= 2.*TOTAL/DX +1
       NX1= NX-1
       NC= TOTAL/DX +1+NNP
       NC1=NC-1
       NS=  NNP+1
       NP=  NS+NNP
       XP(1)= -FLOAT(NC-NP) *DX
       YP(1)= (XP(1)- ZIO2) /SR2
       ZP(1)= (ZIO2+XP(1))/SR2
       X(1)=  -FLOAT(NNP) *DX
       Y(1)=  (X(1)- ZIO) /SR2
       Z(1)=(ZIO+X(1))/ SR2
       DO 11  M=2,NX
       X(M) = X(M-1) + DX
       Y(M)=  (X(M)- ZIO) /SR2
       Z(M)=(ZIO+X(M))/ SR2
       XP(M)= XP(M-1)+DX
       YP(M)= (XP(M)- ZIO2) /SR2
       ZP(M)=(ZIO2 +XP(M))/SR2
   11 CONTINUE
       AJ=  (ZIO-X(NP))/ DX
       R= ZIO/SQRT(T)
       R2= ZIO2/SQRT(T)
       B1=  (CB-CBA)/(2.-ERF(R/SQRT(DBA)))
       B2=  (CAB-CA) /(2.-ERF(R2/SQRT(DAB)))
C
C THIS SEGMENT CALCULATES THE FIRST, APPROXIMATE PROFILE
```

```
C
      IF(K.GT.1)  GO TO 21
      IF(L.GT.1)  GO TO 21
      IF( NTO.EQ.0)  GO TO 306
      WRITE (6,103)
      WRITE (6,200)
  306 DO 20  M=NS,NX1
      N=  2*NS-M
      MN= NX-M+1
      IF(M.GT.NP                )  C(M)= CA+ B2* (2.+ERF(YP(MN)/SDTA)-
     1 ERF( ZP(MN)/SDTA))
      IF( M.LE.NP                  ) C(M)=
     1CB-B1* (2.-ERF((R+Y(M))/ SDTB)+ERF(Y(M)/SDTB))
      IF(M.LE.NP) C(N)= C(M)
      IF (NO.GT.0.OR.NTO.EQ.0)  GO TO 20
      IF(M.GT.NC)  GO TO 20
      KK= M-NS+1
      IF( KK.EQ.45 .OR.KK.EQ.95.OR.KK.EQ. 145.OR.KK.EQ.195 )WRITE(6,103)
      WRITE (6,201)  M, X(M), C(M)
   20 CONTINUE
      IF( L.EQ. 1)  WRITE(6,103)
      C(NX)= C(NX-1)
   21 J = J+1
C
C THE CALCULATIONS FROM THIS POINT DOWN TO STATEMENT 37 ARE THE ACTUAL
C CALCULATIONS.  EVERY TIME AN ITERATION IS COMPLETED THE PROGRAM
C RECYCLES BACK TO THIS POINT.
C
      DO 210 M=1,NX
      IF( M.GT.NP .AND. C(M).GT. CAB ) C(M)= CAB
      IF( M.LE.NP .AND. C(M).LT.CBA ) C(M)= CBA
  210 CONTINUE
```

```
      CALL COEF
      DO 22  M=2,NX
      MN= NX-M+1
      ANEW(M)= (Z(M)/D(M)+Z(M-1)/D(M-1))* (-DZ)
      ANEY(M)=  (ZP(M)/D(MN) + ZP(M-1)/D(MN+1))* (-DZ)
   22 CONTINUE
      TOTNEW(1)=  (  2.*   Z(1)/D(1)) *(-DZ)* AJ
      TOTNEY(1)=  (-2.*ZP(1)/D(NX)  ) *(-DZ)* AJ
      DO 24  M=2,NX
      TOTNEY(M)=  TOTNEY(M-1)  + ANEY(M)
      TOTNEW(M)=  TOTNEW(M-1)  + ANEW(M)
   24 CONTINUE
      TOTNZ=  TOTNEW(NP) - Z(NP)/ D(NP)* DZ *AJ*2.
      MM=NX-NP
      TOTNY= TOTNEY(MM) -ZP(MM)/D(NP+1) *DZ*(1.-AJ) *2.
      SNU(1)= EXP(-TOTNEW(1))/D(1) *(-DZ)*AJ
      SNY(1)=-EXP(+TOTNEY(1))/D(NX)*(-DZ)*AJ
      DO 25  M=2,NX
      MN= NX-M+1
      ARNEW= -(EXP(-TOTNEW(M-1))/D(M-1) + EXP(-TOTNEW(M))/D(M))*0.5*DZ
      SNU(M)=  SNU(M-1) +ARNEW
      ARNEY= (EXP(-TOTNEY(M-1))/D(MN+1)+ EXP(-TOTNEY(M))/D(MN))*.5*(-DZ)
      SNY(M)=  SNY(M-1) + ARNEY
   25 CONTINUE
      SNUZ= SNU(NP)-(EXP(-TOTNZ)/ DBA+EXP(-TOTNEW(NP))/ D(NP))*0.5*DZ*AJ
      SNYZ= SNY(MM)- (EXP(-TOTNY)/DAB+EXP(-TOTNEY(MM))/DAB) *0.5*DZ*(1.-
     1 AJ)
      IF(NTE.LE.0)  GO TO 347
      WRITE(6,103)
  347 CONTINUE
      WRITE(6,312) L,ZIO
      DO 28  M=NS,NX1
```

```
      MN= NX-M+1
      NN= (NX-NP) -MN+2
      N=  2*NS-M
      IF( M.LE.NP                    ) CP(M)=
     1CB-B1* (2.-ERF(R/ SQRT(DBA)) *(SNU(M) + SNU(N))/SNUZ)
      IF(M.GT.NP) CP(M)= CA+B2*(2.-ERF(R2/SQRT(DAB))*(SNY(MN)+SNY(NN))/
     1 SNYZ)
      IF(M.GT.NC)  GO TO 348
      IF( NTE.GT.0 )                 WRITE(6,108) M,X(M),CP(M)
  348 CONTINUE
      IF ( CP(M).LT.0.0 )  GO TO 26
      IF ( CP(M).GT.CB )  GO TO 27
      GO TO 28
   26 WRITE (6,112)  M, L
      CP(M) = 0.0
      GO TO 28
   27 WRITE (6,113)  M, L
      CP(M) = CB
   28 IF( M.LE.NP)  CP(N)=  CP(M)
      CP(NX)= CP(NX-1)
      DO 31 M=NS,NC
   31 DI(M) = CP(M) - C(M)
      DO 29  M=1,NX
      IF( M.GT.NP .AND.CP(M).GT. CAB )CP(M)= CAB
      IF( M.LE.NP .AND.CP(M).LT.CBA )CP(M)= CBA
   29 C(M) = CP(M)
  135 CONTINUE
C
C  SUMAXF IS THE FINAL INTEGRAL OF COMPOSITION OVER DISTANCE. IF THE SOLUTION
C  IS CONSERVATIVE, THIS SHOULD EQUAL THE INITIAL VALUE 'H'.
C
   36 SUMAXF= 0.0
```

```
      DO 37  M=NS, NC1
      IF( M.EQ.NP) SUMAXF= SUMAXF+ (ZIO-X(NP))* (CP(NP)+CBA)*0.5
     1+(X(NP+1)-ZIO) * (CP(NP+1)+ CAB) *0.5
      IF( M.EQ.NP) GO TO 37
      SUMAXF= SUMAXF +  ((CP(M)+ CP(M+1)) *0.5 *DX )
   37 CONTINUE
      WRITE(7,666)SUMAXF,ZIO
  666 FORMAT('SUM=',E15.7,10X,'INTERFACE POSITION=',E15.7)
      IF(L.LT.5)  MAGIC=1
      IF(L.GE.5 .AND. L.LT.10)  MAGIC=2
      IF(L.GE.10)  MAGIC=4
       ZIN=  ZIO+ (CB*H-SUMAXF) /FLOAT(MAGIC)
      IF(L.LT.20)  GO TO 131
C
C THIS SEGMENT CALCULATES THE DIFFERENCES BETWEEN THE COMPOSITIONS IN
C LAST PROFILE AND THE NEXT TO THE LAST PROFILE AND WRITES THEM OUT.
C
      WRITE (6,103)
      WRITE (6,114)
      DO 349 M=NS,NC
      KK= M-NS+1
      IF( KK.EQ.45 .OR.KK.EQ.95.OR.KK.EQ. 145.OR.KK.EQ.195 )WRITE(6,103)
  349 WRITE (6,115)  M, X(M), DI(M)
C
C                     OUTPUT OF FINAL RESULTS
C
      IF ( NO.GT.0 )  GO TO 63
      WRITE (6,103)
      WRITE (6,104)  ( ABLE(I), I=1,40 )
      HMOD=CB*H
      WRITE(6,116) T ,HMOD, SUMAXF
      WRITE(6,136)  ZIO
```

```
      NFIT=NC-NS+1
      DO 335 M=NS,NC
      KK= M-NS+1
  335 WRITE(4,121) D(M), CP(M),X(M)
      DO 560 J=1,NFIT
      X(J)=X(NS+J-1)
  560 CP(J)=CP(NS+J-1)
      WRITE(6,103)
   63 CONTINUE
      IF( ZIN.LE.0.)  GO TO 300
  126 CONTINUE
  300 IF ( LPAL.NE.NTDC )  GO TO 305
      CALL PLOTS(0,0,50)
      CALL PLOT(1.5,3.5,-3)
      CALL SCALE(DIST,6.5,NUMB,1)
      CALL SCALE(COMPO,4.5,NUMB,1)
      CALL NEWPEN(3)
      NFIT1=NFIT+1
      NFIT2=NFIT+2
      NUMB1=NUMB+1
      NUMB2=NUMB+2
      X(NFIT1)=DIST(NUMB1)
      X(NFIT2)=DIST(NUMB2)
      CP(NFIT1)=COMPO(NUMB1)
      CP(NFIT2)=COMPO(NUMB2)
      CALL AXIS(0.,0.,'DIST. (CMS)',-11,6.5,0.,DIST(NUMB1),DIST(NUMB2
     1))
      CALL  AXIS(0.,0.,'CONCENTRATION.',13,4.5,90.,COMPO(NUMB1),COMPO(NU
     1MB2))
      CALL LINE(X,CP,NFIT,1,2,1)
      CALL LINE(DIST,COMPO,NUMB,1,1,2)
      CALL SYMBOL(4.0,4.0500,.100,2,0.,-1)
```

```
      CALL SYMBOL(4.25,4.0,.100,'EXPT. PROFILE',0.,13)
      CALL SYMBOL(4.0,3.80,0.100,1,0.,-1)
      CALL SYMBOL(4.25,3.75,.100,'FITTED PROFILE',0.,14)
      CALL VPISYM(1.,6.,15,KTIL,0.,80)
      CALL PLOT(12.0,0.0,999)
      STOP
      END
C
C        / DIFFUSION COEFFICIENT CALCULATION BY LOG INTERPOLATION.
C
      SUBROUTINE COEF
      COMMON   NX, RD(20 ), CR(20 ), D(1001), C(1001),ND
      DO 4  M=1,NX
      DO 2 I=2,ND
      IF( C(M) .LT. CR(I))  GO TO 2
      D(M)=  RD(I) * (RD(I-1)/ RD(I)) ** ((C(M) -CR(I))/(CR(I-1)-CR(I)))
      GO TO 4
    2 CONTINUE
    4 CONTINUE
      RETURN
      END
```

APPENDIX 4

Operation of Perkin Elmer Sputtering Sytem

In this section, certain salient features of the Perkin Elmer[102] Randex Model 2400-8J Sputtering System will be described. The intent of this endeavour is to familiarize a beginner with the sputtering system* and to provide step-by step instructions for the operation of the unit.

RF Sputtering systems can be used to deposit a wide variety of materials onto substrates as ceramics, metals, plastics, glass and semi-conductors. Resulting thin films can range in thickness from a few Angstroms up to a fraction of a millimeter.

These sputtering systems can also sequentially deposit upto three different materials onto a single substrate. Also, these systems can be used for sputter- etching, a process in which material is removed from, rather than deposited on, the substrate.

The Sputtering Process

---

* Note: No attempt is being made to be thorough in this respect. Every attempt is being made to be consise and as a result, this section is not an instruction manual. For further details reference should be made to the Instruction Manual[114].

Sputtering is a momentum transfer process in which atoms from a cathode/target are driven off or sputtered by bombarding ions. In this process the momentum of the bombarding particles is more important than energy. For example, a hydrogen or helium ion accelerated to 3000ev will cause very little sputtering compared to an ion of argon (which is chemically inert) with the same 3000ev energy, simply because the much lighter hydrogen or helium ion has a lower momentum.

Sputtered atoms travel until they strike a substrate, where they deposit to form the desired layer. As individual atoms they can be chemically active and form compounds with the ions and atoms of the bombarding gas. This is the reason inert argon is used as the bombarding gas. In some applications, however a reactive gas is purposely added to argon so that the deposit is a film of chemical compound, and the process is termed reactive ion sputtering.

When argon ions strike the target, their electrical charge is neutralized and they return to the process as atoms. If the target is an insulator, the neutralization process results in a positive charge on the target surface. This charge may grow large enough that the bombarding ions are repelled and the sputtering process stops. To continue the process, the polarity must be reversed to attract enough

electrons from the discharge to eliminate the surface charge. This periodic reversal of polarity is done automatically by applying RF voltage onto the target assembly (hence the term RF sputtering) of interest here is the diode rectifier-like behaviour of the target and discharge system. This is caused by the vast difference in mobilities of ions and electrons, since the latter are much faster, they are attracted in much greater numbers to the target during the positive half-period of the RF voltage than are ions during their half-period.

System Description The Perkin Elmer 2400-8 sputtering system consists of:

* Impedence matching network
* Control panel
* J-arm (anode) and targets (cathode) assembly
* vacuum chamber
* auto pumpdown control panel

Impedance Matching Network

The impedance matching network is located in the top of the unit (figure 50). This network matches the impedance of the cathode /discharge/ anode (substrate table) system to the standard 50-ohm impedance of the coaxial line which

brings RF power from the generator. Without a proper match, the RF power generator cannot deliver the power for the sputtering process. Instead, reflected waves travel back in the coaxial cable causing standing waves and heating of the cable and certain components in the power generator. The matching network is designed to allow independent matching of the real and imaginary parts of the impedance automatically. Proper matching can be achieved even with wide variations in deposition parameters such as target size, target-to-substrate distance, argon pressure, etc. Impedance matching is controlled manually by the LOAD and TUNE controls on the front panel (see figure 51).

Control Panel

The following controls and indicators are located on the control panel (see figure 51)

MODE SELECTOR SWITCH: Allows selection of any the following operating modes:

SPUTTER DEPOSIT: In this mode all the RF power is applied to the target, i.e., only the target is bombarded by ions and sputtered. Although substrate table is grounded some self bias is developed on the substrate table which is read on the TARGET BIAS meter.

SPUTTER ETCH: All RF power is applied to the substrate table and material is removed (etched away) from the sub-

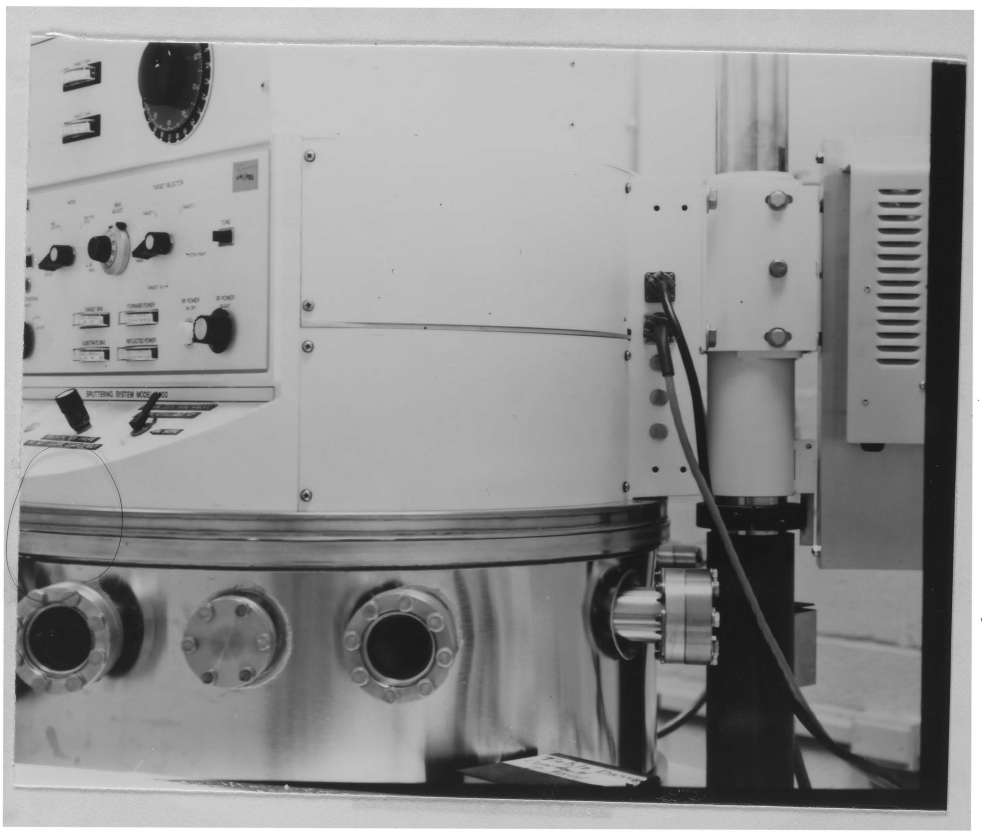


Fig. 50 Side view of the Perkin Elmer Sputtering Unit, showing control panel, hoist, view ports & bell jar.



Fig. 51 Control Panel.

strates by ion bombardment. Self bias is read on the TARGET BIAS meter.

DC BIAS: This mode is essentially the same as sputter deposit. However, instead of grounding the substrate table, a DC bias can be applied to it from an external DC power source.

TARGET SELECTOR: Connects the output of the matching circuit to any one of the three targets and the substrates. This switch has 4 positions. At TARGET 1 the RF power is connected to the left target as viewed from the front of the unit, TARGET 3 is to the right when viewed from the front of the unit and 2 is at the rear. The sputter etch station is in the front.

BIAS ADJUST control: Active only in the BIAS SPUTTER operating mode. This control adjusts the percentage of RF power applied to the substrate table. Varying the amount of power will vary the negative self-bias on the table. This bias is measured by the SUBSTRATE BIAS meter*. The meter essentially measures the energy with which ions from the discharge strike the substrate table.

---

* Note: Although deflection type meters are provided for reading target and substrate bias forward and reflected power, these values (especially the substrate bias in the BIAS sputter mode) can be read off very accurately on digital meters. Provisions for hook up of these meters (for the system in our laboratory) have been made at the top left of the control panel (Figure 51) and the proper markings are found on the unit itself.

LOAD control: Adjusts the inductive coupling between the primary and secondary circuits of the matching network.

TUNE control: Adjusts the parallel capacity in the target circuit of the matching network.

POWER ON/OFF switch: Actuates, through a special logic circuit, a high-voltage relay in the RF power generator. The ON/OFF function is also interlocked by a pressure interlock switch so that the RF voltage cannot be applied to the targets while they are exposed to atmospheric pressure. Applying high RF voltage to targets exposed to air can result in arcing and breakdown around the edges of the target.

POWER ADJUST Control: Governs the power output from the RF generator. This quantity is measured and displayed on FORWARD POWER meter.

REFLECTED POWER meter: Measures the amount of RF power flowing back from the sputtering unit to the generator due to improper adjustment of the matching network. This reflected wave combines in the cable with the forward wave to form standing waves which can cause heating or even damage to the cable. With power adjustment of the LOAD and TUNE Controls, readings on the REFLECTED POWER meter should not exceed 10 to 15 watts for any amount on the FORWARD POWER meter. It should be noted that a small residual amount of reflected power is due to transitions on the cable (such as connections, etc.) and cannot be eliminated.

TABLE POSITION switch: This five-position switch actuates a meter which positions the substrate table opposite any one of the three targets or in the fourth position (ETCH) where the substrate table faces a surface which collects etched off material. The fifth position of the switch (CONT) causes the substrate table to rotate continuously and is especially useful when a 21-inch-diameter annular substrate table is used instead of the J-arm substrate table.

Below the control panel are two valves: the argon shut-off valve and the argon metering valve (figure 51).

Argon Shut-off valve: This is connected in series with the argon metering valve. In operation, the argon metering valve is adjusted to give the desired working pressure of argon and the shut-off valve is then used to close and open the argon flow without changing the setting of the metering valve.

Metering valve: This is a stainless steel needle metering valve equipped with a precision micrometer head for accurate and repeatable settings. Turning the head clockwise closes the valve. The proper setting is empirically determined and depends on the desired argon pressure as well as the system pumping capability.

CAUTION

NEVER TRY TO CLOSE THE METERING VALVE COMPLETELY,

AS THIS WILL DAMAGE THE NEEDLE AND SEAT.

J-arm (anode) and target (cathode) assembly

As decribed earlier, this system has provision for mounting up to three targets to be sputtered separately or even sequentially on to any substrate. The target materials can be bonded onto the cathode using various techniques such as brazing, soldering or epoxy bonding. The target assembly consists of an insulator, cover plate and the target material. The cover has inlets and outlets so that the target can be water cooled.

The substrate table or the J-arm is free to rotate and move under any target. The arm itself is located at the center top unit, and can be adjusted to any height. This adjusts the distance between any target and the substrate table (anode) and the usual distance is 1.5 inches.

Around the targets, Dark Space Shields and Ground Rings can be installed. The purpose of the dark space shield is to focus the discharge, provide grounding surfaces for the discharge and also prevent cross-contamination of targets by sputtered material. When a target smaller than 8 inches in diameter (the standard size for the 2400-8J model) is used then a Dark Space Shield Adapter Kit is used to limit the

discharge to the target material, thus protecting the backing plate from ion bombardment.

Vacuum Chamber

The vacuum chamber is a large stainless steel bell jar provided with ports (one of them being a view port) for installation of additional measuring devices (such as mass spectrometers, etc). The bottom of the chamber is open to the pumping system through a cold trap. At the top, the chamber is sealed off with the sputter head. The sputter head can be raised or lowered by a hoist (see figure 50) as will be described in the next section. A filament igniter is part of the sputtering head assembly. Made of theriated tungsten wire, the igniter circuit ionizes the plazma when the Power Switch is turned on and Power is applied. Once a plasma is obtained the circuitry automatically turns the igniter off.

Auto Pumpdown Control Panel

The Pumpdown Control provides Automatic or Manual pumpdown of the vacuum system and features pushbutton, failsafe operation. It is totally interlocked and provides maximum protection to the vacuum system. Output relays are delayed in sequence, leaving each valve enough time to close before another is opened. The controller also includes a Liquid Nitrogen Level Control with adjustable timer.

The control panel (figure 52) has the following two position toggle switches (in the Manual mode up position means ON, and down position means OFF).

1. Gas valve
2. Throttle valve
3. High-Vacuum Pump
4. High-Vacuum Valve
5. Foreline Valve
6. Roughing valve
7. Mechanical pump
8. Vent valve

The line diagram on the pumpdown control panel (figure 52) shows the functions of these various valves. The control panels also has a digital gauge control that can be used to read the vacuum readings as well as argon pressures. When the FUNCTION SELECTOR SWITCH is on the EMISSION settings, vacuum readings are displayed. When set on the ST1 or ST2 positions, argon pressure reading are displayed.

The pumping system includes a mechanical (roughing) pump, cryo-pump (high vacuum pump) and a liquid nitrogen

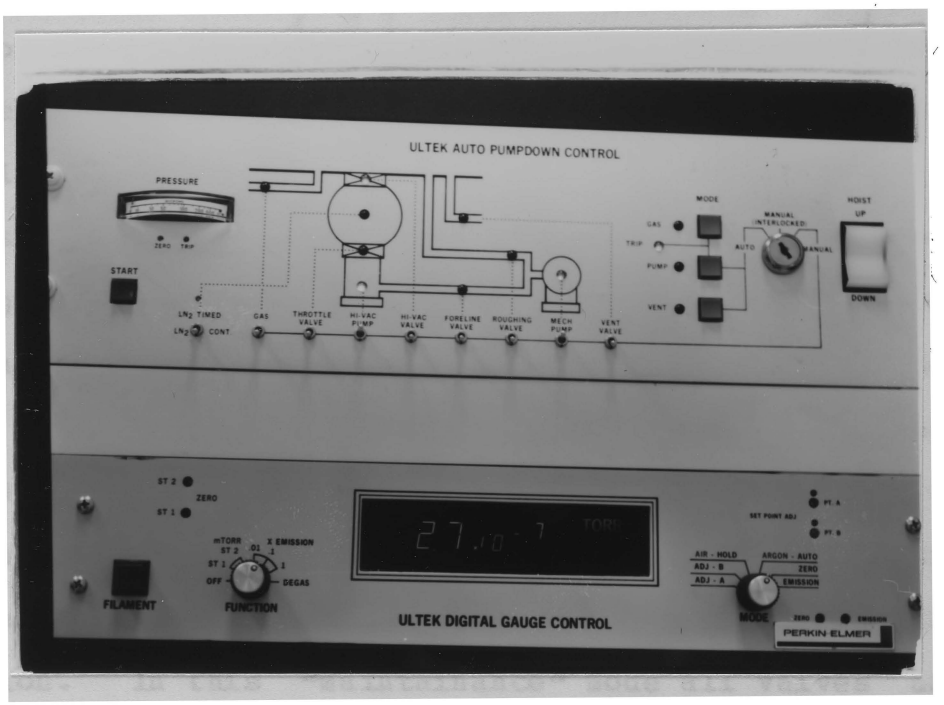


Fig. 52 Perkin Elmer auto pumpdown control panel.

cold-trap (figure 53). The cryo-pump is operated by means of the compressor shown in figure 54.

A hole in the control panel labeled TRIP (figure 52), sets the point of cross-over from the roughing pump to the high vacuum pump. This cross-over is usually set between 10 to 100 microns depending on the reactivity of the target materials. Also provided on the control panel is a 3 position liquid nitrogen toggle switch. The bottom position of the switch is OFF, the center position is for continuous delivery of liquid nitrogen to the cold trap and the top position is for timed delivery. The liquid nitrogen timer adjusts time between fills from 3 minutes to 2 hours. This time can be increased by turning the timer clockwise.

The pumpdown controller has three modes of operation:
MANUAL- used for servicing only. In this mode the front panel Key Switch (figure 52) is in the MANUAL position and the switch on the rear panel is in the INTERLOCK DEFEAT position. In this "maintainance" mode all valves are driven directly with no interlocking.
Interlocked manual- for manual system operation. In this case the Key switch is in the MANUAL/INTERLOCKED position. Valves are driven by switches, but they work only if the swiches are thrown in the right sequence and if proper pressures are established. No time delays are used in this mode.

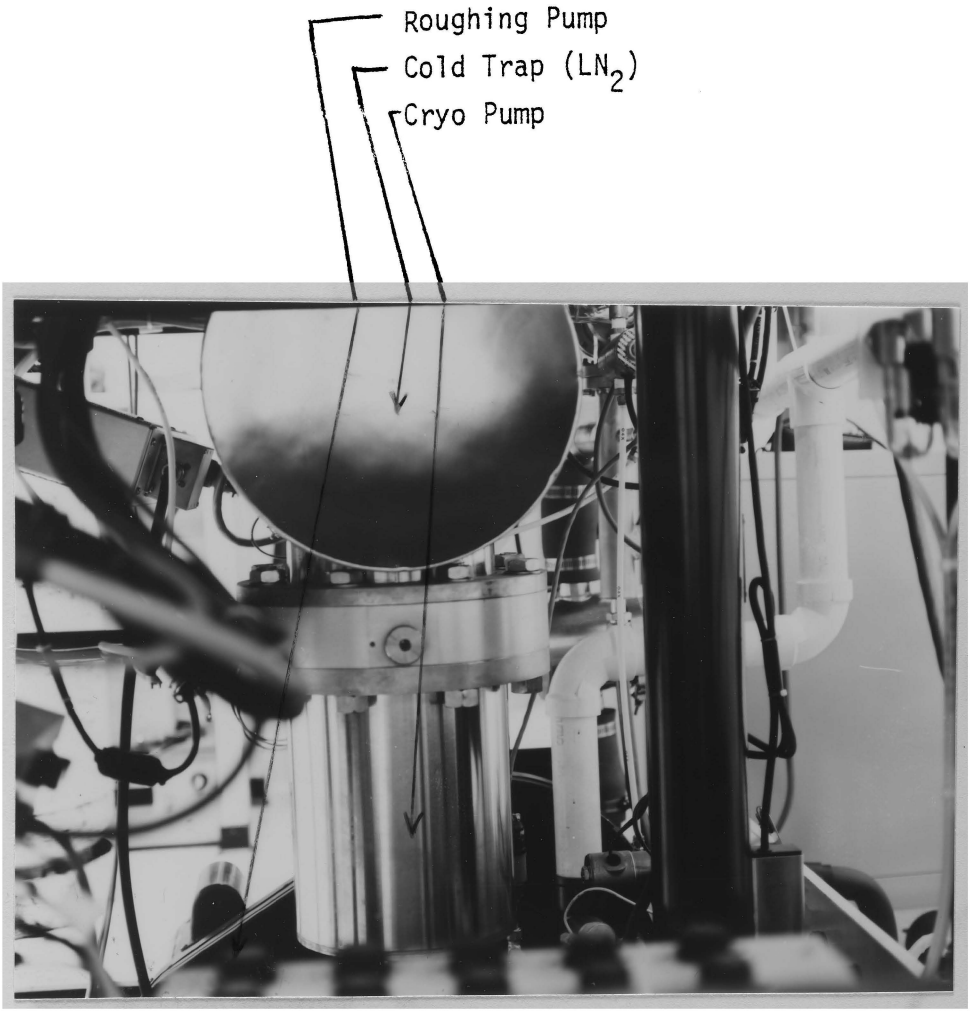


Fig. 53 Photograph showing the vaccum units.

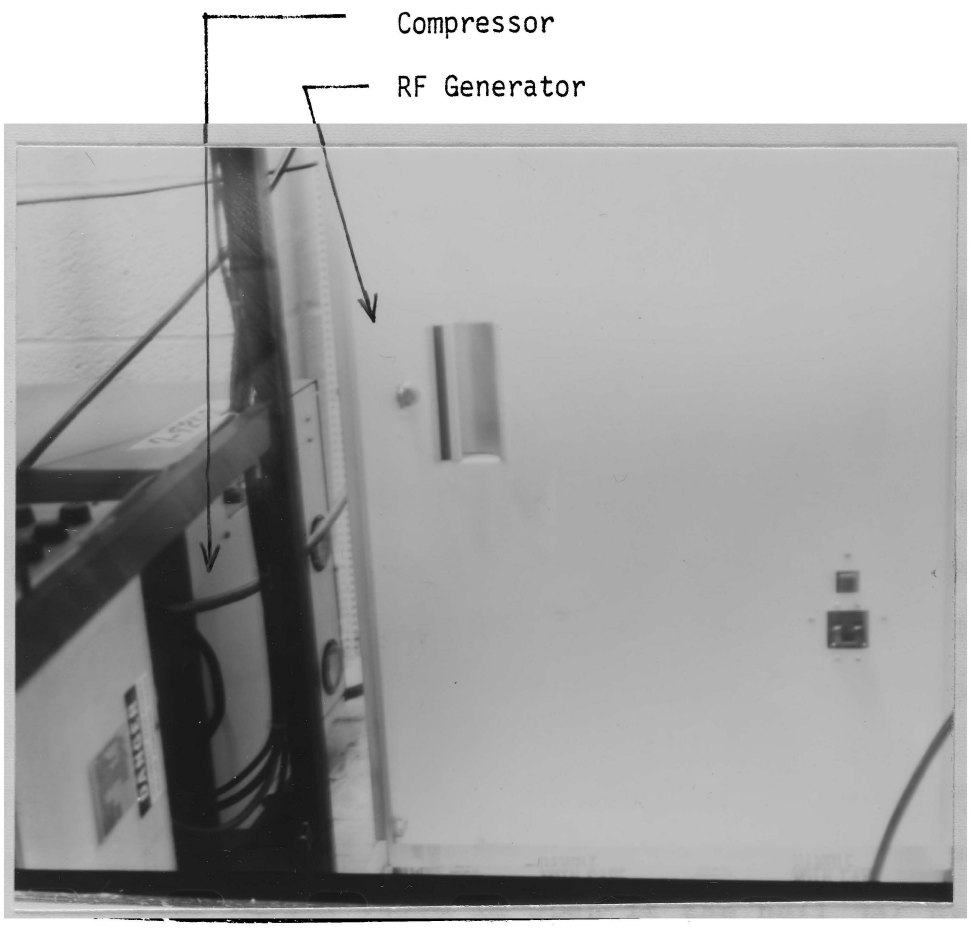


Fig. 54 Photograph showing the RF Generator & Compressor.

Auto- for automatic operation. The Key switch is in the AUTO position and all operations are fully automatic with interlock signals, pressure levels and time delays.
The AUTO mode has the following four conditions:

1. Vent pushbutton- If this button is activated, the high vacuum valve is closed, roughing valve is closed and the vent valve is open. The GAS push-button can be used to interrupt venting.

2. Pump push button - If this button is activated, the foreline valve will be closed, vent valve closed and, if the hoist is down, the roughing valve is opened. The bell jar is pumped down to the preset cross over pressure (TRIP) and the controller goes into the standby condition. The GAS pushbutton can be used to interrupt the pumping.

3. STANDBY condition - In this case, the roughing valve is closed, foreline valve is opened and the high vacuum valve is open if the bell jar pressure is below the TRIP point. The bell jar pressure is shown on the T.C. Gauge Meter(upper left corner of figure 53) and the cross over pressure (TRIP) can be adjusted from 10 to 500 microns.

4. GAS pushbutton - When this is activated, the high vacuum valve must be open, the optional throttle valve is closed and the gas valve is opened. After this pushbutton has been activated, the PUMP pushbutton shuts off the gas.

To activate any of these three modes (VENT, PUMP or GAS), these pushbuttons must be used simultaneously with the START pushbutton.

The HOIST CONTROL switch on the control panel allows the sputter head to be moved up or down. The proper positions are marked on the panel (figure 52).

Regeneration of the Cryopump:

After operating for some time, cryopumps must be regenerated to remove the gas molecules that have been adsorbed on their interior surfaces. The required frequency of regeneration depends upon how often the cryopump is used and on the types of gas molecules that are pumped in the vacuum system.

The regeneration process is comprised of three stages:

1. The cryopanels on the interior of the pump are warmed to room temperature. This drives adsorbed molecules into the vapour phase. The pump is

vented with dry nitrogen gas to accelerate this process, which lasts for up to one hour.

2. The cryopump is evacuated with a roughing pump for thirty minutes and during this time the contaminant gas continues to be removed.

3. The pump's cryopanels are cooled to operating temperature. Two hours are required for this stage, after which the cryopump is ready for use.

The required frequency of regeneration depends on how often the cryopump is used and the types of gas molecules that are pumped in the vacuum system. The cryopump may be regenerated when the compressor's absorbent is changed after 9000 hours of compressor use. In sputtering systems, the pump's capacity is exhausted after approximately one month of use, although a weekly recycling routine should maintain a high reserve of pumping capability.

CONCISE OPERATING INSTRUCTIONS
FOR SPUTTER DEPOSITION
(Including Regeneration of the Cryopump)

1. Make sure the MAINS POWER (on the wall) is ON (turn it ON by pushing START button)

2. Turn the Key Switch on the Pumpdown Control panel to the Manual mode.

3. Turn the MECHANICAL PUMP ON (by throwing the toggle switch on front panel, up).

4. Turn the VENT IN (by turning the Key Switch on front-center panel to the right -these switches are located below the argon control valves - yellow light indicates that the vent is open).
   Open the valve on the dry nitrogen bottle and purge the cryopump with 20ps, dry nitrogen for 45 minutes to an hour (depending on pump usage)
   After the desired length of time, close the vent by turning the Key Switch off.

5. Turn the ROUGHING PUMP Key Switch on (front center panel - red light indicates that the pump is on) Rough for approximately an hour and turn the pump off.

   Turn the FUNCTION SELECTOR Switch on the Digital guage control panel to the "mTorr" settings (red markings).

   If the increase in pressure readings on the digital display is less than 1m Torr/min., you are ready to switch over to the CRYO PUMP. If not, repeat the roughing procedure and try again.

6. Turn the MAIN Key Switch on control panel to AUTO mode.

   Note 1 : When this is done, throwing any of the toggle switches on front panel, up or down will not accomplish anything different from what is predetermined by the AUTO mode.

   Note 2 : The 3 position Liquid Nitrogen toggle switch however has to be turned to the position desired. This will not work automatically.

7. Start the CRYO PUMP by turning the 2 position toggle switch on the COMPRESSOR, up (figure 54).
   Wait for approximately 4 hours or till the temperature gets down to 14°K (Temperature gauge on the Cryo pump shows this).
   Pump for approximately 1 hour under the above conditions

8. Turn the Liquid Nitrogen toggle switch to the center position (continuous delivery). Open the valve on the Liquid Nitrogen tank. Wait till the COLD TRAP is full (the red indicator light stays on till the trap is full and then comes on intermittently - see diagram on control panel, figure 53).

9. Open the valve on the Argon cylinder and regulate the pressure to 2-3 psi. Reduce the pressure on the dry nitrogen cylinder to 3-4 psi.

10. Push the VENT and START buttons on the front panel simultaneously. You can hear the safety switch click. Then, raise the chamber by holding the HOIST Switch in the UP position.

11. Check the distance between anode and cathode. The set distance at present is 1.5. Reset if neccessary - refer to the instruction manual.

12. Lower the Chamber completely by holding the HOIST Switch in the DOWN position.

13. Turn the RF GENERATOR ON

(Trip switch near the bottom of the generator- green light indicates that the generator is ON)

Note 1: Wait at least 90 seconds when the generator is turned on, before doing anything else. Allow 5 minutes cool down time when the RF power switch on module is turned off, before shutting the RF generator off.

Note 2: The RF generator powers the J-arm table and everything on the top module (sputter head).

14. Push START and PUMP buttons on front panel simultaneously. The roughing valve is automatically opened in the Auto mode.

Watch the pressure gauge at top left of front panel. The needle rises till the trip point on

the gauge and the trip light on front panel goes out.

The roughing valve closes automatically and the pressure gauge needle goes back to zero. The high pressure valve opens and the throttle valve light comes on. The needle rises again.

15. Turn the Function Selector switch to the EMISSON setting (black readings).

Push the FILAMENT switch (red) button ON. Note the pressure readings on the DIGITAL DISPLAY. When the pressure reaches approx. $1x10^{-6}$ Torr, turn the Function Selector switch to DEGASS position. The pressure will rise initially but will decrease afterwards. When the pressure is relatively stable, stop the degassing by turning the selector switch to either the 1, 0.1 or 0.01 settings. Wait till the desired vacuum is achieved.

16. Turn the Function Selector Switch to ST2 (red settings). Push the START and GAS buttons on the front panel, simultaneously. The throttle valve opens. Open the black manual valve on top module

by pulling the lever towards you, till it stops in the center or upward position this is marked on the unit.

Adjust the opening micrometer slowly till the Argon pressure reaches the desired value (as seen on the digital display).

Note: Do NOT close the micrometer valve completely as this will damage the needle valve beneath it.

17. Turn the TABLE SELECTOR Switch to the ETCH position. The table will automatically move to a position away from the targets.

Note: The table drive controls are already set for the corect speed (40% of maximum) and direction (reverse), according to the specifications and may not have to be readjusted.

18. Turn the MODE Selector Switch to SPUTTER ETCH position.

19. Push the POWER button ON (while button ligths up - igniter is ON)

Turn the continuously variable RF POWER ADJUST knob slowly till the desired power is obtained (check FORWARD POWER meter reading)

The REFLECTED POWER (meter reading) must be as close to zero as possible. Therefore, it may be neccessary to fine TUNE with the TUNE switch (upper right of top module). (Turn it to the right or left until the Reflected Power is close to zero.)

Note down the Forward Power, Reflected Power, Target Bias and Substrate Bias meter readings. Sputter Etch for the desired length of time.

20. Turn the RF Power Adjust Knob all the way down

(This is neccessary since the J-arm table will not rotate to the desired position when the power is NOT reduced to zero - except when the Table Selector Switch is in the Continuous Mode.)

Note: It may be sometimes useful or essential (especially if it is being used after a long time) to clean the target for about a minute. To do this, the table is left in the ETCH position and the Mode Selector Switch is turned to the SPUTTER DEPOSIT position. The TARGET SELECTOR Switch is

turned to select the target to be cleaned and used for Sputtering. Increase the Power to approx. 500 watts and Sputter Deposit (without any samples beneath) for a minute or so. Turn the RF Power adjust all the way down - it is not neccessary to shut the RF Power Switch off each time this is done.

21. Turn the Table Selector Switch to the desired target that needs to be sputtered. The table will rotate slowly to the desired position.

    (You may wish to note the vacuum achieved before sputtering - Turn Function Selector Switch to the Emission Mode settings and read from digital display.)

    Also, check the Argon pressure and adjust if neccessary.

22. Increase the power to the desired value and tune. Note the Power and Bias readings on the meters. After Sputter Depositing for the required length of time, turn the RF Power Adjust down and the RF Power Switch Off.

23. Turn Table Selector Switch to the ETCH position. The table swings to the front side of the unit. Allow about 15 minutes Cool Down Time.

24. Push the START and VENT buttons simultaneously to vent the chamber.

    When the Safety Switch clicks, raise the chamber UP by holding the HOIST Switch in the UP position.

25. Remove the Samples and lower the chamber. Rough the chamber by pushing the START and PUMP buttons. After the pressure gauge needle reaches the trip point, the chamber is sufficiently rougned and maintained until the next time.
    Leave the Main Key Switch in the Auto Mode.
    Turn the RF power generator (trip switch) OFF.
    Leave the Main Power ON.

CLEANING PROCEDURES

If different materials are to be sputter deposited each time, the system has to be cleaned thoroughly. Certain design features incorporated

to facilitate periodic maintainance and cleaning. The frequency of cleaning will depend upon the amount of use and the acceptable limit of contamination of the chamber. Residual deposits on the chamber walls and the dark space shields could cause an increase in the degassing rates which neccessitate a longer pumpdown.

To clean the dark space shields, first the electrical power must be disconnected from the power generator. Release the sputtering unit to air and lift it by the hoist to gain access to the dark space shields. Unscrew the space shields and clean them by bead-blasting or other suitable methods. Etch clean (chemical) is not desirable as there may be uneven cleaning as well as pitting of the dark space shields. Vapor degassing or an acetone and alcohol wash after the bead-blasting is essential. The bead-blasting also leaves a roughened surface which promotes adhesion of the deposited material and reduces flaking.

Minor cleaning of the substrate platform, especially to remove film flakes can be performed without removing the substrate platform assembly out of the bearing housing. Lossen the clamps

holding the shield of the substrate platform. Slip the shield down over the platform support and clean out film flakes. The disc above the substrate heaters can also be removed and bead blasted.

The rest of the bell jar and sputter head surfaces can be cleaned with 50% Nitric acid. Rubber gloves should be worn when this is done. Care should also be taken not to allow the acid to touch the o-ring on the bell jar, igniter etc. The chamber should next be cleaned with water-free acetone and alcohol, in that sequence. The chamber should be left open so that the remaining acid fumes leave the chamber. The vacuum chamber is then ready for the next sputter-deposition.

```
C                                APPENDIX 5
C
C
C
C
C
C     THIS PROGRAM CALCULATES COMBINATIONS OF H,K,L VALUES                INT00010
C     ALONG WITH VALUES OF 2THETA, SIN/LAMBDA,F FOR EACH ATOM,            INT00020
C     F**2, P, LP, S.R.I.I., AND D.                                       INT00030
                                                                          INT00040
      COMPLEX *8 CMPLX,FT,F1(900),F2(900),CFJ(2,900)                      INT00050
      DIMENSION U(2,20),V(2,20),W(2,20),F(900),FF(900),FFF(900),          INT00060
     1H(900),K(900),L(900),X(900),Y(900),Z(900),SF(900),NQ(200),SL(900),INT00070
     2ASF(200),AT (2,900),IFAC(900),LP(900),CFT(2,900),CFF(900),          INT00080
     3CF(2,900),FG(900),LLP(900),FFG(900),AA(2,4),BB(2,4),CC(2)           INT00090
      DIMENSION ATEQ(1,400)
      REAL NQ,LP,LLP                                                      INT00100
      INTEGER H,K,L,   X,Y,Z ,SF1,SF2 ,QP                                 INT00110
      CALL ERRSET(208,256,-1)
    4 FORMAT (3F9.5)                                                      INT00120
    1 FORMAT(3I3,F6.2,I2)                                                 INT00130
  888 FORMAT('1')                                                         INT00140
  171 FORMAT(30X,' THE TABLE FOR TI3AL IS AS FOLLOWS:'///)                INT00150
  165 FORMAT(5X,'HKL',7X,'2THETA',6X,'SIN/LAMBDA',6X,'F1',11X,'F2',11X,'INT00160
     1F**2',10X,'P', 8X,'LP',19X,'S.R.I.I.',5X,'D')                       INT00170
   91 FORMAT(3X,F8.5,5X,F8.5,5X,F8.5)                                     INT00180
   92 FORMAT(10X,3I2, 6X,2F9.5,10X,9F9.5)                                 INT00190
                                                                          INT00200
      PI=4.*ARCOS(0.)                                                     INT00210
      P=360./PI                                                           INT00220
      READ (5,1)NUM,N,JNJ,AMTH,ICRYST                                     INT00230
C     IF ICRYST = 1 WE HAVE A CUBIC SYSTEM
C     IF ICRYST = 2 WE HAVE A HEXAGONAL SYSTEM
```

```
C      IF ICRYST = 3 WE HAVE A TETRAGONAL SYSTEM
       NUM=0                                                          INT00240
       J=0                                                            INT00250
C                                                                     INT00260
C CALCULATE HKL'S                                                     INT00270
C                                                                     INT00280
       DO 400 I=1,12                                                  INT00290
       DO400 II=1,I                                                   INT00300
       DO 400 III=1,9                                                 INT00310
       IF(J.EQ.0) GO TO 350                                           INT00320
       NUM = NUM+1                                                    INT00330
       H(NUM)=I-1                                                     INT00340
       K(NUM)=II-1                                                    INT00350
       L(NUM)=III-1                                                   INT00360
350    J=1                                                            INT00370
400    CONTINUE                                                       INT00380
C                                                                     
C CALCULATE SIN THETA                                                 INT00390
C                                                                     INT00400
       IK=0                                                           INT00410
       DO 500 NI=1,NUM                                                INT00420
       IK=IK+1                                                        INT00430
       H(IK)=H(NI)                                                    INT00440
       K(IK)=K(NI)                                                    INT00450
       L(IK)=L(NI)                                                    INT00460
       F(IK)=((1.54051**2)/4.)*((4./3.)*(H(IK)**2+K(IK)**2+H(IK)*K(IK))/
      1(7.429**2)+((L(IK)**2)/(5.139**2)))
       FF(IK)=SQRT(F(IK))                                             INT00490
       IF (FF(IK).GE.1.0) GO TO 90                                    INT00500
       FFF(IK)=ARSIN(FF(IK))*P                                        INT00510
       FFG(IK)=2.*FFF(IK)                                             INT00520
       GO TO 500                                                      INT00530
```

```
   90 IK=IK-1                                                          INT00540
500   CONTINUE                                                         INT00550
C                                                                      INT00560
C SORT HKL'S ACCORDING TO THETA                                        INT00570
C                                                                      INT00580
      NUM=IK                                                           INT00590
      FFG(IK+1)=200.                                                   INT00600
300   J=1                                                              INT00610
      DO 200 I=1,IK                                                    INT00620
      IF(FFG(I).LE.FFG(I+1)) GO TO 200                                 INT00630
      J=2                                                              INT00640
      LH=H(I)                                                          INT00650
      LK=K(I)                                                          INT00660
      LL=L(I)                                                          INT00670
      AF=F(I)                                                          INT00680
      AFFG=FFG(I)                                                      INT00690
      H(I)=H(I+1)                                                      INT00700
      K(I)=K(I+1)                                                      INT00710
      L(I)=L(I+1)                                                      INT00720
      F(I)=F(I+1)                                                      INT00730
      FFG(I)=FFG(I+1)                                                  INT00740
      H(I+1)=LH                                                        INT00750
      K(I+1)=LK                                                        INT00760
      L(I+1)=LL                                                        INT00770
      F(I+1)=AF                                                        INT00780
      FFG(I+1)=AFFG                                                    INT00790
200   CONTINUE                                                         INT00800
      IF(J.EQ.2) GO TO 300                                             INT00810
      QP=N-JNJ                                                         INT00820
C                                                                      INT00830
C READ AND PRINT ATOMIC POSITIONS                                      INT00840
      WRITE(7,444)AMTH
```

```
  444 FORMAT('MONOCHROMATOR ANGLE=',F7.4)
C                                                                       INT00850
      DO 5 J=1,JNJ                                                      INT00860
      READ(5,4) U(1,J),V(1,J),W(1,J)                                    INT00870
    5 WRITE(6,91)U(1,J),V(1,J),W(1,J)                                   INT00880
      IF (JNJ.EQ.N) GO TO 911
      DO 60 JK=1,QP                                                     INT00890
      READ (5,4) U(2,JK),V(2,JK),W(2,JK)                                INT00900
   60 WRITE(6,91)U(2,JK),V(2,JK),W(2,JK)                                INT00910
  911 CONTINUE
C                                                                       INT00920
C CALCULATE STRUCTURE FACTORS AND ROUND IF LESS THAN .0005              INT00930
C                                                                       INT00940
      DO 8 IJ=1,NUM                                                     INT00950
      DO 8 JII=1,2                                                      INT00960
      IF (JII.EQ.1)NN=JNJ                                               INT00970
      IF (JII.EQ.2)NN=QP                                                INT00980
      SF3=0.0                                                           INT00990
      SF4=0.0                                                           INT01000
      IF (NN.EQ.0) GO TO 8
      DO 7 JI=1,NN                                                      INT01010
      SF3=SF3+COS((U(JII,JI)*H(IJ)+V(JII,JI)*K(IJ)+W(JII,JI)*L(IJ))*PI) INT01020
      SF4=SF4+SIN((U(JII,JI)*H(IJ)+V(JII,JI)*K(IJ)+W(JII,JI)*L(IJ))*PI) INT01030
    7 CONTINUE
      IF(ABS(SF3).LT.0.0005) SF3=0.0                                    INT01050
      IF(ABS(SF4).LT.0.0005) SF4=0.0                                    INT01060
      IF (JII.EQ.1) GO TO 20                                            INT01070
      F2(IJ)=CMPLX(SF3,SF4)                                             INT01080
      GO TO 8                                                           INT01090
   20 F1(IJ)=CMPLX(SF3,SF4)                                             INT01100
    8 CONTINUE                                                          INT01110
      IK=0                                                              INT01120
```

```
C                                                                       INT01130
C ELIMINATE STRUCTURE FACTORS=0                                         INT01140
C                                                                       INT01150
      DO 100 NI=1,NUM                                                   INT01160
      A=REAL(F1(NI))                                                    INT01170
      B=AIMAG(F1(NI))                                                   INT01180
      C=REAL(F2(NI))                                                    INT01190
      D=AIMAG(F2(NI))                                                   INT01200
      IF (A.EQ.0..AND.B.EQ.0..AND.C.EQ.0..AND.D.EQ.0.) GO TO 100        INT01210
      IK=IK+1                                                           INT01220
      X(IK)=H(NI)                                                       INT01230
      Y(IK)=K(NI)                                                       INT01240
      Z(IK)=L(NI)                                                       INT01250
      F(IK)=F(NI)                                                       INT01260
      FF(IK)=SQRT(F(IK))                                                INT01270
      F1(IK)=F1(NI)                                                     INT01280
      F2(IK)=F2(NI)                                                     INT01290
      FG(IK)=.770255/FF(IK)                                             INT01300
      FFF(IK)=ARSIN(FF(IK))*P                                           INT01310
      FFG(IK)=FFG(NI)                                                   INT01320
      SL(IK)=FF(IK)/1.54051                                             INT01330
  100 CONTINUE                                                          INT01340
C
C  DETERMINE THE MULTPLICITY
C
      DO 1100 NIJ=1,IK                                                  INT01490
      IF(ICRYST.EQ.1)ISTART=48
      IF(ICRYST.EQ.2)ISTART=24
      IF(ICRYST.EQ.3)ISTART=16
      IF(ICRYST.EQ.2)ITYPE=3
      IF(ICRYST.EQ.3)ITYPE=2
      IFAC(NIJ)=ISTART                                                  INT01500
```

```
      IF(ICRYST.EQ.1)GO TO 555
      IF(X(NIJ).EQ.Y(NIJ)) IFAC(NIJ)=IFAC(NIJ)/2                        INT01510
      IF(X(NIJ).EQ.0.OR.Y(NIJ).EQ.0) IFAC(NIJ)=IFAC(NIJ)/2              INT01520
      IF(X(NIJ).EQ.0.AND.Y(NIJ).EQ.0) IFAC(NIJ)=IFAC(NIJ)/ITYPE         INT01530
      IF(Z(NIJ).EQ.0) IFAC(NIJ)=IFAC(NIJ)/2                             INT01540
      GO TO 666
  555 IF(X(NIJ).EQ.Y(NIJ).AND.X(NIJ).NE.0.AND.Z(NIJ).NE.0)IFAC(NIJ)=24
      IF(Y(NIJ).EQ.Z(NIJ).AND.Y(NIJ).NE.0.AND.X(NIJ).NE.0)IFAC(NIJ)=24
      IF(Z(NIJ).EQ.X(NIJ).AND.Z(NIJ).NE.0.AND.Y(NIJ).NE.0)IFAC(NIJ)=24
      IF(X(NIJ).EQ.Y(NIJ).AND.Z(NIJ).EQ.0)IFAC(NIJ)=12
      IF(Y(NIJ).EQ.Z(NIJ).AND.X(NIJ).EQ.0)IFAC(NIJ)=12
      IF(Z(NIJ).EQ.X(NIJ).AND.Y(NIJ).EQ.0)IFAC(NIJ)=12
      IF(X(NIJ).EQ.Y(NIJ).AND.Y(NIJ).EQ.Z(NIJ))IFAC(NIJ)=8
      IF(X(NIJ).NE.Y(NIJ).AND.Z(NIJ).EQ.0)IFAC(NIJ)=24
      IF(Y(NIJ).NE.Z(NIJ).AND.X(NIJ).EQ.0)IFAC(NIJ)=24
      IF(X(NIJ).NE.Z(NIJ).AND.Y(NIJ).EQ.0)IFAC(NIJ)=24
      IF(X(NIJ).EQ.Y(NIJ).AND.X(NIJ).EQ.0.AND.Z(NIJ).NE.0)IFAC(NIJ)=6
      IF(Y(NIJ).EQ.Z(NIJ).AND.Y(NIJ).EQ.0.AND.X(NIJ).NE.0)IFAC(NIJ)=6
      IF(X(NIJ).EQ.Z(NIJ).AND.X(NIJ).EQ.0.AND.Y(NIJ).NE.0)IFAC(NIJ)=6
C
C  THE LORENTZ POLARIZATION FACTOR CORRECTED FOR A MONOCHROMATOR
C
  666 LLP(NIJ)=(1+(COS(AMTH  /P      )**2)*(COS(  FFG(NIJ)/P      )**2))INT01550
     1/(1+(COS(FFG(NIJ)/P      )**2))                                   INT01560
      LP(NIJ)=(1+COS(  FFG(NIJ)/P      )**2)/(F(NIJ)*COS(FFF(NIJ)/P     INT01570
     1 ))*(LLP(NIJ))                                                   INT01580
 1100 CONTINUE                                                         INT01590
C
C  CALCULATE THE ATOMIC SCATTERING FACTORS FROM FUNCTION GIVEN
C  IN X-RAY CRYSTALLOGRAPHY TABLES.
C
      DO 1222 JJ=1,2
```

```
      DO 1221 II=1,4
      READ(5,406) AA(JJ,II),BB(JJ,II)
406   FORMAT(2F14.7)
1221  CONTINUE
1222  CONTINUE
      READ(5,406) CC(1),CC(2)
      DO 141 JJI=1,IK                                              INT01600
      AT(1,JJI)=0.0
      AT(2,JJI)=0.0
      DO 999 KLK=1,4
      AT(1,JJI)=AT(1,JJI)+(AA(1,KLK)*EXP(-1.0*BB(1,KLK)*(SL(JJI)**2)))
      AT(2,JJI)=AT(2,JJI)+(AA(2,KLK)*EXP(-1.0*BB(2,KLK)*(SL(JJI)**2)))
999   CONTINUE
      AT(1,JJI)=AT(1,JJI)+CC(1)
      AT(2,JJI)=AT(2,JJI)+CC(2)
      ATEQ(1,JJI)=(1.0000*AT(1,JJI)+1.0000*AT(2,JJI))
      CFJ(1,JJI)=(AT(1,JJI)*F1(JJI))+(AT(2,JJI)*F2(JJI))           INT01610
      CFJ(2,JJI)=CONJG(CFJ(1,JJI))                                 INT01620
      CFF(JJI)=CFJ(1,JJI)*CFJ(2,JJI)                               INT01630
  141 CONTINUE                                                     INT01640
      DO 887 JJI=1,IK
  887 WRITE(6,885)AT(1,JJI),AT(2,JJI)
  885 FORMAT(2E15.7)
      DO 161 NIN=1,IK                                              INT01650
      CFT(1,NIN)=CFF(NIN)*LP(NIN)*IFAC(NIN)                        INT01660
  161 CONTINUE                                                     INT01670
      DO 600 IJ =1,IK                                              INT01680
600   WRITE (6,92)X(IJ),Y(IJ),Z(IJ),F1(IJ),F2(IJ)                  INT01690
      CRT=0.0                                                      INT01700
      DO 162 NMN=1,IK                                              INT01710
  162 IF (CFT(1,NMN).GT.CRT) CRT=CFT(1,NMN)                        INT01720
      DO 163 JMN=1,IK                                              INT01730
```

```
163 CFT(2,JMN)=(CFT(1,JMN)/CRT)*10.                                    INT01740
    WRITE (6,888)                                                      INT01750
    WRITE (6,171)                                                      INT01760
    WRITE (6,165)                                                      INT01770
    DO 164 NMJ=1,IK                                                    INT01780
164 WRITE (6,166)X(NMJ),Y(NMJ),Z(NMJ),FFG(NMJ),SL(NMJ),AT(1,NMJ),AT(2,INT01790
   1NMJ),CFF(NMJ),IFAC(NMJ),LP(NMJ),CFT(1,NMJ),CFT(2,NMJ),FG(NMJ)      INT01800
166 FORMAT(3X,3I2,4X,F9.5,5X,F8.5,5X,F8.5,5X,F8.5,5X,F9.2,5X,I4,4X,F9.INT01810
   15,1X,E15.7,3X,F6.3,2X,F9.6)                                        INT01820
    WRITE(6,888)                                                       INT01830
345 STOP                                                               INT01840
    END                                                                INT01850
```

APPENDIX 6

Structure and atomic positions of $TiAl_3$

$TiAl_3$ (body centered tetragonal, Ga_2Hf type)[25]

a=3.849 A

c=8.610 A

Z=2 (8 atoms per unit cell)

Density (X-ray)=3.354

c/a=2.237

Origin at center, Equivalent positions:

(0,0,0 ; 0.5,0.5,0.5) +

Ti: 2a (0,0,0)

Al(1): 2b (0,0,0.5)

Al(2): 4d (0,0.5,0.25) ; (0.5,0,0.25)

Space Group I4/mmm

Structure and atomic positions of Ti Al

Ti_3Al (hexagonal, SmN_3 type)[47]

a=5.77 A

c=4.62 A

Z=2 (8 atoms per unit cell)

Density (X-ray)=3.002

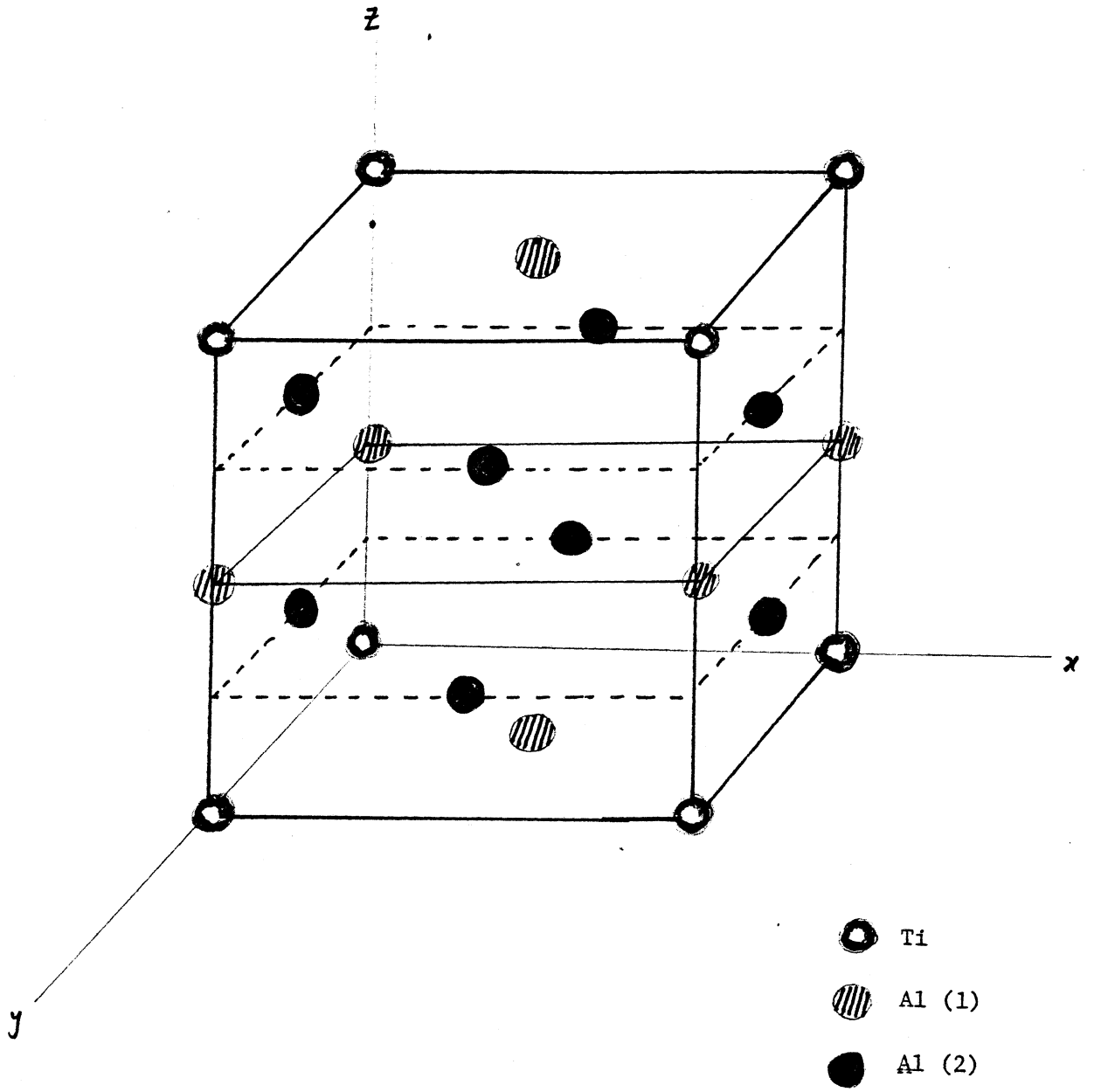


Figure 55: The TiAl unit cell.

No superlattice reflections were observed[47] at temperatures above 600°C.

Equivalent positions:

Ti(6h): (x,2x,0.25) - location 1

(-2x,-x,0.25) - location 2

(x,-x,0.25) - location 3

(-x,-2x,0.75) - location 4

(2x,x,0.75) - location 5

(-x,x,0.75) - location 6

Al(2c): (0.3333,0.6667,0.25)

(0.6667,0.3333,0.75)

The value of x can be chosen from the studies on any of the following compounds (the final choice depends on the atomic radii of the elements of the elements in Ti_3Al and those in the compounds given):

alpha AlCe	0.829
Cd_3Mg	0.833
Cd_3Si	0.833
Co_3Mo	0.8373±3
Co_3W	0.844
beta-Fe Sn	0.840
Ni_3Sn	0.833
SnTi	0.833

For the simulations in the present investigation, a value of 0.833 was chosen for reasons mentioned earlier.

APPENDIX 7

Table showing Integrated Intensities and two-theta positions for Ti.

hkl	Two-theta	Intensity	Rel. Int.
100	35.081	0.278E 05	24.74
002	38.400	0.286E 05	25.38
101	40.156	0.113E 06	100.00
102	52.985	0.158E 05	14.02
110	62.935	0.180E 05	15.96
103	70.631	0.186E 05	16.52
200	74.137	0.267E 04	2.37
112	76.190	0.197E 05	17.51
201	77.334	0.142E 05	12.58
004	82.254	0.266E 04	2.36
202	86.730	0.351E 04	3.11
104	92.688	0.306E 04	2.72
203	102.319	0.806E 04	7.16
210	105.762	0.263E 04	2.33
211	109.009	0.156E 05	13.86
114	114.219	0.104E 05	9.28
212	119.206	0.536E 04	4.76
105	122.248	0.824E 04	7.33
204	126.291	0.287E 04	2.55
300	129.418	0.600E 04	5.33
213	139.318	0.216E 05	19.19
302	148.352	0.182E 05	16.19

Table 37

Integrated Intensities and Two Theta Positions for Ti_5Si_3 Obtained from Theoretical (computer) Calculations

HKL	Two Theta	Intensity	Rel. Int.
001	17.240	0.52E06	14.09
101	22.119	0.42E06	11.38
110	23.936	0.79E05	2.11
200	27.707	0.21E06	5.70
111	29.649	0.51E06	13.70
201	32.817	0.15E06	3.94
002	34.887	0.95E06	25.51
210	36.933	0.11E07	30.32
102	37.664	0.15E06	4.07
211	41.027	0.37E07	100.00
300	42.098	0.74E06	19.81
112	42.754	0.30E06	8.19
301	45.808	0.21E06	5.77
310	51.146	0.10E06	2.78
212	51.712	0.26E06	6.87
221	52.333	0.11E06	3.04
311	54.380	0.40E05	1.08
302	55.787	0.91E05	2.45
400	57.225	0.48E05	1.29
113	59.361	0.13E06	3.58
222	61.557	0.56E05	1.51
321	65.770	0.79E05	2.12
410	66.547	0.31E06	8.43
213	66.737	0.40E06	10.84
402	68.801	0.15E06	4.10
411	69.325	0.14E06	3.88
303	70.268	0.51E05	1.38
500	73.541	0.11E06	2.97
004	73.673	0.18E06	4.82

Table 37 Continued

HKL	Two Theta	Intensity	Rel. Int.
223	75.426	0.19E06	5.04
313	77.117	0.82E05	2.20
412	77.392	0.53E05	1.42
420	78.619	0.13E06	3.54
331	79.568	0.36E06	9.69
421	81.234	0.42E05	1.13
502	84.053	0.27E06	7.17
214	85.386	0.16E06	4.29
511	86.192	0.82E05	2.19
323	87.079	0.12E06	3.15
304	88.676	0.15E06	4.00
422	88.991	0.77E05	2.08
413	90.365	0.38E05	1.03
314	95.253	0.37E05	1.00
431	96.062	0.38E05	1.01
520	96.777	0.44E05	1.18
333	100.275	0.77E05	2.06
610	103.454	0.11E06	3.09
611	106.117	0.45E05	1.21
414	108.717	0.21E06	5.72
215	108.901	0.27E06	7.39
440	112.086	0.62E05	1.65
612	114.355	0.11E06	2.96
504	115.821	0.11E06	3.00
531	116.718	0.38E05	1.03
433	117.713	0.11E06	2.92
620	119.384	0.59E05	1.57
424	121.436	0.17E06	4.48
523	121.492	0.19E06	5.07
621	122.384	0.24E06	6.35
532	125.760	0.82E05	2.19
514	127.413	0.50E05	1.36
006	128.134	0.52E05	1.40

Table 37 Continued

HKL	Two Theta	Intensity	Rel. Int.
710	129.346	0.40E05	1.06
622	132.040	0.44E05	1.19
711	132.760	0.58E05	1.57
415	136.491	0.78E05	2.11
434	141.220	0.63E05	1.69
443	141.295	0.10E06	2.72
216	144.902	0.64E05	1.73
800	146.581	0.43E05	1.15
524	146.813	0.14E06	3.72
631	148.313	0.41E06	11.09
306	151.104	0.38E05	1.02
623	153.513	0.23E06	6.14
335	153.801	0.49E06	13.17
720	157.023	0.11E06	2.83
425	157.809	0.67E05	1.80
542	158.185	0.22E06	6.03
614	162.092	0.73E06	19.70
226	164.049	0.56E05	1.50
721	164.927	0.47E05	1.21
632	170.306	0.14E06	3.77

The vita has been removed from the scanned document

Control of Interface Reactions in SiC/Ti Composites
And An X-ray Diffraction Study of
Interdiffusion Between Al Thin Films and Ti Substrates

by

Venkatraman B. Rao

(ABSTRACT)

In SiC/Ti composites, the physical-chemical behaviour at the interface at fabrication temperatures, is important. Ideally, only a thin bonding film is desired after fabrication with zero growth during the actual service conditions. In this study, two mechanisms which lower the growth rate of silicides about the SiC/Ti interface were investigated. Planar composites that incorporated Mo_5Si_3 or Al films, were compared with the uncoated SiC/Ti standards to investigate the "barrier" and "rejection" mechanisms respectively. Also, SiC/Ti_3Al/Ti composites were used to study the effectiveness of the two mechanisms combined, with the Ti_3Al acting as a barrier and with Ti(Al) retarding the reaction by rejection. Samples were vacuum-annealed at 875°C for various times and examined by X-ray diffraction techniques. The results from the SiC/Al/Ti and SiC/Ti_3Al/Ti composites indicated that silicide formation would be retarded in the presence of an Al saturated Ti matrix. Also, the formation of a Ti_3Al layer near the SiC/Ti interface serves as an effective barrier to diffusion of Si atoms. In the SiC/Mo_5Si_3/Ti composites however, the dissociation of the Mo_5Si_3 phase formed during sample preparation results in additional silicide formation at the interfaces. If stoichiometric Mo_5Si_3 films are sputter-deposited, they could be used as effective barrier.

The inter-diffusion of Al films, sputter deposited on Ti substrates, at elevated temperatures have been analyzed. Samples were vacuum annealed at 635°C and 900°C for various times and then examined using X-ray diffraction. In each case, intensity bands from alpha-Ti and diffraction lines from an intermetallic compound have been observed. For subsequent annealing times, the integrated intensities from the compound decreased slightly, indicating that the compound partially decomposed and released Al into the alpha-Ti lattice. This resulted in an alpha-Ti diffracted intensity band that results from a range of compositions. Intensity bands from Ti(101) were used to obtain composition profiles for Al in alpha-Ti, by using X-ray diffraction techniques and computer simulations. In each case, mass conservation of Al atoms was used to determine the interface motion. It was assumed that the Al profiles extend continuously into the disordered Ti_3Al and Ti_2Al composition regions. This assumption was verified by preparing a Ti_2Al (disordered) powder standard and obtaining accurate lattice parameters. An iterative solution was used to determine composition dependent diffusion coefficients of one-dimensional zones, for two-phase systems. Diffusion zones extending from a few tenths to several microns have been examined. Al diffusion coefficients in alpha-Ti and the Ti_3Al phase have been determined. Activation energies were calculated from the diffusion coefficients at 635°C and 900°C and compared with those obtained from a melting point correlation. Lower activation energies from the present investigation indicated that there was some grain boundary diffusion at these intermediate temperatures.